FisEs 2011

XVII Congreso de Física Estadística

Libro de resúmenes

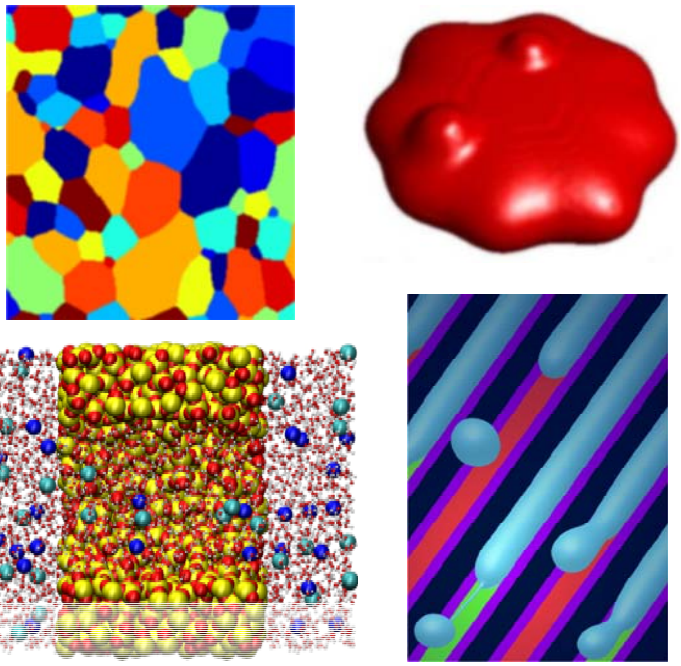

Barcelona, 2-4 Junio de 2011

Facultad de Física, Universitat de Barcelona

UNIVERSITAT DE BARCELONA

B:KC Barcelona Knowledge Campus
Campus de Excelencia Internacional

UPC UNIVERSITAT POLITÈCNICA DE CATALUNYA BARCELONATECH

Cubierta: composición con cuatro figuras seleccionadas entre las contribuciones al congreso. En sentido horario, y empezando por el panel superior izquierdo, J. C. R. E. Oliveira *et al*. (P-117); G. R. Lázaro *et al.* (P-82); R. Ledesma-Aguilar *et al.* (O-14); J. Sala *et al*. (P-147).

Banner: skyline de Barcelona adaptado de imagen © vectorine, www.fotolia.es.

Maquetación y compilación: comité organizador FisEs11.

Comité Científico

- Carlos Cabrillo (Instituto de Estructura de la Materia, CSIC)
- Rodolfo Cuerno (Universidad Carlos III, Madrid)
- Enrique de Miguel (Universidad de Huelva)
- Elvira Guàrdia (Universitat Politècnica de Catalunya)
- Diego Maza (Universidad Navarra)
- Miguel Ángel Muñoz (Universidad de Granada)
- Ignacio Pagonabarraga (Universitat de Barcelona)
- Miguel Ángel Rodríguez (Universidad de Cantabria)
- María José Ruiz (Universidad de Sevilla)
- Pedro Tarazona (Universidad Autónoma de Madrid)
- Raúl Toral (Universitat de les Illes Balears - CSIC)
- Juan A. White (Universidad de Salamanca)

Comité Local

- Giancarlo Franzese (Universitat de Barcelona)
- Elvira Guàrdia (Universitat Politècnica de Catalunya)
- Marta Ibañes (Universitat de Barcelona)
- Jordi Ignés (Universitat de Barcelona)
- Jordi Martí Rabassa (Universitat Politècnica de Catalunya)
- Ignacio Pagonabarraga (Universitat de Barcelona)

Índice General

Parte I
Conferencias invitadas

Thermodynamics of a small system in a μ,T reservoir

Dick Bedeaux*
Department of Chemistry, Norwegian University of Science and Technology, Trondheim 7491, Norway

Due to advances in experimental techniques operating at the nanoscale, it is possible to compute properties from density fluctuations by studying "snapshots" of particle configurations. Thermodynamics on a small scale is different from thermodynamics in bulk systems. We show how the molar enthalpy h and the inverse thermodynamic correction factor Γ^{-1} depend on system size and how these properties can be computed from fluctuations at the nanoscale. We find a $1/L$ finite size effect for all thermodynamic quantities for a small system in contact with a reservoir, where L is the length of the system in a single dimension.

* dick.bedeaux@chem.ntnu.no

La teoría del coarse-graining, aplicaciones y problemas abiertos

Pep Español*
Departamento de Física Fundamental
Universidad Nacional de Educación a Distancia
28040 Madrid

Con el propósito de simular de manera eficiente sistemas moleculares de muchos átomos durante tiempos largos se suelen introducir modelos de grano grueso de los cuales se espera que capturen las características más relevantes del sistema en cuestión a costa de detalles que se espera sean poco importantes. De esta forma, por ejemplo, se suelen introducir potenciales efectivos que se obtienen a partir de la función de distribución radial de centros de masa. Sin embargo, es bien conocido que estos potenciales efectivos reproducen bien las propiedades de equilibrio (por construcción) pero suelen dar resultados muy pobres para las propiedades dinámicas (difusión, correlaciones, etc.)

En este trabajo partimos de la teoría de Zwanzig de operadores de proyección[1]. Esta teoría constituye una teoría completa y práctica[2] para la formulación de descripciones de grano grueso y es, de hecho, una formulación muy elegante de la mecánica estadística fuera de equilibrio. Mostraremos cómo se pueden construir con esta teoría modelos de grano grueso a partir de la dinámica microscópica del sistema en dos ejemplos en particular: polímeros estrella descritos en términos de sus centros de masa (ver figura)[2] y modelos discretos para la hidrodinámica[2],[3].

Sin embargo, existen varios problemas abiertos que necesitan ser abordados para que la construcción genérica de modelos de grano grueso:

- *Cómo seleccionar las variables de grano grueso.* La teoría nos dice, dadas las variables de grano grueso, cómo se mueven, pero no ofrece ningún método para "detectar" cuales pueden ser las variables apropiadas.
- *Efectos no-Markovianos,* Una de las hipótesis básicas en el formalismo es la separación de escalas temporales entre las variables seleccionadas y el resto. Esto no siempre se cumple.
- *La maldición de la dimensionalidad*: Los términos de arrastre y difusión de la ecuación de Fokker-Planck obtenida en la teoría de Zwanzig dependen de todas las variables relevantes y son funciones en un espacio de muchas dimensiones, difícil de muestrear[5].
- *Transitividad.* El resultado de pasar de un nivel microscópico 0 a un nivel mesoscópico 1 y de éste a otro nivel macroscópico 2, debe producir idéntico resultado que si obtenemos el nivel macroscópico 2 directamente a partir del microscópico 0.

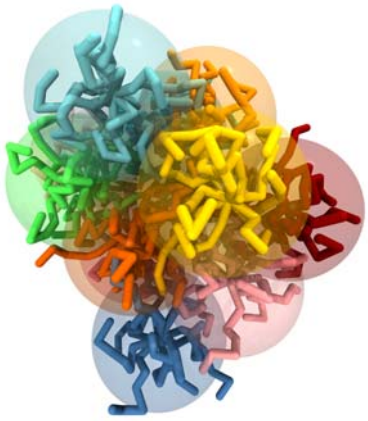

Figura 1. Descripción de grano grueso de un fundido de polímeros estrella

* pep@fisfun.uned.es

[1] *Memory Effects in Irreversible Thermodynamics*, R.Zwanzig, Phys. Rev. **124**, 983 (1961)

[2] *Mori-Zwanzig formalism as a practical computational tool*, Carmen Hijón, Pep Español, Eric vanden-Eijnden, Rafael Delgado-Buscalioni, Faraday Discussions **144** 301-322 (2010).

[3] *Microscopic derivation of discrete hydrodynamic variables*, P. Español Jesús G. Anero, e I. Zúñiga, J. Chem. Phys.**131**, 244117 (2009)

[4] *On the definition of discrete hydrodynamic variables*, P. Español e I. Zúñiga, J. Chem. Phys. **131**, 164106 (2009)

[5] *Obtaining fully dynamic coarse-grained models from MD*, P. Español e I. Zúñiga, aceptado en Physical Chemistry Chemical Physics DOI:10.1039/C0CP02826F.

Frustrated nematic order in spherical geometries

Alberto Fernandez-Nieves*
School of Physics
Georgia Institute of Technology

When nematic liquid crystals are confined between spheres to form shells, complex defect structures emerge. These structures are characterized by a varying number of point defects and disclination lines, all complying with the topological constraints imposed by the spherical geometry. Interestingly, even if the shell thickness per se is what brings about shells with different number and type of defects, it is the thickness inhomogeneity what determines the actual defect arrangement[1]. We will present the rich phenomenology we observe in our shells, where defects move continuously and/or discontinuously as a function of thickness inhomogeneity. In addition, we will also briefly discuss our recent approach to the generation of non-spherical surfaces, such as a torus[2], which we hope to use in the near future to address frustration in these closed surfaces.

* alberto.fernandez@physics.gatech.edu

[1] T. Lopez-Leon, V. Koning, S. Devaiah, V. Vitelli, A. Fernandez-Nieves, Nature Physics (accepted).
[2] E. Pairam, A. Fernandez-Nieves, Phys. Rev. Lett. **102**, 234501 (2009)

Graphene and its unique properties

Francisco Guinea*
Instituto de Ciencia de Materiales de Madrid. CSIC

Graphene, two dimensional membrane one atom thick is a novel material which shows features not found previously in other systems. It is a two dimensional metal whose properties can be tuned, chemically inert, extremely stiff, charge carriers behave as relativistic particles, etc. Some of these properties, along with the research to elucidate their origin and consequences, will be reviewed.

* paco.guinea@icmm.csic.es

Elastic Instabilities Lead To Novel Material Properties

Tom Mullin
Manchester Centre for Nonlinear Dynamics
University of Manchester
Oxford Road, Manchester M13 9PL, UK
tom@reynolds.ph.man.ac.uk

Periodic elastomeric cellular solids with holes arranged on a square lattice give rise a novel uniform transformation of the structure when subjected to uniaxial compression. The original pattern is transformed into a more complex one above a critical load. The results of a numerical investigation reveal that the pattern switch is triggered by a reversible elastic instability. The phenomena were discovered at the *mm* length-scale and, surprisingly, have recently been shown to also operate at the nanoscale. The mechanism has proved to be useful for the imprinting of complex patterns in photonic crystals so that new band gap structures can be induced in a controlled way. Controllable, negative Poisson ratio effects have also been revealed and these also have potential over a wide range of scales

On the short range order of liquid phases

L. C. Pardo, M. Rovira-Esteva, S. Pothoczki, A. Ottochian, J. Ll. Tamarit
[1] *Grup de Caracterització de Materials, Departament de Física i Enginyeria Nuclear, ETSEIB, Universitat Politècnica de Catalunya, Diagonal 647, 08028 Barcelona, Catalonia, Spain*

The structure of disordered systems and its implication in their dynamics is far to be understood. In the case of the liquid phase, for example, it was believed that the structure had no effect on the dramatic slowing down of molecules giving rise to a glass. Actually the opinion that liquids can not be described only by their density, but also by an order parameter characterizing their short range order is growing. In this work we present a way to quantify the short range order of molecules in disordered systems by means of angular bivariate analysis.

The positional order is determined defining an axis system having into account the molecular symmetry and studying the probability distribution function of the azimuthal and equatorial angles for the centers of mass of the neighboring molecules(an example can be seen in the figure). On what concerns the orientational order it depends on molecular position. To have this dependence into account we study separately the relative orientation of two molecules as a function of their position. We present three examples where the aforementioned method has been successfully used.

The first example is devoted to the effect of dipolar moment in the molecular ordering of quasitetrahedral molecules. Choosing CCl_4 as a reference[1] molecule devoid of dipolar moment. We disentangle the effect of the electrostatic interaction on CCl_3Br and CCl_2Br_2. The second example concerns the structure of the high and low temperature liquids for trans-dichloroethylene[2]. In this case, in order to study the differences in the molecular ordering it was necessary to study separately the effect of two configurations in the molecular coordination number of molecules. Finally we account for the crucial role of conformational disorder on the interplay between inter- and intramolecular structure. To highlight such a case, we will show recent results on a Freon derivative with two conformers[3], trans, devoid of dipolar moment, and gauche, with a dipolar moment of 0.26 D .

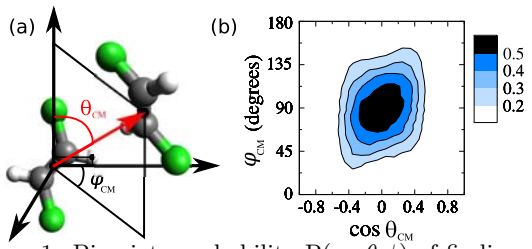

Figura 1. Bivariate probability P($cos\theta$,ϕ) of finding a first neighbour molecule around a reference one

* luis.carlos.pardo@upc.edu

[1] L. C. Pardo, J. Ll. Tamarit, N. Veglio, F. J. Bermejo, and G. J. cuello, Phys. Rev. B **76**, 134203 (2007)
[2] M. Rovira-Esteva, A. Murugan, L. C. Pardo, S. Busch, M. D. Ruiz-Martín, M.-S. Appavou, J. Ll. Tamarit, C. Smuda, T. Unruh, F. J. Bermejo, G. J. Cuello, and S. J. Rzoska, Phys. Rev. B **81**, 092202 (2010)
[3] L.C. Pardo, F.J. Bermejo, J.Ll. Tamarit, G.J. Cuello, P. Lunkenheimer, and A. Loidl, J. Non-Cryst. Solids **353**, 999 (2007)

Multiscale mobility networks and the large scale spreading of infectious diseases

José J. Ramasco*
Instituto de Física Interdisciplinar y Sistemas Complejos IFISC (CSIC-UIB), 07122 Palma de Mallorca, Spain
Complex Networks Lagrange and Epidemiology Laboratories, ISI Foundation, Viale S. Severo 65, 10133, Torino, Italy

Epidemiology is one of fields where the application of the theory of complex networks is crucial. Infectious diseases such as the influenza or the HIV transmit from person to person using mainly connections of social networks. Whether a disease propagates across the world or is restricted to a localized area depends on the structure and properties of these networks. Contact networks are characterized by a multiscale structure with people interacting within local areas and displacing by car, bike, train, etc, to nearby communities where they can carry or contract a disease. This propagation mode reminds thus of a spatial diffusion process. However, a new element has been introduced during the last century. This new factor is airplane traveling that allows for fast connection of very far apart geographical areas. The recent propagation of the H1N1 influenza epidemic until becoming a flu pandemic offers a good example of the effect that long-range traveling has in the global spreading of an infectious disease. The outbreak was first detected in Mexico City in mid March as an anomalous increase in the number of cases of influenza, the Mexican authorities recognized the circulation of a new strain on April 23, just after the analysis performed by the American Center of Disease Control (CDC), and for then it had already extended to the US, and would arrive at Spain a few days later on April 28. An extraordinary propagation velocity crossing thousands of kilometers in a matter of weeks.

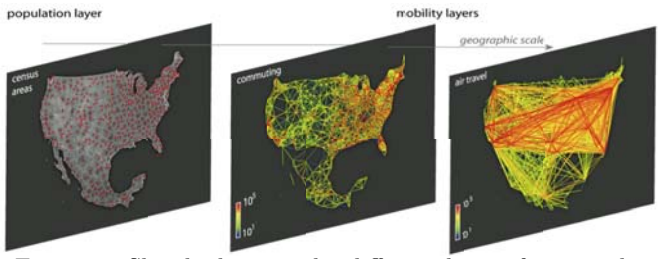

Figura 1. Sketch showing the different layers forming the GLEaM modeler.

In order to study the interplay between small-scale human mobility (commuting flows) and long-range airline traffic in shaping the spatio-temporal pattern of a global epidemic we (i) analyze mobility data from 30 countries around the world and find a gravity model able to provide a global description of commuting patterns up to 300 kms; (ii) we integrate in a worldwide structured metapopulation epidemic model population level data, airline mobility data and the commuting information as illustrated in Figure 1. The different time-scales of the mobility processes are integrated by using a time-scale separation approach for evaluating the force of infection due to multiscale mobility processes in the disease dynamics. This is the origin of the GLobal Epidemic and Mobility (GLEaM) modeler for the spreading of infectious diseases[1–3]. Commuting flows are found, on average, to be one order of magnitude larger than airline flows. However, their introduction into the worldwide model shows that the large scale pattern of the simulated epidemic exhibits only small variations with respect to the baseline case where only airline traffic is considered. The presence of short range mobility increases however the synchronization of subpopulations in close proximity and affects the epidemic behavior at the periphery of the airline transportation infrastructure.

Apart from these results, the GLEaM modeler has been also used in several other applications(which will be briefly described) such as the estimation of the disease parameters of the the H1N1 pandemic[4], the inference of the level of use of antibiotics during the pandemic[5], a comparison between metapopulation models and agent-based models[6] or the assessment of the efficacy of travel restrictions to delay the propagation of a pandemic disease[7].

* jramasco@ifisc.uib-csic.es

[1] D. Balcan, V. Colizza, B. Gonçalves, H. Hu, J.J. Ramasco and A. Vespignani, Proc. Natl. Acad. Sci. (USA) **106**, 21484 (2009).
[2] D. Balcan, B. Gonçalves, H. Hu, J.J. Ramasco, V. Colizza, and A. Vespignani, Journal of Computational Science **1**, 132 (2010).
[3] The application is available online at `http://www.gleamviz.org`
[4] D. Balcan *et al.*, BMC Medicine **7**, 45 (2009).
[5] P. Bajardi *et al.*, Emerging Health Threats Journal **2**, e11 (2009).
[6] M. Ajelli *et al.*, BMC Infectious Diseases **10**, 190 (2010).
[7] P. Bajardi, C. Poletto, J.J. Ramasco, M. Tizzoni, V. Colizza and A. Vespignani, PLoS ONE **6**, e16591 (2011).

First-principles simulation of biomolecular processes

Carme Rovira*

† *Computer Simulation & Modeling Laboratory (CoSMoLAB), Parc Científic de Barcelona, Baldiri Reixac 10-12, 02028 Barcelona, Spain and Institut de Química Teòrica i Computacional (IQTCUB).*

‡ *Institució Catalana de Recerca i Estudis Avançats (ICREA), Passeig Lluís Companys 23, 02010 Barcelona*

Molecular (atomistic) simulation (MS) is a rapidly growing area of computer science that is having an enormous impact on science and technology, because of the increasing need to understand the microscopic details of matter and because of the phenomenal growth in computing power in recent years.[1] Molecular dynamics (MD) is one of the most used MS techniques. In MD, some form for the interaction among atoms needs to be assumed. This is at the same time a strength and a limitation, especially for the study of chemically complex processes such as when covalent bonds break up and new ones form (e.g. chemical reactions) and in general for those processes in which significant electronic reorganizations or polarization play a role. One of the most powerful methods currently available to describe such complex processes is first-principles or ab initio molecular dynamics (AIMD), which is based on Density Functional Theory. Since the pioneering work of Car and Parrinello in 1985,[2] AIMD experienced a rapid development, being now commonly used in many areas of science. In this talk I will show a few recent applications performed in our group in the fields of biochemistry and biophysics,[3] such as the decomposition of hydrogen peroxide by catalase enzymes[4] and the study of conformational free energy landscapes of carbohydrates.[5–7]

* crovira@pcb.ub.es

[1] W. F. van Gunsteren, D. Bakowies, R. Baron, I. Chandrasekhar, M. Christen, X. Daura. P. Gee, D. P. Geerke, A. Glättli, P. H. Hünenberger, M. A. Kastenholz, C. Oostenbrink, M. Schenk, D. Trzesniak, N. F. A. van der Vegt and H. B. Yu, Angew. Chem. Int. Ed. **45**, 4064 (2006).

[2] R. Car and M. Parrinello, Phys. Rev. Lett. **55**, 2471 (1985)

[3] C. Rovira, in *Methods in Molecular Biology,* **305***, Protein-Ligand Interactions: Methods and Applications*, ed.: G. U. Nienhaus, Humana Press, Totowa NJ, pp. 527-566 (2005).

[4] M. Alfonso-Prieto, X. Biarnés, P. Vidossich and C. Rovira, J. Am. Chem. Soc. **131**, 11751 (2009).

[5] A. Ardèvol, X. Biarnés, A. Planas and C. Rovira, J. Am. Chem. Soc. **132**, 16058 (2010).

[6] X. Biarnés, J. Nieto, A. Planas and C. Rovira, J. Biol. Chem. **281**, 1432 (2006).

[7] L. Petersen, A. Ardèvol and C. Rovira, P. Reilly, J. Am. Chem. Soc. **132**, 8291(2010).

¿ Cuan de normales son las anomalías en el transporte y difusión de partículas brownianas ?

José M. Sancho
Departament d'Estructura i Constituents de la Matèria, Facultad de Física, Universidad de Barcelona

Desde el trabajo seminal de Einstein[1] se sabe que el transporte (o bien la velocidad de arrastre de partículas en un fluido) no es independiente de la dispersión o difusión de las mismas. Sabemos que esta velocidad es debida a una fuerza y por la tanto es una propiedad determinista que debería explicarse simplemente con la mecánica newtoniana. En cambio la difusión es una consecuencia de las fluctuaciones térmicas y para partículas libres bajo una fuerza constante F es,

$$D = \frac{k_B T}{\lambda} = k_B T \frac{dv}{dF}, \qquad (1)$$

donde $k_B T$ es la energía térmica disponible para la partícula, y γ es el coeficiente de fricción de Stokes. La segunda igualdad es una generalización que nos dice que la difusión es proporcional al coeficiente de transporte obtenido usando mecánica clásica: $v = F/\gamma$. La expresión anterior es muy llamativa pero como veremos solo se cumple en el caso particular resuelto por Einstein.

Sistema normales: Si consideraríamos como sistemas normales los que obedecen la expresión de Einstein entonces pocos sistemas normales existen. Sobre la base de que las partículas a una temperatura finita experimentan fluctuaciones térmicas y que bajo una fuerza F fija se mueven, definimos el transporte y la difusión como los siguiente promedios estadísticos,

$$v = \lim_{\tau\to\infty} \frac{< x(\tau) >}{\tau}, \quad D = \lim_{\tau\to\infty} \frac{< \Delta^2 x(\tau) >}{2\tau}. \qquad (2)$$

Si estos límites existen sin problemas se considera que el sistema es normal. Hay que aclarar aquí que en un experimento o simulación no alcanzamos tal límite pero esperamos obtener un valor asintótico estable. Si por el contrario observamos algún comportamiento diferente entonces podemos pensar en una anomalía que clasificamos en, débiles o fuertes.

Anomalías débiles

Estas son de varios tipos:

- Difusión gigante o fuerte aumento de D para ciertos valores de F.
- Difusión nula a pesar de que la temperatura es finita.
- Aparición de una componente ortogonal de la velocidad respecto de la fuerza $\vec{F}$. Este efecto es el responsable de la separación de partículas diferentes para una misma fuerza ("sorting").

Anomalías fuertes

Estas se caracterizan por el hecho de que la velocidad o la difusión no son constantes en el tiempo. Aparecen cuando el sistema presenta desorden. Tenemos los siguientes casos:

- Subdifusión: $D(\tau)$ decae en el tiempo.
- Superdifusión: $D(\tau)$ aumenta en el tiempo.
- Subtransporte: $v(\tau)$ decae en el tiempo.

Las anomalías fuertes pueden verse en la figura adjunta.

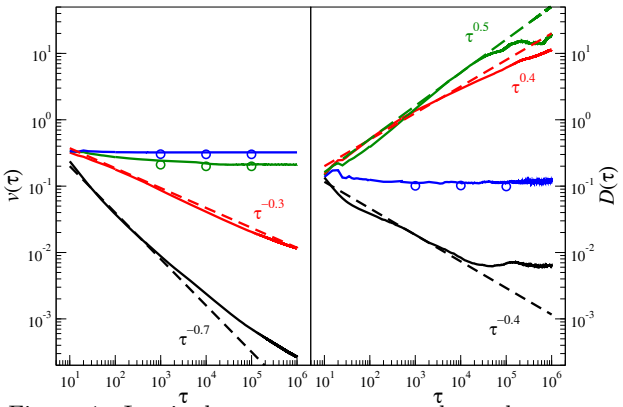

Figura 1. Izquierda: transporte normal y subtransporte. Derecha: difusión normal, super y subdifusión[5]. Cada línea corresponde a una longitud de correlación del desorden que sin embargo es débil: $\sigma = 0.05$. A menor longitud de correlación mayor es la anomalía.

El origen de todas las anomalías es la presencia de un potencial no lineal que puede ser periódico, débilmente desordenado o totalmente aleatorio. Sin embargo basta una dinámica simple como la ecuación de Langevin sobre amortiguada,

$$\gamma \dot{x} = -U'(x) + F + \xi(\tau), \qquad (3)$$

para ver una gran variedad de anomalías. $\xi(\tau)$ es el conocido ruido térmico. El potencial no lineal está separado en dos partes, $U(x) = (1-\sigma)V_p(x) + \sigma V_r(x)$: la primera es un potencial periódico y la segunda es un potencial aleatorio (desorden). El parámetro σ controla el peso relativo de cada parte. La simulación numérica de la ecuación de Langevin depara muchas más sorpresas.

Todo este escenario será explicado en la charla así como los fundamentos teóricos de cada anomalía[2–5].

[1] A. Einstein, Ann. Phys. **17**, 549 (1905)
[2] J.M. Sancho, et al. PRL**92**,250601(2004)
[3] A.M. Lacasta, et al. PRL**94**,160601 (2005)
[4] K. Lindenberg, et al. PRL**98**,020602(2007)
[5] M. Khoury, et al. PRL**106**, 090602(2011)

The emergent dynamics of collective cell migration

Xavier Trepat[1,2,3*]
[1] *Institut de Bioenginyeria de Catalunya*
[2] *Facultat de Medicina, Universitat de Barcelona*
[3] *Institució Catalana de Recerca i Estudis Avançats*

In essential physiological functions including morphogenesis, wound healing, and tissue regeneration, the prevalent mode of cellular migration is innately collective. Collective cellular migration is also recognized as being a ubiquitous mechanism of invasion in epithelial cancers. In order for a cell collective to migrate cohesively, it has long been suspected that each constituent cell must exert physical forces not only upon its extracellular matrix but also upon its neighboring cells. I will present the first comprehensive maps of these distinct force components. Further, I will provide evidence that physical forces within the monolayer develop dramatic heterogeneities, both in space and in time, that emerge spontaneously, propagate over great distances, and cooperate over the span of many cell bodies. To explain the severe ruggedness of this force landscape and its role in collective cell guidance, the well know mechanisms of chemotaxis, durotaxis, haptotaxis are clearly insufficient. In a broad range of epithelial and endothelial cell sheets, collective cell migration is governed instead by a newly discovered emergent mechanism of innately collective cell guidance − phlithotaxis.

* xtrepat@ub.edu

ZCAM, Spanish node of the CECAM network

Michel Mareschal*
Zaragoza Scientific Center for Advanced Modeling (ZCAM)

CECAM's workshops and tutorials have been given a reputation of scientific excellence and have been associated with the leading position of European scientists in computational condensed matter. The growing importance of this field had led to creating Cecam nodes in Europe, among which Zcam, the Spanish node located in Zaragoza. In this short presentation, I will list present opportunities Zcam is offering the community, both in terms of instruments and in terms of topics currently discussed.

* mmaresch@ulb.ac.be

Parte II
Orales

Delayed Coupling Theory of Vertebrate Segmentation

Saúl Ares[1*], Luis G. Morelli[1,2], Leah Herrgen,[2] Christian Schröter,[2] Frank Jülicher,[1] Andrew C. Oates[2]
[1] *Max Planck Institut for the Physics of Complex Systems, Dresden, Germany*
[2] *Max Planck Institute for Molecular Cell Biology and Genetics, Dresden, Germany*

The body plan of all vertebrate animals has a segmented organization that is reflected in the repeated arrangement of vertebra and ribs. This structure forms during the development of the organism by a process termed segmentation. The segments —called somites— form sequentially along a linear axis, one by one, with a precisely controlled timing, see Fig. 1. This timing is set by a genetic clock, is realized by oscillations of the levels of certain proteins in individual cells[1]. The genetic oscillations of cells in the tissue are coordinated by a molecular signaling system that introduce a coupling of neighboring cellular oscillators. This gives rise to a collective spatio-temporal pattern which consists of waves that travel and eventually stop and arrest in a periodic arrangement of somites. Signaling gradients ranging over larger distances control the slow down and arrest of the cellular oscillators and guide spatio-temporal patterns during segmentation. We have developed a theoretical description of somitogenesis based on a coarse grained representation of cellular oscillators as phase oscillators. Slow intercellular communication introduces a time delay in the coupling between oscillators.

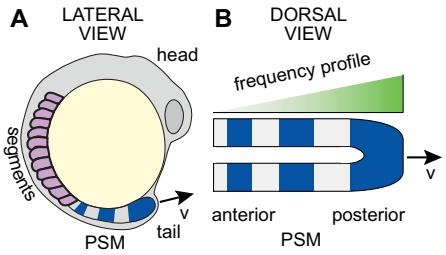

Figura 1. (A) Schematic lateral view of a zebrafish embryo showing formed segments (purple) and waves of gene expression (blue) in the unsegmented tissue, the presomitic mesoderm (PSM). The tail grows with velocity v. (B) From a dorsal view the PSM is a U-shaped tissue. A frequency profile along the PSM causes faster genetic oscillations in the posterior PSM.

The spatio-temporal patterns of genetic oscillations are described by coupled sets of phase oscillators which are arranged in space. The state of a single oscillator is characterized by the phase $\theta_i(t)$, where i labels the oscillator. The dynamic equations for the phases are given by[2]

$$\dot{\theta}_i(t) = \omega_i(t) + \frac{\varepsilon_i(t)}{n_i} \sum_j \sin\left[\theta_j(t-\tau) - \theta_i(t)\right] \qquad (1)$$

where the sum is over all neighbors j of cell i. Here, ε denotes the coupling strength and τ is the time delay involved in coupling. We solve these equations in one or two-dimensional space with moving boundary at one end of the system. The posterior boundary is extended towards one side by the addition of new oscillators at a rate v/a, where v is an extension velocity and a the distance between neighboring cells. We consider a frequency profile which is moving together with the expanding end.

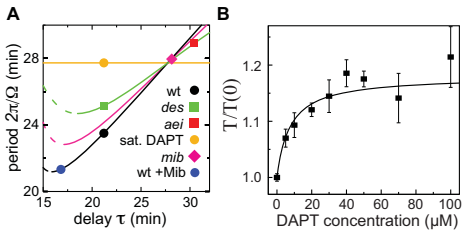

Figura 2. (A) Collective period Ω as a function of time delay τ for different coupling strengths (solid lines). The symbols indicate operating points for wild-type and different mutants as indicated. (B) Experimentally determined collective period $T = \Omega/2\pi$ (symbols) as a function of DAPT concentration, which is a drug that influences coupling strength. The theoretical prediction of the delayed coupling theory is shown as a solid line.

Our theory makes key predictions regarding the effects of coupling and coupling delays on the collective oscillator patterns. After an initial transient dynamics, the system settles in a spatio-temporal limit cycle with collective frequency Ω which obeys the relation

$$\Omega = \omega_A - \varepsilon \sin(\Omega\tau). \qquad (2)$$

This frequency is governed by the autonomous frequency ω_A of the fastest oscillators at the posterior side, modified by effects of coupling described by the coupling strength ε. This implies that changes in coupling strength would lead to changes in oscillation period and thus in variations of the wavelength of cyclic gene expression patterns as well as the resulting segment length. Furthermore, the theory predicts the existence of a dynamic instability when the delay is reduced. We have experimentally verified all these predictions[3]. In this way we have: a) discovered the first period mutants of the segmentation clock (see Fig. 2); b) made the first characterization, to our knowledge, of a natural system of coupled oscillators where coupling delay plays a significant role.

* saul@pks.mpg.de

[1] O. Pourquié, Science **301**, 328 (2003).
[2] L.G. Morelli, S. Ares, L. Herrgen, C. Schröter, F. Jülicher, A.C. Oates, HFSP J. **3**, 55 (2009).
[3] L. Herrgen, S. Ares, L.G. Morelli, C. Schröter, F. Jülicher, A.C. Oates, Curr. Biol. **20**, 1244 (2010).

Deterministic optical rogue waves

Cristian Bonatto, Cristina Masoller
Departament de Física i Eng. Nuclear, Universitat Politècnica de Catalunya, Edif. GAIA, Rambla de Sant Nebridi s/n, 08222 Terrassa, Barcelona, Spain

José R. Rios Leite
Departamento de Física, Universidade Federal de Pernambuco, 50670-901, Recife, Brazil

Michael Feyereisen, Stéphane Barland, Massimo Giudici and Jorge R. Tredicce
Université de Nice Sophia Antipolis, Institut Non-Lineáire de Nice, UMR 6618, 06560 Valbonne, France

Rare extreme events can be observed in different systems in nature. A typical example are rogue waves observed in the oceans, where waves higher than 30 meters are more or less common phenomena. This fact is in contradiction with the Gaussian models often used to describe fluctuations of the wave height in the sea[1,2]. Scientific interest on extremely high waves increased substantially during the last decade not only in oceanographic studies but also in other systems such as capillary waves[3] and optical waves[4–7]. Both, from the theoretical and from the experimental points of view there are several questions still remaining unsolved. The physical mechanisms that originate them, the way they develop, the probability for them to occur , the type of system able to generate such extreme events, and the connections between extreme events in systems which are apparently completely different, are being the subjects of intensive research.

In this work we investigate, both experimentally and theoretically, the appearance of rare giant pulses or rogue waves in a semiconductor laser subject to optical injection. We perform a detailed experimental characterization of the parameter region where rogue waves appear, and compare the experimental observations with numerical results from the simplest rate-equation model.

A typical experimental time series, where a sporadic large intensity pulse is observed, is shown in Fig. 1(a). Figure 1(b) shows a numerical time series obtained for the laser model, in a good qualitative agreement with the experiment. To investigate the rarity of the large pulse events, histograms for the laser intensity were measured, as shown in Fig. 2. Figure 2(a) shows a typical histogram for a time series without rogue waves and Fig. 2(b) shows an histogram with rogue waves. In this case, the probability distribution function of the pulse amplitude displays clear non-Gaussian features, with a long tail and an abnormality index that confirm the rogue wave character of the intensity pulsations.

The analysis of the theoretical model allows to discuss the main mechanisms associated with the appearance of rogue waves. Parameter regions where rogue waves occur are identified and is shown that the rogue waves can be understood as a result of a deterministic nonlinear process. The role of noise in the system is investigated and its influence to induce or inhibit rogue waves is discussed.

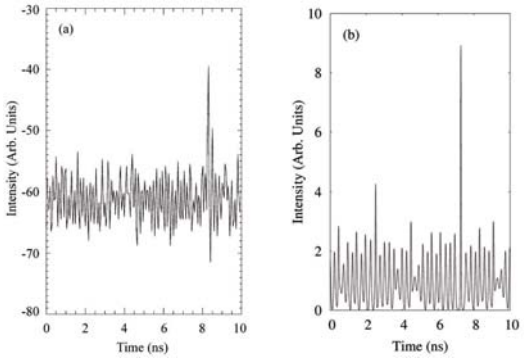

Figura 1. Time trace for the laser intensity showing the occurrence of a large rare event obtained by (a) measuring experimentally the laser intensity and (b) simulating the theoretical model.

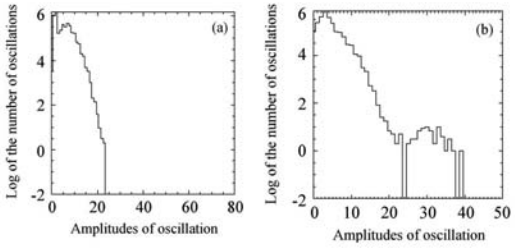

Figura 2. Experimental histograms obtained for the laser intensity showing the cases (a) without rogue waves and (b) with rogue waves.

[1] M. S. Longuet-Higgins, Phil. Trans. Roy. Soc. A **249**, 321 (1957).
[2] S. Aberg and G. Lindgren, Prob. Eng. Mech. **23**, 359 (2008).
[3] M. Shats, H. Punzmann and H. Xia, Phys. Rev. Lett. **104**, 104503 (2010).
[4] D. R. Solli, C. Ropers, P. Koonath, B. Jalali, Nature **450**, 1054 (2007).
[5] J. M. Dudley, G. Genty and B. J. Eggleton, Opt. Express **16**, 3644 (2008).
[6] A. Mussot, A. Kudlinski, M. Kolobov, E. Louvergneaux, M. Douay and M. Taki, Opt. Express **17**, 17010 (2009).
[7] A. Montina, U. Bortolozzo, S. Residori, and F.T. Arecchi, Phys. Rev. Lett. **103**, 173901 (2009).

Instabilities of conducting fluid layers in cylindrical cells under external forcing

Javier Burguete*, Montserrat Miranda
Departamento de Física y Matemática Aplicada, Universidad de Navarra
Edificio Los Castaños, Irunlarrea 1, E-31008 Pamplona

Flows created in neutral conducting fluids remain one of the less studied topics of fluid dynamics, despite their importance both in fundamental research (dynamo action, turbulence suppression) and applications (continuous casting, aluminum production, biophysics).

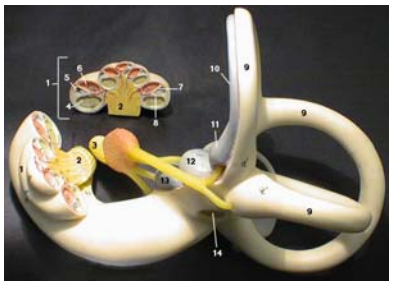

Figura 1. Inner ear model. The equilibrium (spinning) is controlled by the three circular channels placed on the right side and oriented in the three spatial axes. The left part corresponds to the cochlea, where the sound waves are converted in electrical signals.

One of these challenging topics is the interaction between electrolytes and high magnetic fields. This point is relevant in biophysics, because of the secondary effects reported by patients in MRI devices. Between these effects are vertigoes, i.e. the sensation of motion or spinning when the body is at rest. The equilibrium in the human body is controlled by the inner ear, in the vestibular cavity, by three toroidal channels filled with endo- and perilymph (K^+ or Na^+ electrolytes). When an alternating magnetic field is applied to one of these channels it behaves as a coil, an induced current is produced and a radial Lorentz force acts on the fluid.

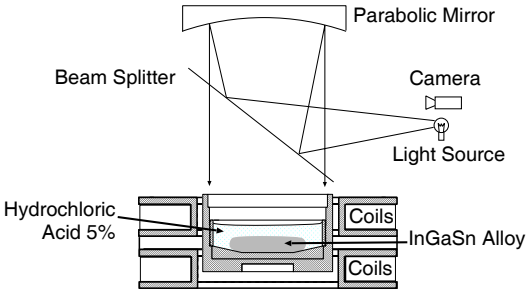

Figura 2. Lateral view of the experimental setup. Very small surface deflections can be easily registered near the threshold.

Having in mind this application, but with a simpler geometry, we present the effect of a time-dependent magnetic field parallel to the axis of circular cavities. As explained above, due to the Lenz′s law, the time-dependent magnetic field generates an azimuthal current, that produces a radial force. This force produces the destabilization of the static fluid layer, and a flow is created.

The geometry of the experimental cell is a disc layer with external diameter smaller than 94 mm, with or without internal hole. The layer is up to 20mm depth, and we use an In-Ga-Sn alloy as conducting fluid. There are no external currents applied on the problem, only an external magnetic field. This field evolves harmonically with a frequency up to 10Hz, small enough to not to observe skin depth effects. The magnitude ranges from 0 to 0.1 T. With a threshold of 0.01T a dynamical behaviour is observed, and the main characteristics of this flow have been determined: different temporal resonances and spatial patterns with different symmetries (azimuthal wavenumbers m=3,4,5,8,...).

To our knowledge there are very few experimental works on this field. Only the group of Y. Fautrelles in Grenoble has performed some measurements but in a strongly non-linear regime[1]. On the other hand, our system allows a much more precise threshold determination and spatial symmetry description, so we can compare with the theory that predicts the instability without threshold[2].

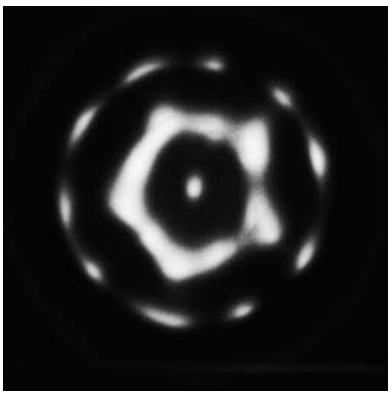

Figura 3. Top view of the fluid layer. The surface is deflected presenting an azimuthal $m = 5$ mode.

* javier@fisica.unav.es - http://fisica.unav.es/mhd/

[1] F. Debray and Y. Fautrelle, Adv. in Turb. IV, in: Appl. Sci. Res., vol. 51, Kluwer (1993) p 31. F. Ingwiller, F. Bonnel, Y. Fautrelle, S. Daugan, and J. Etay Actes du 9eme FLUVISU (2001) p 18

[2] Y. Fautrelle, A.D. Sneyd, European Journal of Mechanics B/Fluids 24 (2005) 91-112

Mecánica Estadística del Sistema Inmune

J. Currie[1], M. Castro[2], Grant Lythe[1], C. Molina-París[1]
[1] *Department of Applied Mathematics, School of Mathematics, University of Leeds, Leeds, LS2 9JT, UK*
[2] *Grupo de Dinámica No-Lineal and Grupo Interdisciplinar de Sistemas Complejos (GISC), Escuela Técnica Superior de Ingeniería (ICAI), Universidad Pontificia Comillas, E28015, Madrid, Spain*

Los vertebrados superiores tienen complejos sistemas inmunológicos que les permiten sobrevivir en un ambiente lleno de agentes infecciosos y también para luchar contra comportamientos celulares anómalos como los tumores. Las células inmunes permanecen inactivas en un individuo sano y entran en acción sólo cuando el cuerpo está en peligro, por ejemplo, durante las infecciones[1].

El sistema inmune es un sistema complejo de células y moléculas (contiene más de 10^7 *clones* distintos) que se comunican mediante un mecanismo estándar de contacto célula-célula y mediante la secrección de ciertas moléculas.

Sin duda, la realización de tareas complejas en este proceso de respuesta ante la amenaza de agentes patógenes (aprendizaje, reconocimiento, memoria, ...) requiere una aproximación propia de la Física Estadística, máxime teniendo en cuenta que involucra escalas de tiempo tan dispares como los segundos (tiempo característico de *sensing*) y los días (tiempo característico en el que el cuerpo humano padece una infección)[2].

En esta comunicación se describen distintos problemas fundamentales desde el punto de vista inmunológico y algunas respuestas desde la Mecánica Estadística.

En particular, se abordan dos problemas, uno a la escala de la célula (y su motilidad) y otro respecto a la dinámica de los receptores de las llamadas células T (células del sistema inmune que son producidas en el *timo*, de ahí su nombre).

En el primer problema, hay un debate interesante tratando de entender si las células difunden aleatoriamente o responden quimiotácticamente a estímulos producidos por otras células.

Como se muestra en la figura 1, una hipótesis de balance entre fluctuaciones térmicas y disipación viscosa permite estimar la difusividad como función de la masa de la célula y, por tanto, discriminar entre un movimiento puramente difusivo y otro dirigido[3].

En el segundo problema, se hace uso de ecuaciones estocásticas (fuera del equilibrio) para responder a la siguiente pregunta: ¿cuál es la cantidad que determina la decisión de una célula T de *responder* a un estímulo?

En este contexto, se han postulado diferentes hipótesis siendo la visión más aceptada la que afirma que son cantidades de equilibrio como las afinidades de la reacción receptor-ligando o el tiempo de vida media de uno de esos enlaces a nivel molecular las que determinan esta respuesta inmune. Nosotros mostramos que dicho proceso es puramente estocástico y que por tanto dichas cantidades de equilibrio no dan una respuesta completamente satisfactoria[4].

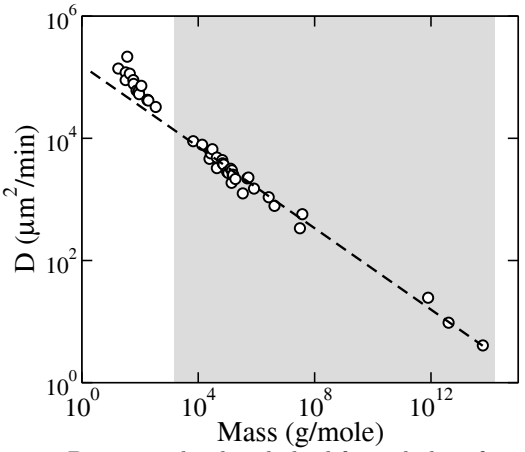

Figura 1. Diagrama log-log de la difusividad en función de la masa (tomada de la Ref.[5]). La línea recta discontinua es un ajuste a la ley fenomenológica $D \sim M^{-1/3}$.

* marioc@upcomillas.es

[1] C.A. Janeway, P. Travers, M. Walport, and J.D. Capra, *Immunobiology: the immune system in health and disease*, (Current Biology London, 1996).
[2] A. Perelson y G. Weisbuch, *Immunology for physicists*, Rev. Mod. Phys. **69**, 1219 (1997).
[3] M. Castro, *A physicist approach to immunology*, capítulo del libro *Current Mathematical Models in T cell Biology*, editado por G. Lythe y C. Molina-París (Springer, 2011).
[4] J. Currie, M. Castro, G. Lythe, C. Molina-París y E. Palmer, *Time is precious, so what does a T cell measure (sense): equilibrium quantities or stochastic events?*, preprint (2011).
[5] R.A. Freitas, *Nanomedicine, Volume I: Basic Capabilities*, (Austin, TX: Landes Bioscience, 1999).

Nonuniversal results induced by diversity distribution in coupled excitable systems

L. F. Lafuerza, Pere Colet, R. Toral
IFISC, Instituto de Física Interdisciplinar y Sistemas Complejos, CSIC-UIB, Campus UIB, 07122 Palma de Mallorca

Synchronization phenomena play a prominent role in many branches of science. They have been analyzed in terms of phase models which successfully describe systems of weakly coupled limit cycle oscillators. In particular, the Kuramoto model[1] has become paradigmatic to describe the emergence of synchronization in an ensemble of oscillators with diversity among the individual units. Diversity in the oscillators is usually introduced by taking their natural frequencies from a probability distribution. Although, on general grounds (central limit theorem), this distribution should be well approximated by a Gaussian form, theoretical studies usually consider a Lorentzian form since it allows for an easier analytical treatment. It is generally believed that the main results concerning the global synchronization properties are qualitatively independent of the precise form of the distribution as long as it is symmetric and unimodal.

We consider a variant of the Kuramoto model for an ensemble of globally coupled active rotators[2]:

$$\dot{\phi}_j = \omega_j - \sin\phi_j + \frac{K}{N}\sum_{l=1}^{N}\sin(\phi_l - \phi_j) \quad j = 1, ..., N. \quad (1)$$

A natural frequency $\omega_j < 1$ (respectively, $\omega_j > 1$) corresponds to an excitable (respectively, oscillatory) behavior of the rotator j when it is uncoupled. K is the coupling intensity. Diversity is introduced by considering that the ω_j's are distributed according to a probability density function $g(\omega)$, with mean value $\overline{\omega}$ and variance σ^2.

For $\overline{\omega} \lesssim 1$ the system displays three different regimes: (i) for small diversity, almost all units are at rest at similar fixed points; (ii) increasing diversity one enters a dynamical state in which a macroscopic fraction of units fire at (roughly) the same time; (iii) for even larger diversity, the system reenters a desynchronized state.

We had developed an approximate theory to describe this diversity-induced collective firing[3]. The theory was independent of the form of the natural frequencies distribution and was also applicable to identical units subject to noise. A recent method developed by Ott and Antonsen[4] allows to solve exactly this model (and a large family of related ones) in the infinite number of oscillators limit and in a number of cases that include the Lorentzian $g(\omega)$. Childs and Strogatz[5] used this method to obtain the full bifurcation diagram of the complex variable $r(t)$ for the Lorentzian distribution. Contrarily to our results, their exact solution implies that there is no transition to collective firing increasing the diversity for $\overline{\omega} < 1$ as illustrated in Fig.1 (right). Regime (ii) takes place for the parameter region located to the right of the solid line signaling the SNIC (saddle node on the invariant circle) bifurcation. The SNIC line always starts at $\overline{\omega} = 1$ with positive slope, so for $\overline{\omega} < 1$ increasing disorder one never encounters Regime (ii).

We show that, quite generally, the Ott-Antonsen method can be successfully applied to any non-singular $g(\omega)$ provided one solves numerically an integrodifferential equation[6]. For the Gaussian distribution the SNIC starts at $\overline{\omega} = 1$ with a negative slope (Fig.1(left)). Therefore for $\overline{\omega} < 1$, as disorder increases one finds first regime (i), then crosses the SNIC lower boundary entering in regime (ii) and finally crosses the reentrant upper boundary entering in regime (iii) where a stable steady state is present again. Region (ii) moves upwards and broadens increasing the coupling K. The same result is obtained using the Ott-Antonsen method solved numerically (circles) and using an alternative approach we have developed[6] (solid line). Besides the Gaussian, we find that this reentrance is generic for all distributions with well defined moments[6].

The diversity induced transition to collective firing is a genuine transition. Singularly enough it is not present for a Lorentzian distribution, for which the first moment integral is only defined as a principal value. The non-generic behavior of the system with a Lorentzian distribution of natural frequencies warns about its indiscriminate use in order to understand generic properties of coupled oscillators.

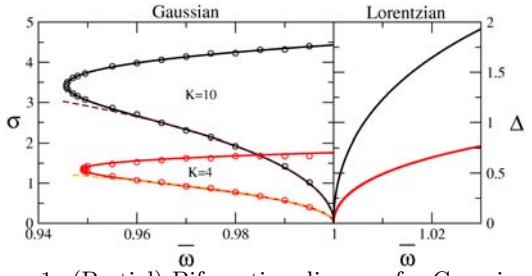

Figura 1. (Partial) Bifurcation diagram for Gaussian (left) and Lorentzian (right) distributions.

[1] Y. Kuramoto, *Chemical Oscillations, Waves and Turbulence* (Springer-Verlag, New York, 1984).
[2] Y. Kuramoto, in *International Symposium on Mathematical Problems in Theoretical Physics*, 1975, p. 39.
[3] C. J. Tessone, A. Scire, R. Toral, and P. Colet, Phys. Rev. E **75**, 016203 (2007).
[4] E. Ott and T.M. Antonsen, Chaos **18**, 037113 (2008).
[5] L.M. Childs and H.S. Strogatz, Chaos **18**, 043128 (2008).
[6] L.F. Lafuerza, P. Colet and R. Toral, Phys. Rev. Lett. **105**, 084101 (2010).

Leyes de Potencia y Leyes de Escala en la Distribución de Energía de los Huracanes

Álvaro Corral*, A. Ossó, J.E. Llebot
Centre de Recerca Matemàtica
Edifici Cc, Campus Bellaterra
E-08193 Barcelona, Spain

The influence of climate variability and global warming on the occurrence of tropical cyclones is a controversial issue. Existing historical databases on the subject are not fully reliable, but a more fundamental hindrance is the lack of basic understanding regarding the intrinsic nature of tropical-cyclone genesis and evolution. It is known that tropical cyclones involve more than a passive response to changing external forcing, but it is not clear which dynamic behaviour best describes them. Here we present an approach based on the application of the power dissipation index (PDI), which constitutes an estimation of released energy[1], to individual tropical cyclones. A robust law emerges for the statistics of power dissipation index, valid in four different ocean basins and over long time periods. In addition to suggesting a description of the physics of tropical cyclones in terms of critical phenomena, the scaling law enables us to quantify their response to changing climatic conditions, with an increase in the largest power dissipation index values with sea surface temperature or the presence of El Niño phenomenon, depending on the basin under consideration.

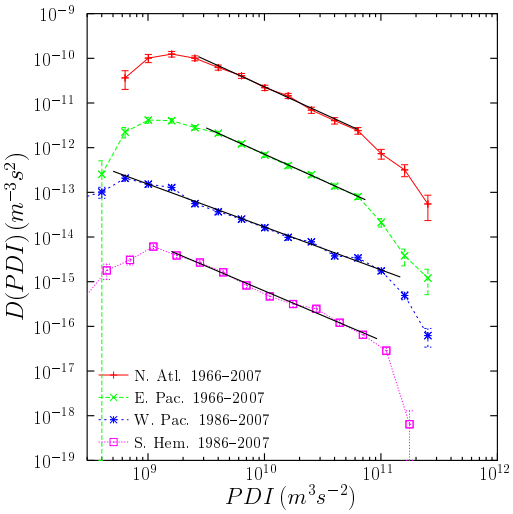

Figura 1. **Power-law distributions of tropical-cyclone PDI values.** PDI probability densities for tropical cyclones in the North Atlantic, Northeastern Pacific, Northwestern Pacific, and Southern Hemisphere basins. The period considered is either 1966-2007 or 1986-2007, depending on the reliability of the records. The values in the vertical axis are divided by the factors 1, $\sqrt{1000}$, 1000 and $\sqrt{1000^3}$, to separate the curves for clarity. The distributions are consistent with a power law (straight lines) over some portion of their range, with exponents $\alpha = 1.19 \pm 0.06$, 1.175 ± 0.05, 0.96 ± 0.02 and 1.11 ± 0.04, from top to bottom and the Kolmogorov-Smirnov (KS) test yields $p-$values larger than 20 % in all basins. Deviations from the power law at large PDI values reflect the finite size effect.

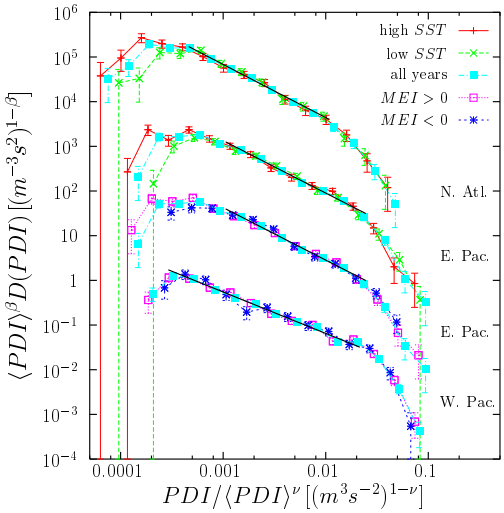

Figura 2. **Scaling of PDI distributions conditioned to sea surface temperature (SST) and El Niño.** PDI probability densities calculated separately for years with high or low SST and for years with $MEI > 0$ (El Niño) or $MEI < 0$ (La Niña). Tropical depressions (storms whose maximum v_t is below 34 knots, 1 knot = 1.85 km/h) are excluded from the Northwestern Pacific dataset, in order to give all basins the same treatment. Time periods and vertical offsets are as in Fig. 1. In all cases the data can be fit by a power law, being the worst one that of the North Atlantic with low SST, which yields $\alpha = 1.26 \pm 0.08$ with a $p-$value equal to 9%.

In this way, we demonstrate that the recent upswing in North Atlantic hurricane activity[2] does not involve tropical cyclones that are quantitatively different from those in other sustained high-activity periods before 1970[3].

* acorral@crm.es

[1] Emanuel, K. Increasing destructiveness of tropical cyclones over the past 30 years. Nature 436, 686–688 (2005).
[2] Goldenberg, S. B., Landsea, C. W., Mestas-Nuñez, A. M. & Gray, W. M. The Recent Increase in Atlantic Hurricane Activity: Causes and Implications. Science 293, 474–479 (2001).
[3] Corral, A., Ossó, A. & Llebot, J. E. Scaling of Tropical-Cyclone Dissipation. Nature Phys. 6, 693–696 (2010).

Límite a la descripción hidrodinámica en el modelo de Maxwell para gases granulares

J. J. Brey, M. I. García de Soria*, P. Maynar
Física Teórica. Facultad de Física
Universidad de Sevilla
Aptdo. de Correos 1065. 41080 Sevilla

Las ecuaciones hidrodinámicas para gases granulares han sido derivadas, en el límite de baja densidad, a partir de la ecuación de Boltzmann para esferas o discos duros inelásticos[1]. Sin embargo, los métodos empleados son formales y no permiten establecer la existencia de la descripción hidrodinámica en sí misma. En el caso de esferas o discos duros elásticos, el conocimiento del espectro del operador de Boltzmann linealizado[2] permite resolver el problema de forma satisfactoria. En el caso inelástico, los modos hidrodinámicos han sido identificados en el límite de longitud de onda grande[3,4], pero casi nada se conoce sobre la parte cinética del espectro.

En este trabajo, analizamos la validez de la descripción hidrodinámica usando una ecuación de Boltzmann inelástica simplificada, la del modelo de Maxwell inelástico[5–7]. Esta ecuación cinética se obtiene a partir de la ecuación de Boltzmann inelástica para esferas o discos duros, sustituyendo la frecuencia de colisión dependiente de la velocidad relativa por un valor medio efectivo proporcional a la velocidad térmica.

Las autofunciones del operador de Boltzmann linealizado homogéneo para moléculas de Maxwell correspondientes a los modos hidrodinámicos pueden ser calculadas, identificándose también algunos modos no hidrodinámicos[8]. Se muestra que por debajo de un valor del parámetro que caracteriza la inelasticidad, uno de los modos cinéticos decáe más lentamente que uno de los modos hidrodinámicos. Como consecuencia de esto, no existe, en este régimen de parámetros, una descripción hidrodinámica cerrada. También se discuten algunas implicaciones de este comportamiento en los coeficientes de Navier Stokes.

* gsoria@us.es

[1] J.J. Brey, J.W. Dufty, C.S. Kim, and A. Santos, Phys. Rev. E, **58**, 4638 (1998).
[2] J.A. McLennan, *Introduction to Nonequilibrium Statistical Mechanics* (Prentice-Hall, Engle-wood Cliffs, NJ, 1989).
[3] J.J. Brey, J.W. Dufty, and M.J. Ruiz-Montero, in *Granular Gas Dynamics*, edited by T. Poeschel and N. Brilliantov (Springer-Verlag, Berlin, 2003).
[4] J.W. Dufty and J.J. Brey, Phys. Rev. E **68**, 030302(R) (2003).
[5] A.V. Bobylev, J.A. Carrillo, and I.M. Gamba, J. Stat. Phys. **98**, 743 (2000).
[6] E. Ben-Naim and P.L. Krapivsky, Phys. Rev. E **66** 011309 (2002).
[7] M.H. Ernst and R. Brito, J. Stat. Phys. **109**, 407 (2002).
[8] J.J. Brey, M.I. García de Soria, and P. Maynar, Phys. Rev. E **82**, 021303 (2010).

Hidden Symmetries in Nonequilibrium Systems

P.I. Hurtado, C. Pérez-Espigares, J. del Pozo, P.L. Garrido
Instituto Carlos I de Física Teórica y Computacional. Universidad de Granada. Spain.

Fluctuations arise universally in Nature as a reflection of the discrete microscopic world at the macroscopic level. Despite their apparent noisy origin, fluctuations encode fundamental aspects of the physics of the system at hand, crucial to understand irreversibility and nonequilibrium behavior [1,2,3,4]. In this work we focus on the large deviation properties of the currents present on systems at nonequilibrium steady states and, in particular, on the joint statistics of the current and any system configurational properties (say the density or energy spatial distribution) both averaged over a long but fixed time interval. When this time interval is set to infinity all system observables tend to their corresponding steady state value. However for long but finite times it is known that the joint statistics exhibits complex structure which couples a given current fluctuation with a precise value of the complementary observable studied. The hidden symmetries appear at this level of description. We find that all the isometric values of current fluctuations (e.g. currents related by rotations) have the same values of some associated configurational property. This allows us to derive an isometric fluctuation relation which links in a strikingly simple manner the probabilities of any pair of isometric current fluctuations. This relation, which results from the time-reversibility of the dynamics, includes as a particular instance the Gallavotti-Cohen fluctuation theorem [5] in this context but adds a completely new perspective on the high level of symmetry imposed by time-reversibility on the statistics of nonequilibrium fluctuations. The new symmetry implies remarkable hierarchies of equations for the current cumulants and the nonlinear response coefficients, going far beyond Onsager's reciprocity relations and Green-Kubo formulae. We confirm the validity of the new symmetry relation in extensive numerical simulations. This opens an unexplored route toward a deeper understanding of nonequilibrium physics by bringing symmetry principles to the realm of fluctuations.

References

[1] Bertini L, De Sole A, Gabrielli D, Jona-Lasinio G, Landim C (2001) Fluctuations in stationary nonequilibrium states of irreversible processes. *Phys. Rev. Lett.* 87:040601.

[2] Bodineau T, Derrida B (2004) Current fluctuations in nonequilibrium diffusive systems: an additivity principle. *Phys. Rev. Lett.* 92:180601.

[3] Bertini L, De Sole A, Gabrielli D, Jona-Lasinio G, Landim C (2007) Stochastic interacting particle systems out of equilibrium. *J. Stat. Mech.* P07014.

[4] Hurtado PI, Garrido PL (2009) Test of the additivity principle for current fluctuations in a model of heat conduction. *Phys. Rev. Lett.* 102:250601.

[5] Gallavotti G, Cohen EGD (1995) Dynamical ensembles in nonequilibrium statistical mechanics. *Phys. Rev. Lett.* 74:2694-2697.

Prisoner's Dilemma on a sizeable network: An experiment with human subjects

Jelena Grujić[1], Constanza Fosco[1], Lourdes Araujo[2], José A. Cuesta[1], Angel Sánchez[1,3]
[1] *GISC, Dpto. de Matemáticas, Universidad Carlos III de Madrid, Leganés*
[2] *NLP and IR, Dpto. de Lenguajes y Sistemas, UNED, Madrid*
[3] *BIFI, Universidad de Zaragoza, Zaragoza*

The mechanisms underlying the emergence of cooperation among unrelated individuals are as yet an unsolved puzzle. Many theoretical models have shown that the existence of structure in a population can help understanding the widespread emergence of cooperation, particularly in the framework of the Prisoner's Dilemma (PD), but the results of these models largely depend on details such as the type of spatial structure or the evolutionary dynamics. Therefore, experimental work suitably designed to address this question is needed to probe these issues.

We have designed an experiment to test the emergence of cooperation when humans play PD on a network whose size is comparable to that of simulations[1]. In our experiment, volunteers played a PD game with each of their eight neighbors taking only one action, either to cooperate (C) or to defect (D), the action being the same against all the opponents. The resulting payoff was calculated by adding all eight interaction payoffs. Payoffs of the PD game were set to be 7 cents for mutual cooperation, 10 cents for a defector facing a cooperator, and 0 cents for any player facing a defector (i.e., the same weak PD setup of Nowak and May[2]). The full experiment consisted of three parts: experiment 1, control, and experiment 2. In experiment 1 players remained at the same positions in the lattice with the same neighbors throughout the experiment. In the control part we removed the effect of the lattice by shuffling players every round. Finally, in experiment 2 players were again fixed on a lattice, albeit different from that of experiment 1.

We find that the cooperation level declines to an asymptotic state with low but nonzero cooperation (Fig. 1). Regarding players' behavior, we observe that the population is heterogeneous, consisting of a high percentage of defectors, a smaller one of cooperators, and a large group that shares features of the conditional cooperators of public goods games, except that the players are not influenced only by how much cooperation they observe but also by how they themselves behaved in the previous round (Fig. 2). We propose an agent-based model based on the coexistence of these different strategies that is in good agreement with all the experimental observations.

The large size of our experimental setup and the data analysis allow us to answer two important questions. First, we have observed that the existence of a lattice giving structure to a population playing a PD does not lead to an increase of the cooperation level; the residual level is around 20% which is typical in public goods experiments and has also been observed on 4×4 lattices[3]. Second, regarding the manner in which people update their strategies, we have not found evidence in favor of imitate-the-best behavior. Our findings also indicate that both heterogeneity and a "moody" conditional cooperation strategy, in which the probability of cooperating also depends on the player's previous action, are required to understand the outcome of the experiment. These results could impact the way game theory on graphs is used to model human interactions in structured groups.

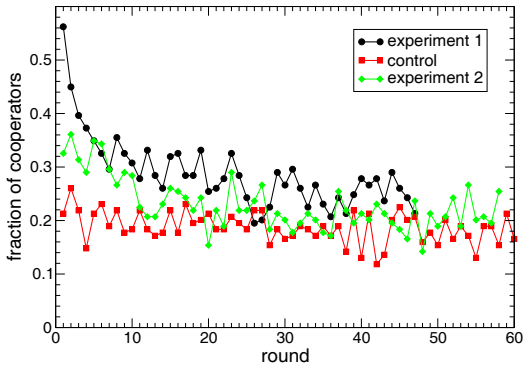

Figura 1. Fraction of cooperators in every round of the three parts of the experiment. The cooperation level declines to a low but non-zero level.

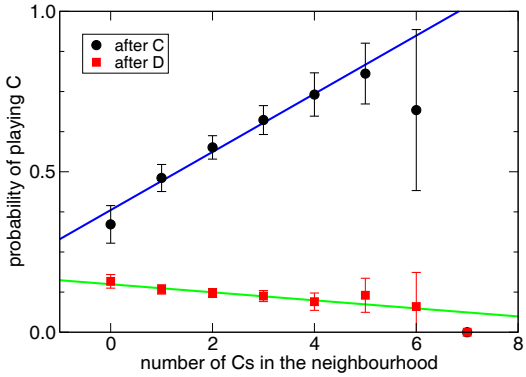

Figura 2. "Moody" conditional cooperators. Probabilities of cooperating after playing C or D, conditioned to the context (number of cooperators in the previous round).

[1] Grujić J, Fosco C, Araujo L, Cuesta JA, Sánchez A, PLoS ONE **5**, e13749 (2010)
[2] Nowak MA, May RM, Nature **359**: 826–829 (1992)
[3] Traulsen A, Semmann D, Sommerfeld RD, Krambeck HJ, Milinski M, Proc Natl Acad Sci USA **107**: 2962–2966. (2010)

Statistical mechanics approaches to complex network inference and reconstruction

R. Guimerà*, M. Sales-Pardo**
ICREA and Departament d'Enginyeria Química
Universitat Rovira i Virgili, Av. dels Països Catalans 26
43007 Tarragona

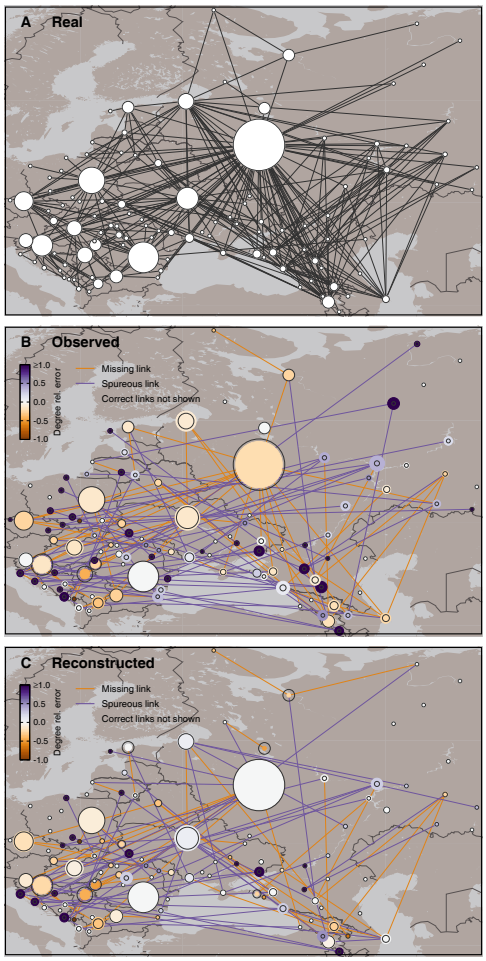

Figura 1. Reconstruction of the air transportation network of Eastern Europe. **A**, The true air transportation network. The area of each node is proportional to its betweenness centrality, with Moscow being the most central node in the network. **B**, The observed air transportation network, which we build by randomly removing 20% of the real links and replacing them by random links. **C**, The reconstructed air transportation network that we obtain, from the observed network, applying the heuristic reconstruction method described in the text and methods. For clarity, in **B** (respectively, **C**) we do not depict the correct links, but only: (i) missing links in orange, which exist in the true network but not in the observation (reconstruction), and (ii) spurious links in blue, which do not exist in the true network but do exist in the observation (reconstruction). As in **A**, the area of each node is proportional to its betweenness centrality, with the black circle representing the true betweenness centrality of each node. The color of each node represents the relative error in the degree of the node, with respect to the true degree.

Network analysis is currently used in a myriad of contexts, from identifying potential drug targets to predicting the spread of epidemics and designing vaccination strategies and from finding friends to uncovering criminal activity. Despite the promise of the network approach, the reliability of network data is a source of great concern in all fields where complex networks are studied. We present a general mathematical and computational framework to deal with the problem of data reliability in complex networks[1]. In particular, we are able to reliably identify both missing and spurious interactions in noisy network observations. Remarkably, our approach also enables us to obtain, from those noisy observations, network reconstructions that yield estimates of the true network properties that are more accurate than those provided by the observations themselves. We will illustrate the methods with examples from systems biology (metabolome and proteome) and from the social sciences (the voting patterns of US Supreme Court justices).

* roger.guimera@urv.cat
** marta.sales@urv.cat

[1] Guimera, R, Sales-Pardo, M., Missing and spurious interactions and the reconstruction of complex networks, *Proc. Natl. Acad. Sci. U. S. A.* **106**, 22073-22078 (2009)

Caracterización y Modelización de Sistemas Dinámicos no Lineales. Medidas de Desorden Dinámico y "Self-Correlation".

Juan Antonio Hernández Álvarez*, Rosa María Benito, Juan Carlos Losada
Grupo de Sistemas Complejos, ETSI, Agrónomos
Universidad Politécnica de Madrid
28040 Madrid

A lo largo de los años se han desarrollado multitud de técnicas e inventado indicadores destinados a caracterizar sistemas no lineales en general y caóticos en particular. Unos pocos, pero importantes ejemplos son: el "Exponente de Lyapunov"[1], la "Entropía de Kolmogorov"[2], "La sección de Poincaré"[3] y distintas definiciones de dimensión como puedan ser la "Fractal"[4] y la de Hausdorff[5]. Estos indicadores, diseñados para hacer mediciones sobre un sistema, reflejan el gran interés existente en la caracterización, que persigue en no pocas ocasiones la obtención de información sustancial que pueda ser útil en la construcción de modelos fiables, siempre con la esperanza de que presenten las mismas características que el sistema original.

Especial mención merece el estudio de aquellos sistemas que presentan un comportamiento caótico. El "Caos Determinista"es una disciplina completamente desarrollada como teoría en las últimas décadas, aunque ha sido en años recientes cuando ha llegado la verdadera avalancha de hallazgos de comportamiento caótico en multitud de sistemas físicos y sociales. Algunos de estos descubrimientos han tenido lugar en campos tan dispares como puedan ser las series económicas[6], el viento[7], los procesadores de computador[8] o las poblaciones de células[9].

Aunque la teoría de Sistemas Dinámicos no Lineales está firmemente desarrollada desde hace tiempo, nuevos enfoques han aparecido en fechas recientes. Algunos de ellos son: el estudio de redes complejas derivadas de una serie temporal[10], la combinación de medidas de complejidad con la entropía de Shannon[11] y la detección de patterns prohibidos en series temporales[12].

En este trabajo se pretende explicar una nueva metodología para caracterizar sistemas no lineales, basada en la medida de ciertas características de una serie temporal que hemos denominado "Dynamical Order"y "Self-Correlation"[13]. La primera se corresponde con lo desordenado que es el movimiento de la serie temporal en un espacio de estados bidimensional, mientras que la segunda es una medida de auto-correlación no lineal. Asimismo, se presentan los productos "Escalar"y "Perpendicular"convenientemente promediados a lo largo de la serie temporal, como indicadores para la medición de las mencionadas características.

La misma técnica puede ser empleada, tanto en órbitas provenientes de un sistema de ecuaciones, como en una serie temporal obtenida experimentalmente. La técnica básica es la misma. La metodología está definida para el estudio de sistemas no lineales en general, tanto teóricos como experimentales, independientemente de cualquier clasificación a priori del objeto a estudiar.

El objetivo perseguido es doble, por un lado caracterizar el sistema y por otro definir modelos fiables construidos sobre dicha caracterización. Dos aplicaciones bien distintas son presentadas para ilustrar la teoría general: la caracterización de un sistema caótico de dos dimensiones y la obtención de modelos para series temporales telefónicas obtenidas de una operadora nacional de telecomunicaciones.

Son relevantes varios aspectos que afloran en la aplicación del método expuesto, y que están relacionados con indicadores bien conocidos como son el "Exponente de Lyapunov"y la "Información mutua". El "Producto Escalar"promedio puede ser utilizado como complemento del primero y el "Producto Perpendicular"promedio puede suponer una mejora del segundo en determinados sistemas.

---

* jantonio.hernandez@iberbanda.es

[1] A. Wolf, J. B. Swift, H. L. Swinney and J. A. Vastano, Physica D, **16**, 285 (1985).
[2] A. N. Kolmogorov, Dokl. Akad. Nauk SSSR, **124**, 754 (1959).
[3] H. Poincaré, Gauthier-Villars et fils (1892).
[4] B. B. Mandelbrot, W. H. Freeman & Co. (1983).
[5] F. P. Hausdorff, Math. Annalen, **79**, 157 (1919) .
[6] D. Guegan, Ann. Rev. Control, **33**, 89 (2009).
[7] T., E. Karakasidis and A. Charakopoulos, Chaos Solit. Fract. **41**, 1723 (2009) .
[8] Z. Halbiniak and I. J. Jozwiak, Chaos Solit. Fract. **31**, 409 (2007).
[9] M. Laurent, J. Deschatrette and C. M. Wolfrom, PLoS ONE, **5**, 9346 (2010) .
[10] J. Zhang and M. Small, Phys. Rev. Lett. **96**, 238701 (2006).
[11] O. A. Rosso, H. A. Larrondo, M. T. Martin, A. Plastino and M. A. Fuentes, Phys. Rev. Lett. **99**, 154102 (2007).
[12] J. M. Amigo, S. Elizalde and M. B. Kennel, J. Comb. Theory A, **115**, 485 (2008) .
[13] J. A. Hernández, R. M. Benito and J. C. Losada, Int. J. Bifurcation and Chaos, accepted for publication (2010).

Universalidad en el flujo de un medio granular a través de un orificio

A. Janda*, I. Zuriguel, A. Garcimartín, D. Maza
Grupo de Medios Granulares†
Departamento de Física y Matemática Aplicada
Facultad de Ciencias, Universidad de Navarra
31080 Pamplona

El flujo de un medio granular a través de un orificio es un claro ejemplo de las peculiaridades de este tipo de materiales. Si bien una descripción hidrodinámica de este proceso pudiera parecer factible, la realidad es que mediante ella no es posible reproducir rigurosamente el comportamiento de los granos. En la literatura está ampliamente aceptado que el flujo de descarga de un silo viene determinado por la dinámica de las partículas en la cercanía del orificio[1]. Aunque se ha especulado sobre las escalas características de este proceso, no existen pruebas experimentales sobre la forma de los perfiles de velocidad y fracción de compactación a la salida. Por otro lado, existe un debate sobre la influencia en el flujo de la aparición de atascos cuando la salida es de tamaño comprable a los granos, así como sobre la posible existencia de un tamaño crítico del orificio por encima del cual no se producirían[2–4].

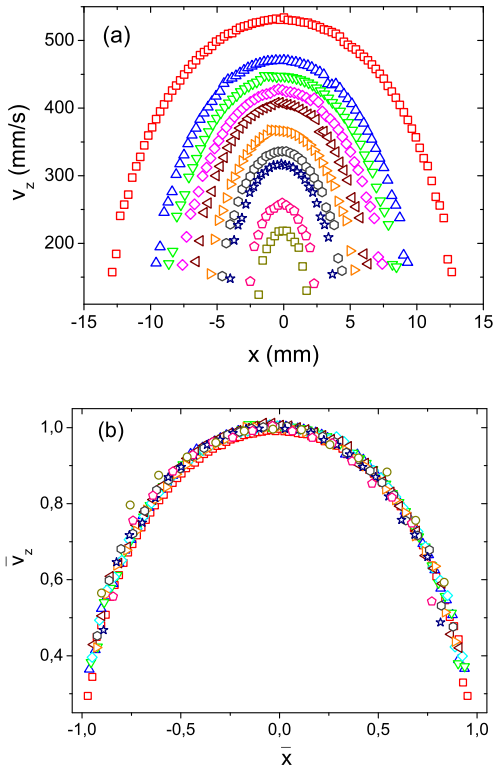

Figura 1. (a) Perfiles de la componente vertical de la velocidad a lo largo del orificio de salida. Los distintos símbolos corresponden a diferentes tamaños de la abertura. (b) Se han representado los mismos datos que en (a) pero reescalados de manera apropiada para mostrar su comportamiento universal.

Con el fin de arrojar luz sobre estas cuestiones, se han estudiado sistemáticamente las propiedades del flujo en un amplio rango de tamaños de la salida. Durante la descarga se han determinado experimentalmente con una gran resolución espacial y temporal los campos de velocidad y fracción de compactación en el orificio. Así, se han encontrado las escalas características del flujo y estudiado las propiedades de los perfiles de dichas magnitudes en función del tamaño de la abertura. Sorprendentemente se obtiene un comportamiento universal del flujo[5] y sus fluctuaciones, tanto para aberturas pequeñas en las que los atascos son frecuentes, así como para orificios grandes donde el flujo es prácticamente continuo. Hasta donde nosotros sabemos, este resultado es la primera prueba experimental que demuestra que el flujo es un estado bien definido del sistema e independiente de la aparición de atascos. Además, esta característica es coherente con la no existencia de un tamaño crítico de orificio.

* ajandaga@alumni.unav.es
† `http://fisica.unav.es/granular/`

[1] R. M. Nedderman, "Statics and Kinematics of Granular Materials", Cambridge University Press, Cambridge, (1992).
[2] I. Zuriguel, A. Garcimartín, D. Maza, L.A. Pugnaloni and J.M. Pastor, "Jamming during the discharge of granular matter from a silo", Phys. Rev. E **71** (2005), 030301.
[3] A. Janda, I. Zuriguel, A. Garcimartín, L.A. Pugnaloni and D. Maza, "Jamming and critical outlet size in the discharge of a two-dimensional silo", Europhys. Lett. **84** (2008), 44002.
[4] K. To, "Jamming transition in two-dimensional hoppers and silos", Phys. Rev. E **71** (2005), 060301(R).
[5] Janda Galán, Alvaro. "Análisis experimental del proceso de descarga de medios granulares en silos." Tesis de Doctorado, Universidad de Navarra (2010).

Natural Correlations in Networks: Origin and Effects

Samuel Johnson*, Joaquín J. Torres, J. Marro, Miguel A. Muñoz
Dpto. de Electromagnetismo y Física de la Materia, and
Institute Carlos I for Theoretical and Computational Physics,
Universidad de Granada, 18071 Granada, Spain.

In recent years it has become apparent that a fundamental aspect of many complex systems is the structure of the underlying network of interactions between the elements. The origins and effects of statistical properties such as degree distributions, short paths, clustering or community structure have been analysed in great detail. One such feature of empirical networks is the existence of correlations between the degrees of neighbouring nodes – a node's degree being the number of neighbours it has. Networks with positive correlations are *assortative*, since nodes of a kind tend to group together, or assort, whereas negatively correlated ones are *disassortative*. This property has been shown to be highly relevant for their behaviour. For instance, assortative networks have lower percolation thresholds and are more robust to targeted attack, while disassortative ones make for more stable ecosystems and are more "synchronizable".

A striking characteristic of empirical networks is that they are seldom uncorrelated. Rather, social networks – in which the nodes are people and the edges represent professional, sexual or any other form of interaction – are usually assortative. Conversely, almost all other networks, whether biological (genetic, ecological, neural...), information-related (linguistic, the Web...), or technological (the internet, power-grids...), are significantly disassortative.

Whence these non-trivial correlations? Do they, in each case, serve some functional purpose? Or do they share a common origin? The positive correlations of social networks are perhaps to be expected, since humans seem to group together deliberately according to all kinds of features. In other words, the elements themselves put energy into the system, driving it from equilibrium. On the other hand, negative correlations have been shown to appear in highly heterogeneous networks when only one edge per pair of nodes is allowed – but this effect alone does not account for the degree of disassortativity observed.

We show that there is a general reason for the "natural" (i.e., equilibrium) state of heterogeneous networks not to be neutral but, in general, disassortative[1]. To do this, we develop an analytical method to partition the phase space of networks compatible with given constraints into equally correlated regions. We obtain the Shannon entropy (which coincides, asymptotically, with the Gibbs entropy for intensive constraints) for each partition, and determine the degree of assortativity that maximizes this magnitude. At equilibrium – i.e., in the absence of correlating mechanisms – the system can be expected to find itself in this largest volume of phase space. Contrasting our predictions against empirical data, it turns out that the correlations of many networks can indeed be explained in this way (for example, the metabolic, Web page and protein networks in Fig. 1). On the other hand, some networks with identifiable anticorrelating mechanisms (such as the P2P network or the internet) are more disassortative than if they were at equilibrium, while social networks (the actors graph) are far more assortative – indicating that there are homophilic processes at work.

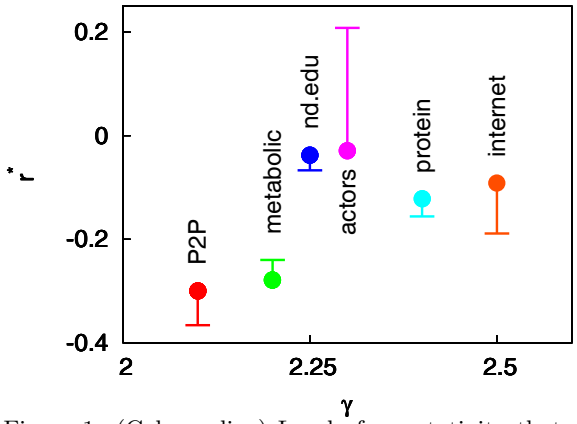

Figura 1. (Color online) Level of assortativity that maximizes the entropy, r^*, for various real-world, scale-free networks, as predicted theoretically against scale-free exponent γ. Bar ends show the empirical values.

We go on to show how our method can be used to study the effects of correlations in any kind of network. In particular, we apply it to a neural-network model and find that assortativity greatly enhances the robustness to noise of such a system[2].

* samuel@onsager.ugr.es

[1] S. Johnson, J.J. Torres, J. Marro, and M.A. Muñoz, "Entropic origin of disassortativity in complex networks," *Phys. Rev. Lett.* **104**, 108702 (2010).

[2] S. de Franciscis, S. Johnson, and J.J. Torres, "Enhancing neural network performance via assortativity", *Phys. Rev. E*, in press (2011).

Wetting-controlled drop emission in forced microfluidic filaments

R. Ledesma-Aguilar[*,†], R. Nistal[*], A. Hernández-Machado[*], I. Pagonabarraga[‡]
[*] *Departament d'Estructura i Constituents de la Matèria*
Facultad de Física
Universidad de Barcelona
08028 Barcelona
[†] *The Rudolf Peierls Centre for Theoretical Physics*
University of Oxford
1 Keble Road, Oxford
OX1 3NP, United Kingdom
[‡] *Departament de Física Fonamental*
Facultad de Física
Universidad de Barcelona
08028 Barcelona

The controlled formation of micron-sized drops is of great importance in microfluidic technological applications. Here we present a novel, wetting-based, destabilization mechanism of forced microfilaments on either hydrophilic or hydrophobic dry stripes, that leads to the periodic emission of droplets[1].

The drop emission mechanism is triggered above a critical forcing, where the contact line no longer follows the leading edge of the filament. We propose a dynamical model which includes the effects of wetting, capillarity, viscous friction and the driving force to determine the interface cofiguration at the threshold. We compare our theory to lattice-Boltzmann simulations and microfluidic experiments, accounting for the emission threshold and hence the size and emission period of droplets, which can be controlled independently.

Our results show that the critical filament velocity depends strongly on wetting, and exhibits a qualitative different behaviour on hydrophilic and hydrophobic stripes, which arises from the dependency of viscous dissipation on the shape of the advancing interface. Our results suggest that this new kind of instability in contact lines is general to advancing fronts[2], and opens new possibilities of exploiting wetting to handle interfaces at the microscale.

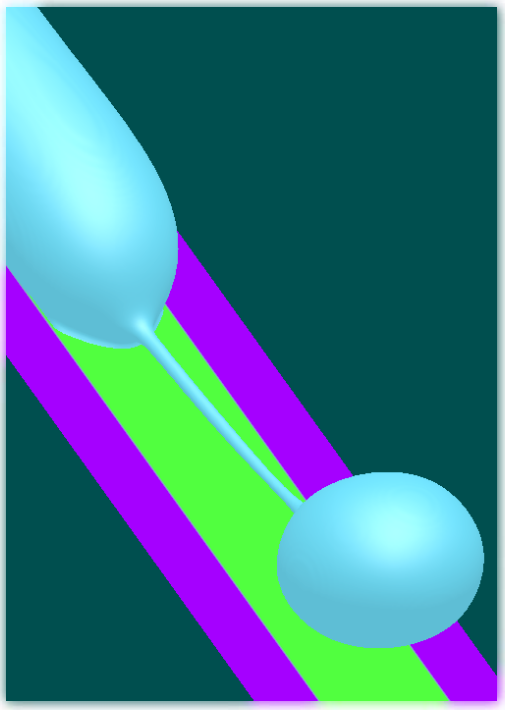

Figura 1. Drop emission in microfilament forced on a hydrophilic substrate (Lattice-Boltzmann simulation).

[1] R. Ledesma-Aguilar, R. Nistal, A. Hernandez-Machado and I. Pagonabarraga, *Nature Materials*, 2011 (accepted)
[2] C. Duez, C. Ybert, C. Clanet and L. Bocquet, *Nature Physics*, **3**, 180 (2007)

Self-assembly of viral capsids

Antoni Luque*, David Reguera
Facultad de Física
Universidad de Barcelona
08028 Barcelona

Viruses are biological entities that can infect a wide variety of organisms -from bacteria to mammals-, causing diseases that have a huge ecological, medical, and economical impact. In their simplest form, viruses are constituted by an infective genetic material (DNA/RNA) and a protective protein shell, called *capsid*, which is generally built in a spontaneous assembly process from several copies of the same or similar proteins. In addition, viral shells have a well-defined size in the nanometer range, are usually highly symmetric, and show relevant mechanical properties. All these features have spread the interest for viral capsids in different nanoscience fields, where several technological and biomedical applications have been developed.

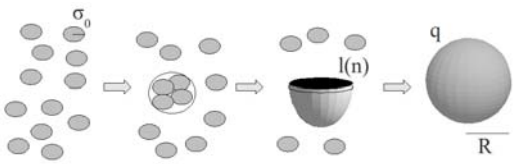

Figura 1. Assembly of a viral capsid. We illustrate the process of formation of a viral shell. The spontaneous aggregation of single subunits produces a sequence of intermediates until a closed capsid is formed.

Here we focus on the self-assembly of viral capsids (see Fig. 1). *In vivo* and *in vitro* experiments have shown that empty viral shells can be formed in different conditions, for instance, of pH or salt concentration, leading to different kind of structures. Several studies have pointed out that the free energy minimization principle governs the origin of these viral structures[1,2], and that the assembly of viral capsids should be regarded as a thermodynamic process[3].

In this contribution, we will show that the assembly and disassembly of viruses have important analogies with the standard vapor-liquid phase transition. We will also demonstrate that classical nucleation theory could be adapted to study the self-assembly of viral capsids[4], which provides a solid thermodynamic and kinetic framework to understand viral shell assembly.

In particular, we will investigate in detail the case for spherical capsids, which are the most abundant type of viral shells. We will propose a simple continuum thermodynamic model that captures the main ingredients of viral assembly, and is in agreement with simulation studies[5] (see Fig. 2). Then, we will develop the classical nucleation theory of viral capsids for this particular model. We emphasize that this theory will be in agreement with several experiments that show different aspects of virus assembly, e.g., assembly-disassembly hysteresis, capsid production lag time, or capsid formation sigmoidal curves.

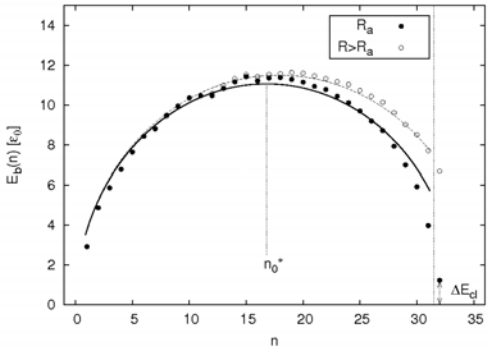

Figura 2. Line energy. We show the simulation (points) and theoretical (curves) results for two radii of a spherical capsid made of 32 capsomers (protein tiles). The rim of an intermediate structure (see Fig. 1) is an interface between the free subunit and capsid phases, and has associated a line energy responsible for the energy barrier represented. The points in the last part of the assembly (right) show an interesting phenomena during capsid closure: the implosion effect.

Therefore, this represents an interesting example of how basic physical principles can explain and guide the understanding of biological systems. Due to the generality of the concepts involved, the study could also be adapted to other systems in other scientific fields, such as soft condensed matter.

* toniluque@ub.edu

[1] R. Zandi, D. Reguera, R. F. Bruinsma, W. M. Gelbart, and J. Rudnick. (2004). Origin of icosahedral symmetry in viruses. *Proc. Natl. Acad. Sci. USA 101*:15556–15560.

[2] A. Luque, R. Zandi, and D. Reguera. (2010). Optimal architectures of elongated viruses. *Proc. Natl. Acad. Sci. USA 107*:5323–5328.

[3] R. F. Bruinsma, W. M. Gelbart, D. Reguera, J. Rudnick, and R. Zandi (2003) Viral self-assembly as a thermodynamic process. *Phys. Rev. Lett.* 90:248101.

[4] R. Zandi, P. van der Schoot, D. Reguera, W. Kegel, and H. Reiss (2006) Classical nucleation theory of virus capsids. *Biophys. J.* 90:1939–1948

[5] A. Luque, D. Reguera, A. Morozov, J. Rudnick, and R. Bruinsma (2011) The assembly of spherical shells: Line Energy, Implosion and Closure Catastrophe (Unpublished).

Complex networks and glassy dynamics: walks in the energy landscape

Paolo Moretti[1*], Andrea Barochelli[1], Alain Barrat[2,3], Romualdo Pastor-Satorras[1]
[1] *Departament de Física i Enginyeria Nuclear, Universitat Politècnica de Catalunya Campus Nord B4, E-08034, Barcelona, Spain*
[2] *Centre de Physique Théorique (CNRS UMR 6207), Luminy, 13288 Marseille Cedex 9, France*
[3] *Complex Networks Lagrange Laboratory, Institute for Scientific Interchange (ISI), Torino, Italy*

Modeling the mechanical properties of systems that exhibit glassy dynamics represents a major issue, both from the computational and the analytical point of view. Using realistic inter-particle potentials, molecular dynamics simulations suitably describe events over limited time-spans. They provide great insight into microscopic dynamics, yet they may become inadequate in predicting long-time relaxation features for normal laboratory scales. In this light, effective modeling techniques must rely on realistic coarse graining procedures.

A simple way of addressing glassy dynamics is that of considering the system as a random walker in the energy landscape. In the regime where the dynamics is thermally activated, the walker evolves through jumps between different energy minima or *traps*[1]. Both experimental and numerical studies have revealed that the emergence of glassy dynamics, for instance in super-cooled liquids, is accompanied by the observation of strong spatio-temporal heterogeneities, with different regions of the system presenting dynamics that vary from each other even by orders of magnitude. The classical trap model indeed predicts the emergence of glassy features, however it considers a mean-field scenario where heterogeneities are not taken into account.

Here, we propose to study the role of heterogeneities in systems approaching the glass transition, by modeling time evolution as a generalized random walk on a complex energy landscape, pictured as a network of minima[2]. Complex network theory provides a powerful tool to encode the heterogeneity of the energy landscape into statistical properties of the network, such as degree distributions and correlations. We show how to use the tools developed for the study of dynamical processes on complex networks, in order to go beyond the mean-field scenario and move towards a more realistic description of the problem. We consider several non-local transition rates between minima and show that, under very general hypotheses, the existence of a glassy phase depends on a delicate interplay between the network topology and the relationship between energy and degree of a minimum[3]. Interestingly, the network-degree correlations and the details of the transition rates do not play any role in the existence (nor in the value) of the glass-transition temperature.

This approach helps contextualize previous studies that focused on the sampling of specific energy landscapes obtained for small systems[4] and shows how the tools developed in complex network theory can be successfully employed in this context.

---

* paolo.moretti@upc.edu

[1] J. P. Bouchaud, J. Physique I (France) **2**, 1705-1713 (1992).
[2] A. Barochelli, A. Barrat, and R. Pastor-Satorras
[3] P. Moretti, A. Baronchelli, A. Barrat, and R. Pastor-Satorras, submitted, preprint available arXiv:1101.3490
[4] S. Carmi, S. Havlin, C. Song, K. Wang, and H. A. Makse, J. Phys. A **42**, 105101 (2009)

Pattern Formation in Reactive-Fluid Systems

Alberto P. Muñuzuri, Jacobo Guiu-Souto, Dario M. Escala, Alexandra Von Kameke, Jorge Carballido-Landeira*
Group of Non Linear Physics Fac. de Fisicas. Universidade de Santiago de Compostela Campus Sur. 15782 Santiago de Compostela

Highly nonlinear mechanisms for pattern formation have been extensively studied due to the important role they play in Nature. The characteristic discrete nature of the biological systems (cellular compartment) has been recently analyzed. Nevertheless, many of these processes occur in a fluidic medium where hydrodynamic properties are especially relevant. Just no name a few examples; reactant pollutants dispersed in the atmosphere or in oceans; cells in living organisms are embedded in fluids, etc. We will present an analysis of the different properties characterizing the fluids on pattern formation. We consider typical pattern-forming reactions (Belousov-Zhabotinsky reaction like) with and without cell compartment but always in a liquid environment. Different instabilities are considered and the effect on the patterns observed analyzed. A first part of the contribution is devoted to the effect of external forcings on these systems. A well controlled turbulent flow can be generated that helps analyzing the effect of the different parameters on the patterning. Gravity modulations (Faraday type) or centrifugal instabilities (Taylor problem) among others will be considered in this context. A second part of the contribution considers gravity and density forces to be compatible with the propagation velocity of the patterns, so that interaction can be analyzed. Typical gravitational instabilities will be considered by changing viscosities and densities of the fluids under study.

Experimental demonstrations of the different cases discussed will be shown and the results complemented and understood by theoretical and numerical analysis.

---

* uscfmapm@cesga.es

[1] A. von Kameke, F. Huhn, G. Fernandez-García, A.P. Muũzuri and V. Perez-Muũzuri, 'Propagation of a Chemical Wave Front in a quasi two-dimensional Superdiffusive Flow.' *Phys. Rev. E* 81, 066211 (2010)

[2] Jacobo Guiu-Souto, Jorge Carballido-Landeira, Vicente Perez-Villar, and Alberto P. Muũzuri, 'Manipulation of diffusion coefficients via periodic vertical forcing controls the mechanism of Turing pattern formation.' *Phys. Rev. E* 82, 066209 (2010)

Relaxation Dynamics in the Columnar Liquid Crystal Phase of Oblate Hard Spherocylinders: Effect of Transient Cages and Permanent Barriers

Alessandro Patti*, Simone Belli, René van Roij, Marjolein Dijkstra
Debye Institute for NanoMaterials Science and Institute for Theoretical Physics
Utrecht University
Utrecht, The Netherlands

We perform Monte Carlo simulations to analyze the equilibrium dynamics and the long-time structural relaxation decay of columnar liquid crystals (LCs) of disk-like colloidal particles with diameter D and height L. In the wake of recent studies on calamitic (rod-like) colloidal particles in the smectic[1–3] or in the columnar mesophases[4], we now focus on the diffusion of their discotic counterparts, here modeled as oblate hard spherocylinders. In spite of the substantial differences in the equilibrium phase behavior between LCs of calamitic and discotic particles, we find interesting similarities in their rattling-and-jumping diffusion and two-step relaxation dynamics. In all these studies, it was found that to diffuse along the broken 1D (smectic) or 2D (columnar) symmetry direction, a particle must overcome a free-energy barrier of the order of a few k_BT, depending mostly on the packing of the system, but also on the particle anisotropy and on the rotational degrees of freedom. Due to the combined action of transient cages and periodic free-energy barriers, this diffusion presents a non-Gaussian behavior.

More specifically, we find that at fixed packing fraction the barrier height increases with decreasing particle thickness, resulting into a more heterogeneous and non-Gaussian dynamics for thinner platelets, and reducing the inter-column diffusion coefficient. We observe the characteristic two-step relaxation decay of the structure in the plane perpendicular to the column axis. At very short times, the discotic particles freely diffuse in the cage formed by their nearest neighbors. At this stage, the system shows a Gaussian behavior with a linear mean square displacement and a fast exponential decay of the correlation functions. As soon as the particles feel the presence of their surrounding cage, the diffusion slows down significantly, deviations from Gaussianity are observed, and the mean square displacement develops a plateau whose time extension increases with density and/or particle anisotropy. As time passes, an increasing number of particles jumps from a column to another, hence contributing to recover a homogeneous dynamics which results into a second diffusive regime. At the beginning of the long-time diffusion, which indicates the end of the cage regime, the deviations from Gaussian behavior start to decrease and go exponentially to zero. At high densities, the plateau may extend beyond our simulation time and no significant diffusion over the trapping cages is observed.

By contrast, the in-column dynamics is similar to the typical single-file diffusion of one-dimensional dense fluids, with a relatively fast decay of the correlation functions.

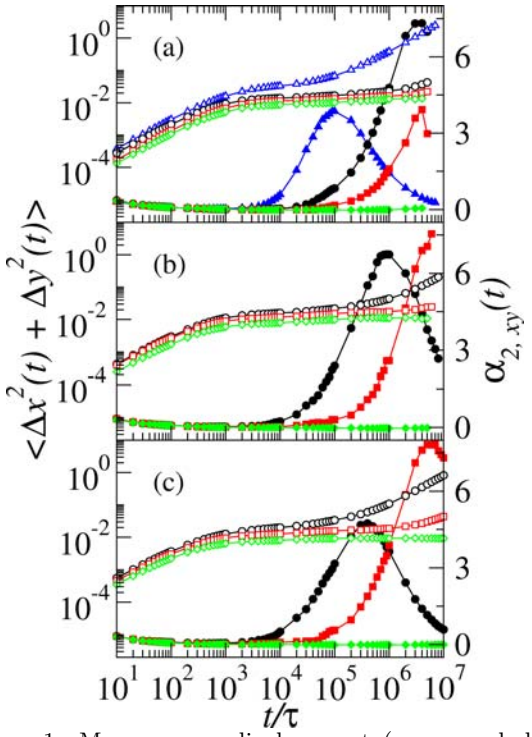

Figura 1. Mean square displacement (open symbols), in units of D^2, and non-Gaussian parameter (solid symbols) in the plane perpendicular to the nematic director, for systems of oblate hard spherocylinders with $L/D = 0.1$ (a), $L/D = 0.2$ (b), and $L/D = 0.3$ (c). Circles, squares, and diamonds refer to packing fractions $\eta = 0.575$, 0.600, and 0.630, respectively. For comparison, also the results at $L/D = 0.1$ and $\eta = 0.500$ are shown (triangles). Note that the vertical axes of MSDs and NGPs are on the left and right, respectively.

* alessandro.patti@iqac.csic.es

[1] A. Patti, D. El Masri, R. van Roij, and M. Dijkstra, *Phys. Rev. Lett.*, 2009, **103**, 248304.
[2] A. Patti, D. El Masri, R. van Roij, and M. Dijkstra, *J. Chem. Phys.*, 2010, **132**, 224907.
[3] R. Matena, M. Dijkstra, and A. Patti, *Phys. Rev. E*, **81**, 021704.
[4] S. Belli, A. Patti, R. van Roij, and M. Dijkstra, *J. Chem. Phys.*, 2010, **133**, 154514.

The helical crack-front instability

A. J. Pons

Edifici GAIA, despatx 1.08 Departament de Física i Enginyeria Nuclear Universitat Politècnica de Catalunya, Campus de Terrassa Rambla de Sant Nebridi s/n, 08222 Terrassa, Spain

Planar crack propagation becomes universally unstable under tension loading (mode I) with the superposition of a shear stress parallel to the crack front (mode III). Under this mixed-mode (I-III) loading configuration, an initially flat parent crack segments into an array of daughter cracks that rotate towards a direction of maximum tensile stress. This segmentation produces stepped fracture surfaces with characteristic 'lance-shaped' markings observed in a wide range of engineering and geological materials. We perform large-scale simulations of mixed-mode I-III brittle fracture using a continuum phase-field method that describes the complete three-dimensional crack-front evolution. We show that the dynamically preferred unstable wavelength is governed by the balance of the destabilizing effect of far-field stresses and the stabilizing effect of cohesive forces on the process zone scale, and we derive a theoretical estimate for this scale using a new propagation law for curved cracks in three dimensions. The simulations reveal that planar crack propagation evolves nonlinearly into a segmented array of finger-shaped daughter cracks which gradually coarsen owing to the growth competition of daughter cracks. The rotation angles of coarsened facets are also compared to theoretical predictions and available experimental data.

---

[1] Pons, A. J.; Karma, A.,*Helical crack-front instability in mixed mode fracture*, Nature, 464, 85-89, **(2010)**.

Estudio mediante geometría intrínseca de procesos de crecimiento cinéticos con rugosidad

Javier Rodriguez-Laguna[†], Silvia N. Santalla[‡*], Rodolfo Cuerno[†]

[†] *Dpt. Matemáticas y Grupo Interdisciplinar de Sistemas Complejos (GISC), Universidad Carlos III de Madrid, 28911 Leganés (España)*

[‡] *Dpt. Física, Universidad Carlos III de Madrid. 28911 Leganés (España)*

Los procesos cinéticos de crecimiento con rugosidad fuera de equilibrio han sidio estudiados extensivamente tanto como un problema fundamental de mecánica estadística como sistemas físicos relevantes en sí mismos, tales como el crecimiento de láminas delgadas, dinámica de fluidos, propagación de frentes de llamas o crecimiento biológico indiferenciado[1].

El Ansatz de Family-Vicsek es un esquema que describe con éxito la mayoría de los sistemas cinéticos con rugosidad. Definamos la rugosidad del sistema W como la anchura promedio de la interfaz. Comenzando con una configuración plana, W crece inicialmente en el tiempo con una ley de potencias, $W \approx t^{\beta}$. Pero para largos tiempos, la rugosidad satura en un valor que depende del tamaño del sistema L con otra ley de potencias: $W \approx L^{\alpha}$. Los exponentes α y β caracterizan el sistema. En la práctica, muchos sistemas diferentes toman los mismos valores para estos exponentes, mostrando un alto grado de universalidad.

Concretamenten, en 1+1D se han identificado varias clases de universalidad, que han sido asociadas a ecuaciones en derivadas parciales estocásticas de evolución temporal de cierta "función altura" $h(x,t)$, tales como la ecuación de Edwards-Wilkinson o la renombrada ecuación de Kardar-Parisi-Zhang. Es interesante notar que dichas ecuaciones, cuyas soluciones son conocidas analíticamente[2], son obtenidas dentro de la aproximación de pendientes pequeñas, impidiendo la formación de marquesinas. Una pregunta relevante, por tanto, es: ¿cambia la clase de universalidad cuando estas restricciones no se aplican?

Proponemos[3] una ecuación en derivadas parciales estocástica definida en 2D, que no introduce ninguna diferencia entre las direcciones de crecimiento e interfacial. Todos los operadores que aparecen son de naturaleza geométrica:

$$v_n(\vec{r}) = A_0 + A_1 K(\vec{r}) + A_2 \nabla^2 K(\vec{r}) + A_n \eta(\vec{r})$$

donde v_n es la velocidad a lo largo de la dirección normal en un punto de la interfaz, $\vec{r}$ es un punto tal, K es la curvatura local, ∇^2 es el operador de Laplace-Beltrami y η es un ruido blanco, decorrelacionado en espacio y tiempo. Así, A_0, A_1, A_2 y A_n son constantes libres.

Nuestra ecuación está complementada con un algoritmo numérico que asegura la naturalidad geométrica del procedimiento, adaptativo con el fin de que la interfaz siempre sea simulada con un grado de resolución suficiente. Las medidas también se llevan a cabo mediante procedimientos geométricamente naturales. Nuestros resultados serán referidos a geometría banda y, asimismo, a geometría circular.

---

* silvia.santalla@uc3m.es

[1] A.-L. Barabási and H. E. Stanley, *Fractal concepts in surface growth* (Cambridge University Press, Cambridge, 1995).

[2] T. Sasamoto and H.Spohn, Phys. Rev. Lett. **104**, 230602 (June 2010)

[3] J. Rodriguez-Laguna, S.N. Santalla, R. Cuerno, JSTAT, submitted (2011).

Thermodynamic tradeoffs in sensory adaptation: the energy-speed-accuracy relation*

G. Lan[1], Pablo Sartori[1,2], S. Neuman[3], V. Sourjik[3], Y. Tu
IBM T.J. Watson Research Center
Yorktown Heights, 10598 NY

INTRODUCTION Adaptation is a fundamental function of living systems. Importantly, adaptation allows sensory systems to maintain high sensitivy over a wide range of backgrounds. An everyday example is the adaptation of the activity (a) of mammalian photoreceptors to prolonged light stimuli (s), by the action of a chemical "memory" (m) through a negative feedback (Fig. 1).

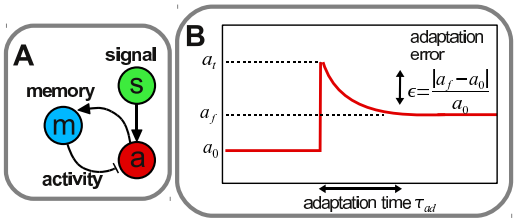

Figura 1. **A** Topology of a sensory system: a stimulus (s) enhances the activity (a) of a receptor, which through a memory (m) mediated feedack recovers to a target value a_0. **B** Adaptive response of the activity a of a sensory system to a step signal. After a transient peak a_t, the final activity a_f recovers to the target a_0 with accuracy $1/\epsilon$ at a speed $\omega_{ad} = 1/\tau_{ad}$.

When leaving a dark room the immediate response of the eye is strong. Right after, the eye becomes insensitive as it is overstimulated by light. However, a few seconds later it adapts to its "ready-to-sense" state, and is then capable of resolving small relative differences in light intensity.

Although the benefits of adaptation are well known, its costs remain poorly understood. In this work we argue that sensory adaptation is a dissipative phenomena, and try to elucidate the energetic cost of sensory systems in maintaining an adapted state.

THE GENERAL CONTINUOUS MODEL We analyze the stochastic dynamics of the *generic* feedback circuit in Fig. 1 responsible for sensory adaptation thorugh Langevin and Fokker-Planck equations. We show that adaptation processes are inherently dissipative, as they violate detailed balance. As a consequence, continuous energy consumption (entropy production) is required to stabilize the adapted state.

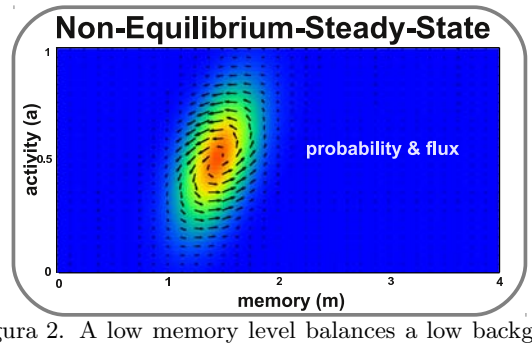

Figura 2. A low memory level balances a low background signal to maintain the activity near the adaptaed state 0.5. This is done at the expense of energy dissipation, as can be readily seen by the pressence of phase-space fluxes.

By using probability flux conservation (Fig. 2), we analytically derive a *universal relation* between the Energy dissipation rate ($\dot{W}$), the adaptation Speed (ω_{ad}), and the adaptation Accuracy ($1/\epsilon$), the ESA relation:

$$\dot{W} \sim -\omega_{ad} c \sigma_a^2 \log(\epsilon/\epsilon_c) \qquad (1)$$

Where σ_a^2 is the variance of activity fluctuations, c depends on the model details, and $k_B T = 1$.

E. COLI CHEMORECEPTOR: MODEL AND EXPERIMENTAL VERIFICATION We then focus on the E. Coli chemoreceptor, the best known example of sensory adaptation. Since the reaction rates are well known, we can perform extensive simulations of the undergoing chemical kinetics.

Through simulations we recover the ESA relation in Eq.1, where ω_{ad} is the rate of the reactions which violate detailed balance. For $\epsilon \sim 1\%$ as meaured, each transition dissipates $\Delta W \equiv \dot{W}/\omega_{ad} \sim 30 k_B T$, roughly the energy of the S-adenosylmethionine (SAM) molecule hydrolized in the chemotaxis pathway.

Our theory predicts that a reduction in the ammount of available SAM in a cell does not change the adaptation accuracy $1/\epsilon$, as $\Delta W \sim 1$SAM is the same. However $\dot{W}$ will decrease, and hence so will ω_{ad}. We measure *in vivo* the response of deenergizing cells. While their adaptation accuracy remains constant, there is a clear decrease in adaptation speed ω_{ad}. This confirms the theoretical prediction derived from the ESA reltion.

---

* Work currently under review in *Science*.
[1] Both these authors contributed equally to this work.
[2] Part of this work was done in the facilities of the Statistical Physics group at the University of Granada.
[3] S.N. & V.S. affilitation is the ZMBHU lab, in Heidelberg.

Flujo de Couette para una impureza inmersa en un gas granular

Francisco Vega Reyes,* Vicente Garzó,†, Andrés Santos‡
Departamento de Física, Universidad de Exremadura, 06071 Badajoz

El estudio de las propiedades de transporte de los medios granulares tiene numerosas aplicaciones tecnológicas e industriales, además de un evidente interés a nivel más fundamental.[1] Por ejemplo, en el caso de medios granulares termalizados y muy poco densos, es posible una descripción de sus propiedades de transporte en el contexto de la mecánica de fluidos. Así, es posible deducir expresiones de los coeficientes de transporte hidrodinámicos clásicos también para *gases granulares*. Las condiciones de transporte y segregación de impurezas inmersas en un gas granular se presenta como uno de los problemas de indudable interés técnico.[2] Por ello, nos proponemos en este trabajo analizar las propiedades de transporte de una impureza granular inmersa en un flujo de Couette.

En nuestro sistema, disponemos de un gas granular de discos/esferas duras lisas idénticas, en el cual se halla presente, en una concentración despreciable, una especie de esferas/discos, también inelásticos, pero que tiene propiedades diferentes a las del gas granular en el que está inmerso. En nuestro sistema simplificado, esas propiedades distintivas pueden ser: o bien el coeficiente de restitución normal, que caracteriza la cantidad de energía cinética perdida en las colisiones, o bien el diámetro o masa de las partículas. Denotaremos, pues, con los subíndices 1 y 2 a la impureza y al gas granular, respectivamente, de manera que denotamos como α_1 y α_2 al coeficiente de restitución normal de la impureza y del gas granular, mientras que $\omega \equiv \sigma_1/\sigma_2$ y $\mu \equiv m_1/m_2$ indicarán, respectivamente, la relación entre diámetros (σ) y masas (m) de ambas especies.

Nuestro gas granular y la impureza se hallan entre dos paredes paralelas e infinitas desde las cuales se calienta (a temperaturas diferentes) y cizalla el gas (geometría del flujo de Couette). En estas condiciones, el estado estacionario de la impureza queda determinado no sólo por sus propiedades físicas sino también por las del gas en el que está inmersa. En cambio, el estado final de la especie del gas no se ve afectado por la presencia de la impureza. De esta manera, y en nuestra geometría, podemos escribir las ecuaciones de Boltzmann para el gas y la impureza, respectivamente, como

$$V_y \frac{\partial}{\partial y} f_2 = J[f_2, f_2], \tag{1}$$

$$V_y \frac{\partial}{\partial y} f_1 = J[f_1, f_2], \tag{2}$$

donde $J[f_i, f_j]$ es la integral colisional de la ecuación de Boltzmann entre las especies i y j.

La solución analítica de las ecuaciones (1) y (2) la hemos aproximado por dos vías alternativas: i) mediante un modelo BGK adaptado a la inelasticidad de las colisiones y ii) mediante el método de los 13 momentos de Grad. Además, hemos obtenido la solución numérica de ambas ecuaciones mediante el método de simulación directa de Monte Carlo (DSMC). Comparamos en este trabajo los resultados obtenidos por estas tres vías, mostrando los valores de los coeficientes de transporte de la impureza. Además, los resultados muestran claramente que la hidrodinámica es no newtoniana, por lo que también analizamos las propiedades reológicas de la impureza.

Otra propiedad interesante en mezclas granulares (incluyendo el caso de impureza) es el cociente de temperaturas granulares de las especies, que resulta ser una constante en estados estacionarios. En la Fig. 1 mostramos los resultados que se derivan para esta magnitud en función de la tasa de cizalladura local a, magnitud que indica la intensidad del flujo de Couette en el gas granular y que también es una constante del sistema en estados estacionarios.

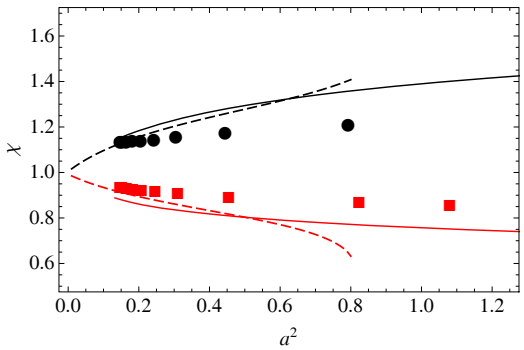

Figura 1. Ratio de temperaturas $\chi \equiv T_1/T_2$ para una impureza con $\mu = 2$ (símbolos y líneas superiores en negro) y $\mu = 0.5$ (símbolos y líneas inferiores en rojo) en función de la tasa de cizalladura. Símbolos: datos DSMC, líneas continuas: modelo BGK, líneas discontinuas: método de Grad.

En nuestro trabajo presentaremos comparativamente los resultados obtenidos por los tres métodos y discutiremos las propiedades de los flujos de Couette de una impureza granular. Mostraremos, además, una clasificación general de los mismos.

* fvega@unex.es
† vicenteg@unex.es
‡ andres@unex.es

[1] F. Vega Reyes, A. Santos, and V. Garzó, Phys. Rev. Lett. **104**, 028001 (2010).
[2] F. Vega Reyes, V. Garzó, and A. Santos, J. Stat. Mech. **P09003** (2008).

Parte III
Paneles

Impact of subdiffusion on the formation and properties of morphogen gradients: a reaction-diffusion approach

Santos Bravo Yuste*, Enrique Abad†, K. Lindenberg ‡
* *Departamento de Física y* † *Departamento de Física Aplicada*
Universidad de Extremadura
06006 Badajoz
‡ *Department of Chemistry and Biochemistry*
University of California, San Diego
La Jolla, CA 92093-0340

Recently, increasing evidence has been gathered on the importance of memory effects in systems where transport and reaction events coexist over biologically relevant time scales. The joint effect of reaction and anomalous transport may bring about unexpectedly strong deviations from results obtained for classical reaction-diffusion systems. Several authors have shown that a rigorous derivation of the relevant reaction-transport equations from mesoscopic models will typically result in the occurrence of mixed reaction-transport terms[1].

An scenario where such equations could find a potential application is morphogen gradient formation[2], a process of utmost importance in developmental biology. Tissue patterning in multicellular organisms is often governed by special signaling molecules called morphogens. Morphogens are produced at localized sites and may undergo degradation as they disseminate through the developing tissue. The combined action of transport and the degradation reaction results in a morphogen concentration gradient which cells across the tissue can sense and interpret. The local morphogen concentration level determines the number and the identity of the genes each cell will express, and thus it also determines its ultimate fate. Hence, there is a direct relation between tissue patterning and the shape of the morphogen gradient[2].

Hornung et al.[3] recently suggested that in some cases cell-to-cell morphogen transport involves successive binding and unbinding events to specific cell surface receptors. Rather than ordinary diffusion, such stochastic events can be viewed as trapping events whose waiting times display a significant dispersion. Consequently, Hornung et al. constructed a 1-d transport model[3] based on the so-called Continuous Time Random Walk (CTRW), which is known to yield subdiffusive behavior in the limit of a large number of jumps. Additionally, they allowed for morphogen degradation at a constant rate per transition between bound and unbound states. However, they assumed that, while bound to the receptors, morphogens were protected against degradation (reaction and transport are thus mutually exclusive). Their approach yields transient concentration gradients, but not stationary morphogen profiles associated with stable tissue patterns, prompting certain authors to assert that the latter were incompatible with anomalous (subdiffusive) transport.

In this work, we relax the assumption made by Hornung et al.[3] and allow for simultaneous degradation and CTRW transport. In our model, the degradation reaction is assumed to be independent of transitions between bound and unbound states and modeled via a first-order death process whose rate coefficient k (reactivity) is in general space-dependent, $k = k(x)$. The underlying CTRW reaction-transport model leads to a reaction-subdiffusion equation (RSE) with a mixed reaction-transport term containing a non-local integro-differential operator (the so-called Riemann-Liouville fractional derivative). For a homogeneous k, our RSE solved for the appropriate boundary conditions yields exponentially decaying stationary morphogen concentration profiles, as opposed to the results found by Hornung et al. However, if the reaction is confined to a small region around the morphogen source, a steady state can be sustained only in the limit of normal diffusion; otherwise, the transport is too slow to stop morphogen accumulation outside the reactive region, leading to a discontinuous concentration profile and a lack of a stationary profile (see fig. 1). In general, we find a large gamut of concentration profiles[4] depending on the specific form of $k(x)$.

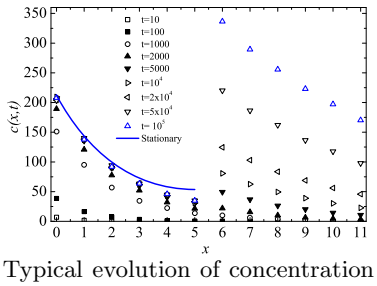

Figura 1. Typical evolution of concentration profiles for a step reactivity $[k(x) = k_0 H(R-x)]$ with $k_0 = 1/1000$, $R = 5.5$

* santos@unex.es

[1] V. Méndez, S. Fedotov, and W. Horsthemke, *Reaction-Transport Systems: Mesoscopic Foundation, Fronts, and Spatial Instabilities* (Springer-Verlag, Berlin, 2010); E. Abad, S. B. Yuste, and K. Lindenberg, Phys. Rev. E **81**, 031115 (2010).
[2] M. Ibáñes and J. C. Izpisúa, Molecular Systems Biology **4**, 176 (2008).
[3] G. Hornung, B. Berkowitz B, and N. Barkai, Phys. Rev. E **72**, 041916 (2005).
[4] S. B. Yuste, E. Abad, and Katja Lindenberg, Phys. Rev. E. **82**, 061123 (2010).

Propiedades del agua en condiciones extremas: región subenfriada y presiones negativas

J.L.F. Abascal, M.A. González, C. Vega
Depto Química-Física I, Facultad de C. Químicas, Univ. Complutense, 28040 Madrid

El anómalo comportamiento del agua y sus consecuencias son conocidos incluso fuera del ámbito estrictamente científico. Es el caso por ejemplo de la existencia de un máximo en la densidad (TMD) a una presión dada. Cuando nos alejamos de las condiciones de temperatura y presión ambiente, las anomalías se hacen aún más notables, especialmente en la zona subenfriada. Para explicar de forma unitaria el comportamiento del agua se ha propuesto la existencia de un segundo punto crítico corrrespondiente a una transición líquido-líquido en la región subenfriada (LLCP)[1]. Aunque ciertos experimentos parecen sugerir la existencia del LLCP, todavía no hay una evidencia experimental concluyente. Por ello, los estudios de simulación pueden arrojar luz sobre este tema. El problema es que la simulación se basa en modelos de agua simplificados por lo que cabe dudar de si representan el verdadero comportamiento del agua en condiciones extremas.

Trabajos experimentales recientes sobre la ecuación de estado del agua en la región subenfriada permiten por vez primera chequear capacidad predictiva de los modelos en la zona en que se presume se encuentra el LLCP. La comparación de estos datos experimentales con las predicciones para el modelo TIP4P/2005[2] muestran una excelente concordancia (tanto cualitativa como cuantitativa). Debe esperarse por tanto que los resultados de simulación de este modelo se aproximen (incluso cuantitaviamente) a los del agua real. Por ello hemos llevado a cabo exhaustivas simulaciones para localizar el LLCP[3]. Hemos calculado también la línea de compresibilidad máxima (línea de Widom) que emana desde el punto crítico y se adentra en la región de presiones negativas. La línea de Widom acaba uniéndose con la línea de densidades máximas justo en el punto en que ésta cambia de pendiente ("retracing TMD").

Consideraciones termodinámicas han demostrado que, en el caso de TMD reentrante, la línea de Widom debe continuar con otra de compresibilidad mínima. Nuestros cálculos con el modelo TIP4P/2005 muestran la continuidad de ambas líneas y su contacto con la TMD a aproximadamente -1000 bar. A partir de este punto la pendiente de la TMD se hace muy pequeña de forma que llega ser más o menos paralela a la espinodal líquido-vapor. Finalmente, hemos investigado la dependencia de la temperatura de fusión con la presión observando que también muestra un reentrante aunque su pendiente es notablemente más abrupta que la de la TMD[4].

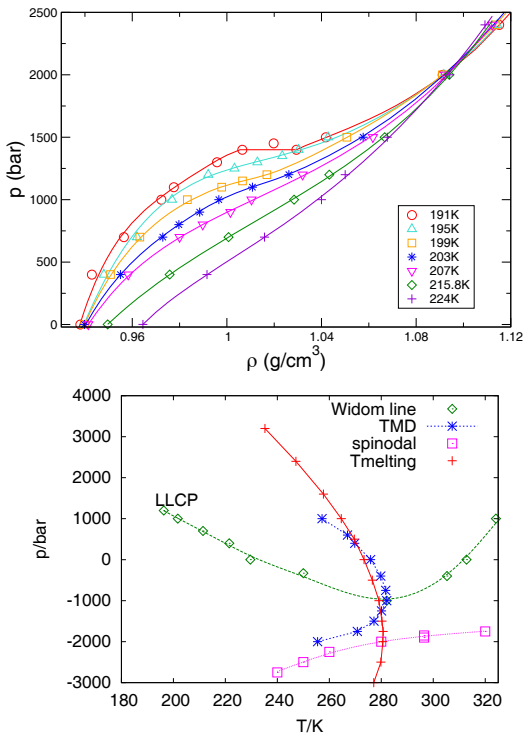

Figura 1. Resultados de simulación para el modelo TIP4P/2005. Arriba: Isotermas en la región subenfriada. Abajo: Líneas de Widom, TMD, spinodal y puntos de fusión

* jlfabascal@quim.ucm.es

[1] P. H. Poole, F. Sciortino, U. Essmann y H. E. Stanley, *Nature* **360**, 324 (1992)
[2] J.L.F. Abascal y C. Vega, *J. Chem. Phys.* **123**, 234505 (2005).
[3] J.L.F. Abascal y C. Vega, *J. Chem. Phys.* **133**, 234502 (2010).
[4] M.A. Gonzalez y J.L.F. Abascal (en preparacion).

Depósitos y Flujo de Partículas con Caras Planas en un Silo

M. Acevedo*, I. Zuriguel, D. Maza
Departamento de Física y Matemática Aplicada, Universidad de Navarra, 31080 Pamplona.

Generalmente, cuando se estudia el comportamiento de los medios granulares, ya sea de forma numérica o de forma experimental, las partículas que los constituyen son esferas o discos dependiendo si se trabaja en 3 ó 2 dimensiones. Sin embargo, estudios recientes muestran que la geometría de las partículas tiene un efecto importante en propiedades granulares tales como: el factor de empaquetamiento, el número de coordinación, la formación de atascos y la propagación de estrés. Por otro lado, el diseño y la explotación de silos de granos requiere de un profundo conocimiento del comportamiento de las partículas tanto en el almacenamiento como en la descarga.

En este trabajo se estudia el depósito y flujo en el interior de un silo de partículas con caras planas y diferente relación de aspecto. Pese al gran interés industrial de este tipo de partículas, existe un gran desconocimiento acerca de su comportamiento debido a la complejidad de las interacciones entre las mismas.

Los principales resultados se exponen en la figura 1. En a) se presenta la distribución de orientaciones de partículas con una relación de aspecto de $d = 5.4$. Después del proceso de carga, la orientación preferente es la horizontal o paralela al sustrato ($\theta = 0$ y $\theta = \pi$), mientras que las orientaciones verticales ($\theta = \pi/2$) son muy poco probables[1,2]. Después de descargar parcialmente el silo, esta distribución de orientaciones cambia hacia una más plana, indicando que es igualmente probable encontrar cualquier orientación tras este proceso.

Los resultados que se muestran en b) corresponden a partículas con relación de aspecto $d = 2.4$. Después del depósito, la distribución es sensiblemente diferente al caso de relación de aspecto $d = 5.4$, ya que la orientación se desvía de la horizontal. Después de descargar parcialmente, se observa que la orientación preferente es la vertical.

En c) se ilustran los resultados para relación de aspecto $d = 1$. Estos resultados muestran que, después de la carga, la orientación más probable es $\theta = \pi/4$ donde la diagonal es paralela a la gravedad. Después de la descarga parcial, resulta que estas partículas giran un ángulo de $\theta = \pi/4$ provocando que la orientación preferida sea la horizontal ($\theta = 0$).

Adicionalmente a estos resultados, se presentarán los obtenidos cuando se varía la velocidad de carga (*Feed Rate*) comparándolos con los anteriormente expuestos.

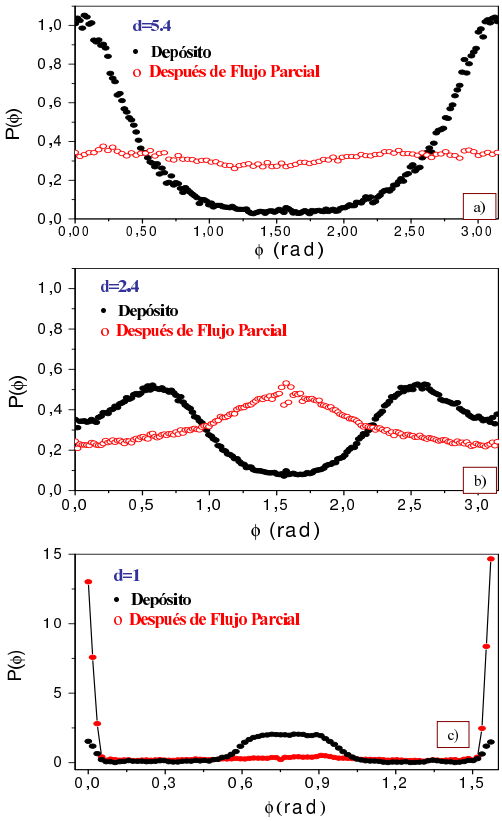

Figura 1. Histogramas de Orientaciones para partículas con diferentes relaciones de aspecto: en a) $d = 5.4$ en b) $d = 2.4$ y en c) $d = 1$.

* macevedo@alumni.unav.es

[1] R. Cruz-Hidalgo, I. Zuriguel, D. Maza and I. Pagonabarraga, J. Stat. Mech. (2010) P06025.
[2] R. Cruz Hidalgo, I. Zuriguel, D. Maza and I. Pagonabarraga. *Phys. Rev. Lett.*, **103**, 1180001 (2009).

Universal critical avalanches in the Coulomb glass

Martin Goethe* and Matteo Palassini†
Departament de Física Fonamental, Universitat de Barcelona
Diagonal 647, E–08028 Barcelona.

The Coulomb glass (CG) is a strongly correlated regime observed at low temperature in Anderson insulators such as dirty metals, amorphous semiconductors, and lightly doped semiconductors. A defining feature of the CG is the extremely slow relaxation of the hopping conductivity (phonon-assisted tunneling between localized states), and related glassy non-equilibrium effects such as aging and memory[1]. It was suggested[2] that these effects reflect an underlying equilibrium "glass phase", which however was ruled out by recent numerical studies[3] down to very low, but finite, temperature T.

In this work we search for glassiness directly at $T = 0$ by investigating charge avalanches in the CG for the first time. We consider the standard CG model[2] consisting of $N/2$ electrons localized on N lattice sites, with $1/r$ pairwise interactions and random local potentials, in a uniform neutralizing background charge. Starting from a random configuration, we quench the system instantaneously to $T = 0$ and let it evolve until it reaches a local minimum, i.e. a stable configuration against all one-electron jumps. We then perturb the system either by inserting one extra electron at an empty site (charge injection), or by displacing an electron from an occupied site to a nearby empty site (dipole injection). Due to the perturbation, other electrons may become unstable and relax to new positions. This in turn can trigger further jumps so that an avalanche forms, until the system stops upon reaching a new local minimum.

It was shown recently[5], in agreement with earlier simulations[6], that the avalanche size distibution $g(S)$ for similar avalanche processes in the infinite-range spin glass and other mean-field models has a power-law behavior

$$g(S) \sim S^{-\tau} \exp[-(S/S_c)^2] \qquad (1)$$

where S is the number of jumps, $\tau > 0$, and S_c a cutoff that diverges for large system sizes. This signals a kind of self-organized criticality[6], which was shown to be related to the marginal criticality[5] of the equilibrium glass phase in these models.

Our goal is to elucidate whether a similar scenario is at play in the CG. Using a new algorithm[4] that allows us to measure $g(S)$ with high statistics for large systems ($N = L^3 \leq 60^3$), we find a power-law tail in agreement with Eq.(1) for both charge and dipole injection, with S_c diverging linearly with L (Fig. 1). We interpret these results in terms of rearrangements of soft long-lived particle-hole pairs (dipoles), and analyse the possible origin of the power-law behavior both from the point of view of branching processes, and of glassy criticality. Finally, we discuss the relationship of the scale-free avalanches with the divergence of the screening length for $T \to 0$. These results shed new light on the elementary excitations in disordered insulators and on the long-debated nature of the CG.

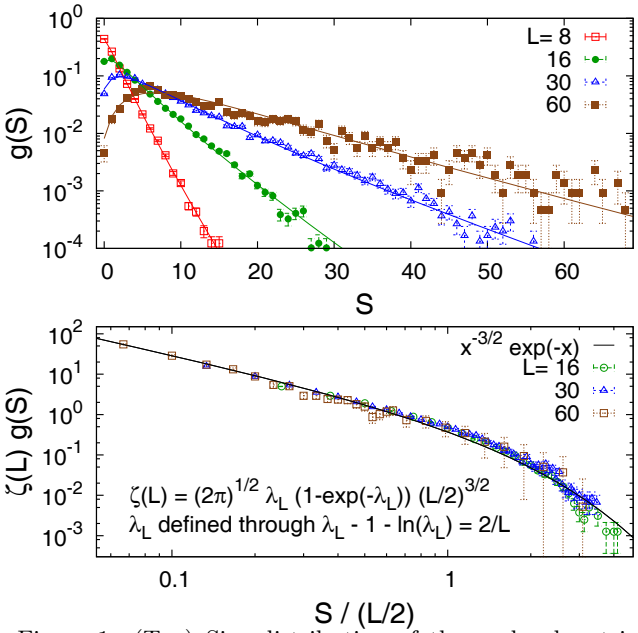

Figura 1. (Top) Size distribution of the avalanches triggered by charge injection, for different linear sizes L. The lines are fits to compound Poisson distributions of Galton-Watson processes. (Bottom) Scaling plot of $g(S)$ for avalanches triggered by dipole injection. In both cases $g(S)$ has a power-law tail with an exponential cutoff, which diverges linearly with L.

* martingoethe@ub.edu
† palassini@ub.edu

[1] A. Amir, Y. Oreg, and Y. Imry, in *Annual Review of Condensed Matter Physics* Vol. 2: 235-262 (2011); arXiv:1010.5767.
[2] M. Müller and L. B. Ioffe, ibid. **93** (2004); S. Pankov and V. Dobrosavljević, ibid. **94**, 046402 (2005); M. Müller and S. Pankov, Phys. Rev. B **75**, 144201 (2007) and references therein.
[3] M. Goethe and M. Palassini, Phys. Rev. Lett. **103**, 045702 (2009); B. Surer et al., ibid. **102**, 067205 (2009)
[4] A. Glatz, V. M. Vinokur, J. Bergli, M. Kirkengen, and Y. M. Galperin, J. Stat. Mech. **P06006** (2008)
[5] P. Le Doussal, M. Müller, and K. Wiese, EPL **91**, 57004 (2010)
[6] F. Pázmándi, G. Zaránd, and G. T. Zimányi, Phys. Rev. Lett. **83**, 1034 (1999)

Stabilization of self-propelling particle clusters

F. Alarcón, I. Pagonabarraga*
Departament de Física Fonamental
Facultat de Física
Universitat de Barcelona
Carrer Martí i Franqués, 1
08028 Barcelona

Suspensions of self-driven organisms are related to a large variety systems of relevant interest which are composed by swimming organisms, such as fish shoals or bacteria colonies. All these systems, referred to generically as *active materials*, are composed by constituents which absorb energy from their surroundings or from their internal metabolism and dissipate it, usually carrying out internal movements, leading to translational or rotational motion[1]. These systems remain out of equilibrium, a feature which leads to unique properties and enhance the ability of these systems to self assemble and develop patterns as a result of their intrinsic motion[2].

We have studied the collective behavior of communities of active particles using a simple model in which the effect of the internal metabolism of the microorganism can be described through the effective fluid flow the particle generates on its surface. This squirmer model, which constitutes a model for ciliated microorganisms and certain types of microrobots, accounts for the correct coupling of the selfpropelling particle to the fluid surrounding it. It is known that this hydrodynamic coupling promotes self-assembly through cluster formation[3], although their stability has not been addressed systematically.

We address systematically the stability of clusters of squirmers, paying special attention to size spanning clusters, responsible for flocking transitions in ensembles of selfpropelling particles in the absence of hydrodynamics[4]. The theoretical prediction, based on linearized hydrodynamics, that squirmer bands are intrinsically unstable[2] has not been analyzed. Previous numerical evidence shows the development of dense squirmer bands coexisting with a dilute fluid suspension. As a result, nonlinear couplings appear as a natural mechanism for band stabilization which we analyze using a lattice Boltzmann (LB) model to describe the fluid and address the appropriate time scales which determine the coupling of the active particles and the fluid while the activity of the particles is characterized using the model described in Ref. [5]. We also address the role of squirmer interactions and geometrical confinement to stabilize squirmer bands and discuss a hydrodynamically-controlled route to flocking.

* ipagonabarraga@ub.edu

[1] Y. Hatwalne, S. Ramaswamy, M. Rao and R. Aditi Simha, *Phys. Rev. Lett.* **92**, 118101 (2004).
[2] S. Ramaswamy and M. Rao, *New Journal of Physics* **9**, 423 (2007).
[3] I. Llopis and I. Pagonabarraga, *Euro. Phys. Lett.* **75**, 999 (2006).
[4] T. Vicsek, A. Czirók, E. Ben-Jacob, I. Cohen and O. Shochet. *Phys. Rev. Lett.* **75**, 1226 (1995).
[5] R. Matas Navarro and I. Pagonabarraga, *Eur. Phys. J. E* **33**, 27 (2010).

Molecular dynamics study of polarizable ion models for molten copper halides

Olga Alcaraz*, Vicente Bitrián and Joaquim Trullàs
Departament de Física i Enginyeria Nuclear,
Universitat Politécnica de Catalunya, Campus Nord, B4-B5
08034 Barcelona, Spain

While the structural properties of molten alkali halides are well reproduced by using rigid ion models (RIM) in which the ions interact throughout the effective pair potentials of Tosi and Fumi,[1] the main features of the experimental structure factors $S(k)$ for molten silver and copper halides cannot be reproduced from the available RIM. However, by using polarizable ion models (PIM), in which the many-body interactions due to the anionic induced polarization are added to those of the effective pair potentials in the form proposed by Vashishta and Rahman,[2] the $S(k)$ for molten AgCl and AgBr is improved,[3,4] and that for molten silver iodide is successfully reproduced.[5,6] Recently, by molecular dynamics (MD) simulation of a PIM for molten CuI, we have also been able to reproduce the main trends of the corresponding $S(k)$, especially the first sharp diffraction peak at about 1 Å which indicates an intermediate range ordering related to the formation of voids with different size due to the inhomogeneous distribution of cations.[7] See Figure 1 where the experimental $S(k)$ is compared with that obtained by MD of a RIM and a PIM. In this work, we complete the series of copper halides with MD of PIM for molten CuBr and CuCl, and we report the corresponding structural and ionic transport properties. The calculated $S(k)$ also reproduce the main trends observed in neutron diffraction (ND) data. Furthermore, we study the polarization effects on the properties of molten copper halides by comparing the PIM and RIM results.

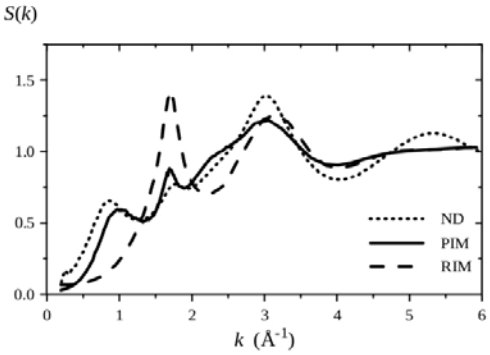

Figura 1. $S(k)$ for molten CuI from ND data of Drewitt et al.[8] (dotted line), and MD results for the PIM (solid line) and RIM (dashed line) models.

* olga.alcaraz@upc.edu

[1] M. P. Tosi and F. G. Fumi, J. Phys. Chem. Solids **25**, 45 (1964). R. Car and M. Parrinello.
[2] P. Vashishta and A. Rahman, Phys. Rev. Lett. **40**, 1337 (1978)
[3] J. Trullàs, O. Alcaraz, L. E. González and M. Silbert, J. Phys. Chem. B **107**, 282 (2003)
[4] V. Bitrián and J. Trullàs, J. Phys. Chem. B **112**, 1718 (2008)
[5] V. Bitrián, J. Trullàs and M. Silbert, J. Chem. Phys. **126**, 021105 (2007)
[6] V. Bitrián and J. Trullàs, J. Phys. Chem. B **112**, 1718 (2008)
[7] V. Bitrián, O. Alcaraz and J. Trullàs, J. Chem. Phys. **134**, 044501 (2011)
[8] J. E. Drewitt, P. S. Salmon, S.Takeda and Y. Kawakita, J. Phys.: Condens. Matter 21, 075104 (2009)

Application of an effective medium theory to heterogeneous reaction-diffusion systems

Sergio Alonso* and Markus Bär
Physikalisch-Technische Bundesanstalt Department 8.4 Mathematical Modelling and Data Analysis Abbestr. 2-12 10587 Berlin Germany

The small scale of the heterogeneities usually allows an effective description of the inhomogeneous system. Specific homogenization theories have been already suggested, but we propose a general effective medium theory based on the homogeneization of reaction-diffusion systems[1,2]. We consider a system where domains of phase 2 (heterogeneities) are randomly dispersed in a medium of phase 1. The reactivity and diffusion of the reactants take different values if they are inside or outside of such domains. If the heterogeneities are small, we can calculate effective values for the diffusion and the reactivity.

Here, we validate the predictions of the effective medium theory by the numerical calculation of the velocity of a wave in reaction-diffusion systems under the presence of static obstacles. We compare the numerical results obtained for bistable[2] and excitable[3] media with the predictions of the effective homogeneous medium theory. We also discuss the applicability of the effective medium theory to slow dynamical evolution of the domains 2.

Some of the results are applied to chemical waves in microemulsions[4] and to electric waves in heterogeneous cardiac medium.

* sergio.alonso@ptb.de

[1] S. Alonso, R. Kapral and M. Bär, Phys. Rev. Lett. 102, 238302 (2009).
[2] S. Alonso, M. Bär and R. Kapral, J. Chem. Phys. 131, 214102 (2009).
[3] S. Alonso, J. Löber, M. Bär and H. Engel, Eur. Phys. J. Special Topics, 187, 31 (2010).
[4] S. Alonso, K. John and M. Bär, J. Chem. Phys. in press (2011).

Estudio Monte Carlo de la fase de spin-glass de sistemas diluidos de dipolos de Ising

Juan J. Alonso[1,*], Julio F. Fernández[2]
[1] *Departamento de Física Aplicada 1, Universidad de Málaga, E-29071 Málaga (España)*
[2] *ICMA, CSIC y Universidad de Zaragoza, E-50009 Zaragoza (España)*

El comportamiento colectivo de sistemas de espines en los que las interacciones magnéticas dipolares son las dominantes ha cobrado un renovado interés. Estos sistemas son raros de encontrar en la naturaleza, aunque algunos materiales, como ferroeléctricos y cristales magnéticos como el $LiHoF_4$ pueden ser bien descritos como sistemas de dipolos. Parte de este interés en los sistemas dipolares proviene también de los avances en la síntesis de arrays de nanopartículas. En estos sistemas, nanopartículas de hasta unos miles de magnetones de Bohr se comportan como simples espines, y, cuando están empaquetados en arrays cristalinos, las interacciones dipolares crean orden magnético a temperaturas accesibles experimentalmente. La anisotropía juega un papel importante en este orden dipolar. Nosotros conside-ramos aquí sistemas en los que la barrera de energía que un dipolo debe superar para invertir su signo es algo mayor que la energía dipolar, de forma que se puedan observar efectos colectivos a temperaturas que no llegan congelar las direcciones de los espines. Este tipo de sistemas pueden ser modelados como cristales de dipolos de tipo Ising.

Nosotros estudiamos aquí el comportamiento de sistemas diluidos de dipolos de Ising. El propósito fundamental es investigar si la *frustración* que proviene del carácter anisotrópico de la interacción dipolar, juntamente con el *desorden* que proviene de la dilución, puede dar lugar a la existencia de una fase de equilibrio de spin-glass (SG). Experimentos con este tipo sistemas muestran comportamientos de no equilibrio de tipo SG, como aging, y relajación no exponencial.

Presentaremos resultados Monte Carlo para sistemas de dipolos con dilución por sitios. Los dipolos ocupan una fracción x de los L^3 sitios de una red SC, y todos ellos están alineados a lo largo de un mismo eje de anistropía cristalina. Para $x_c < x \leq 1$, con $x_c \simeq 0.65$ encontramos una fase antiferromagnética por debajo de una temperatura de transición que tiende a 0 para $x \to x_c$. Para sistemas aún más diluidos encontramos una fase de equilibrio de spin-glass por debajo de una temperatura $k_B T_{sg} \simeq x\varepsilon_d$, donde ε_d es una energía de interacción dipolar entre vecinos próximos. Para caracterizar el posible orden de spin-glass hemos estudiado el overlap de SG q. En particular, (a) la desviación cuadrática relativa Δ_q^2, y (b) ξ_L/L, donde ξ_L es una longitud de correlación de SG. De su dependencia con la temperatura y el tamaño del sistema determinamos T_{sg}. En la fase de SG encontramos: (i) que $\langle \mid q \mid \rangle$ y $\langle q^2 \rangle$ decrecen algebraicamente con L al aumentar L, (ii) distribuciones bimodales anchas de $q/\langle \mid q \mid \rangle$, (iii) que ξ_L/L crece con L hacia valores finitos. Todo ello es consistente con orden débil de largo alcance en la fase de SG.[1]. Finalmente, mostraremos resultados para sistemas diluidos de dipolos de Ising en redes bidimensionales cuadradas que indican que esta fase de equilibrio de SG no existe en sistemas bidimensionales.[2]

* jjalonso@uma.es

[1] J. J. Alonso and J. F. Fernández, *Phys. Rev. B* **81**, 064408 (2010).
[2] J. J. Alonso and B. Allés, *Phys. Rev. B* **82**, 064425 (2010).

Vidrios de espín en cuatro dimensiones en presencia de un campo magnético

R. Álvarez-Baños*, A. Cruz, L. A. Fernandez, J. M. Gil-Narvion, A. Gordillo-Guerrero, D. Iñiguez, A. Maiorano, F. Mantovani, E. Marinari, V. Martin-Mayor, J. Monforte-Garcia, A. Muñoz-Sudupe, D. Navarro, G. Parisi, S. Perez-Gaviro, J. J. Ruiz-Lorenzo, S. F. Schifano, B. Seoane, A. Tarancon, R. Tripiccione, D. Yllanes

Instituto de Biocomputación y Física de Sistemas Complejos
Mariano Esquillor, Edificio I+D
50018 Zaragoza

La solución exacta en la aproximación de campo medio de los vidrios de espín predice características muy interesantes, como la existencia de un número infinito de estados puros y su organización ultramétrica, que hacen de estos materiales el paradigma de los sistemas complejos.

Actualmente se sabe que los vidrios de espín en tres dimensiones presentan una transición de fase entre un estado desordenado paramagnético y una fase de bajas temperaturas conocida como fase *spin glass*. Sin embargo, la naturaleza de esta fase de bajas temperaturas es todavía cuestión de debate. El objetivo de las simulaciones numéricas se centra en determinar cuáles de las predicciones de la solución de campo medio, exacta en dimensión infinita, sobreviven en vidrios de espín más realistas de tres dimensiones, descritos generalmente por el denominado modelo de Edwards-Anderson[1,2].

Una manera de llevar a cabo esta tarea consiste en el estudio del comportamiento de vidrios de espín en presencia de un campo magnético. La solución de campo medio o solución de Parisi predice un transición de fase a temperatura finita, de manera que existe una línea de transiciones en el espacio (T, h), conocida como línea de Almeida-Thouless, que separa la fase paramagnética a altos campos y temperaturas de la fase *spin glass*[3]. Por el contrario, los escenarios *droplet* y TNT predicen la desparición de dicha transición incluso en presencia de un campo externo infinitesimal[4,5]. Estudios numéricos previos ofrecen evidencias tanto a favor como en contra de la existencia de la linea de AT. El objetivo de este trabajo es determinar el comportamiento de vidrios de espín en cuatro dimensiones, en los que se espera que una transición de fase sea más fácil de detectar.

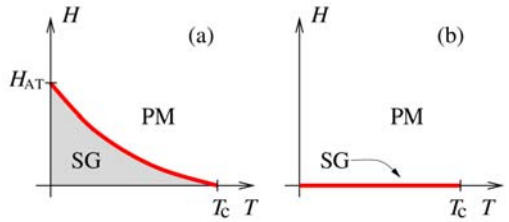

Figura 1. Diagrama de fases en el espacio (T,h), de acuerdo con la solución de campo medio (a) y el modelo *droplet* (b). Figura tomada de la referencia[6].

* raquel.alvarez@unizar.es

[1] M. Mezard, G. Parisi y M. A. Virasoro, *Spin Glass theory and beyond* (World Scientific, 1994)

[2] G. Parisi, *Field Theory, disorder and simulations* (World Scientific, 1994).

[3] E. Marinari, G. Parisi, F. Ricci-Tersenghi, J. J. Ruiz-Lorenzo, F. Zuliani, *Replica Symmetry Breaking in Short Range Spin Glasses: A Review of the Theoretical Foundations and of the Numerical Evidence*, cond-mat/9906076 (1999), *J. Stat. Phys.* **98**, 973 (2000).

[4] D. S. Fisher, D. A. Huse, *Phys. Rev. Lett.* **56**, 1601 (1986); *Phys. Rev. B* **38**, 386 (1988).

[5] F. Krzakala, O. C. Martin, *Phys. Rev. Lett.* **85**, 3013 (2000); M. Palassini, A. P. Young, *Phys. Rev. Lett.* **85**, 3017 (2000).

[6] A. P. Young y Helmut G. Katzgraber, *Phys. Rev. Lett.* **93**, 207203 (2004).

Caos y arritmogénesis en la dinámica del calcio intracelular

E. Alvarez-Lacalle *, I. R. Cantalapiedra, B. Echebarria, A. Peñaranda
Departament de Física Aplicada, Universitat Politècnica de Catalunya, Barcelona.

La muerte súbita debido a arritmias cardiacas es una de las principales causas de muerte en el mundo industrializado. El tipo más grave de arritmia es la fibrilación que se produce cuando las fibras cardiacas se contraen de forma caótica y asíncrona, lo que impide el correcto bombeo de sangre del corazón. Se ha estudiado extensamente el efecto de un desajuste en el balance de las corrientes iónicas en las arritmias cardiacas, a través de las variaciones que producen en el potencial de membrana y la forma del potencial de acción. En la última década, sin embargo, se ha demostrado que desajustes en la regulación del calcio intracelular pueden contribuir a la generación de arritmias. El acoplamiento electromecánico hace que ambas causas estén interrelacionadas

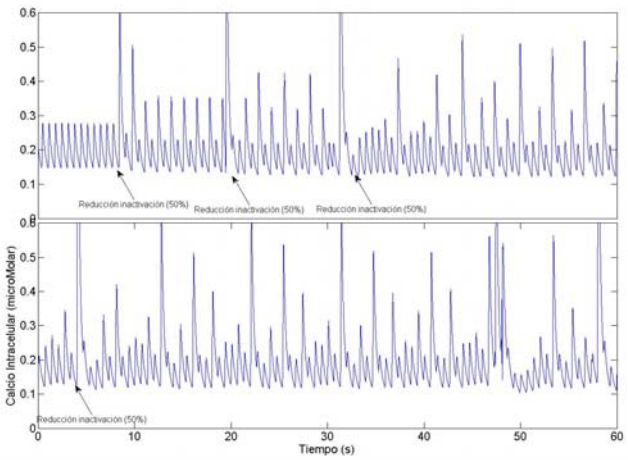

Figura 1. Aparición de alternans en la concentración de calcio intracelular debido a la disminución del tiempo de inactivación del receptor de rianodina.

En este trabajo estamos interesados en arritmias producidas por alternancia en la concentración de calcio intracelular de un batido a otro. La contracción celular se activa con la depolarización de la célula, que provoca la apertura de los canales de Ca de la membrana, permitiendo la entrada de Ca al interior de la célula. El aumento del calcio intracelular origina la liberación de Ca del retículo sarcoplasmático (RS) a través de los canales de receptores de Rianodina (RyR) (Calcium induced Calcium release, CICR). Parte de este Ca se adhiere al sarcómero originando la contracción de la célula. La relajación hacia un nuevo ciclo se consigue mediante la eliminación de Ca hacia el exterior mediante un intercambiador y la reacumulación de Ca en el RS a través de una bomba (SERCA).

Experimentalmente se han observado situaciones patológicas con alternancia en la contracción entre un batido y otro debido a la existencia de alternans en la concentración de Ca intracelular[1]. Generalmente aparecen cuando el ritmo cardiaco aumenta, aunque en algunos casos, se pueden producir a bajas frecuencias de excitación[2,3].

En esta contribución analizamos los efectos que tienen posibles cambios en la activación, inhibición y recuperación de los receptores de rianodina en la aparición de alternans en la concentración de calcio en un módelo de corazón de conejo[4]. Como se observa en la Fig.1 es posible conseguir sucesivas duplicaciones de periodo modificando los parámetros de control del RyR, incluso llegando a obtener dinámicas en apariencia caóticas .

* enrical@fa.upc.edu

[1] Blater L.A. et al, J. Physiol **546** 19 (2003)
Aistrup G.L.et al, Cir. Res. 99 65, (2006)
[2] Diaz M.E., O'Neill S.C. and Eissner D.A., Cir. Res. **99**, 740 (2006)
[3] Picht E., DeSantiago J., Blatter L.A., Bers D.M., Cir. Res. **99** 740 (2006)
[4] Shannon T. R., Wang F., Puglisi, J., Weber, C., Bers, D.M. Biophys. J. **87** 87 5 (2004)

Aggregation of superparamagnetic colloids in magnetic fields: the quest for the equilibrium state

J. S. Andreu[†,‡,*], J. Camacho[†], J. Faraudo[‡]
[‡] *Institut de Ciència de Materials de Barcelona, Consejo Superior de Investigaciones Científicas (ICMAB-CSIC) 08193 Campus de la UAB, Bellaterra, Spain.*

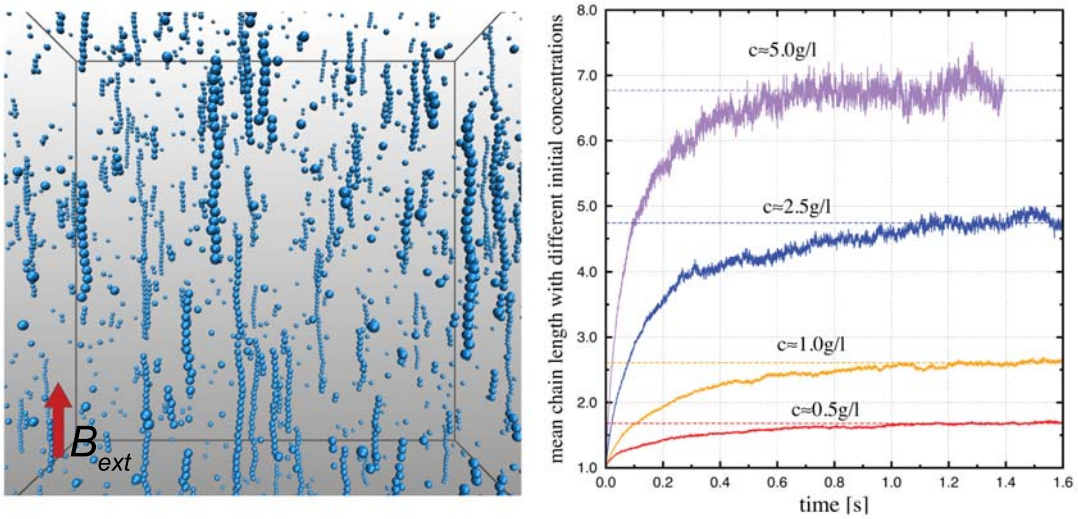

Figura 1. **Left:** Snapshot corresponding to the simulated system with $\phi_0 = 1.05 \times 10^{-3}$ (equivalent to $c \approx 1g/l$) and $\Gamma = 10$. We can observe that chains of colloids align parallel to the applied external uniaxial magnetic field. **Right**: Time evolution of the mean chain length for $\Gamma = 10$ and different concentrations. After a fast transient regime, the mean chain length reaches a constant value depending on the initial volume fraction of colloids ϕ_0 and the magnetic coupling parameter Γ.

Previous experimental[1] and simulation[2] studies of superparamagnetic colloids in a strong external field have systematically shown a nonequilibrium aggregation process in which chains of particles steadily grow in the direction of the applied external field with an average length increasing with a power law with time.

Here we show[3], by employing Langevin dynamics simulations, the existence of a different behavior under the effects of an external magnetic field: after a transient period of chain formation, the system attains an equilibrium distribution of chain lengths. Furthermore, a thermodynamic self-assembly theory supports the simulation results and it also predicts that the average chain length in the equilibrium state depends only on a dimensionless parameter combining the volume fraction of colloids ϕ_0 and the magnetic coupling parameter Γ. The conditions under which this new behavior can be observed are discussed.

This work is supported by the Spanish Government (grants FIS2009-13370-C02-02, PET2008-02-81-01/02 and CONSOLIDER-NANOSELECT-CSD2007-00041), the Catalan Government (grant 2009SGR164) and SEPMAG Tecnologies SL. We acknowledge computer resources and technical assistance provided by the CESGA Supercomputing Center (Finisterrae Supercomputer).

[*] jandreu@icmab.es
[†] Universitat Autònoma de Barcelona.
[‡] Institut de Ciència de Materials de Barcelona.

[1] P. Domínguez-García *et al.*, Phys. Rev. E **76**, 051403 (2007).
[2] F. Martinez-Pedrero *et al.*, Phys. Rev. E **76** 011405(2007).
[3] J. S. Andreu, J. Camacho, J. Faraudo, Soft Matter doi:10.1039/c0sm01424a.

Experimental study of different LFF regimes in semiconductor lasers with an external cavity

Andrés Aragoneses[1], Jordi Zamora-Munt, Jordi Tiana-Alsina, Nicolas Rubido, Cristina Masoller, Maria Carme Torrent

Dept. Física i Enginyeria Nuclear[2], Universitat Politècnica de Catalunya. Rambla Sant Nebridi s/n, Terrassa, 08222 (Spain)

Optical feedback, due to an external mirror in a semiconductor laser, induces instabilities in the laser power output. When the laser works close to its solitary threshold and it is subjected to a small or moderate feedback, sudden irregular power dropouts, followed by gradual power recoveries, appear. These chaotic behaviour, known as Low Frequency Fluctuations (LFF), may show different statistics[3–5], depending on the system's parameters. For pump currents just above the laser's threshold the system may be in a transient regime, where the dropouts are rare and it is predominantly in continuous wave (cw) emission. Increasing slightly the pump current, the system gets to a coexistence regime of cw and LFF. For higher currents, the system shows a sustained LFF regime, with very short periods of cw emission.

For a constant feedback rate and different pump currentes (20.50mA to 22.00mA), we have studied the transition, as the system passes from the transient to the coexistence and to the LFF regimes. In figure 1 the time series of the power output, for the different regimes studied, are shown. In order to characterize the transient and the coexistence regimes, we have obtained long time statistics of the bursts of LFFs and of the periods of stable emission.

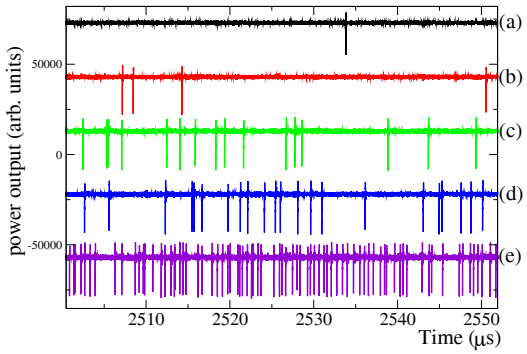

Figura 1. Time series for the different pump currents studied: $I_a = 21.00mA$, $I_b = 21.25mA$, $I_c = 21.50mA$, $I_d = 21.75mA$, $I_e = 22.00mA$. The threshold of the laser was 20.64mA, and the feedback used reduced it 10%

The transient regime, (*a* in figure 1), is interpreted as the system being near a fix point in the phase space. It sporadically jumps from it due to noise, and it quickly returns and remains stably there for a long period. When increasing the pump current to around 21.25mA, the system gets to the coexistence of bursts of LFF and cw emission (*b*-*d* of figure 1). The system spends longer times far from the fix point, showing longer intervals of LFF's, and the rest of the time in the attractor, with cw emission. At pump currents higher than 21.75 mA the system shows a complete LFF regime (*e* in figure 1).

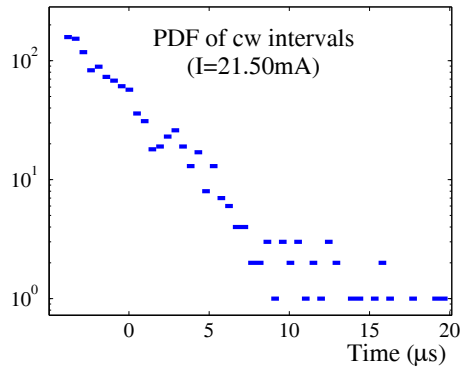

Figura 2. Probability Distribution Function for the continuous wave intervals. The linear plot shown in the lin-log scale can be described in terms of Kramers' formula.

The probability distribution functions (PDF) we obtain show an exponential decay behaviour for the cw intervals (see figure 2). This can be explained in terms of the Kramers' formula. But the PDF of the bursts of LFF show some structure that makes it different from an exponential decay. In order to distinguish between a chaotic or an stochastic origen of the jumps from the bursts of LFF to the cw and vice-versa, we also follow a complexity analysis of the time intervals in the coexistence regime. In this analysis we transform each time series intervals into a symbolic series, so we can study the probabilities of these symbols.

[1] andres.aragoneses@upc.edu

[2] `http://www.donll.upc.edu`

[3] T. Heil, I. Fisher, W. Elsäβer, J. Mulet, C. R: Mirasso "Statistical properties of low-frquency fluctuations during single-mode operation in distributed-feedback lasers: experiments and modeling,**24**, 18, p. 1275 (1999)

[4] A. Torcini, S. Barland, G. Giocomelli, F. Marin "Low-frequency fluctuatinos in vertical cavity lasers: Experiments versus Lang-Kobayashi dynamics", Phys. Rev. A, **74**, p. 063801 (2006)

[5] J. Zamora-Munt, C. Masoller, J. García-Ojalvo "Transient low-frequency fluctuations in semiconductor lasers with ioptical feedback", Phys. Rev. A, **81**, p. 033820 (2010)

Evolución temporal en el flujo longitudinal uniforme de un gas granular Estudio mediante simulaciones en computación grid.

Antonio Astillero*, Andrés Santos†,‡
Departamento de Tecnología de Computadores y Comunicaciones
Universidad de Extremadura, 06800 Mérida (Badajoz)

Un gas granular es un tipo particular de sistema complejo donde una de las características más sobresalientes que lo definen es la disipación de energía que se produce cuando tiene lugar una colisión entre partículas. Como consecuencia, no se verifica el principio de conservación de la energía, haciendo que la dinámica interna del gas sea mucho más rica que la correspondiente a su homólogo molecular.

Una de las formas más extendidas de modelar un gas granular es considerar que está formado por esferas duras inelásticas, donde el grado de inelasticidad de las colisiones viene determinado por el coeficiente de restitución normal α constante[1].

En un trabajo anterior[2], estudiamos la etapa hidrodinámica transitoria en el caso particular del flujo longitudinal uniforme (ULF),[3] tanto desde un punto de vista analítico como computacional (DSMC)[4]. En dicho trabajo, referimos las velocidades de las partículas al sistema de referencia *lagrangiano* que se mueve con la velocidad media del fluido. Haciendo este cambio de sistema de referencia nuestro problema original se transforma en uno independiente del espacio, lo cual permite simular la ecuación de Boltzmann utilizando DSMC de un modo relativamente sencillo sin necesidad de dividir el sistema en celdas.

En el presente trabajo intentamos responder las siguientes cuestiones: ¿qué condiciones de contorno es preciso imponer para que podamos simular el flujo longitudinal inhomogéneo o, en otras palabras, dependiente del espacio? ¿evoluciona un estado inicial inhomogéneo hacia el estado homogéneo? ¿cuál es la duración típica de la relajación hacia el estado homogéneo? Partimos de la condición inicial no homogénea definida por la función de distribución de velocidades[5]:

$$f(\mathbf{r},\mathbf{V};0)=\frac{n^0(x)}{4\pi {V^0}^2}\delta\left(|\mathbf{V}-\mathbf{u}^0(x)|-V^0\right), \tag{1}$$

donde los campos de densidad inicial y velocidad media inicial están dados por

$$n^0(x)=\overline{n}\left(1+\frac{1}{2}\sin\frac{2\pi x}{L}\right), \tag{2}$$

$$\mathbf{u}^0(x)=U\left(\cos\frac{\pi x}{L}-\frac{2}{\pi}\right)\widehat{\mathbf{x}}, \tag{3}$$

respectivamente. Por contra, la temperatura inicial $T^0=m{V^0}^2/3$ es homogénea. La ecuación de Boltzmann para un estado que sólo presenta gradientes a lo largo de la dirección x tiene la forma

$$\partial_t f+v_x\partial_x f=J[f,f]. \tag{4}$$

A continuación efectuamos el siguiente cambio de variables

$$x\to s=\frac{x}{1+a_0t}, \tag{5}$$

$$t\to\tau=a_0^{-1}\ln\left(1+a_0t\right), \tag{6}$$

$$\mathbf{v}\to\mathbf{V}=\mathbf{v}-\frac{a_0x}{1+a_0t}\widehat{\mathbf{x}}, \tag{7}$$

donde a_0 es el gradiente de velocidad inicial. Teniendo en cuenta el cambio anterior, la ecuación (4) queda como

$$\partial_\tau\overline{f}+V_x\partial_s\overline{f}-a_0\frac{\partial}{\partial V_x}\left(V_x\overline{f}\right)=J[\overline{f},\overline{f}]. \tag{8}$$

Entonces, para poder generar el flujo longitudinal uniforme y realizar simulaciones DSMC inhomogéneas podemos utilizar las variables escaladas (5)–(7) y aplicar condiciones de contorno periódicas en $s=\pm L_0$.

Hemos efectuado simulaciones para $\alpha=0.5$ y $a_0=-4\,(\tau^0)^{-1}, -10\,(\tau^0)^{-1}$, analizando la evolución temporal de los perfiles espaciales de densidad, velocidad media y temperatura, respectivamente. Los resultados obtenidos muestran cómo el sistema, partiendo del estado inicial definido por (1)–(3), evoluciona durante la etapa cinética hasta alcanzar las condiciones que definen el flujo longitudinal uniforme.

---

* aavivas@unex.es
http://www1.unex.es/eweb/fisteor/
† Departamento de Física, Universidad de Extremadura, 06071 Badajoz
‡ andres@unex.es
http://www1.unex.es/eweb/fisteor/

[1] N. Brilliantov and T. Pöschel, *Kinetic theory of granular gases* (Oxford University Press, Oxford, 2004).
[2] A. Astillero and A. Santos, *Régimen hidrodinámico transitorio de un gas granular en un flujo compresible*, congreso *Partículas y flujos*, Pamplona (2010).
[3] A. Santos, in Rarefied Gas Dynamics: Proceedings of the 26th International Symposium on Rarefied Gas Dynamics, Takashi Abe, ed. (AIP Conference Proceedings, vol. 1084, Melville, NY, 2009), pp. 93-98
[4] G. A. Bird, in Molecular gas dynamics and the direct simulation of gas flows, Oxford Science Publications, Oxford (1994).
[5] A. Astillero and A. Santos, Phys. Rev. E **72**, 031309-1-20 (2005).

Effects on the histeresis in martensitic transformations

V. Torra[1], A. Isalgue[1], C. Auguet[1,2*], G. Carreras[1]
[1] *CIRG-ETSECCPB-DFA, Universitat Politècnica de Catalunya, Barcelona*
[2] *EPSEB- DFA, Universitat Politècnica de Catalunya, Barcelona*

Shape Memory Alloys (SMA) show a solid-solid structural first order phase transformation from austenite to martensite when a stress is applied in austenite phase, producing changes in length relatively relevant (up to 8-10 %). When the stress is suppressed, the martensite retransforms to austenite. In this way, a hysteresis cycle stress-strain is obtained. The necessary stress mean value to induce the transformation is dependent on the temperature according to the Clausius-Clapeyron thermodynamic equation: as higher is the local temperature, higher is the necessary stress to produce the transformation. The hysteresis cycle induces the damping property of the SMA transforming the mechanical energy in heat, and this property enables the use of SMA as dampers (passive smart materials) in Civil Engineering. The hysteresis cycle induced by the differences between transformation and retransformation stresses and the associated latent heat (dissipated and absorbed) produces the self-heating in the SMA.

Also, in the first cycles of working, it is observed that the hysteresis cycles evolve progressively decreasing their width and reducing the available useful length of the samples (SMA creep), and consequently, decreasing the damping effect. This is an intrinsic effect mainly related to changes in the internal state of the material: plastic deformation in NiTi and plastic deformation plus stabilized martensite in Cu-based alloys.

We studied the influence of the self-heating in the width of the hysteresis in NiTi wires with cycling frequency. In quasi-static cycling it is possible to see the increase of the stress due to the local self-heating. The hysteresis width, for several frequencies, shows the effects of coupling between temperature and stress by a Gaussian shape. An outline of the hysteresis width for CuAlBe is, also, determined. Minor dynamic actions associated to cycling-pause effects are also visualized[1,2].

---

* carlota@fa.upc.edu

[1] V. Torra, A. Isalgue, F. Martorell, F. C. Lovey and Patrick Terriault, *Damping in Civil Engineering using SMA. Part I: Particular Properties of CuAlBe for Damping of Family Houses*, Can. Metall. Quart., 49(2), 179-190 (2010)

[2] V. Torra, A. Isalgue, C. Auguet, G. Carreras, F.C. Lovey, P. Terriault, *Damping in Civil Engineering using SMA. Part II. Particular properties of NiTi for damping of stayed cables in bridges*, submitted to Can. Metall. Quart. (2010)

Buckling transition in quasi-spherical viral capsids

María Aznar, Antoni Luque, David Reguera
Universidad de Barcelona, Dpto. Física Fundamental, Martí i Franqués, 1, 08028 Barcelona Spain.

Viruses are fascinating biological organisms which can self-replicate and infect all types of cells. In their simplest form, they are essentially composed of a protein shell or *capsid* that encloses and protects the genetic material, RNA or DNA. About half of all viral species have a quasi-spherical capsid with icosahedral symmetry characterized by a triangulation number T. This T number, which adopts a discrete set of values, serves as a structural classification for viruses [1]. In turn, viruses with different T numbers can be grouped into families with similar geometrical arrangements of proteins, that are labelled using a second number P. The mechanical properties of these viral capsids play a major role in their stability [2] and have been shown to depend on their structure and T number [3].

Many viruses have a maturation stage, necessary for them to become infective, where the capsid undergoes a buckling transition in which its shape changes from spherical to a flattened icosahedron. In this poster, we will present the results of our studies aimed to analyze the phenomenon of buckling in quasi-spherical viral capsids. In particular, we will discuss how this buckling transition depends on the virus triangulation number T and especially on its class P. We will also discuss the potential biological implications of this buckling phenomenon in the viral stability and life cycle.

References [1] D.L.D Caspar and A. Klug, *Quant. Biol.* **27**, 1-24 (1962)

[2] R. Zandi and D. Reguera, *Phys. Rev. E.* **72**, 021917 (2005)

[3] C. Carrasco, M. Castellanos, P.J. de Pablo, M.G. Mateu, *Proc. Nat. Acad. Sci. USA* **105**, 4150-5 (2008).

Voter models on weighted networks and limits of the mean-field approach

Andrea Baronchelli[1], Claudio Castellano[2], Romualdo Pastor-Satorras[1]

1. Departament de Física i Enginyeria Nuclear, Universitat Politècnica de Catalunya, C. Nord B4, 08034 Barcelona, Spain

2. Istituto dei Sistemi Complessi (ISC-CNR), and Dipartimento di Fisica "Sapienza" Università di Roma, P.le A. Moro 2, I-00185 Roma, Italy

The classical Voter model[1] is a paradigm in the statistical physics approach to social modeling[2]. It describes the spreading of opinions/ideas based on a pure imitation process: at each time step an individual is selected and copies the opinion of a neighbor of hers. In the most common version only two opinions compete in the population, and in finite systems all individuals ends up sharing the same one (i.e. consensus is reached). The model has been extensively studied on different topologies, ranging from regular lattices to complex binary networks. However, the role of heterogeneous connectivity patterns has not been deeply investigated so far, even though many network structures found in technological, biological or social contexts are intrinsically weighted, i.e. connections have widely varying strengths.

Here we present a thorough analysis of the Voter model on complex weighted networks[3]. We write down heterogeneous mean field equations that allow us to estimate the exit probability (i.e. the probability that a given opinion will survive, depending upon the initial conditions) and the consensus time. We focus on networks characterized by power-law degree distribution and point out that the interplay between the degree exponent and the link strength yields an extremely complex phenomenology that can be rationalized in a phase plane adopting simple assumptions. We also introduce the concept of annealed weighted network and discuss how the validity of heterogeneous mean field theory is, strictly speaking, limited to these structures[4]. However, we show that the same approach is able to describe the model accurately also on quenched weighted graphs, provided the link strength is not too strong. We finally discuss the implications of our findings for the modeling of more complex processes on complex weighted networks.

---

* andrea.baronchelli@upc.edu

[1] P. Clifford and A. Sudbury, Biometrika 60, 581 (1973) and R. Holley and T. Liggett, Ann. Probab 3, 643 (1975).

[2] C. Castellano, S. Fortunato, and V. Loreto, Rev. Mod. Phys. 81, 591 (2009).

[3] A. Baronchelli, C. Castellano and R. Pastor-Satorras *preprint* arXiv:1011.2395 (2011).

[4] A. Baronchelli and R. Pastor-Satorras, Phys. Rev. E 82, 011111 (2010).

Percolative analysis of nanoconfined supercooled water

Valentino Bianco, Giancarlo Franzese*
Departament de Física Fonamental, Universitat de Barcelona
Diagonal 647, 08028 Barcelona, Spain

Water is a fundamental substance for all processes involving life. It has many unusual properties compared with other liquids. Recent studies of hydrated biomolecules and nonoconfined water suggest that, surprisingly, the anomalous properties of water are consistent with the hypothesis of the occurrence of a first-order phase transition between two liquids with different densities at low temperature and high pressure. In this hypothesis the phase transition line ends in a liquid-liquid critical point. To validate this hypothesis experiments in nanoconfinement could be very valuable, because they allow to explore the water behavior in a region of temperature that would be otherwise inaccessible for bulk liquid water, as a consequence of inevitable crystallization. We present here a coarse-grained model of water that give insight into the physics of a nanoconfined water monolayer. Our model allows us to analyze the possible existence of a critical point thanks to a mapping into a percolating model.

* vbianco@ub.edu, gfranzese@ub.edu

[1] K. Stokely, M. G. Mazza, H. E. Stanley, G. Franzese, Proc. Natl. Acad. Sci. U.S.A. 107, 1301-1306 (2010).
[2] G. Franzese, F. de los Santos, J. Phys.: Cond. Matt. 21 504107 (2009).
[3] M. G. Mazza, K. Stokely, E. G. Strekalova, H. E. Stanley, G. Franzese, Computer Phys. Comunications 180, 497-502 (2009).
[4] P. Kumar, G. Franzese, and H. E. Stanley, Phys. Rev. Lett. 100, 105701 (2008).
[5] G. Franzese, H. Stanley, J. Phys.: Cond. Matt. 19, 205126 (2007).
[6] G. Franzese, H. Stanley, J. Phys.: Cond. Matt. 14, 2201-2209 (2002).

Turbulent bubble dispersions in microgravity. Drop Tower experiments

Pau Bitlloch, Xavier Ruiz*, Laureano Ramírez-Piscina†, Jaume Casademunt
Departament d'Estructura i Constituents de la Matèria, Universitat de Barcelona
Av. Diagonal, 647, 08028 Barcelona

Dispersed multiphase flows are relevant to many technological applications, often involving turbulent regimes. Examples include particles suspended in liquid or gas flows, droplets in gas flows or bubbly flows. This type of problems combines two of the most challenging problems in fluid mechanics and statistical physics: turbulence and multiphase flows. In particular, both for technological and fundamental interests, it is important to characterize and understand the interaction between the carrying phase and the dispersed phase. This includes not only how the carrying flow affects the transport and spatial distribution of the dispersed phase (one-way coupling) but also how the dispersed phase modifies the nature of the turbulence of the carrying flow (two-way coupling)[1].

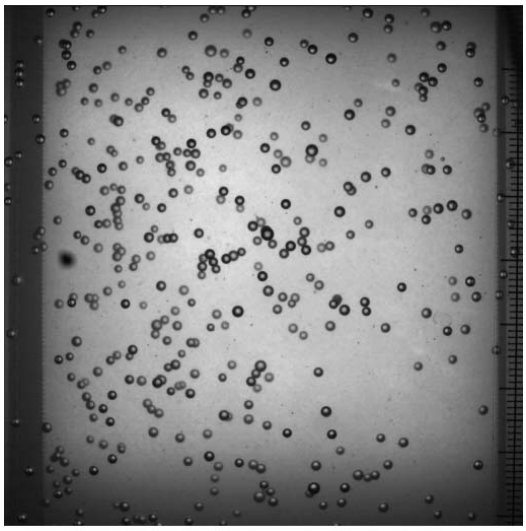

Figura 1. Snapshot of a monodisperse bubble suspension of bubbles of diameter close to 1.5 mm in a turbulent flow in microgravity.

Here we address the problem of turbulent bubbly flows in the absence of gravity. Efficient control of bubble formation and management of turbulent bubbly flows in microgravity environments is indeed crucial for multiple applications in the rocket industry and for life support systems in space. However both practical procedures and fundamental aspects of the physics of bubbly flows in the absence of buoyancy are dramatically different from those in normal gravity, and largely unknown because of lack of data. In particular, the controlled formation and management of a monodisperse bubble suspension is by itself a practical challenge in the absence of buoyancy forces. Recently, a new method of bubble injection has been successfully tested that allows the formation of monodisperse turbulent bubble jets in microgravity[2,3]. Here we present results of a new series of Drop Tower experiments conducted at the ESA facilities at ZARM in Bremen, that exploit the above bubble injection method to create a nearly uniform monodisperse bubble suspension carried by a turbulent duct flow.

The experiment is designed to allow independent control of bubble size, bubble density and the degree of turbulence of the carrying flow. Typical duct Reynolds numbers used are up to 12000. Typical bubble diameter is 1.5 mm, in a duct of 80 cm long and 10x10 cm^2 section, that is, significantly larger than the Kolmogorov turbulent scale, but significantly smaller than the scale of most energetic eddies. Bubble densities keep mean bubble distances comparable to the size of most energetic eddies. This setup is designed to optimize spatial dispersion of bubbles while minimizing the degree of coalescence. The Webber number of bubbles is small enough to maintain the spherical shape, but they cannot be considered as point-like with respect to their interaction with the flow. Under these circumstances, a significant degree of two-way coupling between bubbles and turbulence is expected.

The experiment has proven succesful in creating nearly monodisperse bubble suspensions in turbulent flows in microgravity, under controlled variations of the relevant parameters. This is achieved for the first time. Quantitative information is obtained through the appropriate digital image processing, based on particle tracking methods that yield trajectories of individual bubbles. As a first characterization, we have systematically measured the mean velocity profile of bubbles and the velocity mean square dispersion for different experimental conditions, including variation of Reynolds number, bubble size and bubble density. Preliminary results show that turbulent kinetic energy tends to be decreased by the presence of bubbles for increasing Reynolds number. In addition, our data provide, for the first time, a quantitative characterization of the decay of the so-called pseudo-turbulence, created by the bubbles previously formed with normal gravity, before the drop release.

---

* Universitat Rovira i Virgili
† Universitat Politècnica de Catalunya

[1] S. Balachandar, J. K. Eaton, *Annu. Rev. Fluid. Mech.* 42, 111 (2010)
[2] J. Carrera, X. Ruiz, L. Ramírez-Piscina, J. Casademunt, M. Dreyer, *AIAA Journal* 46, 2010 (2008)
[3] S. Arias, R. González-Cinca, X. Ruiz, L. Ramírez-Piscina, J. Casademunt, *Colloids and Surfaces A: Physicochemical and Engineering Aspects* 365, 52-55 (2010)

A nonlinear mechanism of cell motility in lamellar actomyosin fragments

Carles Blanch-Mercader*, Jaume Casademunt
Departament Estructura i Constituents de la Matèria, Universitat de Barcelona, Av. Diagonal 647, Barcelona, Spain

Directional cell locomotion is one of many biological processes that depends on the development and maintenance of functional asymmetry between parts of a system that were initially equivalent. Morphological instabilities may spontaneously break the symmetry but how the machinery of cell locomotion can couple to the morphology and initiate/sustain motion is not well understood. In actin-based motility on a solid substrate, two main mechanisms of force generation that are powered by the hydrolysis of ATP are present: the collective action of molecular motors (myosin) that exerts contractile forces on the actin network, and the polymerization of actin localized at the cell membrane. Both mechanisms are combined with friction (or adhesion) forces with the substrate to achieve motion.

Lamellar fragments of keratocytes are pieces of the motile machinery of these cells which lack nuclei, microtubules and most organelles, but retain the minimal set ingredients to generate motion. Experimental observations[1] show that the combination of these elementary acto-myosin machinery is indeed capable to generate and sustain spontaneous directional motion through some symmetry-breaking of these lamella. A theoretical understanding of this phenomenon is still lacking. In particular it is not known whether myosin motors play a fundamental role or are essentially auxiliary. Previous theoretical studies[2] based on the theory of active polar gels[3] have shown that a circular lamellar fragment undergoes a morphological instability similar to that of viscous fingering under centrifugal forcing, due solely to polymerization forces, but no sustained motion have been found.

In the present work we demonstrate for the first time that an inherently nonlinear mechanism of cell motility operates combined with the morphological instability of lamellar fragments that is capable to sustain motion, achieving a nontrivial stationary shape of the fragment. We show that this mechanism is operative with only polymerization forces, in the absence of myosin. We base our analysis on the framework of active polar gels in a confined quasi-two-dimensional (Hele-Shaw) geometry. In this regime and in the absence of myosin, the problem can be mapped into a Laplacian free-boundary problem.

The model assumes a polar nematic continuous description of the gel of actin and assumes that the dynamics of the polymerization can be slaved to the slow membrane dynamics. Under the appropriate conditions the flow of actin filaments associated to the treadmilling process can be shown to satisfy Darcy's law and therefore be reduced to a laplacian pressure field with appropriate boundary conditions at the moving boundary[2]. Similarly to the problem of viscous fingering in Hele-Shaw cells[4], the problem can then be formulated by means of conformal mapping techniques. This is a very powerful tool for laplacian problems which allows to explore systematically the weakly nonlinear regime of the instability and thus have an analytical grasp of the nonlinear structure of the problem. At the same time, the method provides a powerful numerical scheme to find solutions deeply into the nonlinear regime.

We have exploited this approach to pursue the instability and have found explicit propagating solutions in the problem without myosin, proving that motion can be sustained with only actin polymerization forces combined with the appropriate morphology of the fragment. We show how a purely linear analysis of the morphological instability misses this point, since motion is only initiated at the nonlinear level. Remarkably, preliminary results also show that an adiabatic reduction of the problem exploiting the separation of time scales close to the instability threshold, may also miss the existence of a finite velocity, implying that the existence of a propagating mode could be associated to a problem of so-called 'asymptotics beyond all orders' such as that of the classical Saffman-Taylor problem[4].

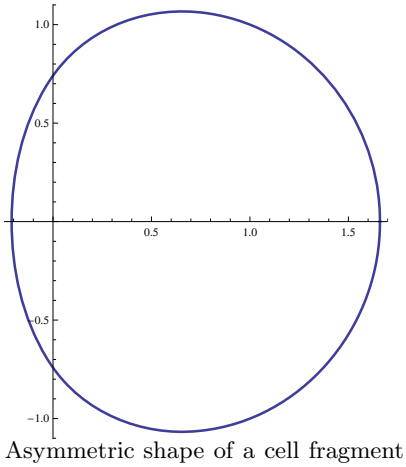

Figura 1. Asymmetric shape of a cell fragment moving at finite velocity from right to left, under the polymerization dynamics of the actin gel, in a 2d confined geometry.

* blanch@ecm.ub.es

[1] A. B. Verkhovsky, T. M. Svitkina, and G. G. Borisy, Curr. Biol. 9, 11 (1999)
[2] A. C. Callan, J.F. Joanny, and J. Prost, Phys. Rev. Lett. 100, 258106 (2008)
[3] K. Kruse, J.F. Joanny, F. Jülicher, J. Prost, and K. Sekimoto, Eur. Phys. J. E 16, 5 (2005)
[4] J. Casademunt, Chaos 14, 809 (2004)

Camino aleatorio, subdifusión, memoria, series divergentes y funciones de Bessel de primera especie

Santos Bravo Yuste*, Enrique Abad+
*Departamento de Física y +Departamento de Física Aplicada
Universidad de Extremadura
06006 Badajoz

La historia de la ciencia nos informa de los numerosos hallazgos matemáticos que, de forma inesperada, surgen del estudio de problemas físicos. En esta comunicación se muestra cómo un problema relacionado con la difusión de cierta clase de caminantes aleatorios lleva al descubrimiento de una nueva forma de definir las funciones de Bessel de primera especie $J_p(x)$ y, además, al descubrimiento de (infinitas) familias de polinomios cuyos miembros $f_{p,n}(x)$ son aproximaciones de $J_p(x)$ que convergen hacia esta función cuando n crece.

El problema físico a resolver consiste en hallar la probabilidad de supervivencia y la distribución espacial de caminantes aleatorios de tiempo de salto continuo (Continuous Time Random Walk, CTRW) donde el tiempo de espera entre saltos está descrito por una distribución de cola larga: $\omega(t) \sim t^{-1-\gamma}$ con $0 < \gamma < 1$. Los caminantes desaparecen cuando llegan a la superficie de una esfera d-dimensional. Un modo eficiente de resolver problemas de este tipo pasa por expresarlos en términos de ecuaciones difusivas. En el caso de distribuciones de cola larga, la ecuación difusiva de la concentración $c(r,t)$ de caminantes es fraccional

$$\frac{d^\gamma c(r,t)}{dt^\gamma} = K\nabla^2 c(r,t),$$

El operador d^γ/dt^γ es una derivada fraccional de Caputo. La ecuación puede resolverse por separación de variables de modo que la solución se expresa como una superposición de modos (sub)difusivos: $c(r,t) = \sum_{n=0}^{\infty} a_n \psi_n(r)\phi_n(t)$, donde $\phi_n(t) \sim t^{-n\gamma}$. La parte espacial de los modos $\psi_n(r)$ es interesante por dos razones. Primero, $\psi_n(r)$ contiene información de la condición inicial para todo n. Por tanto, incluso para $t \to \infty$, la condición inicial del problema puede reconstruirse mediante el análisis de Fourier del modo espacial dominante $\psi_1(r)$. Esto es una manifestación clara de efectos de memoria de largo alcance en problemas con caminantes de cola larga. El segundo aspecto interesante es que $\psi_n(r)$ tienen la forma de una serie de Fourier-Bessel *divergente*. En algunos problemas concretos hemos sido capaces de sumar las series resultantes.[1] Por ejemplo, cuando la concentración inicial de caminantes es constante $c(r,0) = c_0$, la suma de las series divergentes conduce a funciones polinómicas $J_{d/2-1,n}(x)$ definidas por

$$J_{p,n}(x) = \frac{x^p}{2^p p!}\mathrm{Ba}_n^{(p)}\left(\frac{x}{z_p}\right)$$

donde $\mathrm{Ba}_n^{(p)}(x)$ son polinomios de grado $2n$ y z_p es el primer cero de $J_p(x)$. Estos polinomios se generan mediante la aplicación sucesiva del operador integral $\hat{\Lambda}_p[f] = \Lambda_p[f]/\Lambda_p[f]_{x=0}$ sobre la función semilla $f_{p,0}(x) = 1$, siendo

$$\Lambda_p[f] = z_p^2 \int_x^1 \frac{du}{u^{2p+1}} \int_0^u dv v^{2p+1} f(v).$$

Los polinomios $\mathrm{Ba}_n^{(p)}(x)$ o, equivalentemente, las funciones $J_{p,n}(x)$ pueden calcularse de forma recursiva mediante una simple relación algebraica:[2,3]

$$J_{p,n}(x) = \sum_{k=1}^{n} c_{k,n,p}\, J_{p,n-k}(x) - \frac{c_{n,n,p}}{2^p p! z_p^{2n}} x^{2n+p}$$

Los coeficientes numéricos $c_{k,n,p}$ pueden evaluarse también de forma recursiva. Sorprendentemente, resulta que estas funciones constituyen aproximaciones polinómicas de la función de Bessel de primera especie $J_p(x)$. De hecho es posible demostrar que $J_{p,n}(x) \to J_p(x)$ cuando $n \to \infty$, lo cual constituye una definición alternativa de la función $J_p(x)$. Otras elecciones de funciones semilla $f_{p,0}(x)$ conducen a otras familias de funciones $f_{p,n}(x) = \Lambda[f_{p,n-1}(x)]$ las cuales también dan lugar a familias de funciones que tienden a $J_p(x)$ cuando n crece.

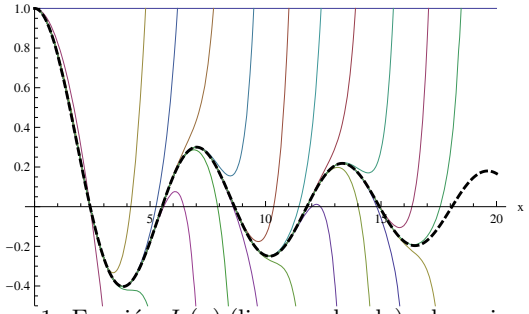

Figura 1. Función $J_0(x)$ (linea quebrada) y las primeras 21 funciones polinómicas $J_{0,n}$ con $n = 0, 1, \ldots 20$ (líneas continuas).

* santos@unex.es
+ eabad@unex.es

[1] S. B. Yuste, R. Borrego and E. Abad E *Phys. Rev.* E **81** (2010) 021105.
[2] S. B. Yuste and E. Abad J. Phys. A: Math. Theor. **44** (2011) 075203.
[3] http://www1.unex.es/eweb/fisteor/santos/Ba/BaPol.htm

Puzzling Out the Mechanical Stability and the Dynamics of the DV Organizer in the Wing Imaginal Disc of Drosophila

Javier Buceta*
Parc Cientific de Barcelona
CoSMo Lab (Computer Simulation and Modeling)
C/ Baldiri Reixac 10-12, 08028 Barcelona, Spain

During the course of development, tissues are subjected to forces that shape the primordia. Within this context we have studied the dynamics and stability of the dorsal-ventral organizer of the wing imaginal disc of Drosophila as cell proliferation advances. Our approach is based on a generalized vertex model to perform in silico experiments that is fully dynamical and takes into account the available experimental data. Thus, in this talk 'll show that our results shed light on the complex interplay between the cytoskeleton mechanics, the cell cycle, the cell growth, and the cellular interactions, in order to shape the dorsal-ventral organizer as a robust source of positional information and a lineage controller. All in all, our results provide novel insights into the developmental mechanisms that drive the dynamics of the DV organizer and set a definition of the so-called Notch fence model in quantitative terms.

* javier.buceta@pcb.ub.es

Grand Canonical Monte Carlo simulations of adsorption using functionalized amorphous silica

Santiago Builes[1,2], Lourdes F. Vega[1,2,3*]

[1] *MATGAS Research Center. Campus UAB, 08193 Bellaterra, Barcelona*

[2] *Instituto de Ciencia de Materiales de Barcelona. (ICMAB-CSIC),Campus UAB, 08193 Bellaterra, Barcelona*

[3] *Carburos Metálicos - Air Products Group. Campus UAB, 08193 Bellaterra, Barcelona*

It is possible to merge the inherent sorptive behavior of amorphous silica with organic groups; increasing the adsorption capabilities of the solid silica. These functionalized materials can be used to capture gases reversibly using adsorption. Effective design of these materials requires a method that can relate the structure of the adsorbent to its performance. This level of understanding can be achieved by using molecular simulations, as they relate the microscopic behavior of the molecules during the adsorption process to the macroscopic behavior of the system, allowing one to search for the best materials for separation purposes.

Although the silica material can be modeled as a rigid structure, the functionalized chains in the surface have to be allowed to move during the adsorption of fluid molecules. The tethered molecules have branched chains. Therefore, for the simulations of adsorption it is necessary to use a method capable of moving branched chains efficiently. The torsion and bending angles in the surface groups can be handled using a coupled-decoupled configurational bias algorithm[1]. Additionally, we used pregenerated Gaussian distributions for the probabilities of generating the bending and torsion angles for the grafted molecules, which are then corrected in acceptance rules[2]. For all the possible substitution sites (surface silanols), we calculate the Rosenbluth factor for replacing the hydroxyl group for the first and second bead in the chain. In our simulations, we consider as the first atom in our chains the oxygen atom bonded to the surface silica.

The results of the simulations are presented for the behavior of CO_2 molecules captured on functionalized amorphous silica. We calculate the adsorption isotherms and isosteric heats of adsorption. As well as specific the adsorption sites, and the orientation and distribution of the adsorbed molecules.

Support for this work was provided by Air Products and the Spanish Government (project CEN2008-1027 CENIT SOST-CO2). Additional support from the Spanish Government (project CTQ2008-05370/PPQ) and by the Catalan Government (2009SGR-666 and a TALENT to S. Builes) is also acknowledged.

---

* vegal@matgas.com

[1] Martin, M. G.; Siepmann, J. I. J Phys Chem B 1999, 103, 4508.

[2] Martin, M. G.; Frischknecht, A. L. Mol. Phys. 2006, 104, 2439

Demographic growth and competition shape the size-area relationship for human languages

Susanna C. Manrubia*, Jacob B. Axelsen, Damián H. Zanette†
Centro de Astrobiología (INTA-CSIC), 28850 Torrejón de Ardoz, Madrid, Spain

According to linguists' classifications, there are about 6.900 languages currently spoken on Earth[1]. Among them, 516 are classified as nearly extinct (with less than 100 speakers), while the ten most abundant languages are spoken by 2.6×10^9 people. The uneven distribution of language sizes, measured as the number of speakers per language, is well fit by a log-normal probability distribution. Its functional form has been explained on the basis of a stochastic multiplicative growth of populations in the last thousand years[2].

We here present results on the correlation between the size P_i of a language i and the area inhabited by its speakers A_i. Our data set includes all living languages plus a set of about 700 recently extinct but listed in the most comprehensible database currently available: the Ethnologue[1]. We have first calculated the distribution of areas corresponding to all languages (see Figure 1) and have observed that it is also compatible with a log-normal function. Further, the representation of the number of speakers as a function of the area of a language yields a dependence $A_i \propto P_i^z$. The analysis of the previous quantities in five different geographic regions (Africa, America, Asia, Europe, and Papua New Guinea) reveals that, while the log-normal shape of the distributions for areas and sizes, as well as the power-law dependence between both quantities are maintained, the parameters of the distributions (average size and dispersion) and the exponent z are region-dependent.

With these data at hand, we have devised a dynamical model for the change of language sizes and areas that relies on the demographic growth of the last ten centuries and includes in an effective fashion the competition for physical space. The model is defined by two rules specifying the growth in language size and language area: 1. At each time step (time is measured in years) the size of a language is multiplied by α_t, a value randomly drawn for each language from a distribution $Q(\alpha)$: $P_{t+1} = \alpha_t P_t$. 2. The change in area for that same language is set to $A_{t+1} = \gamma_t A_t$, where γ_t is chosen as follows. (2.i) If $\alpha_t < 1$, then $\gamma_t = 1$; (2.ii) if $\alpha_t > 1$ but at the same time there is another, randomly chosen population whose growth factor is larger than one, then $\gamma_t = 1$ again. (2.iii) When the size of a language grows and the second population has shrunk it is then possible for the population speaking the first language to increase the area it covers in an amount directly related to the population growth: $\gamma_t = g(\alpha_t)$. The monotonically increasing function $g(\alpha)$ sets the degree of correlation between size and area, and as such determines the value of the exponent z. We assume that, contrary to the population size –which grows exponentially on the average, the total area available is constant. To fulfill this constraint we rescale at each time step the areas, which amounts to dividing by the average value $\bar{\gamma}$ of γ_t: $A_{t+1} \to A_{t+1}/\bar{\gamma}$.

This model admits an analytical treatment in terms of correlated random walks. The parameters of the model can be put in correspondence with the empirical data and some conclusions on the degree of competition between populations in different regions and the effect of the demographic pressure can be extracted.

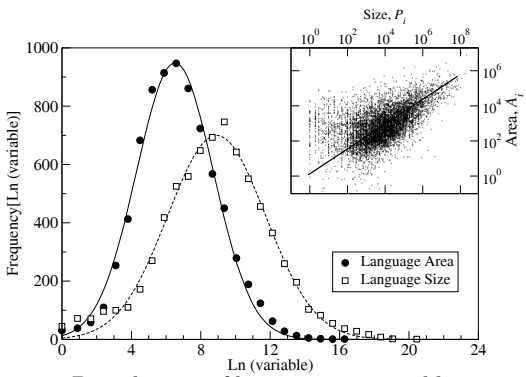

Figura 1. Distribution of language sizes and language areas on Earth. Both functions are compatible with a log-normal probability distribution. Inset: scatter plot of the area A_i and the size P_i of each language i. The two variables are correlated, indicating that the demographic growth conditions to a large extent the area spanned by a language. The straight line has slope 0.7.

* scmanrubia@cab.inta-csic.es
† Centro Atómico Bariloche and Instituto Balseiro, 8400 San Carlos de Bariloche, Argentina

[1] R. G. Gordon, ed., *Ethnologue: Languages of the World*, 15th edition (SIL International, Dallas, 2005). Online version: http://www.ethnologue.com
[2] Zanette, D. H. Demographic growth and the distribution of language sizes. Int. J. Mod. Phys. C **19**, 237 (2008).

A First Passage Time Analysis of Atomic-Resolution Simulations of the Ionic Transport through a Bacterial Porin

Carles Calero*†, Jordi Faraudo†, Marcel Aguilella-Arzo‡
† *Institut de Ciència dels Materials de Barcelona (ICMAB-CSIC), Campus de la UAB, E-08193 Bellaterra, Spain.*
‡ *Biophysics Group, Department of Physics, Universitat Jaume I, 12080 Castelló, Spain.*

Understanding transport of charged solutes across the cell membrane is a problem of paramount importance in biophysics, since it is crucial to regulate many cell functions[1]. This task is undertaken by transmembrane channels, so the characterization of the permeation of charged particles, ions in particular, is essential. In addition, recently there has been a renewed interest to comprehend transport through biological nanochannels for possible applications in biotechnology[2]. Bacterial porins are macromolecular proteins located at the outer membrane that enable the diffusion of small molecules through the lipid bilayer. As porins are well characterized, both structurally and functionally, they represent model systems to study transport through biological nanochannels. In particular, the ionic transport properties of the OmpF porin, a transmembrane nanochannel located at the outer membrane of Escherichia coli, have been extensively studied since the determination of its X-ray structure[3].

In this work, we study the transport of potassium and chloride ions and of water through the OmpF porin[5]. Using the results of extensive all-atom molecular dynamics simulations of the system[4], we employ a first time passage analysis to understand the transport of ions and water through the channel in terms of a one dimensional biased diffusion model. We explore the applicability of such a description and extract the diffusion coefficients and effective forces characterizing the dynamics of the particles in different regions of the channel. These results can be used to describe the ionic transport through the channel with the help of classical 1D models (such as the Piosson-Nernst-Planck approach) with coefficients obtained taking into account all the complexity of the structure of the channel. From our analysis we recognize the appearance and quantify the magnitude of effective entropic forces, which are compared with existing theories[6] on the transport of particles through channels of varying cross section.

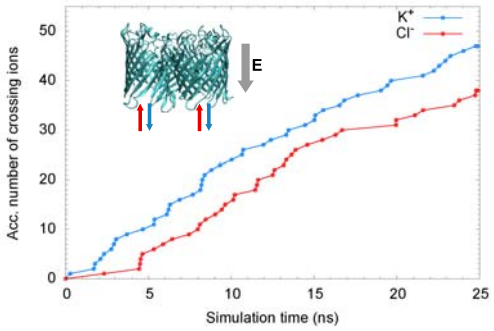

Figura 1. Flux of ions through the OmpF porin, as obtained from molecular dynamics simulations. The inset shows a diagram of the channel, where the directions of the external electric field and of the flux of Cl^- and K^+ ions are represented.

* ccalero@icmab.es

[1] B. Hille, *Ion Channels of Excitable Membranes* (Sinaure, Sunderland, 2001).
[2] G. Maglia, A. J. Heron, W. L. Hwang, M. A. Holden, E. Mikhailova, Q. Li, S. Cheley and H. Bayley, *Nature Nanotechnology* **4**, 437 (2009).
[3] Cowan, S. W., R. M. Garavito, J. N. Jansonius, J. A. Jenkins, R. Karlsson, N. König, E. F. Pai, R. A. Pauptit, P. J. Rizkallah, J. P. Rosenbusch, G. Rummel and T. Schirmer, *Structure* **3**, 1041 (1995).
[4] J. Faraudo, C. Calero and M. Aguilella-Arzo, *Biophys. J.* **99**, 2107 (2010).
[5] C. Calero, J. Faraudo, M. Aguilella-Arzo, accepted in *Phys. Rev. E* (preprint at arXiv:1011.3952v1 [cond-mat.soft]).
[6] R. Zwanzig, *J. Phys, Chem.* **96**, 3926 (1992). D. Reguera and J. M. Rubí, *Phys. Rev. E* **64**, 061106 (2001).

Solvation properties of mono- and di-valent cations in water from DFT molecular dynamics simulations

Ausias-March Calvo[†*], Elvira Guàrdia[†], Marco Masia[‡]
[†] *Departament de Física i Enginyeria Nuclear, Universitat Politécnica de Catalunya, Campus Nord, B4-B5 08034 Barcelona, Spain*
[‡] *Dipartimento di Chimica, Università degli Studi di Sassari, Sardinian Laboratory for Computational Materials Science SLACS (INFM-CNR) and INSTM, Via Vienna 2, 07100 Sassari, Italy*

Structural and dynamical properties of the solvation of mono- and di-valent cations in water at ambient conditions were studied using density functional theory based molecular dynamics simulations. The simulated systems were made of one single ion and 96 water molecules. The ions studied include Li^+, Na^+, K^+, Mg^{2+} and Ca^{2+}. In each case, the length of the cubic box was computed in order to get a density $\rho = 1 g/cm^3$. Periodic boundary conditions were applied. The simulations were performed using the Car-Parrinello scheme[1] as implemented in the CPMD package.[2] The BLYP density functional[3,4] was used for the electronic structure calculations. The cut-off for the wavefunctions was set to 80 Ry, the time step was set to 4 a.u. and the fictitious electron mass was chosen to be 400 a.m.u. Every five time steps, the Wannier centers' coordinates[5,6] were computed (see Fig. 1). A similar procedure was previously used in Ref. 7 to study ion and molecular polarization of halides in water.

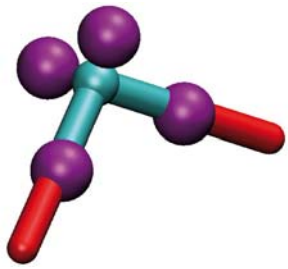

Figura 1. Electronic estructure of the water molecule. Bars represent the oxygen-hydrogen bonds, purple spheres correspond to the location of the electronic pairs.

Production runs of 15 ps in the microcanonical ensemble followed NVT equilibration runs of 3 ps where the temperature was set to 330 K; the initial configurations were generated with classical molecular dynamics simulations of 200 ps. Fig. 2 shows the computed ion-oxygen radial distribution functions. A thorough analysis of the structure and dynamic properties of the first solvation shell molecules will be reported.

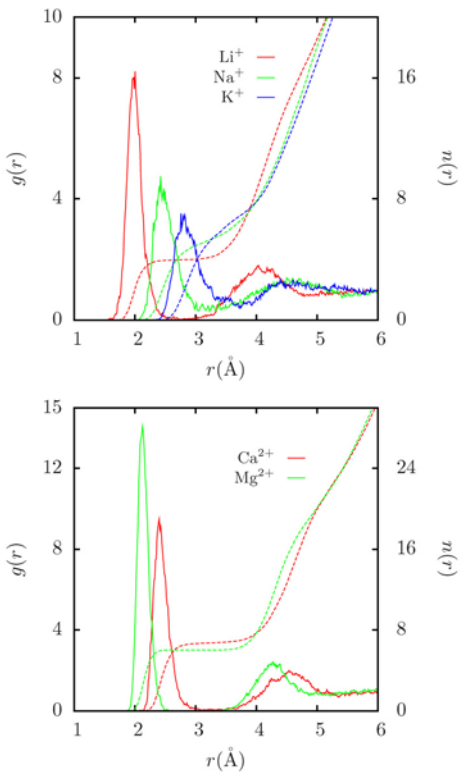

Figura 2. Ion-oxygen radial distribution functions (solid lines) and running coordination numbers (dashed lines).

* ausias.march@upc.edu

[1] D. Marx and J. Hutter, in *Modern methods and algorithms of quantum chemistry*, John von Neumann Institute for Computing, Forschungszentrum Julich, pp.329–477, 2000.
[2] `CPMD version 3.11`,Copyright IBM Corp. 1990-2006, MPI für Festköorperforschung Stuttgart 1997-2001. For downloads see `http://www.cpmd.org` (accessed Dec. 1, 2009).
[3] A. D. Becke, Phys. Rev. A **38**, 3098 (1988).
[4] C. Lee, W. Yang, and R. G. Parr, Phys. Rev. B **37**, 785 (1988).
[5] N. Marzari and D. Vanderbilt, Phys. Rev. B **56**, 12847 (1997)
[6] P. L. Silvestrelli, and M. Parrinello, Phys. Rev. Lett. **82**, 3308 (1999); *erratum*: Phys. Rev. Lett. **82**, 5415 (1999).
[7] E. Guardia, I. Skarmoutsos, and M. Masia, J. Chem. Theory Comput. **5**, 1449 (2009).

Estudio del flujo sanguíneo en una arteria estenótica

Marta Lage[1], Beatriz Rastrollo[1], Alexis Cantizano[1], Mario Castro[2]
[1] *Departamento de Ingeniería Mecánica. Universidad Pontificia Comillas. Madrid, España.*
[2] *Grupo Interdisciplinar de Sistemas Complejos (GISC). Universidad Pontificia Comillas. Madrid, España.*

La Hemodinámica es la parte de la Biomecánica que estudia el flujo sanguíneo en el sistema circulatorio, basándose en los principios físicos de la dinámica de fluidos[1]. Estudia el movimiento de la sangre (campos de velocidades y presiones) y las fuerzas que genera el flujo en los elementos con los que interactúa (vasos sanguíneos y corazón).

En este trabajo se simulará el flujo sanguíneo en una arteria con estenosis. La estenosis es un estrechamiento localizado de la arteria causado típicamente por aterosclerosis[2]. La formación de placa aterosclerótica en arterias coronarias depende, entre otras variables, de la hemodinámica del sistema arterial.

Mediante el uso de software de fluidomecánica computacional (CFD, por sus siglas en inglés), este estudio pretende proporcionar información relevante acerca de las variaciones de presión y distribución de tensiones en una arteria con estenosis, ayudando así a entender, predecir y solucionar este tipo de enfermedades vasculares. Se utilizará la herramienta OpenFOAM, que es un software de cálculo en 3D que puede simular y resolver numéricamente flujos complejos incluyendo reacciones químicas, turbulencia y transmisión de calor, problemas estructurales o incluso electromagnetismo[3].

El trabajo consta de cuatro etapas estándar[4]:

1. **Construcción del modelo:** En esta etapa se define la geometría del problema que se quiere estudiar. En nuestro caso, el flujo en una arteria estenótica. Por simplicidad, supondremos que la arteria es rígida (y por tanto que se pueden despreciar los efectos de la elasticidad de la misma).

2. **Generación del mallado:** El software OpenFOAM es un software que implementa distintos algoritmos de resolución de las ecuaciones de Navier-Stokes basados en volúmenes finitos. Por esta razón, la construcción de un mallado adecuado es crucial para la fiabilidad de los resultados.

3. **Solución del problema:** Como se ha mencionado, OpenFOAM integra el problema mediante la técnica de volúmenes finitos. La estabilidad de estos esquemas depende del número de Reynolds del mismo, por lo que se estudiarán la convergencia de la solución en situaciones biomédicamente realistas.

4. **Visualización y extracción de información:** Por último, se analizarán los resultados del paso 3 tanto gráficamente (visualización del campo de presiones o del campo de velocidades en el interior de la arteria) así como mediante el establecimiento de criterio de riesgo médico (relacionados, en su gran mayoría, con magnitudes como el stress en las paredes de la arteria, la oscilación del *stress* o el tiempo de residencia del fluido en las distintas partes de la geometría del mismo).

La validez del modelo numérico se evaluará comparando con resultados analíticos en situaciones sencillas (como el flujo de Womersley para un fluido newtoniano en un conducto cilíndrico en régimen laminar oscilatorio) y con datos experimentales extraídos de estudios biomédicos[5].

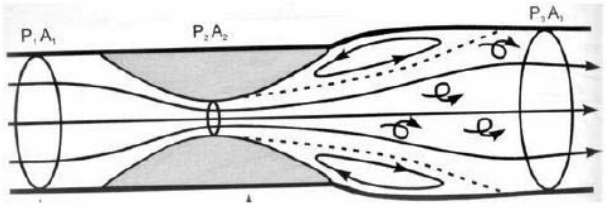

Figura 1. Diagrama esquemático del flujo en las proximidades de una estenosis.

* alexis.cantizano@dim.icai.upcomillas.es

[1] M. Thiriet, *Biomechnics and Mechanics of Blood Flows (vol I)*, (Springer Verlag, 2007).
[2] F. Loth, P. F. Fischer, and H. S. Bassiouny, Ann. Rev. Fluid Mech. **40**, 367 (2008).
[3] OpenFOAM se puede descargar de la página web `http://www.openfoam.com/`.
[4] C. A. Taylor and J. D. Humphrey, Comp. Meth. Appl. Mech. Eng. **198**, 3514 (2009).
[5] S. E. Logan, IEEE Trans. Biomed. Eng. **4**, 327 (2007).

Thermodynamics of feedback controlled systems

Francisco J. Cao*
Departamento de Física Atómica, Molecular y Nuclear, Universidad Complutense de Madrid, Avenida Complutense s/n, 28040 Madrid, Spain

We compute the entropy reduction in feedback controlled systems due to the repeated operation of the controller. This was the lacking ingredient to establish the thermodynamics of these systems, and in particular of Maxwell's demons. We illustrate some of the consequences of our general results by deriving the maximum work that can be extracted from isothermal feedback controlled systems. As a case example, we finally study a simple system that performs an isothermal information-fueled particle pumping.

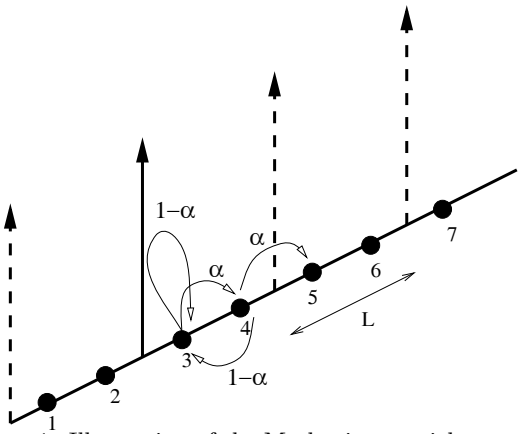

Figura 1. Illustration of the Markovian particle pump with $n = 2$ lattice sites between barriers. This is a simple example of a feedback controlled system that extracts useful work from the entropy reduction due to the information about the system used by an external feedback controller.

* francao@fis.ucm.es

[1] F. J. Cao, M. Feito, *Thermodynamics of feedback controlled systems*, Phys. Rev. E 79, 041118 (2009).

Scale invariance in marine population dynamics

José A. Capitán*[1], Gustav W. Delius†[2]
[1] *Dept. Enginyeria Informàtica i Matemàtiques, Universitat Rovira i Virgili, 43007 Tarragona, Spain*
[2] *Dept. of Mathematics, University of York, York, United Kingdom*

A special property of the open sea that has not been exploited yet from a theoretical point of view in the context of population dynamics is its approximate physical scale invariance. The open sea looks similar at a wide range of scales. Over many orders of magnitude there are no physical features and no strong physical principles that would single out a particular intermediate scale. This kind of scale invariance is not present in terrestrial environments, where not only the geographical constraints set up a scale, but in addition the effects of gravity quickly become important for larger organisms.

As for the marine ecosystem, the main observational evidence for approximate scale invariance is that the equilibrium size distribution of organisms in the open ocean is approximately given by a power law, valid over almost ten orders of magnitude. Several theoretical models have been proposed in the past to derive this steady-state size spectrum.[1–3] In this contribution we interpret the observed size spectrum as a consequence of the scale invariance of the underlying population dynamics. Hence we use this symmetry in the construction and solution of a size-structured dynamical population model. Starting from a Markov model encoding the basic processes of predation, reproduction, maintenance (respiration), and intrinsic mortality (see FIG.1), we derive a partial integro-differential equation describing the dependence of abundance on weight and time. Our model represents an extension of earlier models based on the McKendrick-von Foerster equation.[3] The model is scale-invariant provided the rate functions of the elementary stochastic processes fulfill precise scaling properties. We determine the steady-state power-law solution, whose exponent is determined by the relative scaling between the rates of the density-dependent processes predation and the rates of the density-independent processes reproduction, maintenance, and mortality.

While the population dynamics leads to a power-law steady-state solution, its dynamical stability is not necessarily ensured. The conditions under which this steady state is an attractor are much less well understood. This is an important issue, because the knowledge of what makes marine ecosystems resilient or susceptible to external pressure has become extremely relevant at a time of overexploitation of marine resources. We study the stability of the steady state against small perturbations and find that inclusion of maintenance respiration and reproduction in the model has a strong stabilizing effect (FIG.2). Furthermore, the steady state is unstable against a change in the overall population density unless the reproduction rate exceeds a certain threshold.[4]

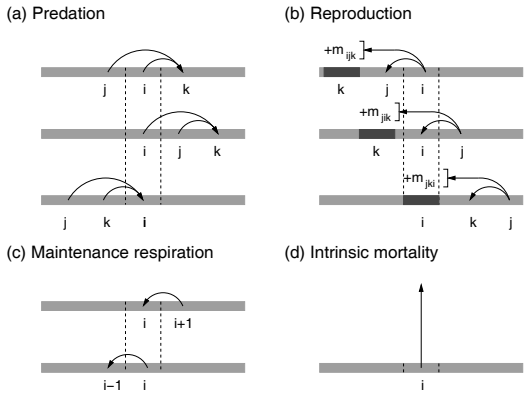

Figura 1. Individual stochastic processes involved in the model that affect the number of organisms in different weight brackets. Arrows indicate the movement of individuals between weight brackets as a consequence of each process.

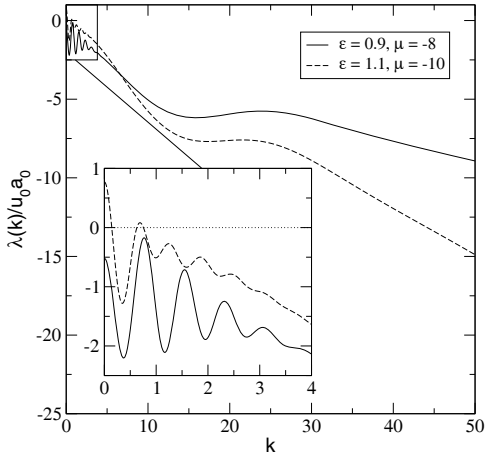

Figura 2. Perturbations of the steady state can be studied using standard Fourier analysis. The inclusion of reproduction and maintenance processes stabilizes the steady state over the whole set of wavenumbers.

* jcapitan@gmail.com
† delius@york.ac.uk

[1] J. Camacho and R. V. Solé, Europhys. Lett. **55**, 774 (2001).
[2] E. Benoît and M.-J. Rochet, J. Theor. Biol. **226**, 9 (2004).
[3] S. Datta, G. W. Delius, and R. Law, Bull. Math. Biol. **72**, 1361 (2010).
[4] J. A. Capitán and G. W. Delius, Phys. Rev. E **81**, 061901 (2010).

Harmonic vibration modifies the Turing pattern morphology from White-Spots to Black-Spots

Jorge Carballido-Landeira*, Jacobo Guiu-Souto, Alberto P. Muñuzuri
Grupo de Física Non Lineal. Facultade de Física
Universidade de Santiago de Compostela
E-15782 Santiago de Compostela, Spain

We investigate the effects of a mesoscopic perturbation on the pattern formation. This perturbation is achieved by adding a vibrational potential term to the free Hamiltonian of the system. We try to elucidate if this perturbation is able to modify the dynamics of Turing patterns on reaction-diffusion system. By using numerical simulations we observed two main effects induced by the forcing: changes from white to black spots towards stripe and labyrinthine configuration and moreover, modifications in the Turing wavelength, mostly observed in White Spots with Hexagonal order.

The morphology of Turing patterns was analyzed by using topological functionals, which allow us to identify the transition between the different Turing scenarios with quantitative measurements of digitized grey-scales images.

* jorge.carballido@rai.usc.es

[1] K. R. Mecke *Phys. Rev. E* 53 04794 (1996).
[2] J. Guiu-Souto, J. Carballido-Landeira, V. Pérez-Villar and A. P. Muñuzuri *Phys. Rev. E* 82 066209 (2010).
[3] M. Okamoto and S. Kondo *Nature Comunications* 1 66, 1071 (2010).

Detección automática de palabras clave en textos cortos

C. Carretero Campos*, P. Bernaola-Galván, A. V. Coronado y P. Carpena
Departamento de Física Aplicada II, Universidad de Málaga. 29071 Málaga

El problema de la detección automática de palabras clave en textos literarios a partir de sus propiedades estadísticas ha sido abordado de maneras muy variadas. La primera aproximación propuesta por Luhn[1] estaba basada en un análisis de la frecuencia de ocurrencia de las palabras en el texto. Sin embargo, métodos que sólo consideran la frecuencia con la que aparece cada palabra funcionan correctamente si se compara con una colección de documentos de referencia (corpus), pero no son suficiente para un único documento. Si aleatorizamos el texto conservamos la frecuencia con la que aparece cada palabra, pero se destruye la información. De modo que la relevancia de una palabra vendrá determinada no por la palabra en sí misma, sino por cómo se distribuye a lo largo del texto. Esta es la hipótesis presentada en Ortuño *et al.*[2], dónde se comprueba que existe una relación entre la cantidad de información que proporciona una palabra y su distribución espacial en el texto: las palabras relevantes tienen una distribución inhomogénea y están concentradas en determinadas regiones del texto formando clusters, mientras que las irrelevantes están distribuidas de manera aleatoria. Así obtienen un método basado en la distribución de las distancias entre apariciones sucesivas de las palabras que detecta adecuadamente las palabras relevantes del texto, pero que presenta algunas debilidades que pueden conllevar identificaciones incorrectas. En Carpena *et al.*[3], se realiza una mejora significativa del método de Ortuño *et al.*[2], combinando la información proporcionada por el clustering de una palabra con la de su frecuencia. Sin embargo, estos métodos no funcionan demasiado bien en textos cortos.

En este trabajo, proponemos incluir la información contenida en las fronteras del texto, que permiten detectar un único cluster; y mejoramos la estimación estadística para palabras con frecuencia pequeña. Al mismo tiempo, con el objetivo de evitar que el singular y el plural de una palabra sean consideradas palabras distintas, los identificamos implementando un algoritmo que contemple las reglas de formación de plurales en inglés, asi como las principales excepciones. Estas mejoras se implementan en la medida de relevancia C_0.

Por otro lado, también se habían propuesto otro tipo de técnicas. Recientemente, Herrera and Pury[4] hacen uso de la entropía de Shannon para definir una medida de relevancia(E_{nor}) basada en el contenido de información de la secuencia de ocurrencias de cada palabra y que necesita una partición previa para su evaluación. Usando "The Origin Of Species" de Charles Darwin como corpus y los capítulos como partición natural, esta medida resultaba ser tan buena o mejor que otras publicadas previamente, que tomamos nosotros como referencia para evaluar la bondad de nuestras mejoras. La bondad de la medida se evalúa con un glosario elaborado manualmente que contiene las palabras relevantes del texto.

Como una de las principales características deseables en un detector de keywords es que funcione correctamente cuando el texto a analizar es corto, consideraremos ese caso. La frecuencia de aparición de las palabras es pequeña lo que complica la estimación estadística. Sin embargo, los textos cortos resultan ser de gran interés porque en él se encuadrarían, por ejemplo, los artículos científicos y las páginas web. Tomamos como modelo de texto corto el capítulo IV de "The Origin Of Species" para poder disponer de un glosario que nos permita comparar la precisión de cada método. Definimos $Pr(n)$ como el número de palabras del glosario entre las n primeras del ranking de relevancia y observamos en la figura 1 como de las 50 primeras palabras que C_0 detecta como relevantes un 60% lo son, mientras que para E_{nor} (considerando los párrafos como partición) sólo un 32%. Un análisis más profundo muestra que los resultados obtenidos para E_{nor} dependen de la partición considerada y que los de C_0 son tan buenos o mejores, tanto en un texto largo y sobre todo en un texto corto, y sin necesitar previamente una elección arbitraria de la partición usada.

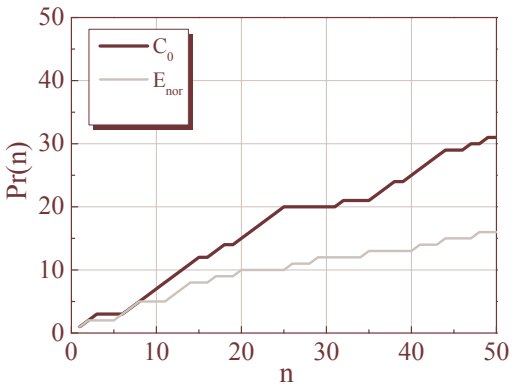

Figura 1. $Pr(n)$ frente a n para las medidas E_{nor} y C_0.

* ccarretero@uma.es

[1] H. P. Luhn, IBM J. Res. Devel. **2**, (1958) 159
[2] M. Ortuño, P. Carpena, P. Bernaola-Galván, E. Muñoz and A. M. Somoza, Europhys. Lett. **57**, (2002) 759
[3] P. Carpena, P. Bernaola-Galván, M. Hackenberg, A. V. Coronado, and J. L. Oliver, Phys. Rev. E **79**, (2009) 035102(R)
[4] J. P. Herrera and P. A. Pury, Eur. Phys. J. B **63**, (2008) 135

Electrocinética DC de suspensiones de partículas concentradas en medios electrolíticos generales

Félix Carrique[1*], Emilio Ruiz-Reina[2]
[1] *Física Aplicada I, Universidad de Málaga, 29071 Málaga (Spain)*
[2] *Física Aplicada II, Universidad de Málaga, 29071 Málaga (Spain)*

En este trabajo se estudia la respuesta de una suspensión coloidal concentrada de partículas esféricas en un medio electrolítico genérico en presencia de un campo eléctrico estático. Se estudia en particular la velocidad estacionaria de las partículas por unidad de campo eléctrico aplicado, o movilidad electroforética. Nuestro modelo tiene en cuenta: 1) los contraiones liberados por las partículas cuando se cargan en solución; 2) los iones H^+ y OH^- de la disociación del agua; 3) los iones producidos por la contaminación del CO_2 atmosférico disuelto en el medio; 4) los iones de un electrolito añadido externamente a la suspensión. El modelo presentado en este trabajo está basado en una nueva descripción realista de la doble capa eléctrica de equilibrio que rodea a las partículas, recientemente desarrollada por los autores[1] así como en modelos electrocinéticos DC[2,3] que incorporan los puntos anteriores 1 a 3. Aquí estamos interesados en los efectos asociados con la presencia de una sal externa añadida al sistema (punto 4). Se conoce que para suspensiones desionizadas realistas, los efectos sobre las propiedades electrocinéticas de las suspensiones que incluyen las consideraciones de los puntos 1 a 3 son enormes. De aquí nuestro interés en extender estos estudios a medios salinos, que incluyen a los desionizados como caso límite cuando la sal externa tiende a cero. El modelo está basado en la estadística clásica de Boltzmann, las apropiadas reacciones químicas, las ecuaciones electrocinéticas estándar y la aproximación de modelo de celda para tener en cuenta las interacciones electrohidrodinámicas entre las partículas en estos medios concentrados. Hemos aplicado el modelo al estudio de la movilidad electroforética DC de las partículas y a la conductividad eléctrica DC para diferentes concentraciones de partículas, densidades de carga superficial de las mismas y concentración del electrolito añadido. Se puede concluir que la presencia de una concentración moderada de sal apantalla la mayoría de los efectos asociados con los puntos 1 a 3, cruciales para medios desionizados, como cabría esperar. Sin embargo, si la concentración de sal es baja se observa que: i) la contaminación por CO_2 juega un papel excepcionalmente relevante para bajas concentraciones de partículas en la suspensión; ii) los contraiones añadidos por las partículas tiene un papel crucial si la concentración de partículas es alta, apantallando progresivamente los efectos de la sal. En el futuro próximo se extenderá el estudio a la electrocinética AC para poder cuantificar en cada rango de frecuencias del campo eléctrico el peso de las diferentes contribuciones a la respuesta electrocinética.

* carrique@uma.es

[1] E. Ruiz-Reina and F. Carrique, J. Phys. Chem. B **112**, 11960 (2008).
[2] F. Carrique and E. Ruiz-Reina, J. Phys. Chem. B **113**, 8613 (2009).
[3] F. Carrique and E. Ruiz-Reina, J. Phys. Chem. B **113**, 10261 (2009).

Self-similarity and chaos in coupled ratchets. Unfolding the complexity of cooperative Brownian motors

Carles Blanch-Mercader, Javier G. Orlandi, Jaume Casademunt
Departament d'Estructura i Constituents de la Matèria
Universitat de Barcelona
08028 Barcelona

Brownian ratchets may be considered as a paradigm of statistical physics where thermal noise rectification under nonequilibrium conditions leads to directed motion and power generation. Some molecular motors in biology, such as monomeric kinesin, are known to exploit directly this noise-based mechanism. Recently it has been shown that one of the reasons to adopt such mechanism in the biological context might be that the ratchet structure is particularly fit to cooperative action. In particular, it has been proved that motors are capable to spontaneously associate and dramatically enhance their collective efficiency, in particular when noise is weak[1,2]. Remarkably a motor cluster is capable to produce a finite power in the limit of vanishing noise intensity, when individual motors would be powerless. This is possible whenever two main conditions are satisfied: (i) the external force is unequally loaded to the participant motors, and (ii) the ratchet states change independently for each motor. These conditions are naturally satisfied in the biological context of intracellular traffic of soft cargoes and affect crucially the collective behaviour of motors. In order to isolate and gain understanding on the underlying deterministic mechanism of motor cooperativity, we study the weak noise limit of the two-motor problem.

We solve exactly the problem of two interacting motors when an external force is applied to the first one, in the limit of vanishing noise. The motors switch states between a fully asymmetric sawtooth potential and a flat potencial. We show that this situation is particularly fit to the collective improvement of the motor performance, and because of its simplicity it can be considered as a paradigm of cooperativity. We show that the problem can be mapped into a random walk on a complex directed graph. The topological structure of the graph depends sensitively on physical parameters, in particular as the external force is varied. Consequently the velocity-force curve of the motor pair becomes fractal. Using graph theory techniques we obtain general properties of the dynamics of the system. We show that the graphs may be finite or infinite and we are able to solve exactly the random-walk statistics in most regions of parameter space. We can thus determine the exact velocity-force curves in most regimes, exhibiting fractal properties.

The sampling of the graph that defines the joint dynamics of the motor pair can in turn be seen as a random alternation of two deterministic evolutions. The respective Poincaré sections of those define two circle maps which are piece-wise linear. The multi-parametric bifurcation structure of those maps is analyzed, showing a complex structure that includes the so-called *big bang* bifurcations[3]. Remarkably, while the two involved maps cannot produce chaos by themselves, the stochastic combination of the two is capable to generate chaos. In this scenario, although the dynamics is stochastic, the phase space of the system can be hierarchically organized in a tree-like structure which is generated by a chaotic map.

In summary, we show that underlying an apparently simple mechanism of cooperativity of coupled ratchets there is a complex mathematical structure. Combining graph theory and concepts from dynamical systems we identify a variety of complex dynamical behaviour, including a high sensitivity response to the external force, self-similar behaviour, and the signature of deterministic chaos in the inner structure of a stochastic system.

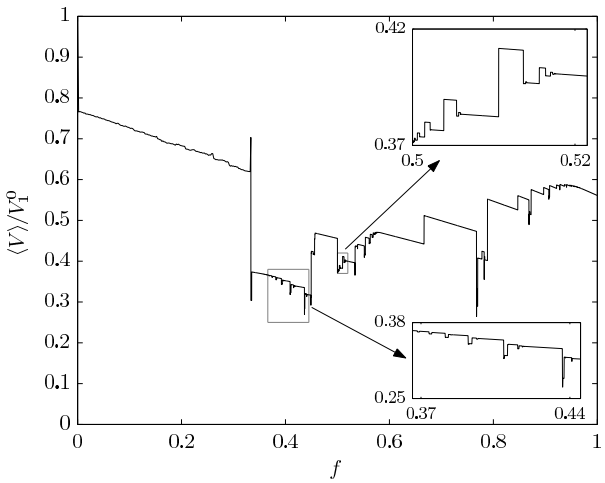

Figura 1. Fractal velocity-force curve. We plot the mean velocity of a motor pair normalized by the velocity of one motor at zero load vs the force normalized to the stall value. The curve in exact for $1/3 \leq f \leq 1$. For $0 < f < 1/3$ it is continuous in a subset of irrationals and the set of discontinuities is infinite with zero measure. The values on this region are approximated by Monte Carlo sampling.

[1] J. Brugués, J. Casademunt, Phys. Rev. Lett. **102**, 118104 (2009)
[2] J. G. Orlandi, C. Blanch-Mercader, J. Brugués, J. Casademunt, Phys. Rev. E **82**, 061903 (2010)
[3] V. Avrutin, M. Schanz, Nonlinearity **19**, 531-552 (2006)

Laminar oscillatory flow of Maxwell and Oldroyd–B fluids: Theoretical analysis and experiments

L. Casanellas*, J. Ortín†
Departament d'Estructura i Constituents de la Matèria
C. Martí Franquès 1, Facultat de Física, Universitat de Barcelona
08028 Barcelona

Wall-bounded oscillatory flows of newtonian and complex fluids are present in many different practical situations. Pulsating flows are of particular interest in physiology in connection with the respiratory and circulatory systems of living beings, in industrial processes such as fluid pumping, secondary oil recovery and filtration, in acoustics, and in the rheological characterization of fluid properties.

In this work we revisit the generic problem of wall–bounded oscillatory flow of a viscoelastic liquid. We focus on the periodic steady state of laminar flow, at small Re. In this approximation the governing equations are linear and therefore accessible to analytical treatment. We consider as constitutive equations the upper convected Maxwell model (UCM) and the more general Oldroyd–B model, that includes a newtonian solvent contribution. We first consider the fluid motion induced by the synchronous oscillation of two parallel infinite walls, each giving rise to a traveling transverse shaer wave. The flow is characterized by the damping length of the amplitude of oscillation of the shear waves, x_0, and their wavelength, $\lambda_0/(2\pi)$. For a Newtonian fluid these two lengths are equal and coincide with the thickness of the boundary layer, leading to overdamped shear waves. However, for viscoelastic fluids $x_0 > \lambda_0/(2\pi)$ and underdamped shear waves can propagate effectively before they are attenuated[1]. In 'narrow' systems (small setup dimensions compared to x_0) the viscoelastic shear waves extend through the whole system and superpose themselves originating an interference pattern inside the fluid domain. This leads to a resonant behaviour with a huge increase of the velocity amplitude at particular frequencies. Computing the phase lag between the velocity at the center of the geometry and the acceleration of the moving plates we see that they move in–phase at these frequencies.

A similar behaviour is obtained in the oscillatory flow within an infinitely long straight cylinder of radius a, induced by the oscillatory motion of a bottom piston and a top endwall. We derive the expression for the vertical velocity along the radial coordinate inside the tube in terms of the characteristic lengths of the corresponding shear waves. For Maxwell fluids the resonances are prominent in 'narrow' systems and the velocity profiles show a complex inflectional structure, with multiple concentric cylindrical layers. However, as we add an increasing newtonian solvent contribution to the model, measured by the viscosity ratio $X = \eta_s/\eta$, the resonances progressively disappear and the magnitude of the velocity and shear rate are drastically reduced (Fig. 1)[2].

We compare our theoretical predictions to experimental results that we have obtained for oscillatory flow in a cylindrical tube with large aspect ratio. The experimental velocity profiles are measured for a wormlike micellar solution, CPyCl-NaSal [100:60], using a time resolved PIV technique. At low amplitudes and frequencies of the driving oscillation the profiles follow the predicted trends. However, at high velocity amplitudes (high shear rates) the experimental profiles deviate from the theoretical predictions, as a result of the non–linearities of the fluid rheology in this regime.

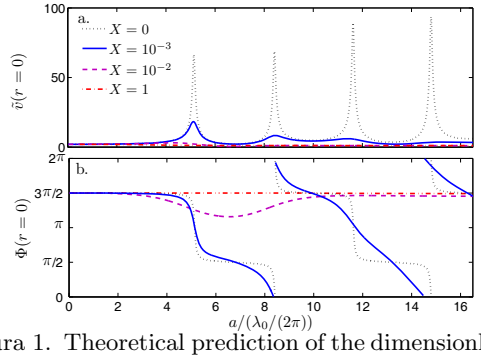

Figura 1. Theoretical prediction of the dimensionless velocity magnitude at the tube axis (a) and time phase lag between the fluid velocity at the tube axis and the pressure gradient (b) vs. the dimensionless ratio $a/(\lambda_0/(2\pi))$, for an Oldroyd-B fluid. Different lines correspond to different values of the viscosity ratio X.

* laurac@ecm.ub.es
† ortin@ecm.ub.es

[1] Mitran, S.M., Forest, M.G., Yao, L., Lindley, B. & Hill, D.B. 2008. *J. Non-Newtonian Fluid Mech.* **154**, 120–135.
[2] Andrienko, Y.A., Siginer, D.A. & Yanovsky, Y.G. 2000. *Int. J. Non–Linear Mech.* **35**, 95–102.

Control of spiral wave dynamics by low energy stimuli

Jorge Castro[1], Matias Rafti[2], Flavio H. Fenton[3], Jorge Carballido-Landeira[1], Alberto P. Muñuzuri[1*]

[1] *Group of Non Linear Physics Fac. de Fisicas. Universidade de Santiago de Compostela. Campus Sur. 15782 Santiago de Compostela. Spain.* [2] *INIFTA. Fac. Cs. Exactas. Dpto. de Química.— Univ. Nac. de La Plata. Argentina.* [3] *Dept. of Biomedical Sciences. Cornell University, Ithaca, NY, USA*

Atrial fibrillation (AF) is the most common sustained cardiac arrhythmia worldwide affecting 2.2 million people in the United States alone. Complications associated with chronic AF include increased risk for both thromboembolism and stroke. Left untreated, paroxysmal AF often progresses to permanent AF, which is resistant to therapy. Although underlying anatomic or pathophysiological factors may fuel this progression, AF itself may lead to its own perpetuation through electric, structural, and metabolic remodeling of atrial tissue. The realization that AF begets AF has led to management strategies that are designed to avoid the progression of AF by reducing the frequency and duration of AF episodes [1]. Among these strategies, a new method to terminate fast atrial tachycardias and AF has been recently developed within the context of animal experimentation [2]. In this method, electrodes located at a small distance from the heart deliver a train of low-voltage shocks at a rapid rate. The idea underlying is that during the low-energy shocks, small intrinsic conductivity discontinuities behave as internal "virtual"electrodes that actually serve as activation sites (or secondary sources) if the field strength depolarizes the tissue beyond the excitation threshold. This method presents many advantages comparing with previous methods.

Although the method has been successfully tested in laboratory animals, a deep understanding of the mechanisms underlying is still to be done. In such a sense, we will present in this contribution results aiming to understand the previous mechanism in a completely different system although equivalent in many senses [3]. We will analyze the same problem within the context of chemical pattern forming chemical reactions (Belousov-Zhabotinsky reaction). Effectively, BZ reaction is considered to be a paradigm for pattern formation research as the mechanisms here studied can be easily extrapolated to more complex systems such as the cardiac tissue. Spiral waves are believe to be responsible of Atrial Fibrilation in the heart and can be easily observed in BZ reaction. In this system, we apply low-energy stimuli and demonstrate the effectiveness of the method. The presence of conductivity discontinuities in the system will also be modeled and the results agree with the experiments in cardiology.

Experimental results and numerical simulations will present clearly the deep mechanism underlying.

---

* uscfmapm@cesga.es

[1] Waktare JE. Cardiology patient page: atrial fibrillation. Circulation. 2002;106:14-16. Heart disease and stroke statistics: 2007 update. Circulation. 2007;115: e69-e171. Nattel S, Opie LH. Controversies in atrial fibrillation. Lancet. 2006;367: 262-272. Wijffels M, Kirchhof C, Dorland R, Allessie MA. Atrial fibrillation begets atrial fibrillation: a study in awake chronically instrumented goats. Circulation. 1995;92:1954-1968.

[2] Fenton FH, Luther S, Otani NF, Cherry EM, Pumir A, Bodenschatz E, Krinsky V, Gilmour RF Jr. ermination of atrial fibrillation using pulsed low-energy far field stimulation Circulation 120, 467-476: 2009

[3] Matias Rafti, Flavio H. Fenton and Alberto P. Muũzuri, in preparation.

First steps in the study of unconventional magnetic fluids

Juan J. Cerdà*, Pedro A. Sánchez, Tomás Sintes
Instituto de Física Interdisciplinar y Sistemas Complejos, IFISC (CSIC-UIB). Universitat de les Illes Balears. E-07122 Palma de Mallorca, Spain.

Unconventional magnetic fluids are suspensions in which magnetic particles have been replaced by more complex magnetic micro and nanostructures like for instance magnetic filaments[1] and shifted-dipole particles[2]. Those fluids are expected to exhibit magnetorheologial and tribological properties very different from ordinary magnetic fluids. A first step towards their characterization is the study of very diluted suspensions in which such unconventional magnetic units are present. Our work includes the study of the phase behavior of such diluted suspensions in bulk as well as near neutral and interacting surfaces. Further insight about the influence of external fields on the phase behavior of such magnetic systems will be also provided.

* joan@ifisc.uib-csic.es

[1] Pedro A. Sánchez, Juan J. Cerdà, V. Ballenegger, T. Sintes, O. Piro, C. Holm, Soft Matter, doi:10.1039/C0SM00772B, (2011).

[2] Sofia Kantorovich, R. Weeber, Juan J. Cerdà, C. Holm, J. Magnetism Magnetic Materials, doi:10.1016/j.jmmm.2010.11.019, (2011);

Nature of Waterlike Liquid-Liquid Criticality

Claudio A. Cerdeiriña, Pablo G. Debenedetti
Department of Chemical and Biological Engineering
Princeton University
08544 Princeton, New Jersey, USA

The study of phase transitions for pure substances in which two liquids of different density coexist in equilibrium acquired great interest in 1992 with water's second critical point hypothesis by Stanley and coworkers[1]. Such waterlike liquid-liquid phase transitions have been observed experimentally for other fluids[2–4] and studied via simulations of water models and of fluids characterized by isotropic core-softened intermolecular potentials (see, e.g., Refs. 6 and 7). At this stage, it seems appropriate to investigate the nature of waterlike liquid-liquid criticality.

One may first inquire about the universality class of this sort of continuous phase transitions. This issue has an obvious intrinsic interest, but it is also relevant with a view to applying finite-size scaling techniques to simulation data[8]. Kurita and Tanaka[5] and Sciortino and coworkers[9] have asserted that, like for the liquid-gas case, waterlike liquid-liquid criticality should be of Ising character. On the other hand, Brovchenko et al.[10] have pointed out that it could belong to the universality class of the random-field Ising model. To the best of our knowledge, there is neither strong experimental evidence nor a detailed enough theoretical analysis on this particular question.

Here we tackle the problem by studying the properties of a simple cell model. Consider the space divided in cells which contain one particle and have two accessible volumes, say, v_+ and v_-. Particles in nearest-neighbor cells interact via a discretized energy ϵ_0, which is supplemented by an additional one $\delta\epsilon$ whenever two adjacent cells are in the '+' state. Such compressible cell liquid (CCL) model can be mapped onto the Ising model, and is in certain respects related to a previously reported water model[11] and in others to the so-called compressible cell gases for asymmetric liquid-gas criticality[12].

Application to water's second critical point entails incorporating entropic effects ascribed to the geometric selectivity of hydrogen bonding. Such a task is accomplished by suitably imposing constraints on the free volume that a particle can explore in its cell. Specifically, when local low-density and low-entropy states are energetically favorable (that is, when low-temperature water's essential microscopic features are implemented), one finds that the slope of the coexistence line in the temperature-pressure plane dp_σ/dT is negative and that the isobaric thermal expansivity α_p diverges to $-\infty$ at criticality, in accord with available information. Correspondingly, 'soft-core-like' behavior (viz., dp_σ/dT ¿0 and $\alpha_p \to +\infty$ as $T \to T_c$) is obtained when low-density and high-entropy states are energetically favorable.

In summary, we will show that (Ising-like) CCL models provide insights into liquid-liquid critical phenomena in pure substances. Some variants are consistent with what has been conjectured for water's liquid-liquid critical point, others with what core-softened models have evidenced. Implications of CCL's for isostructural solid-solid transitions in Cs and certain rare earth metals[13] as well as for crystalline systems with short-range interactions[14,15] will be briefly outlined.

---

* calvarez@uvigo.es

[1] P.H. Poole, F. Sciortino, U. Essmann, and H.E. Stanley, Nature 360, 324 (1992).
[2] Y. Katayama, T. Mizutani, W. Utsumi, O. Shimomura, M. Yamakata, and K.I. Funakoshi, Nature 403, 170 (2000).
[3] G. Monaco, S. Falconi, W.A. Crichton, and M. Mezouar, Phys. Rev. Lett. 90, 255701 (2003).
[4] H. Tanaka, R. Kurita, and H. Mataki, Phys. Rev. Lett. 92, 025701 (2004).
[5] R. Kurita and H. Tanaka, Science 306, 845 (2004).
[6] P.G. Debenedetti, J. Phys.: Condens. Matter 15, R1669 (2003).
[7] S.V. Buldyrev, G. Malescio, C.A. Angell, N. Giovambattista, S. Prestipino, F. Saija, H.E. Stanley, and L. Xu, J. Phys.: Condens. Matter 21, 504106 (2009).
[8] Y. Liu, A.Z. Panagiotopoulos, and P.G. Debenedetti, J. Chem. Phys. 131, 104508 (2009).
[9] C.W. Hsu, J. Largo, F. Sciortino, and F.W. Starr, Proc. Natl. Acad. Sci. U.S.A. 105, 13711 (2008).
[10] I. Brovchenko, A. Geiger, and A. Oleinikova, J. Chem. Phys. 123, 044515 (2005).
[11] G. Franzese and H.E. Stanley, J. Phys.: Condens. Matter 19, 205126 (2007).
[12] C.A. Cerdeiriña, G. Orkoulas, and M.E. Fisher, in preparation.
[13] J.M. Kincaid, G. Stell, and E. Goldmark, J. Chem. Phys. 65, 2172 (1976).
[14] P. Bolhuis and D. Frenkel, Phys. Rev. Lett. 72, 2211 (1994).
[15] C.F. Tejero, A. Daanoun, H.N.W. Lekkerkerker, and M. Baus, Phys. Rev. Lett. 73, 752 (1994).

Coordination of mitotic axes guides morphogenesis of epithelial cysts

Benedetta Cerruti[1*], Alberto Puliafito[1], Annette M. Shewan[2], Keith E. Mostov[2], Guido Serini[1], Antonio Celani[3], and Andrea Gamba[1,4]

[1] *Institute for Cancer Research and Treatment, Str. Prov. 142 km 3.95, 10060 Candiolo, Torino, Italy*
[2] *Department of Anatomy, University of California, San Francisco, California, United States of America*
[3] *Institut Pasteur, Genomes and Genetics Department, Unit "Physics of Biological Systems", Centre National de la Recherche Scientifique Unité de Recherche Associée 2171, F-75015 Paris, France*
[1,4] *Politecnico di Torino, Corso Duca degli Abruzzi 24, 10129 Torino, Italy*

Almost every eucariothic cell is polarized, and the formation of tissues and organs requires the coordination of this polarization in space and time[1]. Typical examples of polarized tissues are epithelia, the 60% of mammalian cell types being of epithelial origins. Epithelia and epithelial-derived tissues serve to divide the organism into compartments, and are often characterized by the presence of a central lumen or luminal network, as observed for instance in kidney, lung, blood vessels and mammary glands. Lumens can serve to isolate specific functions, like in digestion, or to allow the movement of fluids, cells or gases, and lumen dysfunctions are at the basis of very common and often fatal human diseases, like polycystic kidney diseases, hypertension or many epithelial cancers. Despite the apparent differences between the various epithelial tissues, the idea is arising that their formation can be led by general principles, and thus there exist common features underlying their dysfunctions[2].

In order to form multicellular lumens, cells must coordinate the orientation of their apical surfaces, requiring interaction of every cell with the other cells and with the extra-cellular matrix. Hence a first general principle must involve cell-matrix and cell-cell recognition: polarity proteins are key regulators of apical surface and lumen orientation[3], while sensing neighboring cells occurs with a multitude of adhesion receptors. A second general principle must involve apical-basal polarization, spatiotemporally coordinated with neighboring cells, and the generation of a new luminal space: mitotic spindle axes tend to align parallel to the lumen surface[4].

Inspired by this last phenomenologic observation, we investigate if the coordination between successive mitoses is necessary and sufficient for the formation of a central and spherical luminal structure, as observed in physiological cysts, and hence if the absence of this correlation can lead to a multiluminal structure, observed in pathological conditions like cancer and experimentally reproduced in cells where the spindle orientation machinery is disrupted by targeted mutations[4]. We develop a simple lattice model that simulates cystogenesis from its earliest stages. In the model, cell evolution is driven by surface tensions corresponding to different cell-cell and cell-matrix adhesion strengths, and there are two characteristic timescales, the mitotic time and the relaxation time between two mitotic events. Depending on the ratio between these two timescales there exist two possible regimes: an equilibrium regime, in which cells can relax to a global energy minimum before a new division occurs, and an out-of-equilibrium regime. Topological analysis of our experiments on wild-type Madin-Darby canine kidney cells in 3d cultures shows that the physiological regime corresponds to the out-of-equilibrium case. In this regime, a mechanism of spatiotemporal correlation of mitotic spindle axes is mandatory to achieve the formation of a central hollow lumen (fig.1a), while its absence leads to the formation of the pathological multilumen phenotype (fig.1b).

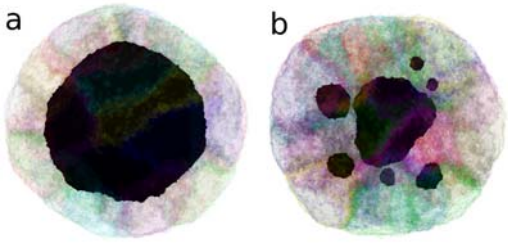

Figura 1. Simulated cyst topology: (a) monolumen and (b) multilumen configurations.

* benedetta.cerruti@ircc.it

[1] L.E. O'Brien, M.M. Zegers, and K.E. Mostov, Nature Rev. Mol. Cell Biol. **3**, 531 (2002).
[2] A. Datta, D.M. Bryant, and K.E. Mostov, Curr. Biol. **21**, R126-R136 (2001)
[3] L.E. O'Brien, T.S. Jou, A.L. Pollack, Q. Zhang, S.H. Hansen, P. Yurchenco, and K.E. Mostov, Nat. Cell Biol. **3**, 831-838 (2001)
[4] Z. Zheng, H. Zhu, Q. Wan, J. Liu, Z. Xiao, D.P. Siderovski, and Q. Du, J. Cell Biol. **189**, 275 (2010)

Capillary rise between parallel plates: Velocity dependence of the capillary pressure

Xavier Clotet*, Jordi Ortín
Dep. d'Estructura i Constituents de la Matèria, Fac. de Física, Universitat de Barcelona
C./ Martí i Franquès 1, 08028 Barcelona

Capillary rise is a process of spontaneous imbibition in the presence of gravity. That is, the displacement at constant external pressure of one fluid by a second immiscible invading fluid that preferentially wets the medium, in a cavity under the effect of gravity. The dynamics of capillary rise was first studied in depth by Green and Ampt in 1911[1] and by Lucas and Washburn a few years later[2,3].

The general equation for the pressure balance at the average interface height for a fluid invading either capillary tube of radius $b/2$ or a Hele-Shaw (H-S) cell of gap thickness b is:

$$\rho\frac{d}{dt}\left(h\dot{h}\right) = \underbrace{\frac{2\gamma\cos\theta}{b}}_{capillarity} - \underbrace{\rho g h\sin\psi}_{gravity} - \underbrace{\frac{\mu}{\kappa}h\dot{h}}_{viscous\ losses} + P_0\,, \tag{1}$$

where the LHS accounts for the variation of the momentum (inertial term) and the RHS is the sum of various pressure contributions. ρ is the density of the fluid and $h(t)$ stands for the mean height of the front measured along the cell as a function of time. γ is the surface tension of the air-fluid interface, θ is the apparent contact angle at the solid-liquid-vapor contact line, g is the acceleration of gravity and the angle ψ measures the inclination of the cell with respect to the horizontal. μ is the dynamic viscosity of the fluid and κ the permeability of the medium. P_0 is the externally applied pressure difference.

We have noticed that for capillary rise experiments in vertical cylindrical tubes there is systematic deviation from the analytical or numerical curves proposed for $h(t)$ when considering a constant contact angle (Extended Solution)[4]. This deviation is partially corrected if a dynamic contact angle is assumed, $\cos\theta_D \propto \beta(\dot{h})^x$, with x in the range[5] $0.33 \leq x \leq 1$.

In the present work we study these deviations for the displacement of air by a perfectly wetting fluid (silicone oil) in laboratory models of porous media (Fig. 1). First, the displacement of the fluid takes place in a rectangular Hele-Shaw cell with uniform gap thickness. Second, the displacement takes place in a Hele-Shaw cell in which the gap spacing takes two possible values randomly distributed in space, mimicking an open fracture. In this medium the capillary pressure fluctuates along the air-fluid interface. In both cases the flow is induced by an imposed externally pressure difference P_0, and the cell is inclined so that a gravitational field $g\sin\psi$ acts as a volume stabilizing force.

The first aim of the study is to check whether a dynamic contact angle approach applies also to our models of porous medium. The second one is to measure the exponent x in the two models (with and without capillary pressure fluctuations) and investigate possible differences between them.

The work consists of systematic experiments carried out at different conditions of cell inclination (ψ) and externally applied pressure difference (P_0). The analysis of the data is done by means of Eq.(1), neglecting the inertia term and replacing the capillarity contribution by

$$\frac{2\gamma}{b}\cos\theta_D = \left[\alpha + \beta(\dot{h})^x\right]\,, \tag{2}$$

where α accounts for the static contribution and β for the dynamic one. Both coefficients together with the exponent x are obtained from fitting the experimental data.

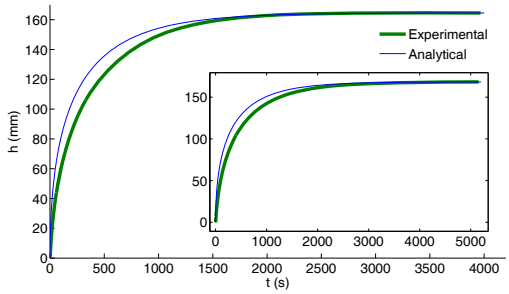

Figura 1. Mean height of the front versus time. Thick line: experimental data for an experiment in a H-S cell without perturbations in the capillary pressure ($\kappa = 0.018$ mm^2)(*main plot*) and with perturbations ($\kappa = 0.013$ mm^2)(*inset*), $\psi = 5°$ and $P_0 = 49$ Pa. The fluid properties are $\mu = 49.9$ mPa·s, $\rho = 998$ kg/m^3 and $\sigma = 20.7$ mN/m. Thin line: analytical solution given by the Extended Solution[4]. Notice the deviation of the analytical curve from the experimental results in both cases.

* xclotet@ecm.ub.es

[1] W.H. Green and G.A. Ampt, J. of Agric. Sci. **IV**, 1 (1911).
[2] R. Lucas, Colloid & Polymer Science **23**, 15 (1918).
[3] E.W. Washburn, Phys. Rev. **17**, 273 (1921).
[4] N. Fries and M. Dreyer, J. Colloid Interface Sci. **320**, 259 (2008).
[5] A. Hamraoui *et al.*, J. Colloid Interface Sci. **226**, 199 (2000), and references therein.

Dynamics of passively phased fiber laser arrays

A. Jacobo[1,2], P. Colet[1], E.J. Bochove[3], Y. Braiman[4], A.B. Aceves[5], R. Deiterding[6], C.A. Miller[7], C. Rhodes[8], S.A. Shakir[9]

1. IFISC, Instituto de Física Interdisciplinar y Sistemas Complejos, CSIC-UIB, 07122 Palma de Mallorca, Spain
2. Max Planck Institute for the Physics of Complex Systems, Nöthnitzer Straße 38, 01187 Dresden, Germany
3. Directed Energy Directorate, Air Force Research Laboratory, Kirtland Air Force Base, New Mexico 87117, USA.
4. Center for Engineering Science Advanced Research Oak Ridge National Laboratory, Tennessee 37831, USA
5. Department of Mathematics, Southern Methodist University, Dallas, Texas 75275, USA
6. Department of Mechanical, Aerospace, and Biomedical Engineering, University of Tennessee, Knoxville, TN 37996, USA
7. Department of Mathematics, University of Tennessee, Knoxville, TN 37996, USA
8. Libration Systems Management, Inc., Albuquerque, New Mexico 87106, USA
9. TASC, Inc., Albuquerque, New Mexico 87106, USA

The goal of scaling fiber lasers to high power levels for applications has created an interest in coherently combine the beams of a number of fibers. However, success in accurately controlling the frequencies and phases of the fields by either passive, active or hybrid means has until now been limited. Studies of the dynamics of passively phased fiber arrays have been published, but the understanding of their instabilities is limited. We consider a passively phased array of N rare earth doped fibers which are coupled through an external cavity. Each fiber is independently optically pumped. The propagation of the signal electrical field and the pump intensity within each fiber can be described by:

$$\frac{\partial E_n}{\partial z} + \left(\beta_0' - \frac{i}{2}g_n'\right)\frac{\partial E_n}{\partial t} = \left(\Gamma_s \frac{g_n}{2} + ik_0 n_2 |E_n|^2\right) E_n \quad (1)$$

$$\frac{\partial I_{pn}}{\partial z} + \beta_p' \frac{\partial I_{pn}}{\partial t} = -\Gamma_p \alpha_n \quad (2)$$

$$\frac{\partial N_{2n}}{\partial t} = \frac{\alpha_n}{\epsilon_p} - g_n \frac{|E_n|^2}{\epsilon_s} - \frac{N_{2n}}{\tau} \quad (3)$$

$$g_n = \sigma_e(\Omega_0)N_{2n} - \sigma_a(\Omega_0)N_{1n} \quad (4)$$

$$\alpha_n = \left(\sigma_a(\omega_p)N_{1n} - \sigma_e(\omega_p)N_{2n}\right) I_{pn} \quad (5)$$

Where $E_n(z,t)$ is the complex slowly varying envelope of the signal electric field in the fiber n with respect to the central frequency Ω_0, and propagation constant β_0. $I_{pn}(z,t)$ is the pump intensity at frequency ω_p. The primes denote derivatives with respect to the frequency at $\omega = \Omega_0$ or $\omega = \omega_p$. β_0' is the signal inverse group velocity while β_p' is the pump inverse group velocity. σ_a and σ_e are the effective emission and absorption cross sections respectively. ϵ_s and ϵ_p are the energies of the photons at the central and pump frequencies. Γ_s and Γ_p are the signal-core and pump-core overlap factors. Finally N_{1n} and N_{2n} are the lower and upper level populations of the medium (with $N_{1n} + N_{2n} = N_{0n}$) and n_2 is the nonlinear refractive index. The above equations are completed with the boundary condition associated to the external cavity coupling

$$E_n(0,t) = \sum_{m=1}^{N} K_{nm} E_m(L_m, t - \tau_{nm}) e^{i(\beta_0 L_m + \Omega_0 \tau_{nm})} \quad (6)$$

where K_{nm} are the coefficients of the coupling matrix, L_m is the length of fiber m and τ_{nm} are the delays in the feedback loop.

By linear stability analysis and numerical simulations we show that, for one fiber, the system has a stable CW regime above threshold, for low pumping powers. We also show that the system can become unstable for high pump intensities first exhibiting pulsating behavior and then becoming chaotic. For two fibers we show that phase locking in a stable CW regime is possible, although this regime becomes unstable when the pump is increased. Instabilities appear for lower powers as the difference in length between the fibers is increased. Examples of these regimes are shown in Fig. 1

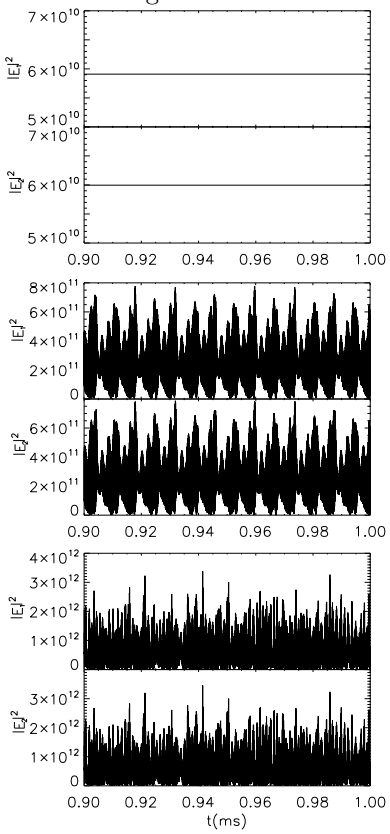

Figura 1. Time traces for two fibers. From top to bottom: CW emission, pulsed behavior, chaotic behavior.

Time delay identification using permutation information theory quantifiers

Miguel C. Soriano, Luciano Zunino, Ingo Fischer, Claudio R. Mirasso
IFISC (CSIC - UIB), Instituto de Física Interdisciplinar y Sistemas Complejos, Campus Universitat Illes Balears, E-07122 Palma de Mallorca, Spain

An important problem in the analysis of a sequence of data points (time series) originating from a given physical process is the identification of time delays. Delay phenomena are intrinsic to many dynamical processes and the identification of a delay would give valuable information about the interaction between the system components.

Autocorrelation function (ACF) and delayed mutual information (DMI) are conventional techniques widely used to identify time delays. However, new alternatives were introduced in recent years in order to perform this task. We are particularly interested in the application of a permutation information theory methodology to unveil delay phenomena from time series[1]. This method relies on the computation of the permutation entropy and the permutation statistical complexity.

We analyze time series originating from an experimental realization of a semiconductor laser with delayed optical feedback and from them construct a probability distribution of their amplitudes. We choose the Bandt and Pompe method to construct the probability distribution[2], which considers the order of neighboring values rather than partitioning the amplitude into different levels. The probability distribution of the generated ordinal pattern for a given time series can be established once an embedding dimension D and an embedding delay time τ are chosen. The embedding dimension D refers to the number of symbols that forms the ordinal pattern. The embedding delay τ is the time separation between symbols which is directly related to the sampling time of the time series (see refs.[1,2] for a detailed derivation and description of the quantifiers).

In our experimental realization of a laser with optical feedback, the laser exhibits chaotic intensity pulsations. Time series are recorded with a sampling time of $\delta_s = 25$ ps. From the length of the feedback loop, the delay time is estimated to be around $\tau_{ext} = 38.5$ ns[3].

In Fig. 1 we plot the normalized permutation entropy and the permutation statistical complexity obtained from the experimental time series as a function of the embedding delay τ for an embedding dimension $D = 8$. We verify experimentally that the permutation entropy is minimized and the permutation statistical complexity maximized when the embedding delay τ of the symbolic reconstruction takes values near τ_{ext}, i.e. for τ close to 1540 samples ($\tau_{ext}/\delta_s = 1540$). We have also found other extrema when the embedding delay matches *harmonics* and *subharmonics* of τ_{ext}.

In summary, time delays present in the system dynamics are detected through the presence of clear extrema of the quantifiers when they are calculated as a function of the embedding delay. The feedback time delay is associated with embedding delay values that minimize the permutation entropy and maximize the permutation statistical complexity, simultaneously. The presence of additional peaks at harmonics and subharmonics of the feedback time delay allow us to better distinguish the delay time.

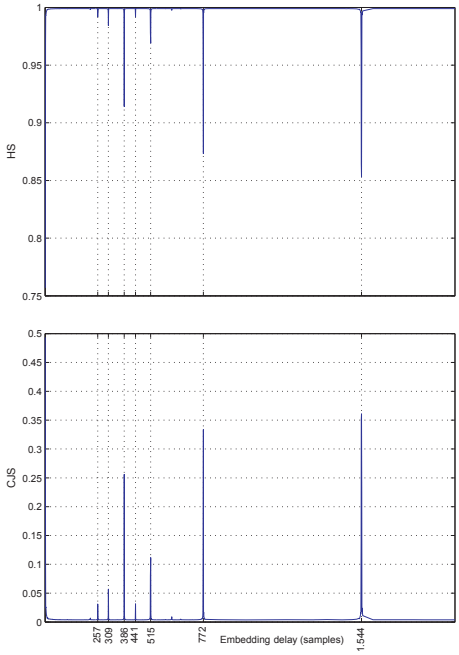

Figura 1. Permutation entropy HS (top) and permutation statistical complexity CJS (bottom) as a function of the embedding delay τ with embedding dimensions $D = 8$ for the experimental time series. Positions of the local extrema associated with the feedback time delay τ_S and its subharmonics are detailed.

* miguel@ifisc.uib-csic.es

[1] L. Zunino, M. C. Soriano, I. Fischer, O. A. Rosso, and C. R. Mirasso, "Permutation information theory approach to unveil delay dynamics from time series analysis," *Phys. Rev. E*, **82**, 046212 (2010).

[2] C. Bandt and B. Pompe, "Permutation entropy - a complexity measure for time series", *Phys. Rev. Lett.*, **88**, 174102 (2002).

[3] M. C. Soriano, L. Zunino, O. A. Rosso, I. Fischer, and C. R. Mirasso, "Time scales of a chaotic semiconductor laser with optical feedback under the lens of a permutation information analysis," *IEEE J. Quantum Electron.*, **47**, 252–261 (2011).

Quasi-stationary analysis of the contact process on scale-free networks

Silvio C. Ferreira,*† Ronan S. Ferreira,†, Romualdo Pastor-Satorras
Departament de Física i Enginyeria Nuclear
Universitat Politècnica de Catalunya, Campus Nord B4, 08034 Barcelona, Spain

Complex network theory represents a general unifying formalism under which is possible to understand and rationalize the intricate connectivity and interaction patterns of many natural and man-made systems. Among their characteristics, probably the most intriguing is the discovery of the apparently ubiquitous scale-free (SF) nature of the connectivity pattern of many systems, described by a probability $P(k)$ that an element (vertex) is connected to other k elements (has degree k), scaling as a power-law of the form $P(k) \sim k^{-\gamma}$, with a degree exponent usually in the range $2 < \gamma < 3$. In recent years, the research community has also devoted a great deal of attention to the study of the dynamical processes on complex networks, which can have important implications in understanding of the behavior of real processes such as the spread of epidemics in social systems or traffic in technological systems as the Internet or transport infrastructures.

Dynamical processes with absorbing configurations are subjects of outstanding interest in non-equilibrium statistical physics that have also found a place in network science. The simplest model allowing absorbing configurations is the classical contact process (CP). In the CP defined in an arbitrary network, vertices can be in two different states, either empty or occupied. The dynamics includes the spontaneous annihilation of occupied vertices, which become empty, at unitary rate and the self-catalytic occupation of an empty vertex i with rate $\lambda n_i/k_i$, where n_i is the number of occupied neighbors of i and k_i is its degree. The model is thus characterized by a phase transition at a value of the control parameter $\lambda = \lambda_c$, separating an active phase from an absorbing phase devoid of active vertices.

The configuration in which all vertices are empty plays a very particular role, since once the system has fallen into this state, the dynamics becomes frozen. For this reason, these states are called absorbing and constitute a central feature in the analysis of finite size systems since, in this case, the only actual stationary state is the absorbing one. Finite size and absorbing states must therefore be handled using suitable strategies, concomitantly with an ansatz for the finite size scaling (FSS) of the dynamics. A widely adopted procedure is the so called quasi-stationary (QS) state,[1] in which the absorbing configuration is suitably excluded from the dynamics.

In this work, we present a study of the QS state of CP on SF annealed networks, combining the QS numerical approach developed in Ref. 1, suitably extended to complex networks, with the theoretical analysis of a approximated one-step process derived from mean-field theory[2,3] and solving the corresponding master equation. Our analysis allows us to obtain information about the probability distribution of activity both close to the critical point and in the off-critical regime, as well as to obtain high quality data for QS relevant quantities, such as the density of active sites or the characteristic times.

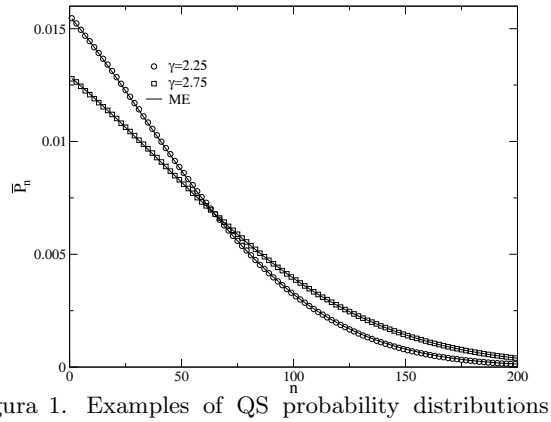

Figura 1. Examples of QS probability distributions obtained in simulations of the critical CP on annealed SF networks and in numerical solutions of the master equation (ME).

The high accuracy of our data (Fig. 1) allows to identify strong corrections to the scaling in the critical quantities that mask the correct finite size scaling exponents obtained analytically by means of an exact mean-field solution. Both critical density and characteristic time show tenuous curvatures as a function of the network size N due to finite size corrections to scaling that may provide incorrect exponents if a simple power law decay is assumed. In annealed networks, for which the critical point is exactly known, we can determine the corrections to scaling analytically and thus recover the theoretical exponents in the finite size analysis, including the abrupt change when the network loses its SF property. The analysis of the supercritical region, on the other hand, hints that those finite size corrections are relevant for very large network sizes, the asymptotic scaling being observable only for extremely large values of N.

* silviojr@ufv.br
† Departamento de Física, Universidade Federal de Viçosa, 36571-000, Viçosa - MG, Brazil

[1] M. M. de Oliveira and R. Dickman, Phys. Rev. E **71**, 016129, (2005).
[2] C. Castellano and R. Pastor-Satorras, Phys. Rev. Lett. **100**, 148701 (2008).
[3] M. Boguñá, C. Castellano and R. Pastor-Satorras, Phys. Rev. E **79**, 036110,(2009).

Simple rules govern finite-size effects in scale-free networks

Sara Cuenda*, Juan A. Crespo†
Departamento de Economía Cuantitativa
Facultad de CC. Económicas y Empresariales
Universidad Autónoma de Madrid
Fco. Tomás y Valiente 5, 28049 Madrid

The growing network with preferential attachment proposed by Barabási and Albert[1] introduced a simple, effective model of networks that would lead to a power-law distribution of the degree of nodes. The results of this model should be understood within the limit of large networks, as some investigations showed the existence of finite-size effects that make the distribution of the degree of nodes depart from the power-law[2–5]. These works show/predict a cut-off degree from which distributions of finite networks created with this model stop from behaving as power-laws, and acknowledge the influence of the initial nodes from which the network grows in the final result. However, a general prediction of the degree distributions of finite networks in terms of the initial nodes has not been made so far.

In this work we find a general, theoretical prediction of the final degree distribution of finite networks growing with preferential attachment in terms of the initial degree distribution. We obtain the expression of the final distribution using two different approaches: the well-known deterministic mean-field approximation, and the more accurate probability distribution of the degree of each node, which considers the stochastic process.

The model that we use is the original introduced by Barabási and Albert[1], in which the probability of a node with degree k of gaining a new link in a network of size t when a new node arrives is $\pi_{k,t} = mk/\sum_i k_i$, where m is the number of *undirected* links of the new node to be attached to the nodes in the network. Since this probability only depends on the state (degree) of each node, we can model the dynamics of every node in order to obtain the final distribution of the network. We did it considering also the initial nodes in the network, which are distributed according to the probability distribution $f_0(k)$.

Using the mean-field approximation we obtain an analytical expression of the final density distribution, which contains the effect of the initial nodes, but with no effects of the dispersion in it. The expression obtained, however, explains previous results on the universality of the cut-off function for finite systems starting from the same initial core[2,3,5]. The theoretical calculation of the stochastic dynamics of every node renders an exact expression of the expected final degree distribution (exact within the limits of the accuracy of $\pi_{k,t}$). Numerical simulations support very well our results, as shown in figure 1.

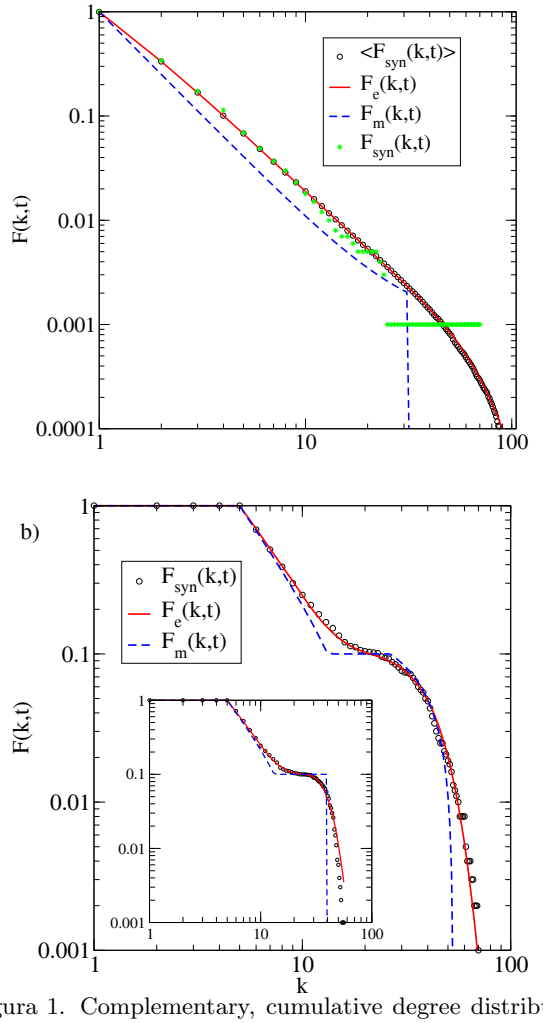

Figura 1. Complementary, cumulative degree distribution of the final network for different initial conditions.

* sara.cuenda@uam.es
† juan.crespo@uam.es

[1] A.-L. Barabási , R. Albert and H. Jeong, *Phys. A* **272**, p. 173 (1999).
[2] S.Ñ. Dorogovtsev, J. F. F. Mendes and A.Ñ. Samukhin, *Phys. Rev. E* **63**, p. 62101 (2001).
[3] P. L. Krapivsky and S. Redner, *J. Phys. A: Math. Gen.* **35**, p. 9517, (2002).
[4] P. R. Guimarães et al., *Phys. Rev. E* **71**, p. 37101 (2005).
[5] B. Waclaw and I. M. Sokolov, *Phys. Rev. E* **75**, p. 056114 (2007).

Replicator dynamics for the n-player Prisoner's Dilemma with "moody" conditional cooperators

Jelena Grujić[1], José A. Cuesta[1], Angel Sánchez[1,2]
[1] *GISC, Dpto. de Matemáticas, Universidad Carlos III de Madrid, Leganés*
[2] *BIFI, Universidad de Zaragoza, Zaragoza*

We have recently performed an experiment to test the emergence of cooperation in the presence of an underlying structure[1]. Human subjects played a Prisoner's Dilemma (PD) with each of their neighbors in a 13×13 square lattice. The results show that the population consisted of cooperators and defectors, who respectively cooperate or defect with high probability regardless of their and their neighbors' previous actions, and "moody" conditional cooperators, whose behavior does depend on those previous actions.

Here we take a first step towards an evolutionary explanation of the aforementioned experimental results. Specifically, we use replicator dynamics to describe the evolution of a set of strategies that mimics the observations, in a simplified context consisting of a well-mixed population of players confronted in iterated n-player PD games. We consider three strategies: cooperators (cooperate with probability p), defectors (cooperate with probability $1-p$) and "moody" conditional cooperators (they cooperate with probability p_D following a defection, and with a probability that increases linearly with the number of cooperating opponents, varying between p_{C0} and p_{C1} when none or all neighbors cooperated). Players played a PD game with each of their $m-1$ opponents taking only one action, either to cooperate (C) or to defect (D), the action being the same against all the opponents; we present results for $m = 2, 3$, and 4.

Denoting by x_i, $i = 1, 2, 3$ the fractions of the three strategies ($x_1 + x_2 + x_3 = 1$), the dynamics of x_i for the case of pairwise PD ($m = 2$) is given by

$$\dot{x}_i = x_i \Big[(A\mathbf{x})_i - \mathbf{x} \cdot A\mathbf{x} \Big] \qquad (1)$$

where A is the payoff matrix, and A_{ij} is the average payoff that strategy i yields when confronted to strategy j in an infinitely long iterated PD. To compute A, we need to find first for every pair of strategies i, j the probability that players play X'Y' in the next round having played XY in the present round (X, X', Y, Y' can be C or D and the first action listed corresponds to the strategy whose payoff is computed, the second action being that of its opponent). This defines a Markov process with transition matrix M, whose stationary probability is obtained by solving the equation $\pi = \pi M$, leading to a payoff for strategy i vs strategy j will be given by[2]

$$A_{ij} = R\pi_{\mathrm{CC}} + S\pi_{\mathrm{CD}} + T\pi_{\mathrm{DC}} + P\pi_{\mathrm{DD}}. \qquad (2)$$

Repeating the calculation for all pairs yields A, the payoff matrix in Eq. (1).

For the cases $m = 3, 4$, we apply the same procedure, except that M matrices will now be 8×8 or 16×16, respectively, since we now need to calculate the transition probabilities for all combinations of actions of three or four players. Thus, for instance, for $m = 3$ the payoff matrix will be a tensor of size $3 \times 3 \times 3$ and the replicator equation will be:

$$\dot{x}_i = x_i \left(\sum_{j,k} A_{ijk} x_j x_k - \sum_{j,k,l} A_{jkl} x_j x_k x_l \right), \qquad (3)$$

and the obvious generalization will hold for $m = 4$.

For all the group sizes, the dynamics exhibits two attractors: a population consisting only of defectors and an interior point with population frequencies comparable to those observed in the experiment. This interior point has a much larger basin of attraction than full defection, and thus it becomes the most probable evolutionary outcome (Fig. 1). While this is the first hint that the experiment results may be understood from an evolutionary viewpoint, more work is needed to ascertain the dependence of the size of the basis of attraction of the interior point as the group size increases.

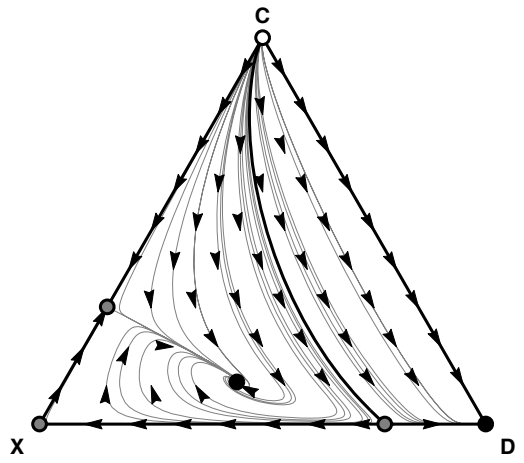

Figura 1. Population dynamics for the pairwise PD with defectors D, cooperators C and "moody" conditional cooperators X. Black circles represent the attractors, gray ones are saddle points and white ones are repellers. Trajectories are plotted in gray and the arrows show the flow of the dynamics. The thick solid line is the separatrix between the two basins of attraction.

[1] J. Grujić, C. Fosco, L. Araujo, J.A. Cuesta, A. Sánchez, Social experiments in the mesoscale: Humans playing a spatial Prisoner's Dilemma PLoS ONE **5**, e13749 (2010).
[2] K. Sigmund, *The Calculus of Selfishness* (Princeton University Press, Princeton, 2010).

Coarse graining en dinámica browniana: modelos de difusión discreta

J. A. de la Torre[1]*, Pep Español[1,2]
[1] *Dpto. Física Fundamental, Universidad Nacional de Educación a Distancia, Apdo. 60141 E-28080 Madrid, España*
[2] *Freiburg Institute for Advanced Studies, Freiburg im Breisgau, 79100, Alemania*

Utilizando el formalismo de Zwanzig proponemos el desarrollo de diversos modelos de grano grueso para formular modelos de difusión discreta. Trabajar con modelos sencillos como el de partículas brownianas no interaccionantes permite centrar el estudio del *coarse graining* en aspectos esenciales del mismo: cómo, dada una descripción microscópica, podemos obtener una descripción macroscópica formalmente equivalente a la anterior con un coste computacional menor. Trabajos previos han utilizado la triangulación de Delaunay y la teoría del *coarse-graining* en un modelo hidrodinámico discreto a partir de la descripción de Smoluchowski[1]. En el presente trabajo, establecido un nivel de descripción para un problema de difusión de partículas coloidales, se hace una descripción de grano grueso en la que se trabaja no ya con las posiciones de las partículas coloidales sino con la concentración, $n_\mu(z)$, en el entorno de un nodo μ definido por la triangulación de Delaunay. Nuestro objetivo es, a partir de este formalismo, desarrollar de forma explícita las ecuaciones de difusión discreta en forma de una ecuación diferencial estocástica que pueda ser simulada y comparada posteriormente con los resultados de la dinámica real del sistema de partículas coloidales.

Si bien la teoría de Zwanzig da una solución formal al proceso de granulado para la probabilidad en forma de una ecuación de Fokker-Planck, ésta queda descrita en términos de dos bloques de información computacionalmente difíciles de calcular: la energía libre y la matriz de fricción. En nuestro trabajo probamos que la matriz de fricción, para perfiles de concentración suficientemente suaves, puede modelarse aproximando el promedio condicional de la concentración por el valor medio de las concentraciones en nodos vecinos. La energía libre queda a su vez bien modelada en el caso de un gran número de partículas coloidales por nodo por un modelo gaussiano no local cuadrático en las concentraciones

Comparando simulaciones de este modelo con la dinámica real obtenida mediante dinámica browniana comprobamos que se verifican tanto las propiedades estadísticas en el equilibrio (a partir del cálculo de la distribución de probabilidad en distintos nodos) como el comportamiento dinámico que se refleja en las correlaciones temporales (Fig. (1)).

Con el objetivo de hacer una simplificación mayor proponemos considerar una energía libre aditiva local. Simulaciones realizadas bajo esta aproximación demuestran que si estamos interesados en propiedades globales del sistema o con una clara separación de escalas (nodos alejados o tiempos largos) esta nueva hipótesis es óptima para simplificar nuestro problema. Sin embargo las distribuciones de probabilidad conjunta para nodos vecinos no se ajustan a la dinámica real del sistema. En el caso de las correlaciones se observa además que al incidir sobre los detalles del proceso (interacción entre nodos vecinos o tiempos cortos) aparecen inexactitudes que nos obligan a considerar el modelo cuadrático.

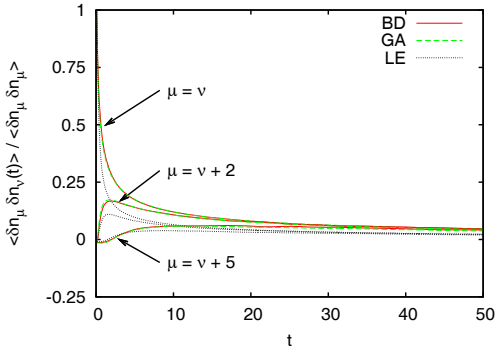

Figura 1. Correlaciones de equilibrio para la dinámica browniana (BD), la aproximación gaussiana (GA) y la hipótesis de energía libre local (LE) para distintas vecindades entre nodos μ y ν.

* jatorre@bec.uned.es

[1] P. Español e I. Zúniga, J. Chem. Phys **131**, 164106 (2009).

Phase diagrams of binary mixtures of patchy colloids with distinct numbers of patches

Daniel de las Heras, José Maria Tavares, Margarida M. Telo da Gama
Centro de Física Teórica e Computacional da Universidade de Lisboa
Avenida Professor Gama Pinto 2
P-1749-016, Lisbon, Portugal

We calculate the phase diagram and the connectivity of the coexisting fluid phases of binary mixtures of patchy colloids, using Wertheim's first order perturbation theory and a generalization of Flory-Stockmayer's theory of polymerization. The colloids are modelled by equisized hard spheres with a number of identical patches on their surfaces, with species distinguished by the number of patches -or functionality-, $f_A^{(1)}$ and $f_A^{(2)}$ (with $f_A^{(2)} > f_A^{(1)}$). We found that the difference in functionality is the key factor controlling the phase behaviour of the mixture. In particular, when $f_A^{(2)} > 2f_A^{(1)}$ the entropy of bonding drives the phase separation of two network fluids and if $f_A^{(1)} > 2$ it changes the topology of the phase diagram of the mixture, from type I to type V. The difference in functionality also determines the miscibility at high pressures: When $f_A^{(2)} - f_A^{(1)} = 1$ the mixture is completely miscible, while closed miscibility gaps are present, above the critical pressure of the less volatile component, when $f_A^{(2)} - f_A^{(1)} > 1$. We argue that this rich phase behaviour is driven by a competition between the entropy of mixing and the entropy of bonding.

Universality of rain event size distributions

Anna Deluca[1*], O. Peters[2,3], A. Corral[1], J. D. Neelin[3], C. E. Holloway[4]
[1] *Centre de Recerca Matemàtica, Spain*
[2] *Dept. of Mathematics and Grantham Institute for Climate Change, Imperial College London, UK.*
[3] *Dept. of Atmospheric and Oceanic Sciences and Institute for Geophysics and Planetary Physics,UCLA, USA*
[4] *Dept. of Meteorology, University of Reading, UK*

Atmospheric convection and precipitation have been hypothesised to be a real-world realization of self-organized criticality (SOC). This idea is supported by observations of avalanche-like rainfall events[1,2] and by the nature of the transition to convection in the atmosphere[4,5]. However, many questions remain open. Here we ask whether the observation of scale-free avalanche size distributions is reproducible using data from different locations and whether the associated fitted exponents show any sign of universality.

We study rain data from all 10 available sites of the Atmospheric Radiation Measurement (ARM) Program, see www.arm.gov, over periods from about 8 months to 4 years[3]. The measurements are from climatically different regions using a standardized technique, making them ideal for our purpose. Precipitation rates were recorded at one-minute resolution with an optical rain gauge.

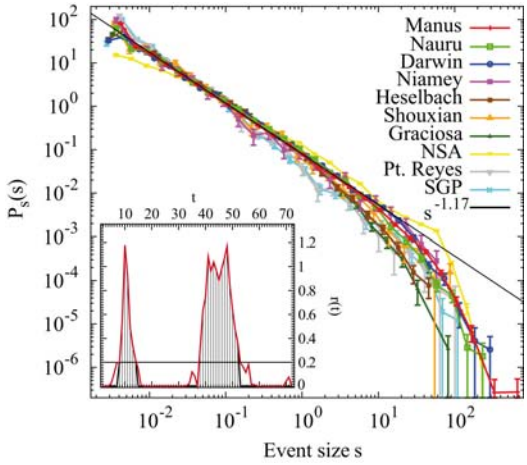

Figura 1. Probability densities of event sizes, s in mm, and a power-law fit (black straight line). Inset: Precipitation rates including two rain events lasting 7 and 15 minutes respectively. Interpreting reported rain rates of less than 0.2 mm/h as zero, the shaded areas are the corresponding event sizes.

Following Ref.[2], we define an event as a sequence of non-zero measurements of the rain rate, see inset in the figure . The event size s is the rain rate, $r(t)$, integrated over the event, $s = \int_{\text{event}} dt\ r(t)$. For each data set, the probability density function $P_s(s)$ in a particular size interval $[s, s + \Delta s)$ is estimated.

The distributions, shown in the figure, are visually compatible with a power law (black straight line) over most of their ranges. A procedure similar to that in Ref.[8] consisting of maximum-likelihood estimation plus a goodness-of-fit test confirms this result: over ranges between 2 and 4 orders of magnitude, all data sets are consistent with a power-law distribution and the estimates of the apparent exponents are in agreement with the hypothesis of a single exponent $\tau_s = 1.17(3)$, except for three problematic data sets from Point Reyes, the Southern Great Plains and Alaska.

Climatic differences between regions are scarcely detectable in event size distributions, which may be surprising on the grounds of climatological considerations. However, the cutoff s_ξ, representing the capacity of the climatic region around a measuring site to generate rain events, changes significantly from region to region, confirming meteorological intuition, and is easily extracted from the moments of the distributions. While the exponents are not significantly different, the larger tropical events are reflected in the greater large-scale cutoff of the tropical distributions.

Similarly, the dry-spell durations (durations of precipitation-free intervals) seem to follow another power law with $\tau_d = 1.2(1)$, and regional differences can be seen in the strength of the diurnal cycle and the cutoff dry spell duration. The broad range of event durations suggests a link to the lack of characteristic scales in the mesoscale regime, where approximately scale-free distributions of clusters of convective activity, for example cloud or precipitation, have been observed to span areas between $\mathcal{O}(1\ \text{km}^2)$ and $\mathcal{O}(10^6\ \text{km}^2)$, see for example Ref.[9]. The observation of scale-free rainfall event sizes suggests long-range correlation in the pertinent fields, a possible indication of critical behaviour near the transition to convective activity.

* adeluca@crm.cat

[1] Andrade R F S, Schellnhuber H J, and Claussen M. *Physica A*, 254(3-4):557–568, 1998.
[2] Peters O, Hertlein C, and Christensen K. *Phys. Rev. Lett.*, 88(1):018701(1–4), 2002.
[3] Peters O, Deluca A, Corral A, Neelin J D and Holloway C E *J. Stat. Mech.*, P11030, 2010.
[4] Peters O and Neelin J D. *Nature Phys.*, 2(6):393–396, 2006.
[5] Neelin J D, Peters O, and Hales K. *J. Atmos. Sci.*, 66(8):2367–2384, 2009.
[6] Arakawa A and Schubert W H. *J. Atmos. Sci.*, 31(3):674–701, 1974.
[7] Tang C and Bak P. *Phys. Rev. Lett.*, 60(23):2347–2350, 1988.
[8] Clauset A, Shalizi C R, and Newman M E J. *SIAM Rev.*, 51(4):661–703, 2009.
[9] Peters O, Neelin J D, and Nesbitt S W. *J. Atmos. Sci.*, 66(9):2913–2924, 2009.

Teorema de fluctuación-disipación para un oscilador activo ruidoso, el haz ciliar del oído interno.

L. Dinis[1,2,*], P. Martin[1], J. Barral[1], J. Prost[1,3], J.F. Joanny[1]
[1] *Institut Curie, CNRS UMR 168, 26 rue d'Ulm 75248 Paris Cedex 05 France*
[2] *Grupo Interdisciplinar de Sistemas Complejos (GISC)*
[3] *ESPCI, 10 rue Vauquelin, 75231 Paris Cedex 05 France*

El teorema de fluctuación disipación (TFD) es un resultado fundamental de la física estadística. Relaciona la respuesta de un sistema a una perturbación externa con la correlación de fluctuaciones en el equilibrio térmico.

Sin embargo, los sistemas alejados del equilibrio no cumplen en general el teorema. Uno de los casos más espectaculares es el de los sistemas cerca de una bifurcación de Hopf. El haz ciliar (*'hair-bundle'*) de las células ciliadas del oído interno de los vertebrados proporciona un ejemplo experimental de uno de estos sistemas[1]. El análisis de las oscilaciones tanto espontáneas como forzadas externamente muestra una fuerte violación del teorema: la temperatura efectiva definida a partir del TFD diverge en torno a la frecuencia espontánea de oscilación ν_0, como se muestra en la figura 1. La divergencia corresponde a un cambio de signo de la parte imaginaria de la función de respuesta lineal, que mide la energía transferida al sistema por parte del forzamiento. Para estímulos de frecuencias menores a la frecuencia de oscilación espontánea, el forzamiento externo recibe en realidad energía del haz ciliar, indicando la presencia de un proceso "activo" interno que mantiene al sistema fuera del equilibrio.

En años recientes han aparecido varias generalizaciones del teorema de fluctuación disipación para sistemas fuera del equilibrio. En particular, el teorema generalizado (TFDG) de Prost *et al.*[2] se aplica a sistemas de markov que evolucionan a partir de un estado estacionario. Utilizando los datos del experimento junto con una descripción del sistema en la forma normal de Hopf, mostramos que el teorema generalizado se cumple aproximadamente si se elige la variable conjugada de la fuerza externa apropiada. El resultado se muestra en la figura 2 en la que se representa la fracción

$$T'_{\rm eff} \equiv \frac{\pi\nu\tilde{C}(\nu)}{\tilde{\chi}''(\nu)} \qquad (1)$$

donde ν es la frecuencia, $\tilde{C}(\nu)$ representa el espectro de potencia de las fluctuaciones en la nueva variable y $\tilde{\chi}''(\nu)$ la parte imaginaria de la función de respuesta lineal de la nueva variable a la perturbación externa. Como se ve en la figura, su valor es aproximadamente 1 para estímulos externos de frecuencias próximas a la frecuencia espontánea. Si bien el resultado no es 1 para toda frecuencia como predice el TFDG, la divergencia que aparecía en la temperatura efectiva en la variable original desaparece completamente.

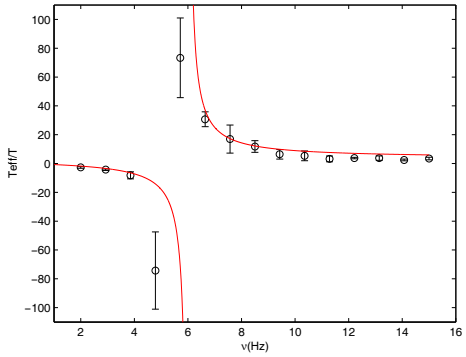

Figura 1. Temperatura efectiva (en unidades de la temperatura del sistema) en función de la frecuencia ν de la estimulación externa.

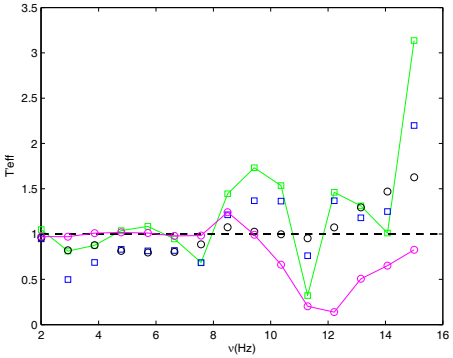

Figura 2. Resultado de la fracción $\frac{\pi\nu\tilde{C}(\nu)}{\tilde{\chi}''(\nu)}$ en la variable conjugada apropiada, calculada según cuatro procedimientos diferentes. El teorema generalizado de fluctuación-disipación predice que la fracción vale 1 para sistemas de markov que evolucionan desde un estado estacionario. En cualquiera de los cuatro métodos, la fracción es cercana a 1 al menos para frecuencias próximas a $\nu_0 \simeq 6$Hz, la frecuencia propia de oscilación.

* ldinis@fis.ucm.es

[1] P. Martin, A. J. Hudspeth and F. Jülicher, *Proc. Natl. Acad. Sci. USA* **98**, 14380 (2001)
[2] J. Prost, J. F. Joanny and J. M. R. Parrondo, *Phys. Rev. Lett.* **9**, 090601 (2009)

Information routing driven by background chatter in signaling networks

Núria Domedel-Puig, Pau Rué, Antonio J. Pons, Jordi García-Ojalvo*
Departament de Física i Enginyeria Nuclear
Universitat Politècnica de Catalunya
Edifici GAIA, Rambla de Sant Nebridi s/n
08222 Terrassa (Barcelona) Spain

Transformation of information into chemical change, signal transduction, is a property of all living cells. Signaling molecules stimulate their receptors, which transmit the signal downstream through a series of protein-protein interactions that modify DNA expression and protein levels. In this manner, information affects cell behavior. The description of signal transduction has classically involved independent signaling cascades -or pathways-, in which information is linearly transmitted from membrane to nucleus. Contributing to this simplified view of cell signaling, experimental studies have usually analyzed pathway stimulation by single inputs, such as variations in one chemical (nutrients, hormones, etc.) or physical property (presence of light, pressure, etc.). However, extracellular media usually contain a complex mix of molecules that have the potential to feed the signaling network with multiple inputs simultaneously[1]. Furthermore, it is now known that proteins of one signaling cascade often interact with proteins of other pathways, forming a dense web of intracellular connections both in eukaryotes and prokaryotes[2]. Finally, the fact that cells process diverse signals under a fluctuating environment provides a source of random variation at the input level that the cell must also deal with[3].

Here we explore the impact of this signal diversity and variation upon the information processing capabilities of a cell signaling network as a whole. In particular, we study how transmission of information coming from one single input is affected by the background activity, or *chatter*, provided by other network inputs. To address this issue in a way that explicitly accounts for the complexity of the system under consideration, we use one of the most comprehensive dynamic models of cell signaling currently available in the literature: a recently published Boolean network for the human fibroblast that involves over 130 protein species[4] (Fig 1). The dynamics of this network are implemented as a set of logic rules, an approach that -despite its simplicity- represents a good choice when building a detailed kinetic model is unfeasible. Indeed, Boolean networks have successfully been applied to modelling numerous biological processes, showing that sequences of events can be reproduced by this type of discrete dynamic models[5].

We have characterized the response of this network to periodic signals under different chatter levels by performing extensive numerical simulations. Our findings suggest that the level of background activity shapes the response of the entire network to the external signal. Indeed, specific levels of background chatter activate different areas of the network, causing the information to travel through chatter-dependent paths (Fig 1). In certain cases, background activity allows input signals to be transmitted to downstream nodes that would be unreachable otherwise. The existence of this chatter-induced information routing appears to rely on the structure and dynamics of a truly biological network, as we find that random versions of the system are unable to display this feature.

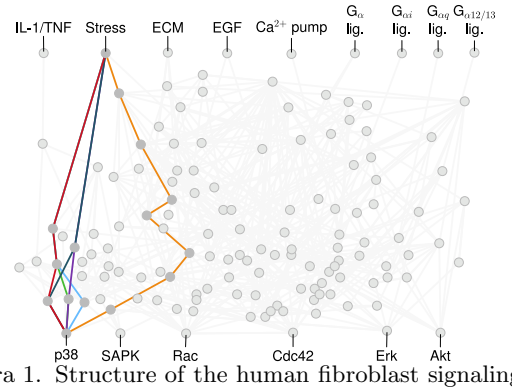

Figura 1. Structure of the human fibroblast signaling network. The network has 9 input nodes (top row), 6 output nodes (bottom), and 124 internal nodes. A periodic stimulation has been applied to input *stress* under different chatter levels. The most utilized paths to node *p38* are then identified based on correlation measures, and shown here in red (high score at low chatter), blue (high score at low and medium chatter), and yellow (top scoring at high chatter levels).

* jordi.g.ojalvo@upc.edu

[1] Natarajan M, Lin K, Hsueh RC, Sternweis PC, Ranganathan R (2006) A global analysis of crosstalk in a mammalian cellular signalling network. *Nature Cell Biology*, 8:571–580.

[2] Oda K, Kitano H (2006) A comprehensive map of the Toll-like receptor signaling network. *Molecular Systems Biology*, 2:2006.0015.

[3] Suel G, Kulkarni R, Dworkin J, Garcia-Ojalvo J, Elowitz M (2007) Tunability and noise dependence in differentiation dynamics. *Science*, 315:1716–1719.

[4] Helikar T, Konvalina J, Heidel J, Rogers J (2008) Emergent decision-making in biological signal transduction networks. *Proc Natl Acad Sci USA*, 105:1913–1918.

[5] Huang S, Eichler G, Bar-Yam Y, Ingber D (2005) Cell fates as highdimensional attractor states of a complex gene regulatory network. *Phys Rev Letters*, 94:128701.

Del colapso gravitatorio a la descomposición espinodal

Alvaro Domínguez[1*], Johannes Bleibel[2], Martin Oettel[3], Siegfried Dietrich[2]
[1] *Física Teórica, Universidad de Sevilla, Apdo. 1065, E–41080, Sevilla*
[2] *Max–Planck–Institut für Metallforschung, Heisenbergstr. 3, D–70569, Stuttgart*
[3] *Institut für Physik, Johannes–Gutenberg–Universität Mainz, WA 331, D–55099, Mainz*

Un gas de Yukawa bidimensional consiste en esferas duras (diámetro σ) que se atraen según el potencial

$$V_{\rm atr}(d) = -V_0 K_0(d/\lambda) \qquad (V_0, \lambda > 0)$$

en términos de la función de Bessel modificada K_0, que exhibe un decaimiento exponencial para $d \gg \lambda$ (correspondiente a una interacción de corto alcance), pero un comportamiento logarítmico para $d \ll \lambda$ (formalmente análogo a la gravitación newtoniana bidimensional y por tanto no integrable en el sentido de la mecánica estadística del equilibrio). Los estudios previos del gas de Yukawa han considerado invariablemente $\sigma \approx \lambda$; nuestro objetivo es estudiar el caso $\sigma \ll \lambda$, de forma que el efecto del comportamiento logarítmico sea patente.

Aparte de su interés intrínseco, este modelo es de importancia práctica porque describe la interacción por fuerzas capilares de partículas coloidales atrapadas en una interfase fluida. Se trata de un sistema que hoy en día se genera y estudia rutinariamente en el laboratorio, para los cuales V_0 y λ dependen de parámetros experimentalmente controlables con relativa facilidad. En particular, una configuración típica involucra $\sigma \approx 1$ μm (partículas coloidales) y $\lambda \approx 1$ mm (longitud capilar).

Nos hemos centrado en el estudio de la inestabilidad de una distribución homogénea de partículas. El problema se ha abordado teóricamente mediante una aproximación de campo medio[1], así como con ayuda de simulaciones de dinámica molecular[2]. Estas últimas permiten la medición de cuantificadores particularmente sensibles a la formación de estructuras en el régimen no lineal (inhomogeneidad alta). Los resultados se pueden resumir en términos del cociente λ/L, donde la escala $L(\gg \sigma)$ caracteriza el tamaño de la distribución de partículas:

- En el límite $\lambda/L \ll 1$ se observa un proceso de descomposición espinodal según la distribución de partículas se separa en una fase gaseosa y otra líquida.

- Por el contrario, en el límite $\lambda/L \gg 1$ se observa una inestabilidad análoga a la del colapso gravitatorio con la formación de cúmulos densos en una distribución diluída de partículas.

La evolución en este segundo límite ocurre sobre una escala de tiempo característica independiente de λ y mucho más corta que la de descomposición espinodal. A pesar de esto, es posible identificar claramente dos etapas reminiscentes de los regímenes de separación de fases y crecimiento de dominios, respectivamente, de la descomposición espinodal. La evidencia sugiere que la transición entre estas dos dinámicas límites es continua como función del parámetro λ.

---

* dominguez@us.es

[1] Domínguez, Oettel, and Dietrich, *Phys. Rev. E* **82**, 011402 (2010).
[2] Bleibel, Domínguez, Oettel, and Dietrich, *preprint* (2011).

Supernormal conduction in cardiac tissue promotes concordant alternans and action potential bunching

Blas Echebarria[1*], Georg Röder[2], Harald Engel[3], Jörn Davidsen[4], Markus Bär[5]
[1] *Departament de Física Aplicada, Universitat Politècnica de Catalunya, E-08028 Barcelona, Spain*
[2] *Max-Planck-Institut für Physik komplexer Systeme, 01187 Dresden, Germany*
[3] *Institut für Theoretische Physik, Technische Universität Berlin, 10623, Germany*
[4] *Department of Physics and Astronomy, University of Calgary, Calgary, Alberta, Canada AB T2N 1N4,*
[5] *Physikalisch-Technische Bundesanstalt, 10587 Berlin, Germany.*

Propagation of pulse trains in excitable media is usually characterized by a so-called dispersion curve that gives the velocity of a pulse in a periodic train as a function of its wavelength. Since a pulse typically is followed by a refractory zone of decreased excitability, the pulse velocity monotonically increases with increasing wavelength (=normal dispersion). In the context of excitable cardiac tissue, normal dispersion corresponds to *normal* conduction. Supernormal conduction (SNC) in excitable cardiac tissue refers to an increase of pulse (or action potential) velocity with decreasing distance to the preceding pulse. Here, we employ a simple ionic model to study the effect of SNC on the propagation of action potentials (APs) and the phenomenology of alternans (beat-to-beat alternations in the duration of the excited phase of the AP) in excitable cardiac tissue. We use bifurcation analysis and simulations to study attraction between propagating APs caused by SNC, that leads to AP pairs and bunching. It is shown that SNC stabilizes concordant alternans in arbitrarily long paced one-dimensional cables. As a consequence, spiral waves in two-dimensional tissue simulations exhibit straight nodal lines for SNC in contrast to spiraling ones in the case of normal conduction[1].

* blas@fa.upc.edu

[1] B. Echebarria, G. Röder, H. Engel, J. Davidsen, Markus Bär, Physycal Review E, in press.

Local routing of the Internet based on a linear projection of complex networks

Pau Erola*, Sergio Gómez, Alex Arenas
Departament d'Enginyeria Informàtica i Matemàtiques
Universitat Rovira i Virgili, 43007 Tarragona (Spain)

Internet is the largest synthetic complex system ever built, with a collection of more than 30,000 networks, each one known as an Autonomous System. In the last few years, Internet is experiencing an explosive growth that is compromising its navigation scalability[1,2] due to its dependence on the Border Gateway Protocol (BGP). The BGP routing protocol requires to maintain an updated view of the network topology, involving a huge amount of data exchange and significant convergence times. The scale-free topology of Internet makes the complex network theory the natural framework to analyze its problems. Here, we propose a local alternative to this routing protocol based on complex networks. Our approach guarantees a high reliability over time and the simulation results show that we are in high percentage close to optimal paths.

In many strongly clustered networks, without a global view of the topology, a message can be routed efficiently. Assuming the hypothesis that the mesoscopic structure provides meaningful insights on this routing property, we analyze the contribution of each node of a network to modules using the projection technique introduced by Arenas *et al.*[3]. This projection is based on a rank 2 TSVD and constructs a plane $\mathcal{U}_2$ where each node has a coordinate pair. For each pair we calculate the polar coordinates (R,θ) and the values R_{int} and R_{ext}. R and θ enlighten about the degree and connectivity pattern of each node, R_{int} informs about the internal contribution of nodes to their corresponding modules, and R_{ext} reflects the boundary structure of modules.

Using these values, we propose a greedy routing algorithm that at each step chooses the neighbor that minimizes the function

$$\begin{aligned}\text{cost}_k &= \beta(\lambda + |\Delta\theta_{k\to j}|)/R_{\text{int}_k} && \text{if } k \in \alpha_j,\\ &= |\Delta\theta_{k\to j}|/R_{\text{ext}_k} && \text{if } k \notin \alpha_j \wedge R_{\text{ext}_k} > 0,\\ &= (\lambda + |\Delta\theta_{k\to j}|)/R_{\text{int}_k} && \text{otherwise;}\end{aligned}$$

where $|\Delta\theta_{k\to j}|$ is the angular distance between the neighbor k and destination j; α_j is the destination community; and λ and β are constants. For more details see [3,4].

This study is also concerned about the reliability of this projection: if data is continuously changing the projection might become obsolete. In our earlier work[5] we defined two measures to quantify the differences between two projections. The first measure is of global reliability and indicates the amount of change in the position of nodes in $\mathcal{U}_2$. It is computed by the *relative error* between the $\mathcal{U}_2$ coordinates of the initial network and the grown network. Nonetheless, the neighborhood of each node in the $\mathcal{U}_2$ plane may differ and be hardly reflected by the measure defined above. Thus, we proposed a norm that reflects these local changes using the weighted distances between nodes. First, we construct the matrices D^z with the $N \times N$ distances between any pair of nodes of the network at stage z. Then, we compute the matrices of weighted distances S^z using a gaussian distribution that prioritizes the stability of closer nodes over the distant ones,

$$S^z_{ij} = D^z_{ij} e^{-{D^z_{ij}}^2/2\left(\sigma R^0_i\right)^2},$$

where R^0_i is the module of the node i, and σ is a constant. Finally, the local measure of reliability is computed as

$$E_{\text{local}} = \left(\sum_{i=1}^{N}\sum_{j=1}^{N}|S^z_{ij} - S^0_{ij}|\right)\left(\sum_{i=1}^{N}\sum_{j=1}^{N}|S^0_{ij}|\right)^{-1},$$

where S^0 and S^z represent the matrices of weighted distances of the initial network and the grown network.

We have selected two snapshots of the AS network[6], June and December 2009, as our test set. With them we construct two undirected and unweighted networks. We have simulated 10^6 paths with a success rate of 93% and an average path of 6 steps (due to the long tail of the distribution). The global error between both projected networks is 18%, however, the local error is only 0.007%. This reinforces the idea that our projection is very robust against evolving data. Likewise, the Figure below shows that the distribution of path length of our greedy algorithm does not significantly degrade.

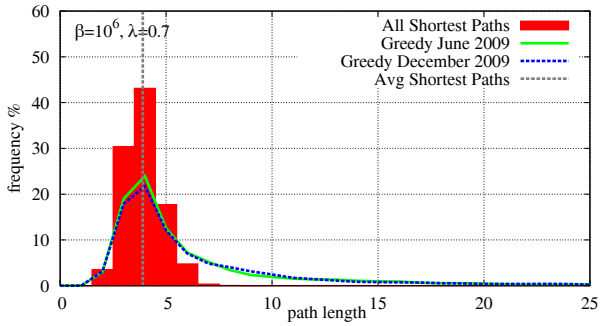

* pau.erola@urv.cat

[1] RFC 4984, *The Internet Architecture Board* (2000)
[2] *Nature Physics 5*, 74–80 (2009)
[3] *New J. Phys. 12*, 053009 (2009)
[4] *Int. J. of Complex Systems in Science 1*, 37–41 (2011)
[5] arXiv:1101.2064 [physics.data-an]
[6] `http://www.caida.org/data/active/as-relationships/`

Changes in buoyancy-driven instabilities by using a reaction-diffusion system

Darío Martín Escala*, Alberto Pérez Muñuzuri
Departamento de Física da Materia Condensada, Grupo de Física Non Lineal†
Facultade de Física ,Univerisdade de Santiago de Compostela
15782 Santiago de Compostela

At the interface generated in the mixing of miscible fluids[1], instabilities can displayed by the difference between the fluids densities and diffusion coefficients. These instabilities generate characteristic patterns that affect the mass transport between the two species.

BZ reaction (Belousov-Zhabotinsky) is a chemical reaction where, due to the autocatalysis of its intermediaries and the difference between diffusion coefficients of the same, are generated chemical oscillations and waves that result in pattern formation when the reaction is carried out in two-dimensional media.

The aim of this study is to analyze the influence of reaction diffusion on the instabilities caused by the contact of two fluids of different density and diffusion coefficient.

The mathematical models involved in these phenomena are solved using numerical methods such as finite differences, finite volumes and finite elements.

* dmescala@gmail.com
† `http://chaos.usc.es/`

[1] T. Bansagi, Jr., D. Horvath, A. Toth, J. Yang, S. Kalliadasis, and A. De Wit. Phys. Rev. E **68**, 055301(R) (2003)
[2] S. Kalliadasis & J. Yang,A. De Wit, Phys. Fluids, **16**, 5,(2004)

A coarse-grained model for water in hydrophobic confinement

Cristian Esplugas*, Giancarlo Franzese
Departament de Fisica Fonamental,
Universitat de Barcelona, Diagonal 647,
08028 Barcelona, Spain

Hydrophobic confinement allows to supercool liquid water well below its melting temperature and is relevant in biology and technological applications. By performing Monte Carlo simulations, we study the effect of hydrophobic confinement on the thermodynamics and dynamics of supercooled water. To this goal, we extend a coarse-grained model previously developed for the case of a water monolayer in hydrophobic nanoconfinement to the case of an arbitrary number of water layers between hydrophobic plates. Here we present our preliminary results about the possible liquid-liquid phase transition, a feature that has been predicted at low temperature and high pressure for bulk water by several theories and models.

* cristian.esplugas@gmail.com

Noise-tolerant signal detection in genetic circuits

Javier Estrada, Raúl Guantes
Departamento de Física de Materiales and Instituto Nicolás Cabrera, Universidad Autónoma de Madrid, Spain

Cells manage information encoded both in amplitude and frequency modulated signals (AM, FM). Biochemical networks processing these signals have to be able to extract infromation from the very noisy intracellular environment. The interactions between the different molecules and their properties (i.e. their sign and strength), determine the signal detection and filtering capabilities of these networks.

We have derived mathematical expressions to predict the response of general two-component modules to AM and FM signals and quantify how noise affects the information transmission. Using these mathematical predictions and running some simulations we have found that, while most of the typical network motifs exhibit a trade-off between AM and FM detection, coherent feed-forward loops can detect simultaneously AM and FM signals. In addition, this network motif exhibits a good noise-tolerant response. Alternatively, incoherent FFL's can work as high-pass filters improving high frequency detection while keeping the overall noise frequency in a lower range. This allows this structure to improve signal detection acting as a noise filter.

Our systematic study remarks the importance of taking into account the nature of the propagated signal (AM or FM) together with the different noise features when studying the response of biochemical networks.

---

* javier.estrada@uam.es

[1] Raúl Guantes, Javier Estrada, Juan F. Poyatos.(2010) Plos One. Vol. 5, Issue 8.

Modelo mesoscópico de interacción DNA-Proteína

R. Tapia-Rojo, D. Prada-Gracia, J. J. Mazo, F. Falo*
Departamento de Física de la Materia Condensada, Universidad de Zaragoza.
Instituto de Biocomputación y Física de Sistemas Complejos, Universidad de Zaragoza.
Instituto de Ciencia de Materiales de Aragón (ICMA) CSIC-Universidad de Zaragoza.
Freiburg Institute for Advanced Studies (FRIAS), University of Freiburg, Freiburg, Germany.

La regulación de la expresión de los genes o su transcripción son procesos que ocurren con la mediación de proteínas que interaccionan con la molécula de DNA de una forma muy selectiva. El mecanismo por el que una proteína encuentra su sitio de ligadura ha sido objeto de investigación en los últimos años. Se han propuesto mecanismos que alternan búsquedas en tres y una dimensión[1], aunque el tiempo en el que la proteína se mueve a lo largo de la cadena es el dominante. Por otra parte, se ha conjeturado que la dinámica la cadena de DNA puede jugar un papel importante en el reconocimiento del sitio de enlace por el factor regulador o por la proteína de transcripción[2]. Por ejemplo, los procesos de transcripción pueden inducirse por el enlace entre la RNA-polimerasa y la apertura de una burbuja en la cadena de DNA[3].

Basándonos en estas ideas proponemos un modelo sencillo de interacción DNA-proteína, que considera una descripción mesoscópica de ambos elementos. Consideraremos la proteína como una partícula que se mueve en una caminata aleatoria a lo largo de la cadena de DNA (1d). La cadena de DNA se modela mediante el modelo de Peyrard-Bishop-Dauxois, en el que las variables relevantes son la apertura de las bases[4]. Introducimos en este modelo, por una parte un término que modela la interacción con el solvente y por otra la dependencia con la secuencia del DNA[5]. La interacción se produce en función de estas variables: posición de la partícula y apertura de las bases.

Hemos aplicado el modelo a tres secuencias de promotores (zonas del genoma donde se regula e inicia la transcripción de un gen) de distintos organismos: un virus (bacteriófago P5), una célula procariota (E. Coli) y una eucariota (colágeno humano). Generamos trayectorias mediante la integración numérica de las ecuaciones del Langevin del modelo. A partir de la mismas hemos hecho un análisis completo del paisaje de energía libre (PEL) del sistema mediante los métodos basados en redes descritos en[6]. La aplicación de estos métodos nos ha permitido: i) Identificar los sitios más probables de unión de la proteína al DNA. ii) Las diferencias de energía libre entre los sitios de unión específicos y no específicos con el DNA. iii) Distinguir entre promotores fuertes y débiles. En la figura podemos observar los resultados para un promotor del virus P5. Es un promotor fuerte y estimamos una energía libre de $\Delta F \approx 10 K_B T$.

El modelo presentado abre el camino a una nueva estrategia para el análisis de secuencias genómicas.

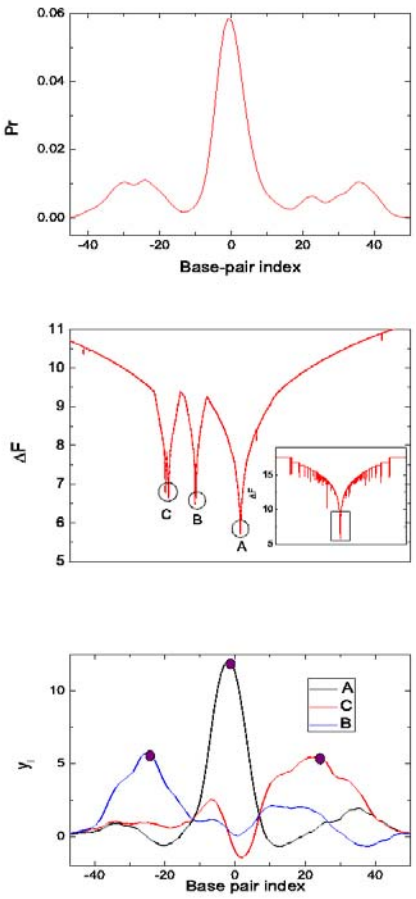

Figura 1. Análisis del promotor del virus P5. (a) Probabilidad de ocupación de la proteina en cada base del promotor. (b) PEL con los tres mínimos más notables. (c) Configuraciones de la cadena DNA y de la proteína para dichos mínimos.

* fff@unizar.es

[1] P.H. von Hippel and O.G. Berg J. Biol. Chem. **264** 675 (1989).
[2] G. Kalosakas, et al., Eur. Phys. Lett.,**68**, 127 (2004)
[3] C.H. Choi et al. Nucl. Acid Research **32**, 1584-1590 (2004).
[4] T. Dauxois, M. Peyrard, and A. R. Bishop, Phys. Rev. E **47**, 684 (1993).
[5] R. Tapia-Rojo, J. J. Mazo and F. Falo Phys. Rev E, 82, 031916 (2010).
[6] D. Prada-Gracia, J. Gómez-Gardeñes, P. Echenique P, F. Falo PLoS Comput Biol 5(6) e1000415. (2009)

Coupled Ising models and interdependent discrete choices under social influence in homogeneous populations

Ana Fernández del Río*, Elka Korutcheva, Javier de la Rubia
Departamento de Física Fundamental
Facultad de Ciencias (UNED), Paseo Senda del Rey 9 28040 Madrid

The study of traditional socieconomic discrete choice problems with interaction (of social norm, role model, or peer pressure type) allows for the use of statistical mechanical tools and models[1]. The simplest possible model is the infinite range Ising model with constant field, which considers completely homogeneous populations (in what concerns social influence, accurate knowledge of the average behaviour of the group and personal or social factors). This simple system already gives rise to interesting socieconomic interpretations[1].

Two such Ising models coupled directly through an additional term in the Hamiltonian have been studied and two different coupling schemes considered. Solutions have been numerically calculated and phase diagram sections constructed for the zero external fields (no pure private deterministic utilities) case.

The non-local model[2] (Weiss type coupling term) can be understood as describing the same decision making process in two groups, where individuals are subject to social influence from both their group and the other one. Examples of interest can be the study of public opinion on a given subject in two neighboring countries (regions, cities, neighborhoods...), companies in two related business sectors and their production technology option...

In the local model[3], coupling is only through each individual, and a single group is considered. Each individual makes two interrelated decisions. This is interesting in many contexts, for example, the interaction between different social pathologies (dropping from school vs teenage pregnancy...), other social traits (joining the labor force vs having a child...), opinion dynamics and political science (voting yes to two different propositions coming from the same party...) and indeed in economical contexts (buying different products of the same/competitor brand...).

Both models have remarkable similarities with a major difference: in the non-local case, for strong enough inter choice coupling, there are no stable solutions. This can be naturally explained as the non-local model *breaking down* when social influence of the *outsiders* is stronger than that exerted by the own peers (frustration).

For both models with zero external fields, either both average choices are zero (paramagnetic phase) or different from zero (ferromagnetic phases). Both models have an unbroken symmetry and so ferromagnetic phases have two physically identical equilibria. Critical curves separating paramagnetic and ferromagnetic phases have been analytically calculated. Note that in the nonzero field case these will still separate regions where social utility matters from regions where it does not. Another feature they have in common is that, if the coupling between both groups or choices is not too big, social interaction can give an outcome which opposes pure private utility (first order phase transition at zero inter-coupling which gives rise to metastability regions and hysteresis).

When compared to the uncoupled case, the interdependence introduces a higher trend to consensus (not favoring any specific direction). It also gives rise to interesting considerations concerning metastability and hysteresis in the light of interacting groups/decisions whose perception/interdependence is reversing. This can be of interest when studying opinion formation in social or political groups when their traditional inter-influence is changing or to study situations such as strong government action to compensate for *natural* reinforcement between undesired trends. Metastability regions involve (socially reinforced) situations in which the groups/options may be prevented from aligning (or disaligning) even when the *conditions seem right*.

There are some additional differences between both models. In the non-local case, metastable equilibria can exist for low temperatures up to $T = 0$. For the local case however, at a small enough temperature, these disappear. Another difference is that in the local case, if social pressure to conform to the norm is small enough or statistical fluctuations large enough, no order will emerge regardless how strong the inter-decision coupling is. Both of these differences can be explained in relation to whether the interdependence between both variables will add an effective term to the social (non-local case) or to the private (local case) deterministic utilities.

When introducing nonzero fields, the paramagnetic phase will disappear and an additional symmetry broken. New metastable equilibria should appear for small enough private utilities and need to be studied in detail. The introduction of quenched disorder in individual deterministic private utilities seems to be a natural next step. These models also need to be tested against real data.

---

* ana.fernandez@invi.uned.es

[1] S.N. Durlauf. How can statistical mechanics contribute to social science?. *Proceedings of the National Academy of Sciences*, 96:10582-10584, 1999.

[2] E.R. Korutcheva and D.I. Uzunov. Ising models and coupled order parameters. *Preprint Joint Inst. Nuclear Research Dubna, E-17-88-467., 1988*

[3] S. Galam, S.R. Salinas and Y. Shapir. Randomly coupled Ising models. *Physical Review B*, 51(5):2864-2871, 1995.

Update rules and interevent time distributions: Slow ordering vs. no ordering in the Voter Model

J. Fernández-Gracia*, V.M. Eguíluz†, M. San Miguel‡
Intituto de Física Interdisciplinar y Sistemas Complejos (UIB-CSIC)
Ed. Instituts Universitaris de Recerca
Campus Universitat de les Illes Balears
07122 Palma de Mallorca,

We introduce a general methodology of update rules accounting for arbitrary interevent time distributions in simulations of interacting agents. In particular we consider update rules that depend on the state of the agent, so that the update becomes part of the dynamical model. As an illustration we consider the voter model in fully-connected, random and scale free networks with an update probability inversely proportional to the persistence, that is, the time since the last event. We find that in the thermodynamic limit, at variance with standard updates, the system orders slowly. The approach to the absorbing state is characterized by a power law decay of the density of interfaces, observing that the mean time to reach the absorbing state might be not well defined.

* juanf@ifisc.uib-csic.es
† victor@ifisc.uib-csic.es
‡ maxi@ifisc.uib-csic.es

Fluctuaciones de Películas Adsorbidas

Eva M. Fernández[1*], Enrique Chacón[1], Pedro Tarazona[2]
[1] *Instituto de Ciencia de Materiales de Madrid, Consejo Superior de Investigaciones Científicas, E-28049 Madrid.*
Departamento de Física Teórica de la Materia Condensada, Universidad Autónoma de Madrid, E-28049 Madrid.

La caracterización de la estructura de la interfase de un fluido es un problema de gran relevancia en física, química, biología y ciencia de materiales. Fenómenos interfaciales tales como adsorción, wetting, prewetting y películas delgadas sobre superficies sólidas, que son resultados de la interacción entre el fluido y el substrato sólido, se encuentran tanto en la naturaleza como en procesos industriales, y juegan un papel importante en catálisis, fabricación de nanoestructuras, biología[1]... El estudio de la superficie fluida, a diferencia de la superficie sólida, presenta un problema añadido debido a la presencia de fluctuaciones térmicas superficiales (ondas capilares) que dificultan conocer la estructura intrínseca (mesoscópica) de dicha superficie.

Durante los últimos años nuestro grupo ha estado estudiando la superficie libre de los líquidos y ha establecido una conexión entre la Teoría de Ondas Capilar (CWT) y el nivel microscópico a través del Intrinsic Sampling Method[2,3] (ISM), el cual ofrece una buena herramienta para extraer la información relevante de la estructura molecular microscópica a partir de simulaciones por ordenador de SOFT-MATTER. El ISM realiza primeramente una análisis percolativo que permite diferenciar las partículas que forman parte del líquido de aquellas que pertenecen al vapor, para posteriormente definir las partículas líquidas constituyentes de la superficie intrínseca[2]. De esta forma se puede obtener la superficie intrínseca de separación entre las dos fases así como el espectro de las ondas capilares asociadas a la interfase, las moléculas que forman parte del líquido y las que forman parte del vapor. Esta metodología ha sido aplicada con éxito al estudio de la interfase líquido-vapor, de líquidos simples, de metales alcalinos, del agua y más recientemente a las interfases entre agua y un líquido hidrofóbico y a membranas del tipo Black Newton Films.

En este trabajo hemos generalizado el ISM al estudio de la superficie de un líquido adsorbido frente a una pared. En una situación de mojado total, hemos estudiado las fluctuaciones, respecto de su valor de bulk, de la posición media de la interfase y la dispersión debido a la presencia de la pared. En este estudio nos centraremos primeramente en las variables del sistema que afectan a las fluctuaciones superficiales y posteriormente nos dedicaremos al estudio de nuestro verdadero objetivo: comprobar, por medio del analisis de las ondas capilares, la validez de los hamiltonianos efectivos, locales y no locales que se usan para el estudio de estos sistemas.

Para una simulación NVT, en el que el número de partículas permanece constante, hemos encontrado que en el comportamiento de las fluctuaciones de la posición media de la anchura del slab adsorbido juegan un papel fundamental la compresibilidad del líquido y la evaporación-condensación de partículas entre el líquido y el vapor. Además hemos encontrado que solamente para slab muy estrechos se hace relevante el potencial efectivo por la presencia de la pared dado el corto alcance de éste. Para interpretar estos resultados hemos desarrollado un modelo sencillo que incorpora la compresibilidad del líquido y la evaporación-condensación y que describe perfectamente el comportamiento de la posición media de la interfase líquido-vapor y el comportamiento de su dispersión en función del tamaño de la capa líquida adsorbida. Hemos de remarcar que esta verificación del modelo no se hubiese podido conseguir sin la gran precisión del ISM en la determinación de la posición de la interfase entre un líquido y un vapor. Por último, en muchas aplicaciones de los hamiltonianos interfaciales efectivos utilizados[4,5] hasta ahora para describir estos sistemas no se han tenido en cuenta los efectos de la compresibilidad y los de evaporación-condensación, por lo cual deben ser revisados. Una vez incorporados estos efectos, para nuestro potencial efectivo de corto alcance y en condición de wetting total, nuestros resultados parecen indicar que una descripción local del hamiltoniano efectivo es suficiente para describir bien el comportamiento de nuestro sistema, aunque es necesario realizar un estudio mas sistemático.

* efernand@icmm.csic.es

[1] D. Bonn, J. Eggers, J. Indekeu, J. Meunier y E. Rolley, Rev. Mod. Phys. 81, 729 (2009).
[2] E. Chacón y P. Tarazona, Phys. Rev. Lett. 91, 166103 (2003).
[3] E. Chacón y P. Tarazona, J. Phys.: Condens. Matter 117, (45), S3493 (2005).
[4] M. E. Fisfer y A. J. Jin, Phys. Rev. B 44, 1430 (1991).
[5] A. O. Parry, J. M. Romero-Enrique, N. R. Bernardino y C. Rascón, J. Phys.: Condesns. Matter 20, 505102 (2008).

Una perspectiva termodinámica al estudio de comunidades microbianas: dinámica y estructura de población en cultivos *in vitro* de *Plasmodium falciparum*

Jordi Ferrer*, Clara Prats, Daniel López
Escola Superior d'Agricultura de Barcelona
Universitat Politècnica de Catalunya
08860 Castelldefels

La variabilidad es una característica esencial de las comunidades microbianas. Los organismos unicelulares muestran gran versatilidad y plasticidad debido a su sensibilidad a las fluctuaciones y hetrerogeneidad de su entorno inmediato. En consecuencia, y como estrategia de adaptación a un entorno natural muy inestable, la población muestra gran diversidad y variabilidad en su estructura y evolución[1].

El análisis termodinámico se emplea en microbiología a escala molecular y celular. Su aplicación a la escala de poblaciones o ecosistemas en su conjunto esta condicionada por la enorme complejidad de los sistemas a tratar. Actualmente, els uso de conceptos y métodos de la termodinámica en biotecnología se plasma en el cálculo de balances para todo proceso (principios de conservación) y el estudio de cinéticas de reacción y de fenómenos de transporte[2].

Sin embargo, el uso de conceptos y herramiebtas de la termodinámica en el análisis de la dinámica de poblaciones conlleva una mejora de la capacidad predictiva y un mayor control sobre los procesos industriales que emplean comunidades microbianas en condiciones controladas. Un ejemplo de ello lo ofrece el uso de la diversidad de una población, definida según la noción física de información, en el campo de la ecología teórica[3].

$$S_x = -\sum_{i=1}^{N} q_i(x) \cdot \log_2 q_i(x),$$

dónde S_x es la diversidad asociada a la característica x medida en bits, *q(x)* es la distribución de dicha diversidad y el subíndice i indica el número de categorías en las que distribuimos *q(x)*.

En el presente estudio, se alnaliza la diversidad de una población de *Plasmodium falciparum* infectando hematíes humanos en condiciones de cultivo estándar. Se toma en cuenta, únicamente, la distribución de edades entre los glóbulos rojos y la distribución de tiempos de infección entre los glóbulos rojos infectados. Se emplean datos experimentales obtenidos por el equipo Experimental Microbiology Group-GSK y se comparan con un modelo computacional basado en el individuo.

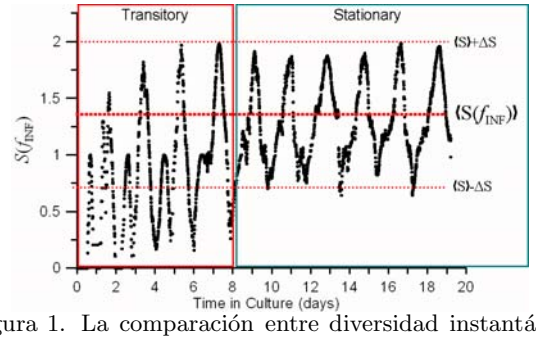

Figura 1. La comparación entre diversidad instantánea y diversidad prevalente de un cultivo permite definir estados transitorios y estacionarios.

El uso de la diversidad de población permite definir regiménes transitorios y estacionarios y establece criterios cuantitativos para la comparación de poblaciones similares con dinámicas parecidas.

Los resultados prácticos que se desprenden del análisis permiten: 1) proponer mejoras en los protocolos de cultivo actuales, 2) establecer criterios de comparación entre los cultivos *test* y *control* en ensayos farmacológicos, y 3) sugerir líneas de desarrollo de los cultivos para mejorar su rendimiento y fiabilidad. El tipo de análisis presentado aquí es muy simple y se puede aplicar a cualquier distribución en cualquier comunidad microbiana.

* jordi.ferrer-savall@upc.edu

[1] Brehm-Stecher BF and Johnson EA Microbiol Molec Biol Rev 68 (2004)
[2] von Stockar U J Non-equil Thermody 35 (2010)
[3] Margalef R Am Nat 97 (1963)

Tuning water transport in carbon nanotubes with a strong perpendicular electric field

Luis Figueras, Jordi Faraudo*
Institut de Ciència de Materials de Barcelona (ICMAB-CSIC),
Campus UAB,
E-08193 Bellaterra, Spain.

Carbon nanotubes are paradigmatic examples of materials with novel and exciting properties arising at the nanoscale. One of the possible applications of these materials is in nanofluidic transport (of water electrolyte or only water) across membranes. In this contribution, we present a molecular dynamics simulation study of water transport along nanotubes. We consider the interesting case of very small radius of the order of the size of a water molecule. In spite of the strong hydrophobic character of the nanotubes, previous simulations[1] have demonstrated the ability of water to fill and permeate across the nanotube. It has been argued that strong hydrogen bonds, formed in the one-dimensional chain of water molecules crossing the channel, make water permeation possible.

In this work, we considered the effect of applying strong electric fields, perpendicular to the flow of water. In this case, we observe a competition between two interactions: the hydrogen bond interaction between neighboring molecules inside the tube and the orientation induced by the electric field (which is perpendicular to the orientation induced by hydrogen bonding). We observe substantial effects for sufficiently strong electric fields (> 1 V/nm), corresponding to an interaction energy between the water dipole and the field of the order of the energy of the hydrogen bond. At these fields, the one-dimensional chain structure of water inside the nanotubes is disrupted (now the tubes are only partially filled) and the permeation of water through the tube becomes more difficult. The flow of water strongly decreases as the electric field increases, even under the effect of strong pressure differences trying to pump water thorough the nanotubes. For electric fields of the order of ~ 4 V/nm, the nanotubes are almost empty (only containing isolated, perpendicularly oriented water molecules) and the flow of water is effectively blocked. Our results suggest that perpendicular electric fields may be convenient ways of tuning and regulating the flow of water in these peculiar nanofluidic devices.

* jfaraudo@icmab.es

[1] G. Hummer, J.C. Rasaiah and J.P. Noworyta, Water conduction through the hydrophobic channel of a carbon nanotube. Nature **414**, 188 (2001).

Regulation of neuronal differentiation at the neurogenic wave front

Pau Formosa-Jordan* [(1)], Marta Ibañes [(1)], Saúl Ares [(2)], José María Frade [(3)]
[(1)] *Departament d'Estructura i Constituents de la Matèria, Facultat de Física, Universitat de Barcelona, Spain*
[(2)] *GISC and Max Planck Institute for the Physics of Complex Systems, Dresden, Germany*
[(3)] *Instituto Cajal, CSIC, Madrid, Spain*

Neurogenesis in the vertebrate embryonic retina is an example of pattern formation of differentiated cells. In this case, cells differentiate into either neural or non neural fates. The choice between these two fates relies on the expression of the so-called proneural genes: this expression induces neural differentiation, while cells become non neural in its absence.This fate choice is regulated spatially through a process termed lateral inhibition with feedback[1]. Such a process is mediated by two kind of proteins, the Notch receptor and the Delta ligand: when Delta ligand anchored in a cell membrane binds to its receptor Notch in a neighbouring cell, it generates a signal towards the cell harbouring the receptor that inhibits the proneural genes. Feedback arises from the fact that (i) all cells can potentially express the receptor and the ligand and then each cell can perform lateral inhibition to its neighbouring cells, and (ii) Delta expression itself can be inhibited by Notch signaling. As a result, neural cells (or equivalently high-expressing Delta cells) differentiate surrounded by non neural cells (or low-expressing Delta cells) in an ordered salt and pepper pattern.

Theoretical studies on lateral inhibition dynamics for pattern formation have focused until now in unrealistic fields of cells with periodic boundary conditions. This combined experimental and theoretical study focuses on a more realistic situation of a fine grained pattern emerging in a discrete multicellular system behind a travelling wave[2] and analyses how its progression depends on the state that is being invaded.

In the retina of chick embryos, the pattern emerges first in the centre of this tissue and spreads out defining a differentiation wavefront which divides the retina in two areas: a differentiating inner domain (the neurogenic domain) and a surrounding undifferentiated region[3–5]. In the inner domain the lateral inhibition process takes place and differentiation of the first neural cells starts. In the undifferentiated region the proneural genes are not expressed, Delta is in high levels and there is no lateral inhibition dynamics. The boundary between both domains moves forward when cells nearby get differentiated. This scenario is what we call a self-regulated wavefront.

The goal of our study is to decipher the role of high Delta expression in the invaded undifferentiated area for proper pattern emergency. For this purpose we have derived an extension of the nonlinear dynamics coupled in space of Collier's model[1]. We have performed an exploration across the parameter space with simulations in two very different scenarios: having Delta (wild-type situation, WT) or not (Delta=0) in the invaded domain of undifferentiated cells. Stochastic simulations have been performed on irregular cell lattices (Voronoi tesselations). The limits of deterministic dynamics and regular hexagonal lattices have been evaluated as well.

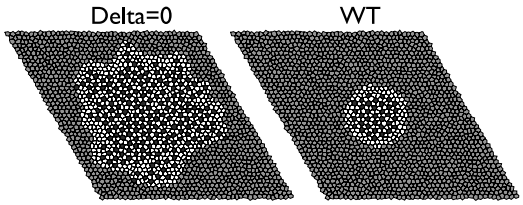

Figura 1. Snapshots from simulation results showing the emerging fine grained patterns in the tissue without Delta (Left) and in the wild type situation (Right) at the same time point. Black cells are neural precursors, white cells are non neural cells that are feeling the lateral inhibition effect and gray cells belong to the undifferentiated tissue being invaded. The morphological instability and fastest growth in the Delta=0 scenario are observed.

Our model shows that the presence of the Delta ahead from the neurogenic wavefront has two important roles in relation to proper pattern emergency. First of all, Delta protein reduces the possibility to have either a massive neurogenic phenotype or sparse patterns, facilitating proper lateral inhibition patterning. Second, the expression of Delta slows down the velocity of the differentiation wave front and promotes its morphological stability. These predictions explain some of the observations made by Rocha et al[6] in a vertebrate embryonic retina and might be extrapolated to other organisms and other neural tissues. Indeed, by applying our theory to the morphogenetic furrow progression in the eye of flies, we reproduce experimental results on front perturbation[7].

* pformosa@ecm.ub.es

[1] J. R. Collier, N.A.M. Monk, P.K. Maini and J. H. Lewis. J. Theor. Biol. **183**, 429-446 (1996).
[2] E. Plahte and L. Øyehaug. Physica D **226**, 117-128 (2007).
[3] C. Prada, J. Puga, L. Pérez-Méndez, R. López and G. Ramírez. Eur. J. Neurosci. **3**, 559-569 (1991).
[4] M. Hu, and S. S. Easter. Dev. Biol. **207**, 309-321 (1999).
[5] Formosa-Jordan P., Ibañes M., Ares S., Frade J.M. Manuscript in preparation.
[6] S. F. Rocha, S. S. Lopes, A. Gossler, and D. Henrique. Dev. Biol. **328**, 54-65 (2009).
[7] N.L. Brown, C.A. Sattler, S.W. Paddock and S.B. Carroll. Cell **80**, 879-887 (1995).

Large decrease of fluctuations for supercooled water in hydrophobic nanoconfinement

Elena G. Strekalova[1], Marco G. Mazza[2], H. Eugene Stanley[1], Giancarlo Franzese[3]*
[1] *Center for Polymer Studies, Department of Physics, Boston University, Boston, MA USA*
[2] *StranskiLaboratorium für Physikalische und Theoretische Chemie, Technische Universität Berlin, Strasse des 17. Juni 135, 10623 Berlin* [3] *Departament de Física Fonamental, Universitat de Barcelona, Barcelona, Spain*

Using Monte Carlo simulations we study a coarse-grained model of a water layer confined in a fixed disordered matrix of hydrophobic nanoparticles at different particle concentrations c. For $c = 0$ we find a 1st order liquidliquid phase transition (LLPT) ending in one critical point at low pressure P. For $c > 0$ our simulations are consistent with a LLPT line ending in two critical points at low and high pressure. For $c = 25\%$ at high P and low temperature T we find a dramatic decrease of compressibility, thermal expansion coefficient, and specific heat. Surprisingly, the effect is present also for c as low as 2.4%. We conclude that even a small presence of nanoscopic hydrophobes can drastically suppress thermodynamic fluctuations, making the detection of the LLPT more difficult[1–3].

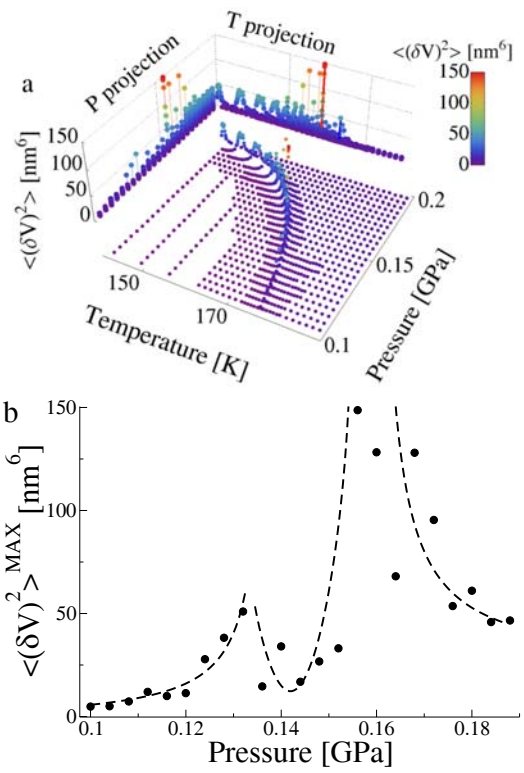

Figura 1. (a) Volume fluctuations $\langle(\delta V)^2\rangle$ for $c = 25\%$ have maxima that follow a locus in the $P - T$ plane that does not change, within the error bars, with c. The projections $\langle(\delta V)^2\rangle$ vs P or vs T clarify that the maxima do not change monotonically with P or T. (b) The projection of maxima of $\langle(\delta V)^2\rangle$ increase approaching $P = 0.132$ GPa and 0.156 GPa, consistent with our estimate of two critical points at ≈ 0.13 GPa and ≈ 0.15 GPa. Dashed lines are guides for the eyes.

* gfranzese@ub.edu

[1] E. G. Strekalova, M. G. Mazza, H. E. Stanley, and G. Franzese, Phys. Rev. Lett. **106**, 145701 (2011).
[2] G. Franzese, Valentino Bianco, and Svilen Iskrov, Water at interface with proteins, Food Biophysics, DOI: 10.1007/s11483-010-9198-4 (2011).
[3] K. Stokely, M. G. Mazza, H. E. Stanley, and G. Franzese, Proceedings of the National Academy of Sciences (PNAS) **107**, 1301 (2010).

Fluctuations and Stochastic Cell State Switching

D. Frigola*, J.M. Sancho, M. Ibañes
Dept. Estructura i Constituents de la Materia
Facultat de Física
Universitat de Barcelona
08028 Barcelona

Introduction. Genetic regulatory networks are biochemical systems which frequently work with very low copy numbers of the relevant molecules, and therefore noise can affect their behaviour in essential ways[1]. An example of this can be seen in the experiments performed by Acar et al. on the galactose signalling network in *S. Cerevisiae* yeast[2]. This is a bistable system with high-concentration (ON) and low-concentration (OFF) states and shows stochastic switching between these states[2]. Acar et al[2] observed that the rate of this switching depended on the state of origin: for the same energy barrier to be overcome, cells switched with a higher rate from ON to OFF than the opposite. We seek to explain this phenomenon through the use of stochastic methods and a simple model.

Methods. The galactose signalling network forms a positive feedback loop mediated by 3 different molecules. To simplify the analysis, we chose to model it as an autoactivating loop (a positive feedback loop with no intermediates) in which the molecule promotes its own production according to a Hill function[3]. The nonlinearity of this function is able to make the system bistable. For this model, the corresponding Master Equation and Fokker-Planck Equation can be derived[4]. The resulting adimensional Langevin Equation reads

$$\dot{x} = A(x) + \sqrt{B(x)}\xi(t)$$

$$A(x) = \frac{ax^2}{x^2+1} - x + R \ , \quad B(x) = \frac{ax^2}{x^2+1} + x + R$$

$$< \xi(t) >= 0 \ , \quad < \xi(t)\xi(t') >= \frac{1}{V}\delta(t-t')$$

where a is the maximal production rate, R is a basal production rate and V is the cell volume. The noise obtained from the proper derivation of the Langevin equation is a multiplicative noise of intensity $\frac{B(x)}{V}$. For the sake of comparison we also did all our calculations with an additive noise of constant intensity.

We did an analysis of the Mean First Passage Time (MFPT) from each of the states, both theoretically (although numerically evaluated) from the Fokker-Planck equation and with simulations, both using the Langevin equation and the Gillespie algorithm (this last one used for the Master Equation).

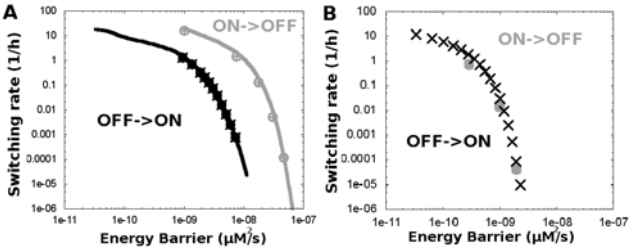

Figura 1. **Multiplicative noise is needed to reproduce the asymmetry in transition rates A** Switching rates versus deterministic energy barrier calculated for the model with multiplicative noise. The continuous lines correspond to the numerically evaluated theoretical expression, and the symbols to Langevin and Gillespie simulations. We can see how at the same energy barrier, the ON to OFF switching rate is different than the OFF to ON rate. This is in agreement with experimental data from Acar et al[2]. **B** Switching rates calculated for the model with an additive noise instead of a multiplicative one. We can see how the asymmetry is lost. Numerically evaluated theoretical expressions have been represented with symbols to be able to distinguish both switching directions.

Results and conclusions. Our results[5] show that a multiplicative noise reproduces the experimentally observed asymmetry in switching rates, whereas an additive noise can not, as seen in figure 1. The meaning of this is that intrinsic fluctuations in the main component of the system (due to the stochasticity of chemical reactions) can explain the experimental phenomenon. This points out that intrinsic fluctuations in the numbers of a molecule can have nontrivial effects in the behaviour of a system, and in some cases (like this one), adding them as a correction (as in the case of additive noise) can leave out relevant information.

* frigola.david@gmail.com

[1] A. Eldar and M.B. Elowitz, *Functional roles for noise in genetic circuits*, Nature **467**, 167 (2010)
[2] M. Acar, A. Becskei and A. van Oudenaarden, *Enhancement of cellular memory by reducing stochastic transitions*, Nature **435**, 228 (2005)
[3] A. Becksei, B. Seraphin and L. Serrano, *Positive feedback in eukaryotic gene networks: cell differentiation by graded to binary response*, The EMBO Journal **20**, 2528 (2001)
[4] Z. Cheng, F. Liu, X. Zhang and W. Wang, *Robustness analysis of celular memory in an autoactivating positive feedback system*, FEBS Letters **582**, 3776 (2008)
[5] D. Frigola, J.M. Sancho & M. Ibañes, *Asymmetric Stochastic switching driven by intrinsic fluctuations in biochemical switches*, Preprint (2011)

Dos escenarios de extinción en redes de interacción planta-polinizador. Aplicación en redes alpinas de alta montaña

Javier Galeano*, Juan Manuel Pastor+, Silvia Santamaría±, Marcos Méndez±
Depto. Ciencia y Tecnología Aplicadas
E.U.I.T. Agrícola Universidad Politécnica de Madrid
28040 Madrid

La desaparición de las interacciones planta-polinización supone una amenaza tanto para las especies de plantas como para la comunidad en general. Este problema es potencialmente muy importante en los ecosistemas de alta montaña, donde las interacciones planta-polinizador juegan un papel clave.

Los primeros estudios que exploraron la tolerancia de las redes de polinizadores a la eliminación de sus nodos sugieren una elevada robustez de la red[1]. Sin embargo, estos estudios que eliminan especies, bien de plantas bien de polinizadores, pueden ser poco realistas desde el punto de vista ecológico.

El presente trabajo queremos estudiar la evolución de las redes de planta-polinizador a los procesos de extinciones utilizando dos escenarios distintos y tres secuencias de extinciones por cada uno de los escenarios. Los dos escenarios que proponemos en el trabajo son: extinción de nodos y la extinción de enlaces. El primer escenario ya ha sido estudiado por Memmott y colaboradores[1] y nosotros proponemos realizar las extinciones eligiendo otro nuevo escenario, que es eliminar interacciones entre especies, es decir, enlaces de la red. Este nuevo escenario, podría simular una disminución gradual en la abundancia de una especie. Dentro de cada uno de los dos escenarios anteriormente citados, realizamos tres secuencias diferentes de extinción: de mayor número de conexiones a menor, de menor a mayor y aleatoria.

Estas simulaciones de extinción se han realizado sobre redes mutualistas reales de planta-polinización en regiones alpinas y sobre redes sintéticas. Debido a que las redes reales suelen ser pequeñas, se utilizaron redes aleatorias para explorar el efecto de la conectancia y la asimetría de las dimensiones de las redes en la robustez.

Las simulaciones, tanto de extinción de nodos como de interacciones, indicaron una gran influencia de ambas características que impide hacer generalizaciones en cuanto a la robustez de las redes de polinización alpinas. Por otro lado, la extinción de interacciones introducida en el presente trabajo sugiere menor robustez que la tradicional extinción de nodos. Es necesario mejorar el conocimiento de las interacciones planta-polinizador en poblaciones en declive para aumentar el realismo en los escenarios simulados de evaluación de la robustez.

---

* javier.galeano@upm.es
+ juanmanuel.pastor@upm.es
± Área de Biodiversidad y Conservación, Universidad Rey Juan Carlos, Móstoles, Madrid.

[1] Memmott J., Waser N. M., and Price M. V. Tolerance of pollination networks to species extinctions, Proc. Biol. Sci., 2004, 271 (1557) pp. 2605-11.

Estudio de la Solvatación de una Molécula de Amoniaco en Nanogotas de Helio Utilizando Técnicas de Difusión de Monte Carlo Cuánticas

Antonio Gamboa*, Jordan A. Ramilowski**, Rosa M. Benito, David Farrelly**
Departamento de Física Aplicada, Universidad Politécnica de Madrid
Av. Complutense s/n, 28040 Madrid, Spain

Los estudios experimentales con gotas de helio tienen una larga historia, que se podría remontar a 1908[1]. Sin embargo, dos importantes avances tecnológicos en los años 90 han brindado la posibilidad de estudiar la interacción de moléculas dopantes inrtroducidas en gotas de ^{4}He. El primero, en 1992, fue la creación de la tecnología que permitió utilizar a las nanogotas de helio como matrices espectroscópicas[2]. El segundo fue el llamado experimento de Andronikashvili microscópico[3,4], el cual permitió observar el comportamiento rotacional de la molécula en interacción con las nanogotas de ^{4}He. Los resultados de estos experimentos utilizando SF_6 y OCS como moléculas dopantes fue sorpresivo, ya que se observaban un comportamiento rotacional de la molécula como el de un rotor libre, pero con una constante rotacional renormalizada(reducida) con respecto a la de la molécula pura. Por ejemplo, en el caso de SF_6, la constante rotacional renormalizada es de aproximadamente un tercio de la que se observaría en fase gaseosa.

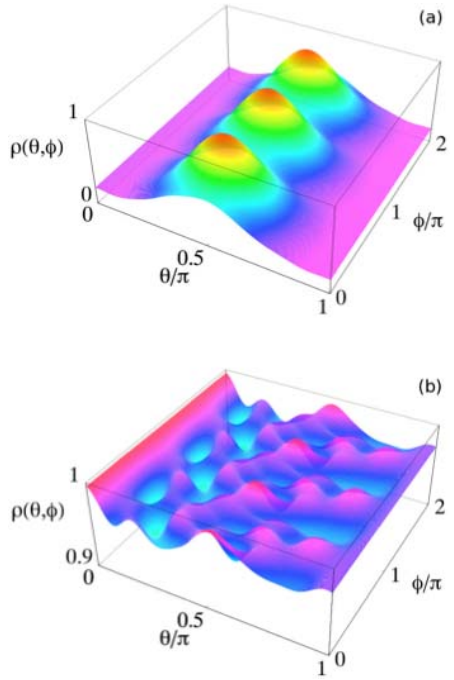

Figura 1. Proyección en el plano $\theta - \phi$ de la densidad $\rho = \sqrt{|\Psi(R_0, \theta, \phi)|^2}$ obtenida de las simulaciones de DMC. En (a), las constantes rotacionales son veinte veces menores que el valor físico real, el cual es utilizado para construir la gráfica mostrada en (b). El comportamiento de la densidad para la molécula real puede considerarse como prácticamente isotrópico (Nótese la diferencia de escalas utilizada)

En este trabajo se realiza la simulación de la dinámica de solvatación de una molécula de amoniaco dentro de una nanogota de ^{4}He conteniendo $N = 1 - 25$ átomos. Para ello se utiliza la técnica de difusión de Monte Carlo, la cual permite obtener el estado fundamental de un sistema cuántico de muchos cuerpos. Los estados excitados han sido calculados utilizando el método del nodo fijo utilizando una separación adiabática entre los movimientos radial y angular de la molécula. Se ha calculado una reducción de la costante rotacional de la molécula de alrededor de un 5 %, lo cual es de acuerdo de manera cuantitativa con experimentos recientes publicados por Slipchenko and Vilesov[5] y en contradicción con la renormalización mucho más grande de $\approx 25\%$ publicada originalmente por Behrens, et al[6] en un artículo anterior.

Asimismo, las simulaciones muestran que, para la molécula de amoniaco, el límite asintótico de saturación no se alcanza hasta $N > 25$. Este comportamiento es similar al que se tiene para otras moléculas lineales como HF, HCl y HBr[7], las cuales tienen unas constantes rotacionales relativamente grandes al igual que la molécula de amoniaco.

Estos resultados corroboran la hipótesis de que las moléculas con constantes rotacionales grandes deben (i) tener una menor renormalización de sus momentos de inercia y (ii) necesitar un mayor número de átomos de ^{4}He para alcanzar el estado de saturación, a diferencia del caso de rotores más pesados, donde la renormalización es alcanzada de manera relativamente rápida principalmente debido a un seguimiento adiabático de los átomos de helio a la molécula.

* a.gsuarez@alumnos.upm.es
** Department of Chemistry, Utah State University, Logan, UT 84322-0300, USA

[1] J. A. Northby, J. Chem. Phys. **115**, 10065,(2001).
[2] S. Goyal, D. L. Schutt, G. Scoles, Phys. Rev. Lett. **69**, 933, (1992).
[3] E. L. Andronikashvili, J. Phys. USSR. **10**, 201, (1946).
[4] S. Grebenev, J. P. Toennies, A. F. Vilesov, Science. **279**, 2083, (1998).
[5] M. N. Slipchenko, A. F. Vilesov, Chem. Phys. Lett. **412**, 176, (2005).
[6] M. Behrens, U. Buck, R. Fröchtenicht, M. Hartmann, F. Huisken, F. Rohmund, J. Chem. Phys. **109**, 5914, (1998)
[7] J. A. Ramilowski, A. A. Mikosz, D. Farrelly, C. Fajin, B. Fernandez, J. Phys. Chem. A. **49**, 12275, (2007)

Modelos primitivos para sistemas con autoensamblado

Noé G. Almarza*
Instituto de Química-Física Rocasolano
Consejo Superior de Investigaciones Científicas
C/ Serrano 119, E-28006 Madrid

Los recientes avances en la preparación de partículas coloidales en cuyas superficies se incorporan centros de interacción *enlazantes* están abriendo un interesante campo de estudio de la química-física supramolecular.[1]

Resulta de gran interés tanto teórico como práctico el análisis del efecto del número y de la topología de los citados centros de interacción sobre el diagrama de fases de estos sistemas.[1]

Por otra parte, el alto grado de direccionalidad de las interacciones presentes en los correspondientes modelos plantea interesantes retos desde el punto de vista de la simulación *molecular*.

En esta contribución se analizará la capacidad de modelos muy sencillos (primitivos) para capturar los rasgos físicos esenciales de los diagramas de fase de estos sistemas complejos. La determinación de los diagramas de fase se lleva a cabo utilizando métodos de simulación de Monte Carlo.

En concreto se presentarán diversos modelos de tipo gas reticular (lattice gas) que dan cuenta de distintos fenómenos peculiares que tienen lugar en los diagramas de fase de sistemas con asociación o autoensamblado molecular:

- Se mostrará como un modelo relativamente simple,[2] definido sobre una red tridimensional, es capaz de dar cuenta de los rasgos esenciales del diagrama de fases de sistemas de partículas anisotrópicas con simetría tetraédrica.[3–5] En particular, el modelo propuesto presenta fases cristalinas de baja densidad estables desde el punto de vista termodinámico.

- Se presentarán resultados del estudio de las transiciones orden-desorden (Véase FIG. 1) de sistemas de segmentos rígidos que se forman por polimerización de monómeros con dos centros de interacción adsorbidos sobre redes ordenadas bidimensionales[6,7].

- Finalmente se presentarán algunos resultados recientes[8] en los que se demuestra que un sencillo modelo de tipo gas reticular puede exhibir equilibrios líquido-vapor *exóticos*[9] en los que la densidad del líquido puede disminuir al reducirse la temperatura dando lugar a lo que se conoce en la literaura reciente como líquidos vacios (empty liquids)[1].

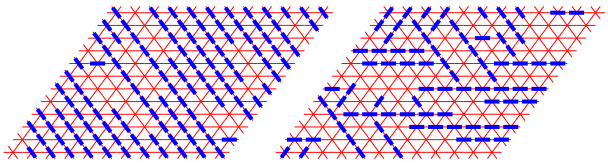

Figura 1. Ejemplos de configuraciones ordenada (derecha) y desordenada (izquierda) para un modelo de segmentos rígidos autoensamblados (SARR)[6,7] sobre redes triangulares.

* noe@iqfr.csic.es

[1] F. Sciortino, Collect. Czech. Chem. Commun. **75**, 349 (2010).
[2] N.G. Almarza, and E.G. Noya, Mol. Phys. **109**, 65 (2011).
[3] F. Romano, E. Sanz, and F. Sciortino, J. Phys. Chem. B **113**, 15133 (2009).
[4] F. Romano, E. Sanz, and F. Sciortino, J. Chem. Phys. **132**, 184501 (2010).
[5] E.G. Noya, EG , C. Vega, C. , J.P.K. Doye, and A.A. Louis, J. Chem. Phys. **132**, 234511 (2010).
[6] N.G. Almarza, J.M. Tavares, and M.M. Telo da Gama, Phys. Rev. E **82**, 061117 (2010).
[7] N.G. Almarza, J.M. Tavares, and M.M. Telo da Gama, J. Chem. Phys. **134**, 071101 (2011).
[8] N.G. Almarza et. al, (To be published).
[9] J. Russo, J.M. Tavares, P.I.C. Teixeira, M.M. Telo da Gama, and F. Sciortino, to be published in Physical Review Letters (2011).

Dynamics of encapsulated water

Miquel Garcia-Ratés[†], Pere Miró[‡], Carles Bo[‡,§], Josep Bonet Avalos[†*]
[†] *Departament d'Enginyeria Química, ETSEQ, Universitat Rovira i Virgili, 43007 Tarragona, Spain*
[‡] *Institute of Chemical Research of Catalonia, ICIQ, 43007, Tarragona, Spain*
[§] *Departament de Química Física i Química Inorgànica, Universitat Rovira i Virgili, 43007 Tarragona, Spain*

Confined liquids behave differently than in the bulk. Water is not an exception. Several experimental and theoretical studies have analyzed the effect of confinement of water in different environments such as graphite channels, carbon nanotubes, silica pores, reverse micelles or metal oxide nanocapsules.[1–3] These studies show that the presence of an interface distorts the hydrogen bond (HB) network creating a peculiar layering inside the system or clear distinct regions of bound water and bulky water. However, not only the structural parameters of water are changed as a function of the distance to the wall, but also its dynamics is different as the surface is approached from inside. For hydrophilic surfaces, water molecules have slower dynamics due to the strong HBs with the charged sites of the confining surface. The difference in the dynamics is highly dependent on the water-confining surface interaction and on the geometry of the latter. Reorientational, translational and vibrational dynamics clearly reflect these changes.

We have studied the structure and dynamics of water confined inside a polyoxomolybdate molecular cluster $[\{(Mo)Mo_5O_{21}(H_2O)_6\}_{12}\{Mo_2O_4(SO_4)\}_{30}]^{72-}$ metal oxide nanocapsule by means of molecular dynamics simulations at ambient conditions. The obtained radial density profiles of water oxygen atoms indicate that the characteristic three-dimensional HB network present in bulk water is distorted inside the cavity where water organizes instead in concentric layered structures. Hydrogen bonding, tetrahedral order and orientational distributions analyses reveal that these layers are formed by water molecules hydrogen bonded with three other molecules of the same structure. The remaining hydrogen bond donor/acceptor site bridges different layers as well as the whole structure with the hydrophilic inner side of the cavity. From these results we conclude that the most stable configuration of the layers is thus that of a buckyball with twelve pentagons and a variable number of hexagons (see Fig. 1) depending on the layer.

To study the overall dynamics of the water layers and the possible switch of water molecules between them, we have defined the occupation number of water molecules in a given layer. Exchange of water molecules between layers are rarely observed, due to the stability of the hydrogen bonded layers. At long times, the system shows a power law decay $\nu^{-\alpha}$ with exponents α characteristic of pink noise in properties like the fluctuations in the number of molecules in the layers, $\langle \Delta n_i(0) \Delta n_i(t) \rangle$, and the total dipole moment, $\langle \vec{M}(0)\vec{M}(t) \rangle$ (see Fig. 2). The exponent is surprisingly related to the structure of the layer and, in particular, to its overall tetrahedral order.

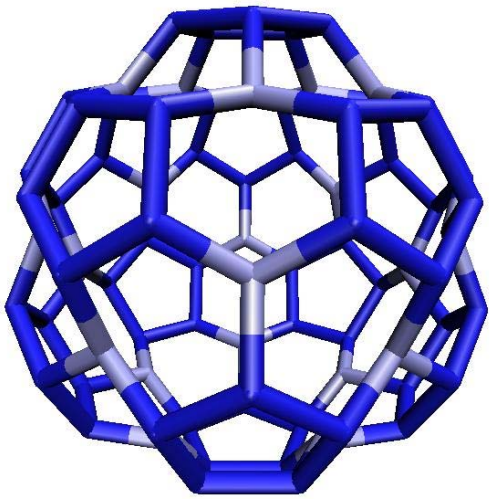

Figura 1. Suggested buckyball-like structure, for water molecules forming $\{H_2O\}_{80}$ layer in our system at $T = 188$ K.

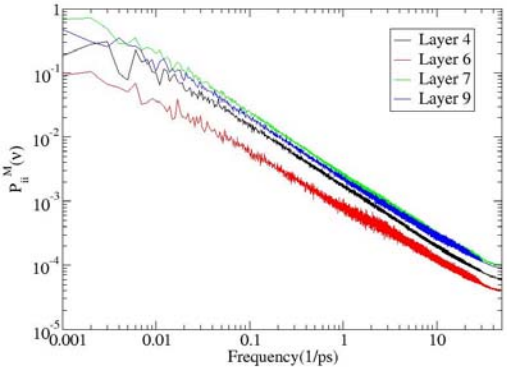

Figura 2. Power spectrum $P_{ii}^{M}(\nu)$ of the total dipole moment correlation function $\langle \vec{M}(0)\vec{M}(t) \rangle$.

Finally, rotational correlation functions and infrared absorption spectra have also been computed.

* josep.bonet@urv.cat

[1] J. Marti, G. Nagy, E. Guardia, and M. C. Gordillo, J. Phys. Chem. B **110**, 23987 (2006).
[2] J. Faeder, and B. M. Ladanyi, J. Phys. Chem. B. **110**, 14304 (2006).
[3] T. Mitra, P. Miro, A. R. Tomsa, A. Merca, H.Bögge, J. B. Avalos, J. M. Poblet, C. Bo, and A. Müller, Chem. Eur. J. **15**, 1844 (2009).

Un obstáculo a la salida disminuye la probabilidad de atasco

I. Zuriguel, A. Garcimartín, A. Janda, C. Lozano*
Departamento de Física y Matemática Aplicada
Facultad de Ciencias, Universidad de Navarra
31080 Pamplona

Una propiedad específica de los medios granulares es que pueden dar lugar a *atascos*. En una tubería, un orificio, o en un estrangulamiento, se puede formar un arco que detenga el movimiento de los granos. El arco no es sino un conjunto de partículas estables frente a los esfuerzos responsables del flujo.

Cómo evitar los atascos es una cuestión de gran relevancia en la industria, y para ello muchas veces se utilizan métodos que implican la inyección de energía (como vibraciones, por ejemplo). Con ello se consigue que el arco se vea sometido a otros esfuerzos diferentes, que provocan su inestabilidad, y se rompa.

Sin embargo, en algunas ocasiones es interesante emplear algún otro método que no implique la inyección de energía al medio y que disminuya la probabilidad de que se formen atascos. Un ejemplo paradigmático puede ser la salida de emergencia de un local de gran capacidad. Colocar un obstáculo frente a la salida (por ejemplo, una columna) puede reducir la probabilidad de atasco, a expensas, quizá, de reducir el flujo (número de partículas que escapan por unidad de tiempo). Es algo que se conoce desde hace algún tiempo[1].

Presentamos aquí los resultados preliminares de un experimento en el que vamos a medir la probabilidad de atasco y el flujo de partículas que salen de un orificio frente al cual se ha colocado un obstáculo. En la figura 1 se muestra un caso en el que se ve un arco que ha taponado la salida.

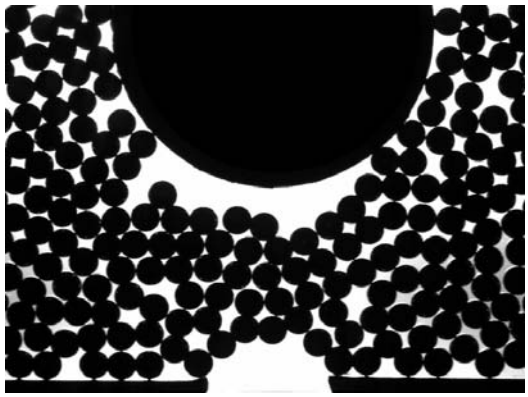

Figura 1. Un arco que tapona la salida, con un obstáculo fijo más arriba.

Los primeros resultados indican que efectivamente la probabilidad de atasco se reduce enormemente, si lo comparamos con el caso de salida libre[2], pero a condición de que el obstáculo se encuentre colocado ni muy cerca ni muy lejos de la salida. Por otro lado, al contrario de lo que sería de esperar, no parece que el flujo de partículas se reduzca notablemente; es más, en algunos casos podría incluso aumentar[3].

---

* `http://fisica.unav.es/granular`

[1] Se pueden ver algunas simulaciones en la página Web de D. Helbing: `http://angel.elte.hu/~panic/`.

[2] A. Janda, I. Zuriguel, A. Garcimartín, L. A. Pugnaloni and D. Maza, "Jamming and critical outlet size in the discharge of a two-dimensional silo", *Europhys. Lett.* **8**4 (2008), 44002.

[3] C. Mankoc, A. Janda, R. Arévalo, J. M. Pastor, I. Zuriguel, A. Garcimartín and D. Maza, "The flow rate of granular materials through an orifice", *Gran. Matt.* **9** (2007), 407–414.

Influencia de la asociación en las funciones respuesta de metanol: efecto de la temperatura y la presión en condiciones supercríticas

P. Gómez-Álvarez*, A. Dopazo-Paz, J. M. Míguez, L. Romaní, D. González-Salgado
Universidad de Vigo. Departamento de Física Aplicada.
As Lagoas s/n. C.P. 32004. Ourense. España.

En un trabajo previo, se desarrolló una metodología[1] para analizar el efecto de la asociación en las funciones respuesta para un líquido puro autoasociado utilizando simulación molecular por el método de Monte Carlo. El procedimiento esencialmente implica expresar la energía residual y volumen del fluido en términos de estas propiedades para dos fluidos hipotéticos, uno compuesto por los monómeros y el otro por las moléculas asociadas. Esto permite escribir las funciones respuesta en una forma perturbativa como combinación del valor de la propiedad en el fluido formado por monómeros y la contribución de asociación (el término perturbativo). El método propuesto fue usado para determinar ambas contribuciones a la capacidad calorífica isobárica y a las derivadas del volumen respecto a la temperatura y la presión para metanol a lo largo de la isobara supercrítica de 50 MPa desde 220 a 1500 K. Se obtuvo que ambos términos influyen para la capacidad calorífica mientras que el término de asociación para las propiedades volumétricas es despreciable.

Aquí, extendemos ese estudio para la evaluación del efecto de la presión. En base a este objetivo, se han llevado a cabo simulaciones a varias presiones desde 25 MPa hasta 4 GPa en el mismo intervalo de temperatura que en el trabajo previo. En base a los resultados, modificar la presión implica importantes e interesantes cambios, fundamentalmente para la capacidad calorífica isobárica y la derivada del volumen respecto a la temperatura, para los que la contribución debida a los monómeros pierde importancia en favor del término de asociación al aumentar la presión. Paralelamente, se ha obtenido una detallada descripción de la estructura de metanol en los intervalos de temperatura y presión considerados.

* ga_paula@uvigo.es

[1] P. Gómez-Álvarez, A. Dopazo-Paz, L. Romaní, and D. González-Salgado, J. Chem. Phys. **134**, 014512 (2011).

La introducción de las interacciones efectivas en la mecánica estadística de las disoluciones: el trabajo de Einstein del año 1905 sobre el movimiento browniano

Juan Luis Gómez Estévez
Dept. Física Fonamental
Facultat de Física,Universitat de Barcelona
Diagonal 647, 08028 Barcelona
jlgomez@ffn.ub.es

En su trabajo sobre el movimiento browniano publicado en 1905 [1], Einstein da, entre otros resultados, una demostración de la ley de Van't Hoff para la presión osmótica de las partículas (solutos) suspendidas en un fluido (disolvente). Su demostración se basaba en su propia versión de la mecánica estadística en el conjunto canónico. Este resultado ha sido raramente citado y discutido pero constituiría la primera utilización, al menos de forma implícita, del método de las interacciones efectivas en la física del estado líquido [2]. En este trabajo, se analiza el método empleado por Einstein , se discuten las hipótesis implícitas empleadas en su artículo y se presenta una formulación correcta de la termodinámica del sistema en términos de una función de partición canónica efectiva. Como resultado final, la ley de Van't Hoff es deducida en forma rigurosa utilizando un método general que permite su extensión formal para sistemas más concentrados.

[1] A. Einstein, Ann, Physik XVII (1905) 549. También en "Investigations on the theory of Brownian movement"por A. Einstein. Editado con comentarios por R. Fürth (Dover, New York, 1956).

[2] D. Frenkel, Physica A 313 (2002) 1.

Self-localized states in one and two dimensions in lasers with external feedback

P.V. Paulau, Damià Gomila*, Pere Colet
IFISC, Instituto de Física Interdisciplinar y Sistemas Complejos (CSIC-UIB)
Campus Universitat Illes Balears, E-07122 Palma de Mallorca, Spain

B. Malomed
Department of Physical Electronics, Faculty of Engineering, Tel Aviv University, 69978, Tel Aviv, Israel

W.J. Firth
Department of Physics, University of Strathclyde, 107 Rottenrow East, Glasgow G4 0NG, UK

Dissipative solitons have long demonstrated their potential for information processing applications. Because of their compactness and extensive use in the information and telecommunication industry, the case of solitons observed in Vertical Cavity Surface Emitting Lasers (VCSEL) is particularly interesting. Different types of transverse localized states have been observed in a number of different configurations. In particular, the existence and stability of vortices in a simple model for VCSEL with frequency-selective feedback were already analyzed in a previous work[1]. Here we use a complex Ginzburg-Landau approach to describe the dynamics of these devices. There is a good qualitative agreement between our results and those from more detailed models. We extend a known analytical one-dimensional self-localized solution to a continuous family of two-dimensional soliton-stripe solutions (Fig. 1). The existence and stability of two-dimensional vortex solitons is also demonstrated. We shown that the radius of the vortices increase linearly with their topological charge (Fig. 2). Moreover, a stripe-soliton can be interpreted as vortex with topological charge $m = \infty$ (and vice versa). Thus, 2D vortex solitons can be interpreted as a soliton-stripe bent into a ring. Complex radial dynamics are observed as a result of the interplay between curvature driven dynamics and moving (Ising-Bloch) transitions (Fig. 3). These general properties of the vortex solutions are applicable to a large group of physical systems.

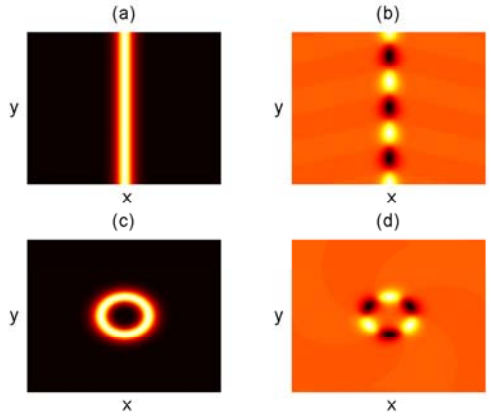

Figura 1. Spatial distribution of the (a) amplitude and (b) real part of the field for an unstable 2D stripe soliton. (c-d) the same as (a-b) for a stable vortex with azimuthal number $m = 3$

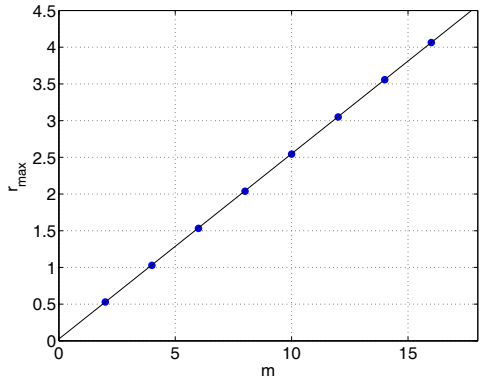

Figura 2. Equilibrium radius of vortex solitons as a function of the topological charge m. Filled circles mark even integer values of m, while the solid line is a linear fitting showing that all points lie on a straight line.

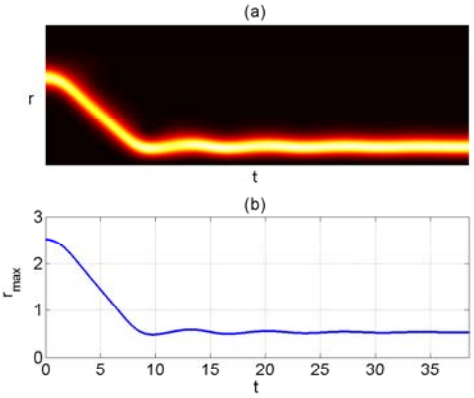

Figura 3. (a) Spatio-temporal dynamics of the radial profile of the field amplitude relaxing towards the equilibrium radius of a vortex with $m = 2$. (b) Dynamics of the position r_{max} of the maximum of the amplitude.

* damia@ifisc.uib-csic.es

[1] P.V. Paulau, D. Gomila, P. Colet, N. Loiko, N. Rosanov, T. Ackemann, and W.J. Firth, Optics Express **18**, 8859 (2010).

Autoorganización de filamentos de proteína FtsZ sobre un sustrato

P. González de Prado,* P. Tarazona
Departamento de Física Teórica de la Materia Condensada
Universidad Autónoma de Madrid
28049 Madrid

FtsZ es una proteína que juega un papel crucial en la división bacteriana, ya que es capaz de formar un anillo proteico directamente relacionado con la constricción de la membrana, proceso que ocurre en ausencia de motores moleculares. Sin embargo, todavía se desconocen los detalles de este mecanismo de autoensamblaje y de la generación de la fuerza de constricción.

Utilizando el microscopio de fuerzas atómicas (AFM) se puede estudiar el comportamiento de FtsZ en solución sobre una superficie con una resolución muy alta, que permite distinguir los diferentes filamentos de FtsZ. Las estructuras observadas se compararan con el resultado de simulaciones Monte Carlo para modelos de red bidimensional en los que se incluyen las interacciones esenciales entre monómeros de FtsZ. Estas interacciones incluyen un enlace longitudinal fuerte que admite una cierta flexibilidad (permitiendo por tanto la curvatura de los filamentos) y una interacción lateral débil.[1]

El trabajo que se presenta trata de avanzar por este camino, centrándose en los últimos experimentos con mutantes de FtsZ. Utilizar estos mutantes permite seleccionar la orientación con la que los monómeros se adhieren a la superficie, generando nuevas estructuras que aportan mucha información sobre las interacciones entre monómeros. De esta forma se explora el papel de la anisotropía del enlace lateral en FtsZ, un factor que hasta el momento no había sido considerado en el problema pero que podría tener importancia en el comportamiento de FtsZ *in vivo*.

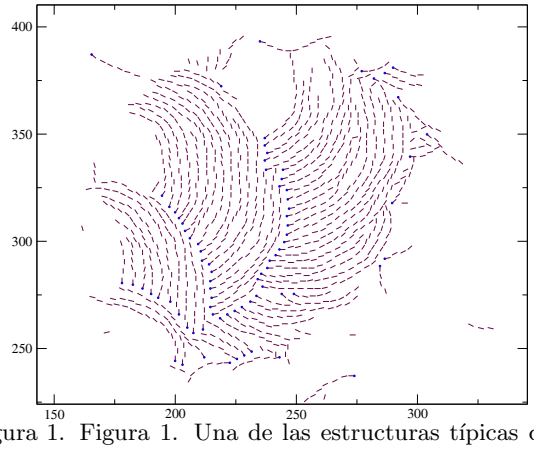

Figura 1. Figura 1. Una de las estructuras típicas que se observan al introducir la anisotropía en el enlace lateral.

* pablo.gonzalezdeprado@uam.es

[1] A. Paez, P. Mateos-Gil, I. Hörger, J. Mingorance, M. Vicente G. Rivas, M. Vélez y P. Tarazona, PMC Biophys. **2**(1):8, (2009).

Mesoscopic perturbation on a reaction-diffusion system modifies the Turing instability

Jacobo Guiu-Souto* , Jorge Carballido-Landeira, Alberto P. Muñuzuri.
Grupo de Física Non Lineal. Facultade de Física
Universidade de Santiago de Compostela
E-15782 Santiago de Compostela, Spain

We study, theoretically and experimentally, the dynamical response of macroscopic Turing patterns to a mechanical periodic forcing which implies a sinusoidal modulation of gravity. Theoretical predictions indicate that the extra energy, due to the forcing, modifies the diffusion coefficient at a microscopic level, producing changes in the Turing domain and in the pattern characteristics, in particular its wavelength. To check the theoretical analysis, we perform numerical simulations with standard models. Experiments were also performed in the closed BZ-AOT system. Experiments as well as numerical and theoretical results show a good agreement.

* jacobo.guiu@rai.usc.es

[1] J. Guiu-Souto, J. Carballido-Landeira, V. Pérez-Villar and A. P. Muñuzuri *Phys. Rev. E* 82 066209 (2010).
[2] A. von Kameke Kameke, F. Huhn, G. Fernández-García, A. P. Muñuzuri and V. Pérez-Muñuzuri *Phys. Rev. E* 81, 066211 (2010).
[3] J. Carballido-Landeira, V. K. Vanag and I. R. Epstein *Phys. Chem. Chem. Phys.* 12, 3656 (2010).

An Age-Dependent Branching Model for Macroevolution

Emilio Hernández-García[1*], Stephanie Keller-Schmidt[2], Murat Tuğrul[3], Víctor M. Eguíluz[1], Konstantin Klemm[2]
[1] *IFISC (CSIC-UIB) Instituto de Física Interdisciplinar y Sistemas Complejos[†], E-07122 Palma de Mallorca, Spain*
[2] *Bioinformatics, Institute of Computer Science, University Leipzig Härtelstr. 16-18, 04107 Leipzig, Germany*
[3] *IST Austria, Am Campus 1, 3400 Klosterneuburg, Austria*

Phylogenetic trees are reconstructions of the evolutionary history of organisms or genes based on present-day genomic information. Branching patterns in phylogenetic trees help to identify and distinguish different evolutionary mechanisms. The imbalance of phylogenetic trees (i.e. the amount of asymmetry between the two subtrees arising in a branching event) exhibits a systematic deviation from the expectation of a purely random tree growth process (such as provided by the Yule or the ERM models). Random tree branching leads to a scaling of the depth of the trees (the mean distance of tips from root) with tree size n as $d \sim \log n$, whereas true phylogenies display a faster depth scaling with size[1]. Some models[2,3] have been already proposed to fit such behavior, but without a clear biological meaning.

Here we introduce an age-dependent growth model based on the hypothesis that speciation rate is a decreasing function of the waiting time since the last speciation. We find that the depth grows as $(\log n)^2$ in leading order with tree size n. This result is in good agreement with the trend observed by exhaustive analysis of the phylogenetic databases TreeBASE and PANDIT (see Fig. 1). Exact likelihood computation of the model on the trees up to 20 tips contained in the databases is performed. Higher likelihoods values are found when compared with a previously suggested model[4].

* emilio@ifisc.uib-csic.es
† http://ifisc.uib-csic.es/

[1] E.A. Herrada, C.J. Tessone, K. Klemm, V.M. Eguíluz, E. Hernández-García and C.M. Duarte, *Universal Scaling in the Branching of the Tree of Life*, PLoS ONE **3**, e2757 (2008).
[2] D.J. Ford *Probabilities on cladograms: Introduction to the alpha model*, PhD Thesis, Stanford University, available in arXiv.org as math/0511246.
[3] E. Hernández-García, M. Tuğrul, E.A. Herrada, V.M. Eguíluz and K. Klemm, *Simple models for scaling in phylogenetic trees*, International Journal of Bifurcation and Chaos **20**, 805-811 (2010).
[4] M.G. Blum and O. François, *Which Random Processes Describe the Tree of Life? A Large-Scale Study of Phylogenetic Tree Imbalance*, Systematic Biology **55**, 685-691 (2006)

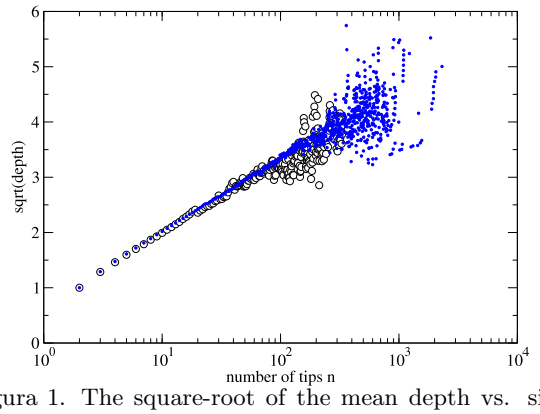

Figura 1. The square-root of the mean depth vs. size of phylogenetic trees contained in databases for species (TreeBASE; empty circles) and proteins (PANDIT; filled circles). The mean depth is averaged for all trees having the same number of tips. In this scale (log-linear), the behavior $d \sim (\log n)^2$ is a straight line. Data from TreeBASE were downloaded from http://www.treebase.org on June, 2007 containing 5,212 phylogenetic trees; data from PANDIT were downloaded from http://www.ebi.ac.uk/goldman-srv/pandit on May 2008 and contains 7,738 protein families.

Control of nematic liquid crystals orientation using paramagnetic asymmetric microparticles

Sergi Hernàndez-Navarro, Pietro Tierno, Josep Claret, Jordi Ignés-Mullol, Francesc Sagués
SOC & SAM group, IN2UB (Institute of Nanoscience and Nanotechnology) and Departament de Química Física, Universitat de Barcelona, Martí i Franquès 1, 08028 Barcelona, Spain

We present a new method to control the orientation of thermotropic nematic liquid crystals (NLC) by means of weak magnetic fields[1]. A NLC with negative dielectric anisotropy is doped with paramagnetic asymmetric microparticles, and then introduced in a cell made of ITO-glass plates with homeotropic anchoring conditions. In the absence of magnetic field, when applying a potential difference between the two ITO-glass plates, the NLC molecules acquire a planar degenerate estate, and the microparticles locally align with the NLC director. The application of a magnetic field parallel to the ITO-glass leads to a collective reorientation of particles and NLC molecules altogether. This phenomenon is already observed with magnetic fields ranging from 1 to 3 mT, far below the magnetic field threshold for the Frederiks transition. This effect, already visible using individual microparticles (Fig. 1), is quite amplified when particles are assembled into clusters.

A simple model is proposed to account quantitatively for the observed reflectivity pattern around an isolated ellipsoid. Similar modeling approaches have been applied to forced free-standing Smectic-C films[2,3]. We start with the usual one-constant approximation to express the elastic free energy as

$$F_{el} = \int \frac{1}{2} K \left(\partial_\alpha n_\beta \partial_\alpha n_\beta\right) d\vec{r}, \tag{1}$$

where K accounts for an average elastic constant, and $\vec{n} = (\cos\phi, \sin\phi, 0)$. A two-dimensional approach is here justified for symmetry reasons and this permits to write the above free energy density in terms of the azimuthal angle $\phi(\vec{r})$:

$$F_{el} = \int \frac{1}{2} K \left(\nabla\phi\right)^2 d\vec{r}. \tag{2}$$

Minimizing eq. (2) under steady state conditions leads to the Laplace equation for in-plane distortions, $\Delta\phi = 0$. This harmonic approximation is easily solved in terms of close- and far-field boundary conditions $\phi(r = r_0) = \phi_p$, $\phi(r = R) = \phi_b$. The first condition refers to the liquid crystal distortion at the contact surface with the ellipsoid and is simply taken as the (measured) angle of rotation of the particle itself. The second prescription refers to the spontaneous azimuth alignment that spans submillimeter regions in the planar NLC configuration. We attribute this phenomenon to the unavoidable presence of orientational quenched disorder on the confining surfaces and, even though it results in weak bulk forces that are easily overcome by the applied magnetic torques, it nevertheless provides a fixed boundary condition far from the colloidal inclusions. We take into account such effect by assuming that at some cut-off distance R from the center of the analyzed particle, the orientation of the liquid crystal recovers its bulk pinned local value ϕ_b. The latter is taken equal to zero according to the initial condition of the experiment. The closed solution of eq. (2) then reads:

$$\phi(r) = \frac{\phi_P \ln\left(\frac{r}{R}\right)}{\ln\left(\frac{r_0}{R}\right)}. \tag{3}$$

Fitting for R and r_0 ($r_0 \leq$ ellipsoid short axis) permits to reconstruct a pattern of transmitted light intensity for arbitrary rotation angles of the magnetic inclusion, which compares favorably well with the experimental data.

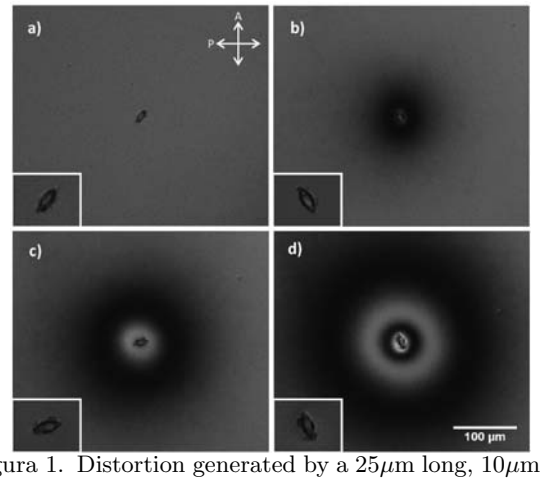

Figura 1. Distortion generated by a 25μm long, 10μm wide ellipsoid rotated CCW inside a 30$\pm$2μm thick cell. The four insets are enlargements (factor 1.8) of the central ellipsoid. Initial (field-free) orientation is taken as 0° (a). The magnetic field (3mT) is applied in (a), and then particle rotates, following the magnetic field, by an angle of 80° (b), 140° (c), and 240° (d).

[1] P. Tierno, J. Claret, F. Sagués and A. Cebers, Phys. Rev. E **79**, 021501 (2009)
[2] Cladis, P. E. and Couder, Y. and Brand, H. R., Phys. Rev. Let. **55**, 2945-2948 (1985)
[3] Eremin, A. and Bohley, Ch. and Stannarius, R., Eur. Phys. J. E **21**, 57-67 (2006)

Amplitude equation description of vertebrate segmentation

Adrián Jacobo[1],* Damià Gomila[2], Manuel Matías[2], Saul Ares[1], Luis Morelli[1,3], Andrew Oates[3], Frank Jülicher[1]
[1] *Max Planck Institute for the Physics of Complex Systems, Dresden*
[2] *Instituto de Física Interdisciplinar y Sistemas Complejos (IFISC), Palma de Mallorca, Spain*
[3] *Max Planck Institute of Molecular Cell Biology and Genetics, Dresden*

The segmentation of the vertebrate body axis is a rhythmic and sequential process controlled by a multicellular clock. This clock operates in the presomitic mesoderm (PSM), a tissue situated at the tail of the growing embryo. Traveling waves of oscillatory gene expression sweep across the field of PSM cells[1,2].

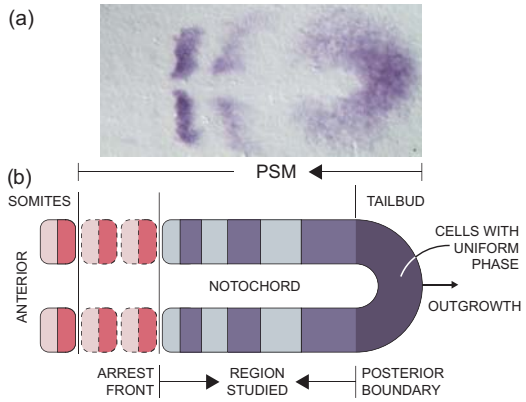

Figura 1. (a) Snapshot of deltaC mRNA expression patterns in the PSM of the developing zebra fish embryo. The cells in the tailbud oscillate homogeneously generating a traveling wave across the PSM. (b) Schematic PSM together with the already determined segments and the most recently formed somites. Figure reproduced with permission from Ref.[2].

This clock has been described either by models of regulatory networks or by simpler descriptions in terms of phase oscillators[2]. While these phase descriptions do not consider amplitude effects, gene regulatory networks are too complex to draw any general conclusion about these effects[1].

To address the effects of the amplitude of the oscillations in the segmentation clock we propose a model based on the Complex Ginzburg-Landau Equation (CGLE):

$$\frac{\partial A}{\partial t} = (\mu + i\omega)A + (b_r + ib)A|A|^2 + (c_r + ic)\nabla^2 A + v\nabla A \qquad (1)$$

The CGLE describes an oscillatory medium close to a supercritical Hopf bifurcation[3], in agreement with accepted gene regulatory network models of the segmentation clock[4]. We added to the equation a drift term to describe the system in the moving PSM reference frame. We also consider a spatial frequency profile, motivated by morphogen gradients in the PSM[2]. The presence of this profile generates the traveling wave pattern.

By taking into account the amplitude of the oscillations in a simple way, we are able to reproduce previous results describing the oscillations in the PSM and to find instabilities which are not present in phase descriptions, and were not described in genetic regulatory networks. These instabilities can lead to distinct regimes, including spatiotemporal chaos (Fig. 2). Our theory suggests possible perturbations to developing embryos that could disrupt the behavior of the segmentation clock and lead to the described regimes.

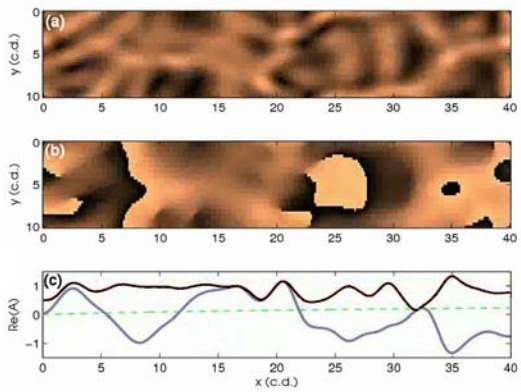

Figura 2. Spatiotemporal chaos in the CGLE. (a) $|A(x,y)|$. (b)$Arg(A(x,y))$. (c) Transversal cut of $|A(x,y)|$ (black line), Re(A(x,y)) (grey line) and spatial frequency profile (dashed line).

* jacobo@pks.mpg.de

[1] Oates, A.C., N. Gorfinkiel, M. González-Gaitán, and C.P. Heisenberg. Nature Reviews Genetics **10**,517 (2009).
[2] Morelli, L. G ., S. Ares, L. Herrgen, C. Schröter, F. Jülicher, and A. C. Oates. HFSP Journal **3**,55 (2009).
[3] Kramer, L., and I. S. Aranson. Rev. Mod. Phys **74**, 99 (2002)
[4] Lewis, J. Curr. Biol. **13**, 1398 (2003).

Equilibrio y ruptura de simetría en gases granulares vibrados

Nagi Khalil*, J. Javier Brey
Física Teórica, Universidad de Sevilla
E-41080 Sevilla, España

Se estudian los estados estacionarios del sistema formado por gases granulares vibrados separados por un pistón adiabático[1,2]. El sistema exhibe una transición de fase de no equilibrio con una ruptura espontánea de simetría. Incluso en el caso en el que los dos gases tienen el mismo número de partículas y las mismas propiedades mecánicas, sus densidades y temperaturas pueden ser diferentes. Este es el caso considerado en lo que sigue.

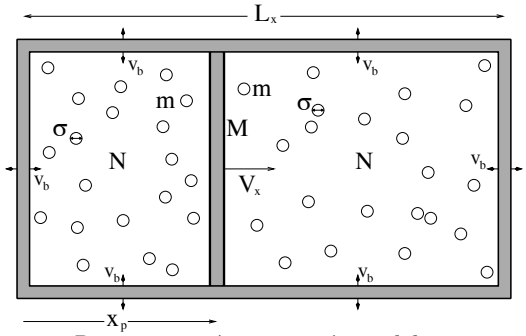

Figura 1. Representación esquemática del sistema estudiado que es análogo al usado en algunos experimentos[2]. N es el número de partículas en cada subsistema de masa m y diámetro σ. M es la masa del pistón, x_p su posición y V_x su velocidad. Las paredes se mueven con un perfil de diente de sierra de velocidad v_b.

Un modelo cinético sencillo, que tiene en cuenta flujos de calor a través del pistón[3,4] y las paredes[3], proporciona una explicación satisfactoria del comportamiento del sistema: el pistón oscila en torno a la posición intermedia del sistema para ciertos valores de los parámetros, haciéndo en otra posición para otros. El parámetro de orden es $|2x_p/L_x - 1|$ y el de control es λ.

$$\lambda = \frac{8NL_x a}{2Ly(2Na+b)+2bL_x},$$

$$a = \frac{\pi(1-\alpha^2)}{8\sqrt{2}}; \quad b = \frac{L_y m}{\sigma M}.$$

$$|2x_p/L_x - 1| = \frac{\sqrt{\lambda^2-4}}{\lambda}.$$

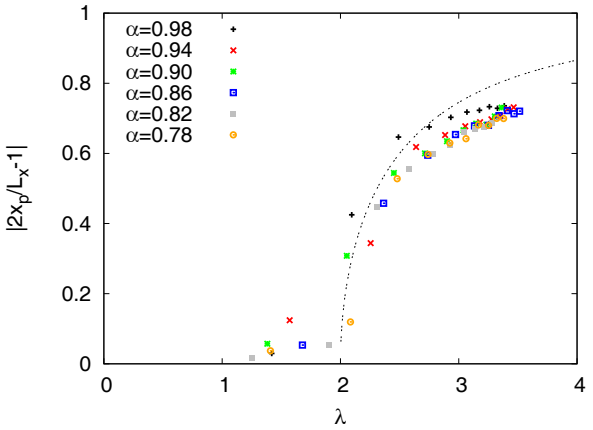

Figura 2. Medida de la ruptura de simetría del sistema como función del parámetro de control[1] λ, para distintos valores del coeficiente de restitución normal α que caracteriza las colisiones entre los granos. Los puntos se han obtenido con de dinámica molecular y la línea discontinua es la predicción teórica.

Un análisis de estabilidad lineal de las ecuaciones determina que sólo cuando es posible una situación simétrica ésta es estable. Para valores de los parámetros del sistema en los que son posibles varias soluciones, el sistema elige una configuración en la que las densidades y las temperaturas de los dos gases son diferentes.

Los resultados de dinámica molecular están en acuerdo con las predicciones teóricas.

* nagi@us.es

[1] J. J. Brey y Nagi Khalil, arXiv:1102.1569v1 (2011).
[2] F. Lechenault y Karen E. Daniels, Soft Matter, **6** 3074 (2010).
[3] J. J. Brey y M. J. Ruiz-Montero, Phys. Rev. E. **79**, 031305 (2009).
[4] J. J. Brey y Nagi Khalil, Phys. Rev. E. **82**, 051301 (2010).

Coupled Ising models and interdependent discrete choices under social influence in homogeneous populations

Ana Fernández del Río*, Elka Korutcheva, Javier de la Rubia
Departamento de Física Fundamental
Facultad de Ciencias (UNED), Paseo Senda del Rey 9 28040 Madrid

The study of traditional socieconomic discrete choice problems with interaction (of social norm, role model, or peer pressure type) allows for the use of statistical mechanical tools and models[1]. The simplest possible model is the infinite range Ising model with constant field, which considers completely homogeneous populations (in what concerns social influence, accurate knowledge of the average behaviour of the group and personal or social factors). This simple system already gives rise to interesting socieconomic interpretations[1].

Two such Ising models coupled directly through an additional term in the Hamiltonian have been studied and two different coupling schemes considered. Solutions have been numerically calculated and phase diagram sections constructed for the zero external fields (no pure private deterministic utilities) case.

The non-local model[2] (Weiss type coupling term) can be understood as describing the same decision making process in two groups, where individuals are subject to social influence from both their group and the other one. Examples of interest can be the study of public opinion on a given subject in two neighboring countries (regions, cities, neighborhoods...), companies in two related business sectors and their production technology option...

In the local model[3], coupling is only through each individual, and a single group is considered. Each individual makes two interrelated decisions. This is interesting in many contexts, for example, the interaction between different social pathologies (dropping from school vs teenage pregnancy...), other social traits (joining the labor force vs having a child...), opinion dynamics and political science (voting yes to two different propositions coming from the same party...) and indeed in economical contexts (buying different products of the same/competitor brand...).

Both models have remarkable similarities with a major difference: in the non-local case, for strong enough inter choice coupling, there are no stable solutions. This can be naturally explained as the non-local model *breaking down* when social influence of the *outsiders* is stronger than that exerted by the own peers (frustration).

For both models with zero external fields, either both average choices are zero (paramagnetic phase) or different from zero (ferromagnetic phases). Both models have an unbroken symmetry and so ferromagnetic phases have two physically identical equilibria. Critical curves separating paramagnetic and ferromagnetic phases have been analytically calculated. Note that in the nonzero field case these will still separate regions where social utility matters from regions where it does not. Another feature they have in common is that, if the coupling between both groups or choices is not too big, social interaction can give an outcome which opposes pure private utility (first order phase transition at zero inter-coupling which gives rise to metastability regions and hysteresis).

When compared to the uncoupled case, the interdependence introduces a higher trend to consensus (not favoring any specific direction). It also gives rise to interesting considerations concerning metastability and hysteresis in the light of interacting groups/decisions whose perception/interdependence is reversing. This can be of interest when studying opinion formation in social or political groups when their traditional inter-influence is changing or to study situations such as strong government action to compensate for *natural* reinforcement between undesired trends. Metastability regions involve (socially reinforced) situations in which the groups/options may be prevented from aligning (or disaligning) even when the *conditions seem right*.

There are some additional differences between both models. In the non-local case, metastable equilibria can exist for low temperatures up to $T = 0$. For the local case however, at a small enough temperature, these disappear. Another difference is that in the local case, if social pressure to conform to the norm is small enough or statistical fluctuations large enough, no order will emerge regardless how strong the inter-decision coupling is. Both of these differences can be explained in relation to whether the interdependence between both variables will add an effective term to the social (non-local case) or to the private (local case) deterministic utilities.

When introducing nonzero fields, the paramagnetic phase will disappear and an additional symmetry broken. New metastable equilibria should appear for small enough private utilities and need to be studied in detail. The introduction of quenched disorder in individual deterministic private utilities seems to be a natural next step. These models also need to be tested against real data.

---

* ana.fernandez@invi.uned.es

[1] S.N. Durlauf. How can statistical mechanics contribute to social science?. *Proceedings of the National Academy of Sciences*, 96:10582-10584, 1999.

[2] E.R. Korutcheva and D.I. Uzunov. Ising models and coupled order parameters. *Preprint Joint Inst. Nuclear Research Dubna, E-17-88-467., 1988*

[3] S. Galam, S.R. Salinas and Y. Shapir. Randomly coupled Ising models. *Physical Review B*, 51(5):2864-2871, 1995.

Analytical solution of a stochastic birth and death process including delay

Luis F. Lafuerza, Raul Toral*
IFISC, Instituto de Física Interdisciplinar y Sistemas Complejos, CSIC-UIB, Campus UIB, E-07122 Palma de Mallorca, Spain

Due to the small number of some molecules involved and of the uncontrolled environment, biochemical processes inside a cell usually need to be described by stochastic models[1]. Some important basic processes (such as transcription, translation or specific degradation) are indeed compound multistage reactions involving the sequential action of different molecules, and by virtue of the central limit theorem, the time to complete such processes should be nearly Gaussian with a well defined characteristic time, rather than exponential. A description including delay is then needed to obtain a reduced model for this kind of processes. It is well known that delay can change qualitatively the behavior of the system, allowing for example the apearence of oscillations[2], and there has been a great interest in delay-induced oscillations in biological systems

Stochastic processes that include delay are analytically difficult due to the non-Markovian character. Most theoretical studies consider a Langevin approach (stochastic differential equations) or systems in discrete time (were delay can be accounted for by increasing the number of variables). None of these approaches is completely suitable to describe chemical reactions inside a cell since the former neglects the inherently discrete nature of the molecule levels and the later considers an arbitrary discretization of time.

In this work we study a general stochastic birth and death process with delayed production and negative feedback. We use a master equation approach that respects the discrete nature of the protein numbers and is continuous in time.
We derive analytica expresions for the stationary probability distribution and the autocorrelation function. We show how the delay increases the amplitude of the fluctuations, changin the character of the system from sub-Poissonian to super-Poissonian as the delay is increased. We also study the effect of distributed delay.

* luis@ifisc.uib-csic.es, raul@ifisc.uib-csic.es

[1] Elowitz MB, Levine AJ, Sigga ED, Swain PS (2002). Science 297:1183-1186.
[2] MC Mackey and L Glass. Science 1977:287-289

Transient dynamics and geometrical properties in an spatial predator-prey model

Karina Laneri*◇, Alejandro Kolton †‡, Manojit Roy §, Mercedes Pascual §
Department of Ecology and Evolutionary Biology
University of Michigan, Ann Arbor, MI, USA

We study numerically an spatial individual-based predator-prey model whose mean-field counterpart is the Lotka-Volterra model. We analyze the transient dynamics towards the steady-states for different space dimensions through equal-time spatial correlation functions, cluster-geometry and cluster-size distributions of the different species. We relate our findings with recent results that display a robust bi-power law between global densities and densities of pairs allowing to write modified mean-field equations that well approximate the exact density dynamics.

* Institut Català de Ciències del Clima (IC3), Barcelona, Catalonia, Spain.
◇ klaneri@ic3.cat
† Departament de Física Fonamental, Universitat de Barcelona, Barcelona, Catalonia, Spain.
‡ CONICET, Centro Atomico Bariloche, Bariloche, Argentina.
§ Department of Ecology and Evolutionary Biology, University of Michigan, Ann Arbor, MI, USA.

Fluctuaciones grandes y función de grandes desviaciones en un sistema disipativo sencillo

A. Lasanta*†, A. Prados† Pablo I. Hurtado‡
†*Física Teórica. Universidad de Sevilla, Apdo. de Correos 1065, Sevilla 41080, Spain*
‡ *Instituto Carlos I de Física Teórica y Computacional, Universidad de Granada, Granada 18071, Spain*

En este trabajo se estudian las fluctuaciones de la energía disipada en un modelo disipativo sencillo. El sistema es un modelo de red unidimensional compuesto por N partículas, cada una caracterizada por una energía ρ_i $(i = 1, ..., N)$. Cuando se produce una interación entre dos partículas (vecinos más próximos), una parte de la energía del par se disipa y el resto se reparte aleatoriamente entre ellas[1]. Además sus extremos están acoplados a dos baños térmicos a temperatura T, alcanzando el sistema un estado estacionario caracterizado por perfiles de temperatura no lineales.

Figura 1. Representación esquemática del sistema.

Para tiempos grandes pero finitos, la disipación promediada temporalmente (D) fluctúa cumpliendo un principio de grandes desviaciones[2]

$$P(D) \sim e^{\tau N G(D)}. \quad (1)$$

Partiendo de la teoría hidrodinámica fluctuante[3,4], hemos calculado la función de grandes desviaciones, tanto numéricamente como analíticamente en el límite de disipación (ν) pequeña. Asimismo mediante técnicas Monte Carlo avanzadas[5], que nos permiten acceder a las colas de la distribución de probabilidades, hemos comprobado un buen acuerdo entre teoría y simulación para fluctuaciones grandes.

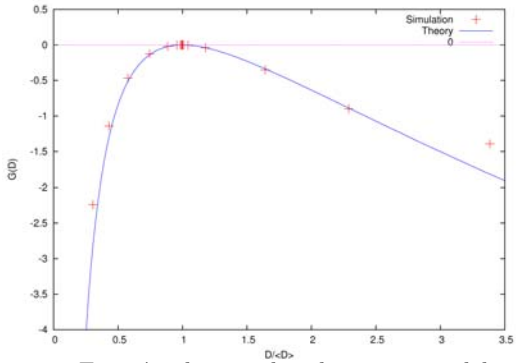

Figura 2. Función de grandes desviaciones del sistema. Comparación teoría-simulación para $\nu = 0.01$.

* alasanta@us.es

[1] D. Levanony and D. Levine. Phys. Rev. E, **73** 055102 (2006).
[2] H. Touchette. Physics Reports, **478** (2009).
[3] L. Bertini, A. De Sole, D. Gabrielli, G. Jona-Lasinio, and C. Landim. Phys. Rev. Lett., **87** 040601 (2001).
[4] T. Bodineau y M. Lagouge. J. Stat. Phys. **39** (2010).
[5] C. Giardina, J. Kurchan and L. Peliti. Phys. Rev. Lett., **96** 120603 (2006).

Stable shapes in the discocyte-equinocyte transition of the Red Blood Cell

Guillermo R. Lázaro[1*], Kathryn Melzak[3], Ignacio Pagonabarraga[2], Aurora Hernández-Machado[1]

[1] *Departament d'Estructura i Constituents de la Materia, Universitat de Barcelona*
[2] *Departament de Fisica fonamental, Universitat de Barcelona*
[3] *CIC biomaGUNE, Parque tecnológico de San Sebastian, Guipuzcoa*

Red blood cells are essential cells in our life since they are the unique oxygen transporters.They have a well defined stable shape, the biconcave discocyte. Their amazing mechanical properties allow them to undergo very large deformations while flowing across the thinnest capilaries, and they are able to resist to high turbulence flows in the main arteries as well.

If the membrane elastic properties are changed then the shape also changes and its functionality will be affected. There are many agents able to induce these changes: an increase in the pH of the surounding fluid, the depletion of ATP, etc... It has been demonstrated that indepentdly of the agent acting, the new shapes are always the same and are usually known as the "stomatocyte-discocyte-equinocyte"transition of the red blood cell.

This transition was first studied in the 80's[1], but until now one-cell experiments were not possible and specific studies of the RBC membrane properties have been developed very recently[2],[3].

In order to understand the physical principles that govern this transition, different elastic energies describing the membrane have been proposed. Some consider the bending of the membrane as the driven force and others focus on the elastic in-plane properties of the cytoskeleton. The most succesful is the area-difference elasticity model (ADE)[4],

$$H_{ADE} = \frac{\kappa_B}{2}\int (J - c_o)^2 dA + \frac{\bar{\kappa}\Pi}{2AD^2}(\Delta A - \Delta \ \ A_0)^2 \tag{1}$$

where the first term is the usual Canham-Helfrich free energy which penalizes the membrane bending and the second term accounts for the effects of the diference in area between the inner and the outer leaflet.

The equinocyte shape is asociated with a relative excess density of lipids in the outer monolayer of the membrane, after the action of some agent that induce a difusion of lipids from the inner monolayer. Since the diffusive time of the lipids from one leaflet to the other are tipically of 20 hours, it is difficult for the cell to relax and, in this sense, the equinocyte can be seen as a metastable state.

In our experiments we show how the cell can recover - in a short period of time- its initial shape using an atomic force microscopy tip. The tip produces a puncture in the cell membrane breaking the hydrophobic barrier that inhibits the spontaneous lipids diffusion. For that reason, when the AFM tip is inside the membrane, lipids can diffuse freely and the rearrangement of lipids allows the cell to relax to a lower energy configuration.

We fit the observed shapes by using the modified Cassini ovals, a family of curves that are known to reproduce the cross section of the discocyte. From here we can compute the energies of these shapes and obtain the energy landscape of the transition. This allows us to identify the relevant terms of the Hamiltonian (1) and its dependence on the control parameters.

Results show that the equinocyte-type shapes are local minima for high spontaneous curvature c_0 and prefered area-difference ΔA_0 , but as expected the global minima is the discocyte.

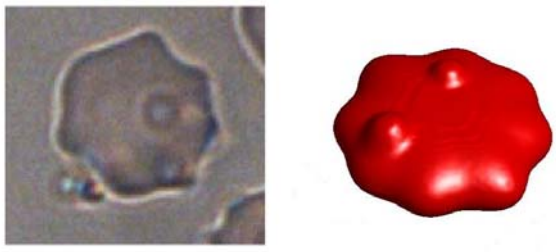

Figura 1. Discoequinocyte, comparison of experimental and analytic shapes.

* lazaro@ecm.ub.es

[1] J. E. Ferrell, K.J. Lee and W.H. Huestis, *Biochemistry* 24, 2849-2857, 1985.
[2] Y. Park *et al.*, *PNAS* 107, 6731-6736, 2010.
[3] Y. Park *et al.*, *PNAS* 107, 1289-1293, 2010.
[4] G. Lim, M. Wortis and R. Mukhopadhyay, *PNAS* 99, 16766-16769, 2002.

Quantum annealing of a hard combinatorial problem

Daniel Lecina Casas*, Matteo Palassini**
Facultat de Física
Universitat de Barcelona
Diagonal 647, 08028 Barcelona

Hard (NP-complete) combinatorial problems appear in many fields of study. An example are constraint satisfaction problems (CSPs), where one must decide if a set of N discrete variables can satisfy M constraints. Any CSP can be mapped into the q-coloring problem (q-COL): given a graph with N nodes and M edges, the aim is to find a configuration in which connected nodes have different colors chosen among q possibilities. q-COL is NP-complete, hence an efficient algorithm (i.e. with a running time polynomial in N) to solve q-COL would solve efficiently all NP problems. It can be mapped into the antiferromagnetic Potts model by defining a Hamiltonian equal to the number of unsatisfied constraints:

$$H_1 = \sum_i \sum_{j\in\partial i} \delta_{\sigma_i\sigma_j} \qquad (1)$$

where $\sigma \in \{1,\dots,q\}$ and ∂i is the set of nodes connected to i. Hence, a graph is solvable if the ground state energy of Eq. (1) is zero.

In this work, we present an investigation on the use of quantum annealing (QA)[1,2] for finding the ground state of H_1, using Erdős-Rényi random graphs with $q = 3$ as a test ground[3]. Given a generic classical Hamiltonian H_1 that we want to minimize, the idea of QA[1] (also called adiabatic quantum optimization[2]) is to promote H_1 to a quantum Hamiltonian $\widehat{H}_1$ and consider $\widehat{H}_\Gamma = \widehat{H}_1 + \Gamma\widehat{H}_2$ where Γ is a tuning parameter and $\widehat{H}_2$ a Hamiltonian that does not commute with $\widehat{H}_1$ and such that we can easily prepare the system in a ground state of $\widehat{H}_2$. The adiabatic theorem of quantum mechanics guarantees that if we start from a ground state of $\widehat{H}_2$ at $\Gamma \gg 1$, and lower Γ slowly enough (i.e. in a time of order at least Δ^{-2}, where Δ is the minimum energy gap between the ground state energy and the first excited state of $\widehat{H}_\Gamma$) the system will end up in the ground state of $\widehat{H}_1$ as $\Gamma \to 0$. Hence, QA could solve efficiently an NP-complete problem if Δ vanished polynomially in N.

Here we propose $\widehat{H}_2 = -\sum_i \sum_j |\sigma_i\rangle\langle\sigma_j|$ and sample from $e^{-\widehat{H}/T}$ at low temperature T via quantum Monte Carlo. To this end, we use the Suzuki-Trotter formula to map the partition function into that of a classical system with an auxiliary imaginary time:

$$-\beta H = -K_2 \sum_{\tau,i,j\in\partial i} \delta_{\sigma_i^\tau\sigma_j^\tau} + \tilde{\Gamma}\sum_{\tau,i} \delta_{\sigma_i^\tau\sigma_i^{\tau+1}} \qquad (2)$$

where τ runs over m copies of the original system, $K_2 = \beta/m$ and $\tilde{\Gamma} \geq 0$, with $\tilde{\Gamma} \to 0$ as $\Gamma \to \infty$ and viceversa. We perform Metropolis sampling from $e^{-H/T}$, decreasing Γ with a linear annealing schedule until we find a putative ground state. We investigate numerically the performance of QA as a function of the number of layers m, the number of Monte Carlo updates τ, and the initial value of $\tilde{\Gamma}$. Our preliminary results suggest that the running time of QA scales exponentially in N. In Fig. 1 we compare the performance of QA with that of (classical) thermal simulated annealing (TA) for $N = 128$ and several values of the constraint density $\alpha = M/N$. The performance of QA improves more rapidly, although the cost associated to the extra $m-1$ layers is such that QA does not improve over TA for these small sizes. Simulations at larger N are in progress.

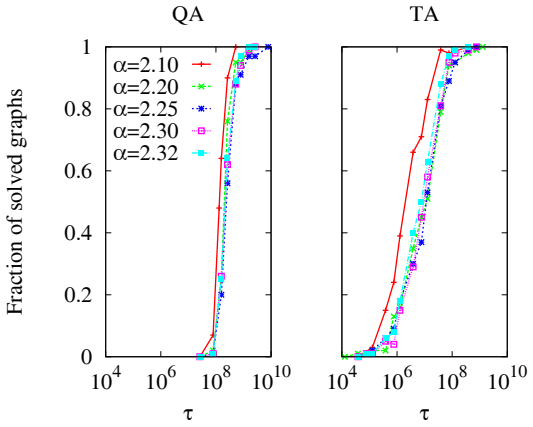

Figura 1. Fraction of instances solved by QA (with $m = 2^4 N$) and TA within τ total Monte Carlo steps. For each value of α we run QA and TA on 100 solvable instances with $N = 128$, with the same linear annealing schedule. Symbols in the right and left panel are the same.

* danilecina@gmail.com.
** palassini@ub.edu

[1] T. Kadowaki, H. Nishimori, Phys. Rev. E, 58, 5355 (1998)
[2] E. Farhi, J. Goldstone, S. Gutmann, J. Lapan, A. Lundgren, D. Preda, Science, Vol. 292 no. 5516 pp. 472-475 (2001)
[3] M. Mézard, M. Palassini, O. Rivoire, Phys. Rev. Lett. 95, 200202 (2005)

Aggregation dynamics and fluctuations in *in vitro* cultures of *Mycobacterium tuberculosis*

I.Llopis*, N.Caceres†, C.Prats, C.Vilaplana†, P-J.Cardona†, D.Lopez
Escola Superior d'Agricultura de Barcelona, Campus del Baix Llobregat, c/ Esteve Terradas, 8
Universitat Politècnica de Catalunya
08860 Castelldefels (Barcelona)

Mycobacterium tuberculosis (Mtb) is the bacillus responsible of the disease tuberculosis, which still today causes millions of deaths among the humanity.

Once it is inoculated in an *in vitro* culture medium, the Mtb may have to adapt to the new environment and, in this case, it remains without replicating for a period. In this phase it has a very low metabolic activity, i.e., it is in the lag phase. After a certain time, it can enter into the exponential phase (log phase), in which it replicates constantly at a certain growth rate. The typical Mtb growth rate in an *in vitro* culture is low compared to other bacterial populations (it duplicates once per day, approximately). As the nutrient resources deplete or the conditions become adverse, the growth rate slows down and the bacteria turn to the stationary phase until the conditions are appropriate for growth again. If the adverse conditions remain for a long time or are especially strong, bacteria may die (death phase). We have observed such growth curve in experiments using *in vitro* cultures (Fig.1), where we count the concentration of colony forming units (CFUs).

The Mtb bacillus has a particular characteristic that is not present in other bacteria and that leads to a curious phenomenon: as it grows, the Mtb tends to cluster in a straight line in the direction of the main axis of the bacteria, due to the lipidic components present in the cell wall, such as the *cord factor*, consequently forming a kind of filament, an elongated aggregate[1]. Thus, the characterization of the different growth phases of Mtb in *in vitro* cultures is linked to the formation of cords, as a form of bacillary resistance. This is shown in the correlation of the number and size of cords with the population growth rate.

We have analyzed, both experimentally and by mathematical models, the morphology and growth dynamics of Mtb in stirred liquid medium. In particular, we have focused on the role of aggregation, and how this aggregation affects their own growth dynamics[2].

We have developed an optical technique to analyze the characteristics of cords in a culture, such as the distribution of sizes, the mean size, the number of aggregates, etc. Microscopic images of a drop of the suspension have been processed by image analysis to determine the relevant information concerning the aggregates. This provides the necessary information to conclude the characterization of the in vitro bacillary growth.

Different cord size distributions are observed in the log phase and the subsequent static phase. When Mtb are replicating constantly, the size distributions are log normal, the majority of the cords are small and, after reaching a maximum at small aggregates, the frequency decreases. However, once in the stationary phase, te population displays a bimodal distribution (Fig.1), where a second peak of the distribution appears at larger aggregates (cords about 100 times larger than the ones that correspond to the first maximum). This bimodal distribution is qualitatively identical during the whole stationary phase[2].

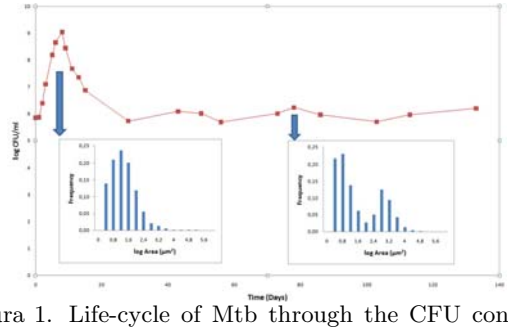

Figura 1. Life-cycle of Mtb through the CFU concentration for the lag, log and stationary phases. Insets: different cord size distributions, in the log phase and in the stationary phase, showing the different shape.

Besides, the experimental measurements during the stationary phase show periodic fluctuations in the CFU concentration, as has been mathematically modelled, which might be related to a certain dynamics of aggregation and disaggregation of cords. Hence, the stationary phase has an approximately constant number of CFUs, but they are breaking and grouping together forming cords all the time.

The European Communitys 7th Framework programme (FP7/2007-2013: STOPLATENT-TB project under grant agreement 200999) and el Ministerio de Ciencia e Innovacion (CGL 2010-20160) collaborated in funding the study.

* isaac.llopis@upc.edu
† Unitat de Tuberculosi Experimental, Institut Germans Trias i Pujol, Universitat Autònoma de Barcelona, CIBERES consortium.

[1] E.Julian, *et al.*, J. Bacteriology 192, 1751 (2010).
[2] N.Caceres, I.Llopis, C.Vilaplana, C.Prats, P-J.Cardona, D.Lopez, *in preparation.*

Renormalization-group corrections of White's approach for the prediction of the property fluctuations in the critical region applied to SAFT equations

F. Llovell[1]*, E. Forte[2], A. Galindo[2], L.F. Vega[1]
[1] *Institut de Ciència de Materials de Barcelona / MATGAS2000 AIE*
Campus de la UAB
08193 Bellaterra, Barcelona
[2] *Department of Chemical Engineering, Imperial College London*
South Kensington Campus
SW7 2AZ London, United Kingdom

The Statistical Associating Fluid Theory (SAFT) is a very successful theory to describe the phase behaviour of complex fluids. The key of the SAFT-based equations is their solid statistical mechanics basis which lets a physical interpretation of the system. In fact, their parameters are molecular, with physical meaning and transferable. It provides a framework in which the effects of molecular shape and interactions on the thermodynamic properties can be separated and quantified.

Although the capability of SAFT-type equations of state has been proved to be very successful in the prediction of thermodynamic properties of complex systems, the theory fails to predict the asymptotic universal behavior of all fluids when approaching the critical region. From a microscopic point of view, the classical theory of critical points corresponds to a mean-field approximation, which neglects local inhomogeneities (fluctuations) in density. It is well known that the nonclassical critical behavior of the thermodynamic properties is a consequence of the long-range fluctuations of an order parameter, the density for the case of pure fluids, the mixture density or the composition for the case of multicomponent systems. The spatial extend of the density fluctuations diverges at the critical point and becomes larger than any molecular scale in the critical region. Only theories which account for these density fluctuations can provide the correct approach to the critical region.

A treatment based on renormalisation group (RG) theory as developed by White and co-workers has proven very successful in improving the predictions of the critical region with different equations of state. The basic idea of RG is a transformation of the system's Hamiltonian into a renormalised one with a reduced number of degrees of freedom (finer microscopic degrees of freedom are integrated out). White and coworkers wrote a formalism as an iterative procedure to account for contributions to the free energy of density fluctuations of increasing wavelengths.

The RG method has been combined with a number of versions of SAFT, by implementing White's earliest ideas[1] with the improvements of Prausnitz and coworkers[2].

The purpose of this contribution is to revise the theory and their implementation and application into SAFT-type equations of state. In particular, it is intended to show some examples of the performance of this methodology into the soft-SAFT equation of state[3], showing a variety of different examples including comparison with molecular simulations and prediction of the critical region of complex mixtures.

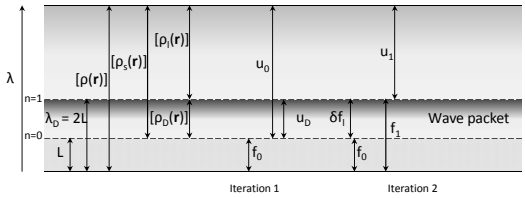

Figura 1. Representation of the iteration procedure.

Finally, some new insights based on the interpretation of White's latter developments[4] are shown to establish a rather straightforward method where the cut-off wavelength becomes the only adjustable parameter. The new implementation has been coupled into the SAFT equation of variable range (SAFT-VR)[5]. Results are compared to computer simulation data of the phase behaviour of chain and associating SW fluids to test the accuracy of the equation.

F. Llovell acknowledges a JAE-Doctor fellowship from the Spanish Government. This work has been partially financed by the Spanish government, Ministerio de Ciencia e Innovación, under project CTQ2008-05370/PPQ. Additional support from the Catalan government, under project 2009SGR-666, is also acknowledged.

* fllovell@icmab.es

[1] J. A. White, Fluid Phase Equilib. 75, 53 (1992)
[2] L. Lue, J. M. Prausnitz, J. Chem. Phys. 108, 5529 (1998).
[3] F. Llovell, J. C. Pàmies, L.F. Vega, J. Chem. Phys. 121, 10715 (2004)
[4] J. A. White, J. Chem. Phys. 111, 9352 (1999).
[5] E. Forte, F. Llovell, J.P.M. Trusler, L.F. Vega, A. Galindo, J. Chem. Phys. accepted (2011)

Slow dynamics in a highly turbulent von Kármán swirling flow

M. López , J. Burguete*
Departamento de Física y Matemática Aplicada
P.O. Box 177 E-31080, Pamplona, Spain.
Universidad de Navarra

In this work we present an experimental analysis of a von Kármán swirling flow and the analysis of the slow dynamics of the mean velocity field.

The experimental device consists in a cylindrical cavity filled with water (Fig. 1). In the lateral walls, two propellers are placed which can rotate independently and modified at will. The aspect ratio $\Gamma = H/D$ has been fixed to $\Gamma = ../Abstracts/lopez_caballero_miguel/1$. The experimental Reynolds number $Re = RV_{prop}/\nu$ defined using the propeller's rim velocity $V_{prop} = 2\pi R_{prop} f$[1]. This number can be varied continuously in the range $Re \sim 10^4 - 10^5$

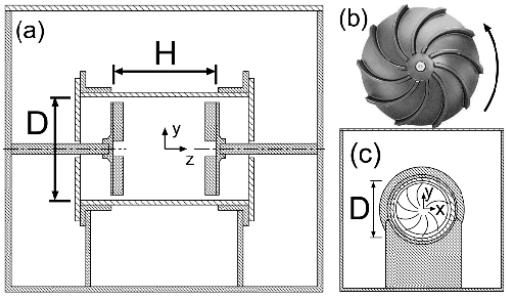

Figura 1. Experimental setup: (a) Section along the axis of the cylinder. The cylinder is placed horizontally, inside a tank. (b) Propeller used in the experiment. The arrow indicates the rotation direction. (c) View of the equatorial plane.

The objective of this research is to determine the effect of the fluctuations in the fluid flow. To achieve this goal, we have characterized the flow in a model experiment (using water). This velocity field, determined only by the hydrodynamics, has been used to find out the effect of the fluctuations in the slow dynamics. We show that the averaged velocity field of the turbulent flow bifurcates subcritically breaking some symmetries of the problem and becomes time-dependent because of equatorial vortices moving with a precession movement[2]. This subcriticality produces a bistable regime, with a hysteresis region for an extremely small range of parameters. Three different time-scales are relevant to the dynamics, two of them very slow compared to the impeller frequency[1].

We have studied the different time scales of the system, analizing the behaivour of a neutrally buoyant spheres assuming that the density of the sphere is homogeneous. Also we change the frequency of the impellers ($1.58Hz$ - $7.92Hz$) to explore another parameter of the system. We follow this volume in a period of time and we compare the results in different spatial scales.

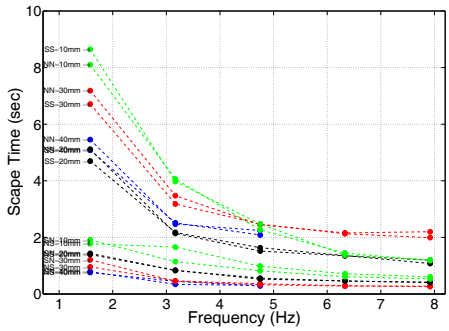

Figura 2. Scape time as a function of the frequency of the propellers for four different size of spheres. In this graphic we see how the scape time decay even if we use different spacial scales.

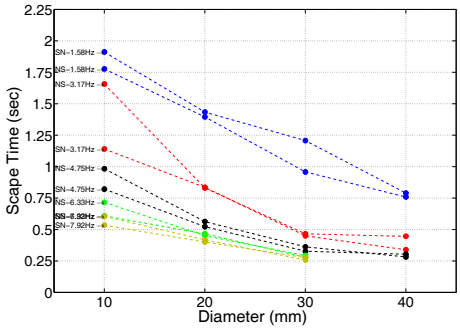

Figura 3. Scape time as a function of the size of spheres for five different frequency's in the propellers. We expected that the scape time was the same for a different spatial scales and for a certain frequency or if the scape time grow as a function of the size of the spheres we could explain the behavior of one of the small scales. But for this result we are searching an explanation.

With this work we conclude that as we increase the Re number the fluctuations inside the flow will increase. Some results concerning the random inversions that appear in the flow remain unexplained.

---

* http://fisica.unav.es/mhd/

[1] J, Burguete et al., IJBC Vol. 19, No. 8 (2009) 2695-2703
[2] A. de la Torre et al., Phys. Rev. Lett. 99, 054101 (2007)

La Compatibilidad como mecanismo de Complejidad en las Redes

J. P. Cárdenas, M. L. Mouronte, R. M. Benito, J. C. Losada*
Grupo de Sistemas Complejos
ETSI Agrónomos. Universidad Politécnica de Madrid
28040 Madrid

Durante la última década un gran número de sistemas complejos reales han sido estudiados bajo la perspectiva de la Teoría de Redes Complejas[1]. Los componentes de los sistemas complejos aparecen relacionados de forma no trivial y en ocasiones poco intuitiva, generando propiedades comunes muy interesantes en los sistemas de los que forman parte[2], como por ejemplo, la presencia de un escalado en la distribución de conectividades de los nodos. Dicha distribución indica que la probabilidad de encontrar un nodo con un número de enlaces (grado) determinado, k, en la red muestra un comportamiento asintótico con la forma $P(k) \sim k^{-\gamma}$. A estas redes se les denomina *libres de escala*, por no tener grado k que las caracterice. Así mismo, este tipo de redes presentan una organización clusterizada de sus componentes y por que entre cualquier par de estos existe, en promedio, una corta distancia a través de enlaces (efecto *small world*)[3].

El origen de esta complejidad puede ser atribuído a los procesos de evolución mediante los que se forman las redes. El tiempo y los mecanismos asociados a estos proceso juegan un papel determinante en la *emergencia* de las propiedades complejas en numerosas redes reales, tanto naturales como artificiales. Esta complejidad ubicua estaría sugiriendo que existen mecanismos o leyes fundamentales tras la evolución de los sistemas, independiente de su origen.

Considerando la existencia de mecanismos comunes que engendran complejidad, las topologías complejas han sido estudiadas a través de modelos generales de red en un intento por encontrar los principios fundamentales que las gobiernan. Un ejemplo bien conocido de estos modelos es el llamado *Modelo de Enlace Preferencial* (PA)[4] que considera una regla en donde un nuevo nodo añadido a la red se enlaza con mayor probabilidad a aquellos más conectados. Este mecanismo de enlace preferencial, que implica conocer en cada paso caracteristicas globales de la red, como es el número total de enlaces, es la base para muchos modelos que reproducen, con éxito, las topologías observadas en la red de Internet y otros sistemas complejos.

En este trabajo se propone un modelo dinámico, Modelo de Enlace Compatible (MEC)[5], en el cual una red compleja puede emerger considerando un simple mecanismo local denominado *compatibilidad*, que representa la afinidad entre los caracteres que definen a los nodos de la red para poder o no conectarse entre ellos. Dichos caracteres son definidos mediante una determinada función de densidad de probabilidad invariante en el tiempo. Hemos encontrado que la naturaleza de esta función de probabilidad es la que determina las propiedades topologigas de las redes generadas según este modelo. Así, si la función de probabilidad sigue ciertas leyes de potencia, las redes presentan propiedades tales como ser libres de escala en el grado de conectibidad, alto clustering o efecto *small world*, de forma que nuestros resultados indican que la compatibilidad entre nodos puede, por si sola, generar la complejidad de los sistemas reales, independiente de su origen.

Presentamos la aplicación del modelo de compatibilidad para estudiar varios tipos de redes complejas de diferente naturaleza: una red interacción proteica y redes semanticas, entre otras.

---

* juancarlos.losada@upm.es

[1] A.L. Barabási, (2009), *Scale-Free Networks: A Decade and Beyond*. Science, 325.
[2] M.E.J. Newman, (2003), *The Structure and Functions of Complex Networks*, SIAM Review, 45 (2)167-256.
[3] D.J. Watts y S.H. Strogatz, (1998), *Collective dynamics of Small-World networks*, Nature 393 440-442
[4] A.-L. Barabási y R. Albert, (1999), *Emergence of scaling in random networks*, Science, 286: 509-512.
[5] J. P. Cárdenas *et al.*, (2010), *Compatibilty as underlying mechanism behind the evolution of networks*. Physica A, 389: 1789-1798.

Análisis experimental de la estabilidad de los arcos en un medio granular

C. Lozano*, I. Zuriguel, A. Garcimartín, G. Lumay‡
Departamento de Física y Matemática Aplicada
Facultad de Ciencias, Universidad de Navarra
31080 Pamplona

Un medio granular es un conjunto numeroso de partículas de similares características que manifiestan comportamientos colectivos. Entre las propiedades inherentes a los medios granulares destaca su capacidad para formar arcos. Se puede definir arco como una estructura espacial de partículas que se sostienen mutuamente. Como los arcos son mecánicamente estables, provocan atascos, que detienen el movimiento ordenado de los granos o al menos lo dificultan.

Para deshacer un atasco, es necesaria una inyección de energía, por ejemplo en forma de vibraciones. Este procedimiento, evidentemente, reviste una gran importancia industrial. En estudios previos[2] se analizó lo que sucede cuando se impone una vibración a un silo de manera continua; ello proporciona una descripción estadística en términos de la probabilidad media de atasco, y cómo la reduce la vibración introducida.

Por otro lado, si se emplean recipientes bidimensionales se pueden observar directamente los arcos, lo cual permite caracterizarlos geométricamente mediante análisis de imágenes[1].

Lo que nos proponemos ahora es estudiar la estabilidad de los arcos en un silo bidimensional, en el cual hay un orificio que deben atravesar los granos. Este tipo de montaje permite observar cada arco individual. El silo se coloca encima de un vibrador electromecánico (véase el esquema de la Figura 1). Con ello se pretende analizar el efecto de la vibración sobre cada arco en particular, y buscar parámetros característicos (como puede ser una amplitud característica, o una frecuencia, o un tiempo de espera).

Figura 1. Esquema del dispositivo experimental propuesto: un silo volteable con un orificio en el centro colocado sobre un agitador electromecánico.

* clozano@alumni.unav.es
`http://fisica.unav.es/granular`
‡ GRASP, Universitè de Liège, B-4000 Liège, Bélgica.

[1] A. Garcimartín, I.Zuriguel, L. A. Pugnaloni, A. Janda, *Phys. Rev. E* **8**2, 031306 (2010).
[2] C. Mankoc, A. Garcimartín, I. Zuriguel, D. Maza, L. A. Pugnaloni, *Phys. Rev. E* **8**0, 011309 (2009).

Arritmias cardiacas producidas por heterogeneidad en la dinámica del calcio

C. Lugo*, E. Alvarez-Lacalle, I. R. Cantalapiedra, B. Echebarria, A. Peñaranda
Departament de Física Aplicada, Universitat Politècnica de Catalunya, Barcelona.

Para que el corazón realice eficazmente su función de bombeo de sangre, es necesario un ciclo cardíaco capaz de propagar el impulso eléctrico de una manera coordinada, produciendo una contracción sincronizada. En algunos casos, sin embargo, fallos en la propagación pueden causar la formación de ondas reentrantes, también llamados rotores, creando regiones en las que la excitación se propaga en caminos cerrados (loops) con una frecuencia mayor a la normal. Esto da lugar a taquicardias monomórficas o polimórficas, dependiendo de si hay una o varias fuentes. Aunque a menudo la taquicardia termina espontáneamente, puede degenerar en fibrilación, un desorden cardíaco en el que los rotores se crean y destruyen continuamente, perdiéndose la sincronía de la excitación y originándose una contracción desordenada de las fibras cardiacas. Si esto sucede en los ventrículos, el corazón pierde la capacidad de bombear la sangre al resto del cuerpo, produciéndose la muerte cardiaca si no se administra un choque eléctrico mediante un defribilador.

Alguno de los factores que favorecen las reentradas son la dispersión de la repolarización del tejido cardiaco, y el bloqueo local de la conducción[1]. Las células cardiacas se depolarizan (el potencial de membrana pasa de $\sim$ -80 mV a $\sim$ 20 mV) cuando les llega el impulso eléctrico, debido a la apertura de diversas corrientes iónicas, aumentando asimismo la concentración del calcio intracelular, que inicia la contracción celular. Una vez depolarizadas, permanecen un cierto tiempo, denominado periodo refractario, en un estado en el que dejan de ser excitables. Así un nuevo impulso que llegue a la célula durante ese periodo no será propagado. Un periodo refractario excesivamente largo, o patologías que reduzcan la capacidad de depolarización celular pueden producir un bloqueo de conducción. Por otra parte inhomogeneidades en el tejido pueden producir diferencias locales en el estado refractario, de forma que una región de tejido se vuelve excitable antes que el resto, y es susceptible a ser reexcitada. Estas inhomogeneidades pueden ser producidas por desajustes en las corrientes de membrana o en la regulación del calcio intracelular. El acoplamiento electromecánico hace que ambas causas estén interrelacionadas.

Nosotros estamos interesados en arritmias producidas por patologías capaces de producir cambios en la concentración de calcio intracelular de un batido a otro. Esto, conocido como alternans[2], se traduce en un potencial de acción largo seguido de uno corto, y puede ser la causa tanto de reexcitación como de bloqueos locales de conducción. A pesar de la importancia de los alternans no está claro el mecanismo que los origina. En este trabajo utilizamos un modelo celular de aurícula humana[3], en el que modificando la dinámica del calcio intracelular podemos estudiar posibles mecanismos que permitan obtener alternans. Simulaciones realizadas en tejido auricular en el que coexisten células normales con células con alternans, nos permitirán investigar la propagación de un estímulo en distintas composiciones del tejido, analizando los efectos de tamaños mínimos y distribuciones espaciales de estas células capaces de producir rentradas y/o bloqueo de conducción.

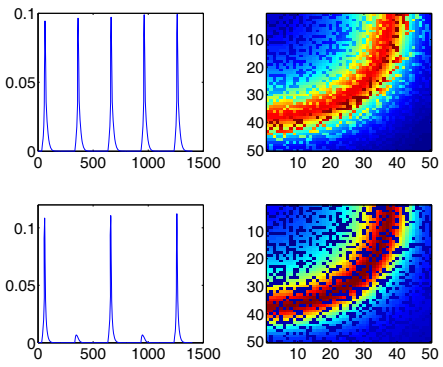

Figura 1. Propagación de un estímulo, generado en una esquina, en un tejido bidimensional con células normales y que presentan alternans colocadas aleatoriamente. En la figura se observa el calcio intracelular en dos batidos consecutivos. La figura de la izquierda muestra la concentración de calcio intracelular para los dos tipos de células.

* carlos.lugo@fa.upc.edu

[1] K.N. Laurita, D.S. Rosembaum, Circ. Res. **87**, 922 (2000); F. Xie, Q. Zhilin, A. Garfinkel, J. Weis, Am J Physiol Heart Circ Physiol **280**, H535 (2001); C. Antzelevitch, Am J Physiol Heart Circ Physiol **293**, 2004 (2007).
[2] L.A. Blater *et al*, J. Physiol **546**, 19 (2003); G.L. Aistrup *et al*, Cir. Res. **99**, 65 (2006)
[3] A. Nygren *et al.* Circ. Res. **82**, 63 (1998)

Feigenbaum graphs: a complex network perspective of chaos

Bartolo Luque, Lucas Lacasa, Fernando J. Ballesteros, Alberto Robledo
Dept. Matemática Aplicada y Estadística
ETSI Aeronáuticos, Universidad Politécnica de Madrid, Spain

We expose a remarkable relationship between nonlinear dynamical systems and complex networks by means of the horizontal visibility (HV) algorithm[1,2] that transforms time series into graphs. In low-dimensional dissipative systems chaotic motion develops out of regular motion in a few number of ways or routes, amongst which the period-doubling bifurcation cascade or Feigenbaum scenario is perhaps the better known and most famous mechanism. This route to chaos appears infinitely many times amongst the family of attractors spawned by unimodal maps within the so-called periodic windows that interrupt stretches of chaotic attractors. In opposition, a route out of chaos accompanies each period-doubling cascade by a chaotic band-splitting cascade, and their shared bifurcation accumulation points form transitions between order and chaos that are known to possess universal properties. Low-dimensional maps have been extensively studied from a purely theoretical perspective, but systems with many degrees of freedom used to study diverse problems in physics, biology, chemistry, engineering, and social science, are known to display low-dimensional dynamics.

The horizontal visibility (HV) algorithm converts the information stored in a time series into a network, setting the nature of the dynamical system into a different context that requires complex network tools to extract its properties. Relevant information can be obtained through this methodology, including the characterization of fractal behavior[3] or the discrimination between random and chaotic series[1,4], and it finds increasing applications in separate fields, from geophysics[5], to finance[6] or physiology[7]. Here we offer a distinct view of the Feigenbaum scenario through the HV formalism, making a complete study of the HV graphs associated to orbits extracted from unimodal maps, which in this context we will call Feigenbaum graphs. We first characterize their topology via order-of-visit and self-affinity properties of the maps. Additionally, a matching renormalization group (RG) procedure leads via its flows to or away from network fixed-points to a comprehensive view of the entire family of attractors. Furthermore, the optimization of the entropy obtained from the degree distribution coincides with the RG fixed points and reproduces the essential features of the map's Lyapunov exponent independently of its sign. A general observation is that the visibility algorithm extracts only universal elements of the dynamics, free of peculiarities of the individual unimodal map, but also of universality classes characterized by the degree of nonlinearity.

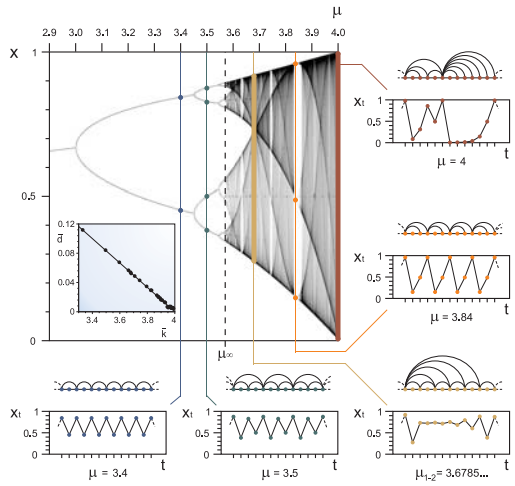

Figura 1. Feigenbaum diagram of the Logistic map $x_{t+1} = \mu x_t(1 - x_t)$, indicating a transition from periodic to chaotic behavior at $\mu_\infty = 3.569946...$ through period-doubling bifurcations. For $\mu \geq \mu_\infty$ the map shows a chaotic mirror image of the period-doubling tree, where aperiodic behavior appears interrupted by periodic windows. Surrounding the central figure, for several values of μ we show time series and their associated Feigenbaum graphs. *Inset:* Numerical values of the mean normalized distance $\bar{d}$ as a function of mean degree $\bar{k}$ of the Feigenbaum graphs for $3 < \mu < 4$ (associated to time series of 1500 data after a transient, and a step $\delta\mu = 0.05$), in good agreement with the theoretical linear relation: $\bar{d}(\bar{k}) = \frac{1}{6}(4 - \bar{k})$.

[1] Luque, B., Lacasa, L., Ballesteros, F. & Luque, J., Horizontal visibility graphs: exact results for random time series. *Phys. Rev. E* **80** (2009) 046103.
[2] Lacasa, L., Luque, B., Ballesteros, F., Luque, J. & Nuno, J.C., From time series to complex networks: the visibility graph. *Proc. Natl. Acad. Sci. U.S.A.* **105**, 13 (2008) 4973.
[3] Lacasa, L., Luque, B., Luque, J. & Nuno, J.C., The Visibility Graph: a new method for estimating the Hurst exponent of fractional Brownian motion. *EPL* **86** (2009) 30001.
[4] Lacasa, L. & Toral, R. Description of stochastic and chaotic series using visibility graphs. *Phys. Rev. E* **82**, 036120 (2010).
[5] Elsner, J. B., Jagger, T. H. & Fogarty, E. A., Visibility network of United States hurricanes. *Geophys. Res. Lett.* **36**, 16 (2009).
[6] Yang, Y., Wang, J., Yang, H., & Mang, J., Visibility graph approach to exchange rate series. *Physica A* **388**, 20 (2009), Pages 4431-4437
[7] Shao, Z.-G., Network analysis of human heartbeat dynamics. *Appl. Phys. Lett.* **96**, 073703 (2010).

Dinámica estocástica y células T

Grant Lythe*, Carmen Molina-París, Mark Day
Applied Mathematics, University of Leeds.

Modelo de de competición y homeostasis

El sistema inmune se encarga de mantenerse preparado para combatir infecciones. Para ello, cuando el cuerpo no está sujeto a infección, un buen repertorio de células T (linfocitos T) es mantenido gracias al balance entre muerte natural y división celular, como consecuencia de estímulos procedentes de antígenos propios.

- Muerte celular: Cada célula T tiene una probabilidad constante por unidad de tiempo, μ, de morir que es independiente de las demás células T.
- Nacimiento de celulas: El estímulo que procede de un APP se comparte entre las células T que lo reconozcan (Fig. III).

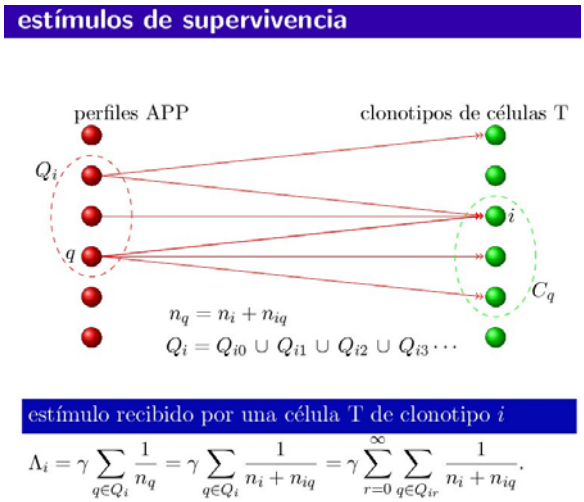

Figura 1. N clonotipos de células T y pueden recibir estímulos de M APPs

La competición entre células (Fig. III). que pertenecen a clonotipos diferentes prolonga la supervivencia de aquellos clonotipos que reconocen (auto)-antígenos distintos a los que reconoce el resto del repertorio de células T. De esta manera, el repertorio de células T cubre el espacio de posibles auto-antígenos de manera mas homogénea (y con menos solapamiento entre clones diferentes) que lo hace un simple proceso aleatorio con distribución uniforme.

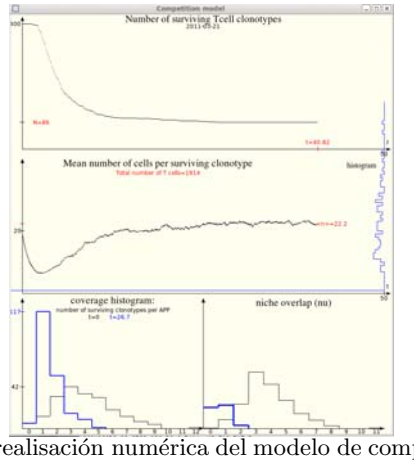

Figura 2. Una realisación numérica del modelo de competición y homeostasis

Encuentros entre células

Un paso esencial en la génesis de una respuesta immune, es el encuentro, en los nodos linfáticos (ganglios), de células T con células dentríticas, las cuales presentan en su superficie antígenos ajenos. Las últimas técnicas de microscopio de láser multifotón nos permiten observar, en tiempo real y *en vivo*, dichos encuentros. Hemos realizado un estudio de las escalas de tiempo de la respuesta inmune, sobre todo el cálculo, analítico y numérico, del tiempo medio de encuentros entre células T y células dentríticas en nodos linfáticos, mediante movimiento Browniano (Fig. III).

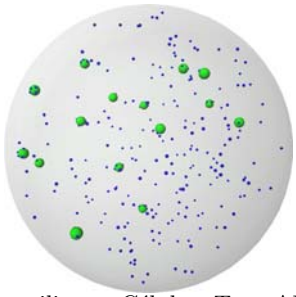

Figura 3. Modelo in silico. Células T y APC siguen caminos Brownianos independientes

[1] grant@maths.leeds.ac.uk
[2] BBSRC MATSYB network *I²M: Immunology, Imaging and Modelling* http://www.maths.leeds.ac.uk/applied/I2M/
[3] FP7 (IRSES) INTI: International Network in Theoretical Immunology http://www.maths.leeds.ac.uk/applied/INTI/
[4] *Mathematical Models and Immune Cell Biology* Springer, 2011.

Ion distribution around charged spherical colloids from molecular dynamics calculations with explicit water molecules

Miroslava Nedyalkova[†], Stoyan Pisov[‡], Francesc Mas[††], Eudald Vilaseca[‡‡], Sergio Madurga[*]
Departament de Química Física i Institut de Química Teòrica i Computacional (IQTCUB)
Facultat de Química, Universitat de Barcelona
Martí i Franquès, 1. 08028 Barcelona (Catalonia, Spain)

Ionisable interfaces are present in many natural and industrial systems. In particular, numerous physical, chemical, and biological processes are governed by electrostatic interactions between charged colloids, surfactant monolayer, functionalized latex and oxide particles, polyelectrolyte, etc.[1] In all these systems, the appearance of electrical forces is due to the surface charges formed in the interface by different charging mechanisms. Therefore, the presence of this surface charge implicates a distribution of ions around the charged surface, which is normally termed electric double layer (EDL).

The objective of this work is to study the electrostatic properties of a model charged colloid particle. In particular, we are interested to find the conditions that gives rise to an overcharging process in this modelled particle. The overcharging phenomenon or charge inversion occurs when the effective charge of a surface exposed to the solution reverses polarity due to an excess of counterions accumulated in the interface. This phenomenon has been previously studied in the BioPhysChem group[2] considering a continuum solvent model (primitive model) and using planar geometry (large colloid particles)[3–5].

In this study, we have performed MD simulations with the GROMACS package to model a large system consisting of a charged colloid particle surrounded by several layers of ions and explicitly including the water solvent molecules. The colloid particle was modeled using a spherical distribution of van der Waals particles. Different surface charge densities of the colloid particle were simulated randomly assigning a negative charge to a set of several van der Waals particles of the colloid surface (from 8 to 370). These surface charged sites represent ionizable functional groups.

In addition, different bulk conditions were simulated using different amounts of monovalent (Na^+) and divalent (Ca^{2+}) counterions. In all cases, the Cl^- ions were used as coions. The dependence of the charge inversion phenomenon of colloidal particles on the concentration of the additional salt has been studied considering different ionic strengths (from 0.1 to 1 M). We observed, that only Ca^{2+} counterions are accumulated in a region close to the surface in an amount that produces a charge inversion. In contrast, the overcharging process was not observed in the monovalent, Na^+, salt solution.

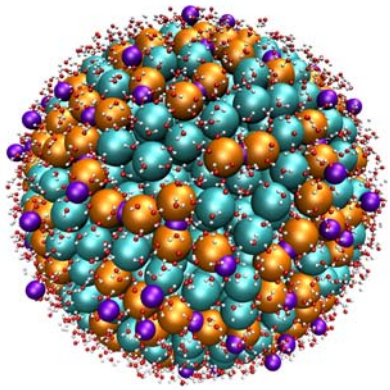

Figura 1. Distribution of Ca^{2+} (in purple) around a charged colloid particle. The first layer of water molecules is also displayed around the negative sites (in orange) and neutral sites (in green) of the colloid particle.

[*] s.madurga@ub.edu
[†] Faculty of Chemistry, University of Sofia, 1164 Sofia, Bulgaria. nhmn@wmail.chem.uni-sofia.bg
[‡] Faculty of Physics, University of Sofia ,1164 Sofia, Bulgaria
[††] fmas@ub.edu
[‡‡] eudald.vilaseca@ub.edu

[1] E. Companys, J.L. Garcés, J. Salvador, J. Galceran, J. Puy, F. Mas Colloid Surface A **306**, 2, (2007).
[2] `http://www.ub.edu/biophyschem/`
[3] S. Madurga, A. Martín-Molina, E. Vilaseca, F. Mas, M. Quesada-Pérez J. Chem. Phys. **126**, 234703 (2007).
[4] S. Madurga, J.L. Garcés, E. Companys, C. Rey-Castro, J. Salvador, J. Galceran, E. Vilaseca, J. Puy, F. Mas Theor. Chem. Acc. **123**, 127 (2009).
[5] S. Madurga, C. Rey-Castro, I. Pastor, E. Vilaseca, C. David, J.L. Garcés, J. Puy, F. Mas J. Chem. Inf. Model. *submitted*.

Virial coefficients and divergence of pressure for hard disks and spheres

M. A. G. Maestre,* A. Santos,† M. Robles,‡, M. López de Haro§
Departamento de Física, Universidad de Extremadura, E-06071 Badajoz, Spain

The virial expansion of the equation of state of a hard-core fluid reads

$$Z(\eta) \equiv \frac{p}{\rho k_B T} \equiv \frac{\widetilde{p}}{\eta} = 1 + \sum_{j=2}^{\infty} b_j \eta^{j-1}, \tag{1}$$

where η is the packing fraction and b_j are the (reduced) virial coefficients. So far, only values up to the tenth virial coefficient have been reported.[1]

Since the compressibility factor of hard-disk and hard-sphere fluids both for the stable and metastable fluid phases is a monotonically increasing function of the packing fraction, one may reasonably wonder at which packing fraction $\eta = \eta_\infty$ the analytical continuation of the compressibility factor diverges, namely one wants to find the value of η_∞ such that

$$\lim_{\eta \to \eta_\infty} Z(\eta) = \infty. \tag{2}$$

Clearly, η_∞ may not be bigger than the maximum packing fraction $\eta_{\max}$ that is geometrically possible (the so-called Kepler's problem).

The aim of this work is to address the question as to whether, using the available information on virial coefficients, one can get a reasonable estimate of η_∞ and whether there may be a systematic method to improve the estimation as more virial coefficients become available.

We have checked that the use of the direct Padé approximants of the compressibility factor Z is not reliable for the purpose of determining η_∞.[2] As an alternative approach, and following an idea of Sanchez,[3] we may formally *invert* the series in Eq. (1), leading to

$$\eta(\widetilde{p}) = \widetilde{p} + \sum_{j=2}^{\infty} c_j \widetilde{p}^{\,j}. \tag{3}$$

In this representation, Eq. (2) is equivalent to

$$\eta_\infty = \lim_{\widetilde{p} \to \infty} \eta(\widetilde{p}). \tag{4}$$

We have constructed (diagonal) $[N/N]$ Padé approximants of the series (3) from the knowledge of the first ten virial coefficients for hard disks and hard spheres. Applying Eq. (4), the estimates $\eta_\infty(N)$ with $N = 1, \ldots, 5$ have been obtained. In addition, making use of the values of b_{11}–b_{16} estimated by Clisby and McCoy,[1] we have also considered $N = 6, 7, 8$. The results, displayed in Fig. 1, are fully consistent with the conjecture $\eta_\infty = \lim_{N\to\infty} \eta_\infty(N) = \eta_{\max}$. Nevertheless, full confirmation must await the availability of higher virial coefficients.

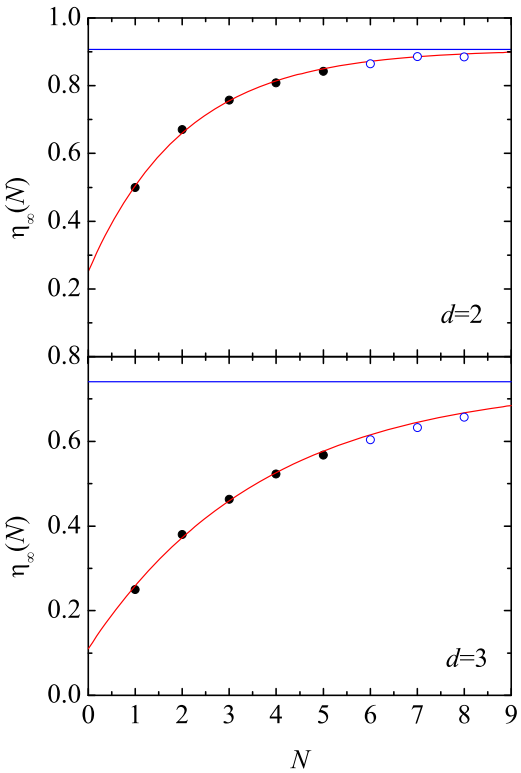

Figura 1. Estimates of η_∞ derived from Padé approximants for the inverse virial expansion (3). The results up to $N = 5$ (filled circles) have been derived from the known values of the virial coefficients, while those for $N = 6, 7, 8$ (open circles) have been obtained from the estimates of the higher virial coefficients. The horizontal lines correspond to the crystalline close-packing value $\eta_{\max}$ for each system. The curves are fits of the points with $N = 1$–5.

* maestre@unex.es
† andres@unex.es
‡ Centro de Investigación en Energía, Universidad Nacional Autónoma de México (U.N.A.M.), Temixco, Morelos 62580, Mexico; mrp@cie.unam.mx
§ Centro de Investigación en Energía, Universidad Nacional Autónoma de México (U.N.A.M.), Temixco, Morelos 62580, Mexico; malopez@servidor.unam.mx

[1] N. Clisby and B. M. McCoy, J. Stat. Phys. **122**, 15 (2006).
[2] M. A. G. Maestre, A. Santos, M. Robles, and M. López de Haro, J. Chem. Phys. (in press).
[3] I. C. Sanchez, J. Chem. Phys. **101**, 7003 (1994).

Energy landscape of constraint satisfaction problems via exhaustive enumeration

S. Mandrà*, M. Palassini†
Departament de Física Fonamental
Universitat de Barcelona
Av. Diagonal 647, 08028 Barcelona.

Constraint satisfaction problems (CSPs) consist in searching for configurations of N discrete variables that satisfy M given constraints, and are of great practical importance in many disciplines, from physics to computer science[1]. In general, CSPs are NP-complete, hence it is believed that the computational time for finding a satisfying configuration (solution), or proving that none exists, for an arbitrary CSP instance grows faster than any power of N. There is currently great interest in random CSP instances extracted from ensembles with fixed density of constraints, $\alpha = M/N$. These exhibit a sharp transition at a satisfiability threshold $\alpha = \alpha_s$ separating solvable and unsolvable instances[2]. Recently, tools from the statistical physics of disordered systems revealed several other transitions in the structure of the solution space. In particular, there is a phase $\alpha_d < \alpha < \alpha_c$ where the solution space breaks into an exponential number of clusters[3–5] (i.e. connected components of the "solution graph" in which links join solutions that differ only in one variable), and a "condensed" phase $\alpha_c < \alpha < \alpha_s$ where the number of clusters becomes sub-exponential.

Despite these advances, little is known about the origin of computational hardness (it was conjectured that computationally hard instances exist only in the condensed phase in a narrow region $\alpha_r < \alpha < \alpha_s$[5,6]), nor about the applicability of the above picture to real-world CSP instances. In this work we study the relationship between computational hardness and cluster organization by exploring exhaustively the solution space of random q-coloring, a prototypical NP-complete problem consisting in coloring the N nodes of a random graph with M edges using only q colors, so that no neighbors share the same color. We developed a parallel version of the DPLL algorithm[7] which reduces significantly the computational time to explore all the q^N possible configurations. Moreover, we devised a fast *hash* algorithm based on the "whitening" procedure[8] to reduce the total amount of memory to store the exponentially (in N) many solutions.

Fig. 1 shows our preliminary results for the complexity $\Sigma(s) \equiv$ log(number of clusters with internal entropy s)/N, where $s \equiv$ log(number of solutions inside the cluster)/N, for Erdös-Renyi graphs with $q = 3$ and $\alpha_c < \alpha = 2.29 < \alpha_r$. The results agree qualitatively with those of the *entropic cavity method*[4] (ECM).

Fig. 2 shows the complexity $\Sigma(s, d)$ restricted to clusters with internal entropy s and Hamming distance d from a fixed configuration. The almost spherical shape of $\Sigma(s, d)$ suggests a simple geometrical organization of the clusters. In particular, the typical distance of clusters at fixed s is $d_{typ}(s) = \text{argmax}_d\, \Sigma(s, d) = 2/3$, which is the distance of random configurations from a fixed configuration. The absence of any geometrical structure might explain why instances are easy to solve for $\alpha < \alpha_r$.

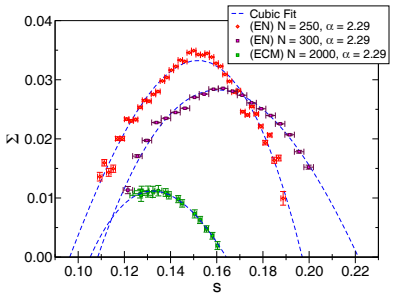

Figura 1. Complexity $\Sigma(s)$ for three random graphs with $\alpha = 2.29$ and $N = 250, 300, 2000$. The data are obtained by exhaustive enumeration (EN) of the solutions for $N = 250, 300$, and with the ECM for $N = 2000$.

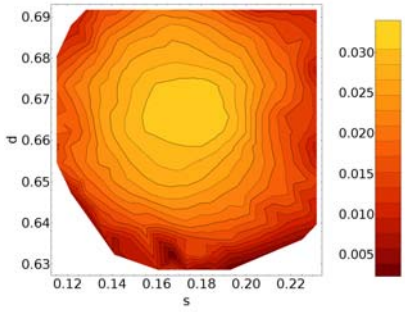

Figura 2. Contour plot of the complexity $\Sigma(s, d)$ for a random graph with $N = 300$ and $\alpha = 2.29$.

* smandra@ffn.ub.es
† palassini@ub.edu

[1] M. Mézard, A. Montanari, *Information, physics and computation*, Oxford University Press (2009)
[2] P. Cheeseman, B. Kanefsky, W. M. Waylor, Proc. of the Twelfth Int. Joint Conf. on Artificial Intelligence (1991)
[3] M. Mézard, G. Parisi, R. Zecchina, Science 297, 5582 (2002)
[4] M. Mézard, M. Palassini, O. Rivoire, Phys. Rev. Lett. 95, 200202 (2005)
[5] F. Krząkała, A. Montanari, F. Ricci-Tersenghi, G. Semerjian, L. Zdeborová, PNAS 104, 25 (2007)
[6] J. Ardelius, L. Zdeborová, Phys. Rev. E 78, 040101 (2008)
[7] M. Davis, G. Logemann, D. Loveland, Communications of ACM 5, 7 (1962)
[8] G. Parisi, arXiv:cs/0212047 (2002)

Intrinsic structure, elastic properties and stability of the Newton Black Film

Hector Martinez*, Pedro Tarazona*, Enrique Chacon†, Fernando Bresme‡
* *Departamento de Fisica Teorica de la Materia Condensada, Universidad Autonoma de Madrid*
† *Instituto de Ciencia de Materiales de Madrid, Consejo Superior de Investigaciones Cientificas (CSIC)*
‡ *Department of Chemistry, Imperial College, SW7 2AZ, London, United Kingdom*

We have studied a kind of thin film, known as "Newton Black Film". These systems are composed of a water layer, confined between two phospholipid membranes of sodium dodecyl sulfate (SDS). We have simulated the NBF's using molecular dynamics simulations. This system is subjected to strong thermal fluctuations, which are present in all soft matter surfaces. The thermal fluctuations blur the surface's intrinsic structure and prevent us from obtaining microscopic information about the interface. In order to solve this problem, we have used different techniques (i.e. "Intrinsic Sampling Method") to define an intrinsic surface which enable us to obtain information of this system at molecular level, subtracting the blurring effects of the thermal fluctuations.

Once we have been able to determine the instantaneous surface (intrinsic surface), we have characterized the system for different thickness of the inner layer of water. We have calculated intrinsic profiles (density profiles referred to the intrinsic surface) to obtain information about the structure properties of the film. Finally we have studied mechanical properties of the NBF, like the bending modulus, using the amplitude of the thermal fluctuations of the membranes, and we have analysed the stability of the system.

---

* hector.martinez@uam.es

[1] E.Chacon y P.Tarazona, Phys.Rev.Lett. 91, 166103 (2003)
[2] P.Tarazona y E.Chacon, Phys.Rev.B 70, 235407 (2004)
[3] Bresme F, Faraudo J, Langmuir, 2004, Vol. 20, pages: 5127-5137
[4] F. Bresme, E. Chacon and P.Tarazona, Phys. Chem. Chem. Phys. 2008, Vol. 10, pages 4704-4715

Temporal Griffiths Phases

Ricardo Martínez*, Federico Vázquez, Juan A. Bonachela, Cristóbal López, Miguel A. Muñoz
IFISC, Inst. de Física Interdisciplinar y Sistemas Complejos (CSIC-UIB),
Campus Universitat Illes Balears,
07122 Palma de Mallorca.

Systems with disorder *quenched-in-space* can exhibit Griffiths phases, characterized by generic algebraic behavior in an extended region of the parameter space, and generic divergences of some quantities as the susceptibility. In this work the effect of *quenched-in-time* external noise on stochastic spatially extended systems is discussed.

On the one hand, the attention is focused on systems with irreversible phase transition to an absorbent state. In this case the Contact-Process (CP)[1] is studied and it is shown that for $d \geq 2$ a "temporal Griffiths phase" (TGP) appears. The TGP is characterized by an algebraic growth of the system mean lifetime and generic divergences of the susceptibility.

On the other hand, systems which exhibit a reversible transition from a disordered to an ordered state are also studied[2]. Taking the Ising Model as representative, numerical and analytic calculation are done, providing results which show the possible extension of TGPs to these kind of systems. Slower decay in the magnetization as a function of an external field in the critical point and the appearence of a region in the control parameter where the magnetization decays with a continuosly varying exponent until the active phase value are observed. This region is shown to exist for different correlations in noise as well as to depend on its amplitude. The influence of the time disorder on the relaxation time is also studyed.

The application of this results is hopeful on the modelling of many problems in Physics, Chemistry or Ecology; where parameters fluctuating in time seem to play and important role, for instance populations subjected to variability in weather conditions[3].

---

* ricardo@ifisc.uib-csic.es

[1] F. Vázquez et al. (Submitted) (2011).

[2] Martínez et al. (in preparation).

[3] E.G. Leigh Jr, J. Theor. Biol. **90**, 213 (1981).

Synchronization in delayed mutually coupled optoelectronic oscillators

Jade Martínez Llinàs*, Pere Colet Rafecas
Instituto de Física Interdisciplinar y Sistemas Complejos IFISC (CSIC-UIB)
Campus Universitat de les Illes Balears, E-07122 Palma, Spain

In this work we study the synchronization between two delayed mutually coupled optoelectronic oscillators with intrinsic delay. In particular we consider the interplay of the different delays in achieving synchronized behavior.

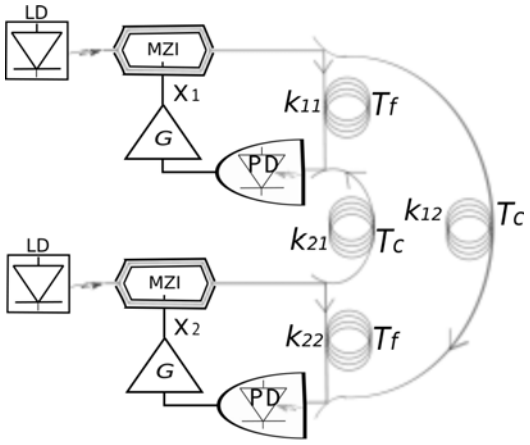

Figura 1. Setup.

The setup is shown in Figura1. Each system has a Mach-Zender Interferometer (MZI) pumped by a cw semiconductor laser (LD). A fraction of light k_{ii} enters the electro-optical loop of oscillator i with self-feedback delay T_f, while a fraction k_{ij} is coupled to oscillator j with coupling delay T_c. The light is detected by a photodiode (PD) and the electrical signal goes through a band-pass amplifier with low and high cut-off characteristic times $\theta_i = 5\mu s$ and $\tau_i = 25ps$, respectively. The dynamics of the electrical signal x_i is:

$$x_i(t) + \tau_i \frac{dx_i}{dt}(t) + \frac{1}{\theta_i}\int_{t_0}^{t} x_i(s)ds = \beta_i C_i,$$
$$C_i = k_{ii}^2 \cos^2(z_{ii}) + k_{ji}^2 \cos^2(z_{ji}) + \\ + 2k_{ii}k_{ji}\cos(z_{ii})\cos(z_{ji})\cos(z_{ii} - z_{ji}),$$

where $i, j = 1, 2$, $z_{ji} = x_j(t - T_{ji}) + \phi_j$, $T_{ii} = T_f$, $T_{ji,j\neq i} = T_c$, ϕ_i is an offset phase and β_i is proportional to the pump power.

Here we keep fixed $k_{11} = k_{12} = 0.5$ and $\phi = 0.25\pi$. For very low values of k_{22} and k_{21} (a configuration similar to unidirectional coupling) increasing β we find steady states, periodic solutions of period $2T_f$ and chaotic solutions. For intermediate values of k_{22} or k_{21}, the $2T_f$ periodic solutions become unstable, but we find other periodic solutions in certain cases. More precisely, when T_c and T_f satisfy the ratio $T_c/T_f = (2m+2)/(2m+1)$ for any integer $m \geq 0$, there are multiple stable periodic solutions with period $T_m = 2T_l/(2m+1)$, being $T_l = T_c - T_f$. In these solutions, x_1 and x_2 are anitisynchronized with zero lag: $x_2(t) = -x_1(t)$. An example is shown in Figura2, where almost square waveforms arise for $\tau_i << T_c = 40ns$, $T_f = 30ns << \theta_i$. Further increasing the pump or the coupling, periodic solutions become unstable and the system gets chaotic. One encounters lag synchronization between x_1 and x_2: $x_2(t) = x_1(t - T_l)$, as it is shown in Figura3.

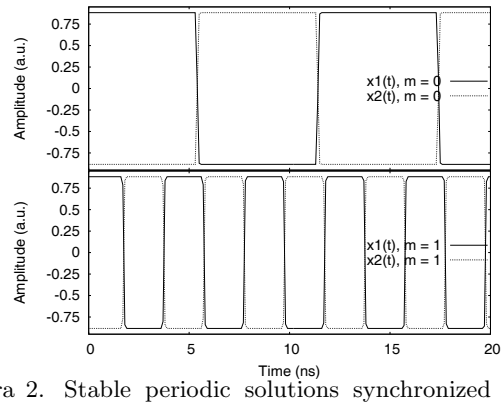

Figura 2. Stable periodic solutions synchronized in antiphase with fundamental frequency (top panel, $m = 0$) and first harmonic (lower panel, $m = 1$). We have taken $\beta = 5$ and $k_{22} = k_{21} \in [0.09, 0.19]$.

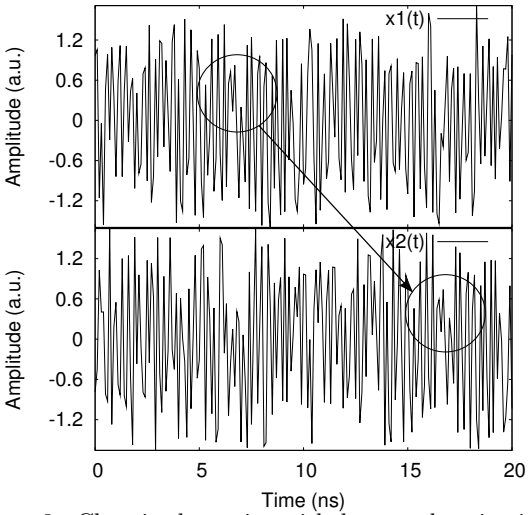

Figura 3. Chaotic dynamics with lag synchronization for $\beta = 10$ and $k_{22} = k_{21} = 0.05$.

* jade@ifisc.uib-csic.es

Determinación de las propiedades interfaciales de la mezcla binaria agua-metano mediante simulación molecular

J.M.Míguez, D. González-Salgado, G. Pérez-Sánchez, J.L. Legido, M.M. Piñeiro*
Departamento de Física Aplicada, Facultade de Ciencias
Universidade de Vigo
36310 Vigo

Después de haber abordado el estudio de las propiedades interfaciales de metano y agua en equilibrio líquido-vapor en una caja bifásica mediante el método de simulación de Monte Carlo, el objetivo de este trabajo es la determinación de estas propiedades para la mezcla binaria correspondiente. Como etapa preliminar[1] se ha calculado usando la ecuación de estado SAFT-VR[2] el diagrama de fases global de la mezcla agua-metano, para determinar los distintos equilibrios de fases que presenta esta mezcla al en un amplio rango de presión y la temperatura, con el objeto de estimar las condiciones en que posteriormente se han realizado simulaciones de las interfases líquido-líquido y líquido-vapor. Se han estimado propiedades interfaciales como la tensión interfacial, calculada a partir de los métodos de Test-Area[3] y de determinación del tensor de presiones[4] y los perfiles de densidad de ambas sustancias, que han sido comparados con los obtenidos mediante la Teoría del Gradiente combinada con la ecuación SAFT-VR Mie[5]. El modelo molecular elegido para describir el comportamiento del metano es una única esfera Lennard- Jones (LJ)[6] mientras que para el agua se ha utilizado el modelo rígido no polarizable conocido como TIP4P/2005[7] que considera cuatro sitios de interacción, de los que tres son cargas eléctricas, y que describe sus propiedades termofísicas con gran eficacia[8].

* mmpineiro@uvigo.es

[1] J. M. Míguez, M. C. dos Ramos, M. M. Piñeiro, F. J. Blas, J. Phys. Chem. B, enviado para publicación (2011).
[2] A. Gil-Villegas, A. Galindo, P. J. Whitehead, S. J. Mills, G. Jackson, A. N. Burgess, A. N., J. Chem. Phys. **106**,4168 (1997).
[3] G. J. Gloor, G. Jackson, F. J. Blas, E. de Miguel, J. Chem. Phys. **123**, 134703 (2005).
[4] G. Jackson ; E. de Miguel, J. Chem. Phys. **125**, 164109 (2006).
[5] T. Lafitte, B. Mendiboure, M. M. Piñeiro, D. Bessières, C. Miqueu, J. Phys. Chem. B **114**, 11110 (2010).
[6] D. Möller, J. Oprzynski, A. Müller, J. Fischer, Mol. Phys. **75**, 363 (1992).
[7] J. L. F. Abascal, C. Vega, J. Chem. Phys. **123**, 234505 (2005).
[8] C. Vega, J. L. F. Abascal, M.M. Conde y J. L. Aragonés, Faraday Discussions **141**, (2009).

Fases nemáticas biaxiales en fluidos de partículas duras con geometría de tipo losa

Yuri Martínez-Ratón[1]*, Szabolcs Varga[2], Enrique Velasco[3]
[1] *Grupo Interdisciplinar de Sistemas Complejos (GISC), Departamento de Matemáticas, Escuela Politécnica Superior, Universidad Carlos III de Madrid, Avenida de la Universidad 30, E28911–Leganés, Madrid, Spain*
[2] *Institute of Physics and Mechatronics, University of Pannonia, P. O. Box 158, Veszprém H-8201, Hungary*
[3] *Departamento de Física Teórica de la Materia Condensada e Instituto Nicolás Cabrera, Universidad Autónoma de Madrid, E-28049 Madrid, Spain*

En este trabajo usamos la técnica del funcional de la densidad basada en el formalismo de la teoría de medidas fundamentales (TMF)[1] para estudiar la estabilidad relativa de la fase nemática biaxial con respecto a fases no uniformes como la esméctica y la columnar en fluidos constituidos por partículas de geometría de tipo losa y que interaccionan de manera dura. Las dimensiones de dichas partículas son en general diferentes $\sigma_1 > \sigma_2 > \sigma_3$. En nuestro modelo usamos la aproximación de orientaciones restringidas (modelo de Zwanzig). Variando la relación de aspecto $\kappa_1 = \sigma_1/\sigma_2$ y fijando $\kappa_2 = \sigma_2/\sigma_3$, calculamos varios diagramas de fases para diferentes valores de κ_2 los cuales incluyen todas las fases uniformes: isótropa, nemáticos uniaxiales con simetría de varillas y de losas (con el director nemático paralelo a la arista mayor y menor de la partícula respectivamente), y la fase nemática biaxial. Calculamos además las inestabilidades espinodales a fases no uniformes con respecto a fluctuaciones con simetría esméctica, columnar y plástico-cristalina. Encontramos, en correspondencia con experimentos recientes[2], que la fase nemática biaxial empieza a ser estable para $\kappa_2 \simeq 2.5$. También, como se ha predicho mediante teorías y simulaciones de partículas biaxiales[3,4], obtenemos una región de estabilidad de dicha fase centrada en $\kappa_1 \approx \kappa_2$ la cual se amplía a medida que κ_2 aumenta. Para $\kappa_2 \gtrsim 5$ la región del diagrama de fases [fracción de empaquetamiento η-κ_1] con $\kappa_2 \approx \kappa_1$ posee una gama de interesantes topologías que cambian cualitativamente con κ_2 (ver figura). En particular, la transición nemático unixial-nemático biaxial, usualmente de segundo orden, es sustituida a bajas densidades y para $\kappa_1 \sim \kappa_2$, por una transición de primer orden entre los dos tipos de nemáticos que luego se conecta a la zona de estabilidad del nemático biaxial de manera peculiar (ver figura). Hemos encontrado que el incremento de la biaxialidad en la anisotropía de las partículas favorece la formación de la fase nemática biaxial. El presente estudio es el primero en aplicar la TMF a partículas biaxiales además de ir más allá de las teorías basadas en el segundo coeficiente del virial. Predecimos además que el diagrama de fases debe de ser asimétrico alrededor de $\kappa_1 \sim \kappa_2$ lo cual es debido al efecto del tercer coeficiente del virial (incluido en nuestra teoría). Nuestro estudio da una pista de cómo sintetizar las partículas del mineral goethita (cuáles deben ser sus longitudes características) para maximizar la probabilidad de encontrar una fase nemática biaxial en dichas suspensiones coloidales.

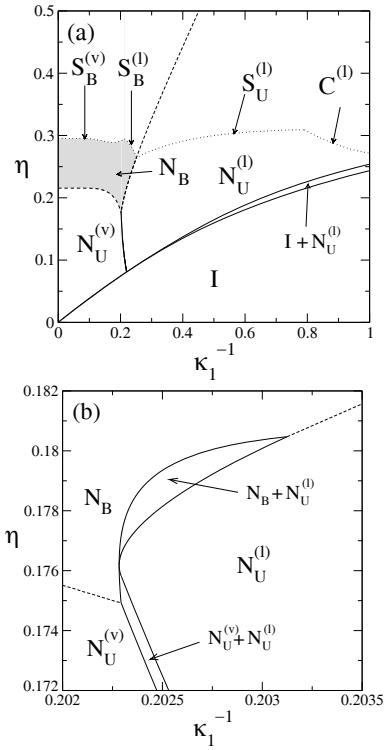

Figura 1. (a): Diagrama de fases η vs. κ_1 de un fluido de partículas biaxiales con $\kappa_2 = 5$. Las etiquetas indican las zonas de estabilidad de las diferentes fases uniformes: I (isótropa), $N_U^{(v)}$ (nemático uniaxial de varillas), $N_U^{(l)}$ (nemático uniaxial de losas), N_B (nemático biaxial), y las inestabilidades espinodales a las fases no uniformes: $S_U^{(l)}$ (esméctico uniaxial de losas), $S_B^{(v)}$ (esméctico biaxial de varillas), $S_B^{(l)}$ (esméctico biaxial de losas) y $C^{(l)}$ (columnar de losas). Las líneas continuas y de trazos indican transiciones de primer y segundo orden respectivamente. Las líneas de puntos indican las inestabilidades espinodales a fases no uniformes. La máxima zona de estabilidad del N_B está sombreada. (b): Ampliación de (a) alrededor de la zona $\kappa_1 \sim \kappa_2$.

* yuri@math.uc3m.es

[1] J. A. Cuesta y Y. Martínez-Ratón, Phys. Rev. Lett. **78**, 3681 (1997)
[2] E. van den Pol, A. V. Petukhov, D. M. E. Thies-Weesie, D. V. Byelov y G. J. Vroege, Phys. Rev. Lett. **103**, 258301 (2009);
[3] M. P. Taylor y J. Herzfeld, Phys. Rev. A **44**, 3742 (1991)
[4] P. J. Camp y M. P. Allen, J. Chem. Phys. **106**, 6681 (1997)

Emergencia de estrategias en juegos iterados con reciprocidad directa

Luis A. Martínez-Vaquero*, José A. Cuesta, Angel Sánchez
Grupo Interdisciplinar de Sistemas Complejos (GISC)
Departamento de Matemáticas, Universidad Carlos III de Madrid
Avda. de la Universidad 30, 28911 Leganés, Madrid

Uno de los mecanismos propuestos para la emergencia de cooperación es la reciprocidad directa[1,2]. Este mecanismo actúa cuando los individuos interaccionan repetidamente, por ello se modela mediante juegos iterados. El objetivo de este trabajo es estudiar sistemáticamente la emergencia de estrategias en juegos iterados con memoria a un paso de tiempo que resultan de sucesivas invasiones por nuevas estrategias que se incorporan al juego a una tasa muy baja.

Los juegos estudiados son juegos simétricos de dos jugadores. Cada uno de éstos puede elegir entre dos posibles decisiones, colaborar (C) o defraudar (D), teniendo en cuenta tanto lo que el oponente como él mismo hicieron en la ronda anterior. Los pagos que recibe un jugador en cada ronda pueden ser R (si ambos colaboran), P (si ambos defraudan), T (si él defrauda y el oponente colabora) o R (si él colabora y el oponente defrauda). Fijando $R = 1$ y $P = 0$, los pares de valores (T, S) parametrizan los distintos juegos.

Se han estudiado tanto juegos clásicos, como el Dilema del Prisionero ($1 \leq T \leq 2$, $-1 \leq S \leq 0$), la Ventisca ($1 \leq T \leq 2$, $0 \leq S \leq 1$), la Caza del Ciervo ($0 \leq T \leq 1$, $-1 \leq S \leq 0$) o la Armonía ($0 \leq T \leq 1$, $0 \leq S \leq 1$), como otros con valores de T y S en la periferia de éstos.

En el juego iterado con memoria a un paso, las estrategias de los jugadores quedan caracterizadas por cuatro probabilidades: la probabilidad que tiene el jugador de colaborar en función de los cuatro posible resultados de la ronda anterior. Para simplificar, y porque estudios previos por simulación sugieren que éstas son las más relevantes[3], sólo se han considerado estrategias *casi* puras, esto es aquellas cuyas probabilidades sólo toman los valores ϵ o $1-\epsilon$, en el límite en el que $\epsilon \to 0^+$. Esto da un total de 16 estrategias. El enfrentamiento entre dos de estas estrategias es una cadena de Markov ergódica entre los cuatro estados (C,C), (C,D), (D,C) y (D,D). Teniendo en cuenta los pagos que cada jugador recibe en estado estacionario, obtenemos una nueva matriz de pagos 16×16 que describe el juego iterado.

Utilizando esta matriz de pagos se ha procedido a invadir cada una de las 16 estrategias por todas las demás. Para ello se considera una población de $N = 1000$ individuos con la estrategia residente y se invade reemplazando 10 de los individuos de la población por individuos con la estrategia invasora. La dinámica procede eligiendo dos jugadores al azar y enfrentando sus estrategias. Si ΔW denota la diferencia de pagos obtenida entre el jugador y su oponente, el jugador cambiará su estrategia por la del oponente con probabilidad $p = (1 + \phi^{-1}\Delta W)/2$, siendo ϕ la máxima diferencia de pagos alcanzable. El proceso se repite hasta que la población muestra una composición de estrategias estable. El resultado de este proceso puede llevar a la prevalencia de la estrategia residente, de la estrategia invasora o a un equilibrio mixto de ambas. Como esto dependerá, en general, de la realización del proceso, éste se repite 100 veces y se determina con qué probabilidad se llega a cada uno de los posibles resultados.

A continuación se procede a invadir los nuevos equilibrios obtenidos, repitiendo el proceso descrito. Cuando todas las posibilidades de invasión se han agotado, el resultado obtenido se puede representar mediante un grafo pesado y dirigido de invasiones, cuyos vértices son los distintos equilibrios obtenidos y cuyos enlaces unen la comunidad invadida con la comunidad resultante tras la invasión, y llevan como peso la probabilidad de que tal transición ocurra y como etiqueta la estrategia invasora que causa la transición.

Analizando los grafos resultantes como cadenas de Markov se pueden identificar conjuntos recurrentes que indican qué estrategias acaban dominando en el proceso. Cada uno de estos conjuntos puede estar formado por una (nodo absorbente) o varias estrategias. Además cada una de ellas puede ser pura o mixta. Para cada conjunto recurrente se ha calculado la probabilidad de absorción media cuando el sistema parte de una comunidad pura, así cómo su distribución de probabilidad en el estacionario.

Con este trabajo por un lado extendemos a un amplio espectro de juegos los estudios previos llevados a cabo por Nowak y Sigmund[4] sobre el papel que juegan las diferentes estrategias y la interacción entre ellas en este tipo de juegos, y por otro caracterizamos completamente el proceso por el que emergen y prevalecen las distintas estrategias o combinaciones de ellas. Merece la pena hacer notar que estos estudios previos se llevaron a cabo mediante simulaciones de mezclas de estrategias y sus resultados no poseen la caracterización cuantitativa que podemos dar en este trabajo. Además, los análisis de invasibilidad que se llevaron a cabo a posteriori con las estrategias dominantes no consideraron estrategias mixtas, cuya importancia pone de manifiesto nuestro trabajo.

---

* luisalberto.martinez@uc3m.es

[1] R. Axelroad, *The Evolution of Cooperation* (Basic Books, New York, 1984).
[2] M.Ñowak, Science **314**, 1560–1563 (2006).
[3] M.Ñowak, *Evolutionary Dynamics* (The Belknap Press of Harvard University Press, Cambridge, 2006).
[4] M.Ñowak, K. Sigmund, E. El-Sedy, J Math Biol **33**, 703–722 (1995).

DNA compaction induced by the anticancer peptide Kahalalide F: a single-molecule study

J. Camunas-Soler, C.V. Bizarro, S. de Lorenzo, X. Sisquella, A. Mata, R. Eritja, F. Albericio, S.B. Dev, F. Ritort
Small Biosystems Lab, Facultat de Física, Universitat de Barcelona, 08028 Barcelona
CIBER de Bioingeniería, Biomateriales y Nanomedicina, Instituto de Salud Carlos III, Madrid, Spain
Nanotechnology Platform, Parc Científic de Barcelona, Universitat de Barcelona, 08028 Barcelona, Spain
Parc Científic de Barcelona, Universitat de Barcelona, 08028 Barcelona, Spain

Kahalalide F is a marine-derived peptide that shows a strong anticancer activity, and that is currently under phase II clinical trials for a variety of cancer types and psoriasis. Interestingly, Kahalalide F kills cancer cells in a way that strongly differs from conventional anticancer compounds, which generally induce cell apoptosis. To the moment, in vitro studies have reported that Kahalalide F induces a broad range of membrane-associated effects such as cell swelling, vacuolization and organelle damage, that lead to a necrosis-like cell death. However the primary mechanism of action of this peptide still remains elusive. Here we show that Kahalalide F directly interacts with nucleic acids inducing its condensation. Using optical tweezers we have characterized the binding of Kahalalide F to dsDNA. As well, the condensation of ssDNA molecules due to its interaction with the peptide has been monitored in real-time as a function of the applied force. These unprecedented results open a new perspective that might be of relevance to elucidate the novel mechanism of action of this peptide. More importantly, the proposed experimental setup can be readily used for the in vitro characterization of other pharmaceutical compounds with limited solubility that are difficult to assess with common bulk techniques.

Emergent structures in bacterial suspensions under gravity

Ricard Matas Navarro*, Ignacio Pagonabarraga
Facultad de Física
Universidad de Barcelona
08028 Barcelona

Bacterial colonies can grow in a wide range of patterns due to the collective behaviour induced by the different interactions between individuals. First, we make a brief review of different continuum models for bacterial colonies. In most of the previous studies the chemotactic interaction is assumed to be the main ingredient to understand the pattern formation. However, it has been shown that a model of reproducing bacteria with a self-propelling velocity which depends on local population density can form stable patterns without need of chemotaxis[1]. After analyzing this model and its different patterns, we study how these are modified under a constant drift between walls, showing the emergence of "rain"processes and progressively localized phases.

* ricardmn@ffn.ub.es

[1] Cates ME, Marenduzzo D, Pagonabarraga I, Tailleur J. PNAS 107:11715–11720.

Nonlocality-induced front interaction enhancement

Manuel A. Matías*, Damià Gomila, Pere Colet
Instituto de Física Intedisciplinar y Sistemas Complejos, IFISC(CSIC-UIB), Campus Universitat de les Illes Balears, E-07122 Palma de Mallorca

Lendert Gelens, Guy Van der Sande
Department of Applied Physics and Photonics, Vrije Universiteit Brussel, Pleinlaan 2, 1050 Brussels, Belgium

The evolution in space and time of a field is classically written in terms of Partial Differential Equations, like the heat equation, being the spatial interaction written in terms of some derivative of the relevant field, a local quantity. More recently considerable effort has been devoted to the study of evolution equations in which spatial interaction is nonlocal, in the form of an integral over an spatial domain[1–3]. Nonlocal interaction terms can appear in Physics and other fields when long-range interaction terms are considered, also as the result of using approximations in reaction-diffusion descriptions and also due to density-dependent effects in biological and ecological systems.

We study[4] a prototypical spatially extended system with two equivalent states connected by monotonic fronts, the 1-D real Ginzburg-Landau equation, with an added spatially nonlocal term,

$$\partial_t E = (\mu - s)E + \partial_{xx}E - E^3 + s\int_{-\infty}^{\infty}\Theta_\sigma(x-x')E(x')dx' \tag{1}$$

being $E(x,t)$ a real field, μ the pump, s the nonlocal strength, and Θ_σ is the spatial nonlocal kernel. Eq. (1) has both a local (diffusive) spatial coupling and also a (linear) nonlocal one.

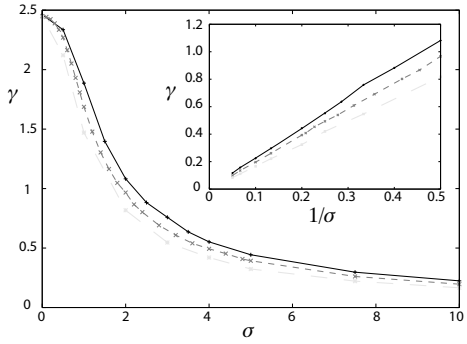

Figura 1. Variation of the exponent γ, as defined in Eq. (2), with σ. The black solid, dark grey dashed and light grey dashed curves have $\mu = 3$, and $s = 0.5, 1, 2$, respectively. The black dotted curve has $\mu = 2$ and $s = 2$.

For attractive interactions we observe an enhancement in the interaction, that ultimately leads to coarsening (like in the local case). From the known *tanh* form of the fronts[5], the interaction can be calculated perturbatively,

$$v(d) = \dot{d} = ce^{-\gamma d}, \tag{2}$$

with v being the relative velocity and d the distance between the fronts. The magnitude of nonlocal effects in front dynamics can be quantified by the deviations from Eq. (2). Thus, Fig. III shows the variation of the exponent γ in (2) for different kernel widths, σ, keeping all the other parameters fixed, for the case of a Gaussian kernel. It can be seen that γ changes about an order of magnitude in the range of σ considered.

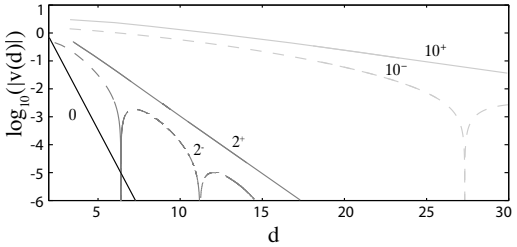

Figura 2. Front velocity as a function of d. $\mu = 3, |s| = 1$, and σ is taken to be 0 , 2 and 10, depicted in the figure as $\sigma^{\mathrm{sgn}(s)}$.

The effect of a spatially nonlocal interaction is more dramatic in the case that the interaction is repulsive (or inhibitory). In this case the exponential law (2) no longer holds. Still, the magnitude of the envelope of the front velocity decreases exponentially (cf. Fig. (2)), while the velocity becomes zero at regular intervals of the distance d between two fronts. At these positions the fronts are locked leading to the formation of localized structures, what is not possible with local interactions.

Nonlocal interactions are common in nonlinear optics, biology, chemistry, and other fields of science, and they can have a constructive role by enhancing the propagation of information between distant parts of the system, and also allowing the system to exhibit new dynamical regimes.

* manuel@ifisc.uib-csic.es http://ifisc.uib-csic.es/

[1] J.D. Murray, *Mathematical Biology*, (Springer, 2002).
[2] G.B. Ermentrout, Rep. Prog. Phys. **61**, 353 (1998).
[3] S. Coombes, Biol. Cybern. **93**, 91 (2005).
[4] L. Gelens, D. Gomila, G. Van der Sande, M.A. Matías, and P. Colet, Phys. Rev. Lett. **104**, 154101 (2010).
[5] P. Coullet, C. Elphick, and D. Repaux, Phys. Rev. Lett. **58**, 431 (1987).

Entropy of continuous mixtures and the measure problem

Pablo Maynar*, Emmanuel Trizac
Facultad de Física
Universidad de Sevilla
41012 Sevilla

In its continuous version, the entropy functional measuring the information content of a given probability density may be plagued by a "measure" problem that results from improper weighting of phase space. This issue is addressed considering a generic collision process whereby a large number of particles/agents randomly and repeatedly interact in pairs, with prescribed conservation law(s). We find a sufficient condition under which the stationary single particle distribution function maximizes an entropy-like functional, that is free of the measure problem. This condition amounts to a factorization property of the Jacobian associated to the binary collision law, from which the proper weighting of phase space directly follows.

* maynar@us.es

A vortex crystal that flows like a liquid: Grain-boundary scars in flat geometry

M. Carmen Miguel[1*], Adil Mughal[2], Stefano Zapperi[2,3]
[1] *Departament de Física Fonamental, Facultat de Física, Universitat de Barcelona, Diagonal 647, 08028 Barcelona*
[2] *ISI Foundation, Viale San Severo 65, 10133 Torino, Italy*
[3] *CNR-IENI, Via R. Cozzi 53, 20125 Milano, Italy*

We investigate the structural transformations of a vortex crystal in the Corbino disk geometry in response to an injected current in the superconducting material. At high enough currents, the vortex crystal exhibits a laminar flow response, with a velocity profile decaying in the same manner as the driving current, as if we were dealing with an uncorrelated vortex liquid phase. Laminar flow can be induced by thermal fluctuations melting the crystal, but also by applying a large current at zero temperature. While the flow profile is the same in the two cases, the underlying vortex structure is completely different. Here we show that in the Corbino disk geometry, a polycrystalline vortex structure flows in a liquid-like manner due to the presence of disclinations and dislocations that induce the necessary curvature in the host crystal. Disclinations in this flat geometry migrate from the sample boundary to the interior of the crystal assisted by the formation of grain-boundary scars, i.e. walls of equally charged dislocations emanating from boundary disclinations. The problem of ground-state configurations including stable grain boundary scars on (positively or negatively) curved surfaces has recently attracted new consideration. Here we show that these topological structures, which in equilibrium conditions would be forbidden in flat geometry, can otherwise be induced and maintained by shear stress. We provide an estimate of the critical current needed to initiate the formation of grain boundary scars in the Corbino disk geometry, and thus to sustain the laminar flow of the vortex crystal, and show that the result is in good agreement with numerical simulations of the vortex array.

* carmen.miguel@ub.edu

El papel de las correcciones de largo alcance en la determinación de las propiedades interfaciales del agua mediante simulación molecular

J.M.Míguez, D. González-Salgado, P. Gómez-Álvarez, J.L. Legido, M.M. Piñeiro*
Departamento de Física Aplicada, Facultade de Ciencias
Universidade de Vigo
36310 Vigo

En simulación molecular el cálculo de las propiedades interfaciales de fluidos descritos a partir de modelos moleculares que incorporan cargas eléctricas requiere un gran tiempo de cálculo. A lo largo de los últimos años, nuevas técnicas de cálculo han sido propuestas para el estudio de estas propiedades en cajas bifásicas de simulación, como por ejemplo el método del Test-Área[1] o el Wandering Interface[2]. Estos métodos innovadores reducen el tiempo de cálculo de forma considerable y mejoran cuantitativamente la estimación de propiedades como: tensión interfacial, densidades de coexistencia, perfil de densidad y anchura de la interfase. Sin embargo, los resultados de estos cálculos dependen enormemente del tamaño del sistema y del tipo de correcciones de largo alcance utilizadas, un hecho que repercute también en los tiempos de cálculo.

En este trabajo, hemos estudiado el papel de las correcciones de largo alcance tipo Janecek[3,4] en la determinación de las propiedades interfaciales del agua, cuyo comportamiento será descrito por los modelos SPC/E[5], TIP4P[6], TIP4P/Ewald[7] y TIP4P/2005[8] que son los que proporcionan una mejor estimación de la curva de coexistencia líquido-vapor. Así, podrá observarse un estudio detallado del valor del radio de corte mínimo a partir del cuál obtenemos una estimación realista de todas estas propiedades incluyendo dichas correcciones de largo alcance.

* mmpineiro@uvigo.es

[1] G. J. Gloor, G. Jackson, F. J. Blas y E. de Miguel, J. Chem. Phys. **123**, 134703 (2005).
[2] L. G. MacDowell y P. Bryk, Phys. Rev. E **75**, 061609 (2007).
[3] J. Janecek, J. Phys. Chem. B **110**, 6264 (2006).
[4] L. G. MacDowell y F. J. Blas, J. Chem. Phys. **131**, 074705 (2009).
[5] H. J. C. Berendsen, J. R. Grigera, y T. P. Straatsma, J. Chem. Phys. **91**, 6269 (1987).
[6] W. L. Jorgensen, J. Chandrasekhar, J. Madura, R. W. Impey y M. Klein, J. Chem. Phys. **79**, 926 (1983).
[7] H. W. Horn, W. C. Swope, J. W. Pitera, J. D. Madura, T. J. Dick, G. L. Hura y T. Head-Gordon, J. Chem. Phys. **120**, 9665 (2004).
[8] J. L. F. Abascal y C. Vega, J. Chem. Phys. **123**, 234505 (2005).

The dynamical strength of social ties in information spreading

Giovanna Miritello[1,2], Esteban Moro [1,3,4], Rubén Lara[2]
[1] *GISC, Departamento de Matemáticas & GISC, Universidad Carlos III de Madrid, 28911 Leganés, Spain*
[2] *Telefónica Research, Madrid, Spain*
[3] *Instituto de Ingeniería del Conocimiento, Universidad Autónoma de Madrid, 28049 Madrid, Spain* & Instituto de Ciencias Matemáticas CSIC-UAM-UCM-UC3M

Quantitative understanding of human communication patterns is of paramount importance to explain the dynamics of many social, technological and economic phenomena. Most studies have focused on the complex *topological patterns* of the underlying contact network and its influence in the properties of spreading phenomena in social networks such diffusion of information, innovations, computer viruses, opinions, etc. In these studies the real temporal activity is aggregated over time giving a static snapshot of the social interaction where ties are described by static strengths which do not include information about the *temporal patterns* of human interaction. In this framework, the dynamics of interaction between individuals is described by a homogeneous Poisson process in which the communication events are uncorrelated events with the same probability to happen.

However, recent studies of human behavior show that humans act in bursts or cascades of events[1], most ties are not persistent[2] and communications happen in the form of group conversations[3]. Thus, since human communication and information transmission are concurrent, the temporal structure of communication must influence the properties of information spreading[4].

In a recent study[5] we investigate the influence of the temporal patterns of human communication in the spreading of information by analyzing the mobile communication of 20 million people during one year. According to previous results[1,3], we observe that human communication is bursty and happens in group conversations. To investigate the influence of these temporal aspects on the spreading of information, we simulate the epidemic SIR model in which an infected node can infect a susceptible node with probability λ. We compare the results with the real time sequence of communication events with the ones when the real time-stamps of the communication events are shuffled (that simulates a homogeneous Poisson process). A significant difference is observed between the real and the shuffled-time data for different regimes of λ: when λ is small, the total reach is bigger for the real data, while the opposite behavior is observed for large λ.

By mapping the dynamical SIR model to a static percolation model where each tie is described by the transmissibility $\mathcal{T}_{ij}$[6], e.g. the probability that the information is transmitted from i to j, we are able to explain the observed behavior.
In particular we show that both the bursty nature of human communications and the existence of group conversations are the two main dynamical ingredients to understand the spreading of information in social networks. These two effects compete in the spreading, favoring (small λ) and hindering (large λ) the information reach when compared with the homogeneous case (Fig.1).

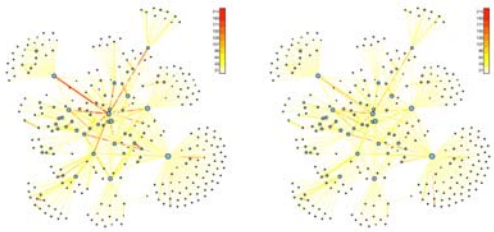

Figura 1. The structure of the mobile call network around a randomly chosen individual. Each link represents at least one call between the two users. The weight of the links assigned on the basis of their transmissibility $\mathcal{T}_{ij}$ for a large value of λ for the shuffled-time (left) and the real (right) case.

Our results indicate that a an effective way to incorporate temporal patterns of communication in the description and modeling of human interaction is through the transmissibility, that represents the *dynamical strength* of the ties.

[1] A.-L. Barabási, *Nature* **435**, 207, (2005); A. Vázquez *et al.*, Phys. Rev. Lett. **98**, 158702 (2007).
[2] G. Kossinets, D. J. Watts, Science **311**, 88 (2006); C. A. Hidalgo and C. Rodriguez-Sickert, Physica A **387**, 3017 (2008).
[3] J.-P. Eckmann, E. Moses, and D. Sergi, Proc. Natl. Acad. Sci. U.S.A. **101**, 14333 (2004); Y. Wu *et al.*, Proc. Natl. Acad. Sci. U.S.A. **107**, 18803 (2010).
[4] J. L. Iribarren and E. Moro, Phys. Rev. Lett. **103**, 038702 (2009); M. Karsai et al. arXiv:1006.2125 (2010).
[5] G. Miritello, E. Moro, R. Lara. arXiv:1006.2125 (2010).
[6] M. E. J. Newman, Phys. Rev. E **66**, 16128 (2002); E. Kenah and J. M. Robins, Phys. Rev. E **76**, 036113 (2007).

Nonequilibrium spin glass dynamics with magnetic field

R. Alvarez Baños[1,2], A. Cruz[2,1], L.A. Fernandez[3,1], J. M. Gil-Narvión[1], A. Gordillo-Guerrero[4,1], M. Guidetti[5], A. Maiorano[6,1], F. Mantovani[7], E. Marinari[6], V. Martin-Mayor[3,1], J. Monforte-Garcia[1,2], A. Muñoz Sudupe[3], D. Navarro[8], G. Parisi[6], S. Perez-Gaviro[1,6], J. J. Ruiz-Lorenzo[9,1], S. F. Schifano[10], B. Seoane[3,1], A. Tarancon[2,1], R. Tripiccione[10], D. Yllanes[3,1]

Instituto de Biocomputación y Física de Sistemas Complejos (BIFI)
Campus Río Ebro, Universidad de Zaragoza,
50018 Zaragoza, Spain

The aim of the work is to study the behavior of the Ising Spin Glass (the Edwards-Anderson model) with a magnetic field out of equilibrium. Simulations with a fixed temperature and with an annealing algorithm have been performed. We have used the special-purpose computes Janus, based on FPGAs, so we managed to reach times up to $0.01s$. We have computed dynamics correlation functions and coherence length. Furthermore, we have studied if the system presents a de Almeida-Thouless line, in order to find if the system behaves like a droplet scenario or a RSB one.

[1] Instituto de Biocomputación y Física de Sistemas Complejos (BIFI), 50009 Zaragoza, Spain
[2] Departamento de Física Teórica, Universidad de Zaragoza, 50009 Zaragoza, Spain
[3] Departamento de Física Teórica I, Universidad Complutense, 28040 Madrid, Spain
[4] Departamento de Ingeniería Eléctrica, Electrónica y Automática, Universidad de Extremadura, 10071, Cáceres, Spain
[5] Dipartimento di Fisica, Università di Ferrara and INFN-Sezione di Ferrara, Ferrara, Italy
[6] Dipartimento di Fisica, INFM and INFN, Università di Roma "La Sapienza", 00185 Roma, Italy
[7] DESY, D-15738 Zeuthen, Germany
[8] Departamento de Ingeniería, Electrónica y Comunicaciones and I3A, Universidad de Zaragoza, 50018 Zaragoza, Spain
[9] Departamento de Física, Universidad de Extremadura, 06071 Badajoz, Spain
[10] Dipartimento di Fisica Università di Ferrara and INFN-Sezione di Ferrara, Ferrara, Italy

Sincronización macrocópica de osciladores de Stuart-Landau

Ernest Montbrió*, Diego Pazó‡
Department of Information and Communication Technologies
Universitat Pompeu Fabra
08003 Barcelona

La sincronización macroscópica es un fenómeno cooperativo por el que una población heterogénea de osciladores se autoorganiza para dar lugar a una oscilación colectiva. Los ejemplos son numerosos[1] en biología pero también en otros ámbitos como la física.

El oscilador de Stuart-Landau (SL):

$$\dot{\varrho} = \varrho(1-\varrho^2), \quad \dot{\theta} = \omega + q(1-\varrho^2). \tag{1}$$

es la forma canónica de un ciclo límite cerca del inicio de las oscilaciones autosostenidas (vía una bifurcación de Hopf). El parámetro ω define la frecuencia angular sobre el atractor $\varrho = 1$, y q es la denominada noiscocronicidad que cuantifica las alteraciones de la frecuencia fuera del ciclo límite.

El modelo básico de sincroniazción macroscópica es un esquema de población de osciladores de SL con acoplamiento de todos con todos :

$$\dot{z}_j = z_j[1 + i(\omega_j + q_j) - (1 + iq_j)|z_j|^2] + \frac{K}{N}(1 + ic_1)\sum_{k=1}^{N} z_k - z_j, \tag{2}$$

donde hemos usado la notación $z_j = \varrho_j e^{i\theta_j}$. La ec. (2) es una versión de campo medio de la ecuación de Ginzburg-Landau compleja con desorden.

En esta comunicación se muestran soluciones explícitas analíticas para la sincronización de la ec. (2). Nuestros resultados son una generalización de resultados anteriores.

---

* ernest.montbrio@upf.edu
‡ Instituto de Física de Cantabria (IFCA), CSIC-Universidad de Cantabria, 39005 Santander.

[1] S. H. Strogatz, *Sync: The emerging science of spontaneous order.* (Hyperion Press, New York, 2003).

Estudio Computacional de un medio granular húmedo forzado

Silvio René Morales Suárez*, Ignacio Pagonabarraga Mora†
Facultad de Física
Universidad de Barcelona
08028 Barcelona

Un *medio granular* se compone de partículas macroscópicas, *granos*, que pueden encontrarse en el vacío o inmersas en un fluido. Entre estas no actúan fuerzas atractivas, solo fuerzas disipativas de repulsión, lo que lleva a que las colisiones sean inelásticas y no se conserve la energía mecánica del sistema. El carácter disipativo de estas colisiones es el responsable de que los medios granulares, en dependencia de las condiciones en que se encuentren, se comporten como un sólido, líquido o gas.

El comportamiento peculiar, y la importancia que tienen para la industria materiales con estas características, ha hecho que en los últimos años el estudio científico de medios granulares haya experimentado un desarrollo considerable.

La mayor parte de los estudios que se han realizado sobre este tipo de material se centran en medios granulares secos en los que sólo se tiene en cuenta la interacción entre las partículas.

En muchas situaciones se puede despreciar el efecto que ejerce el fluido donde se encuentran los granos y tratar el sistema como un medio granular seco, pero en otras[7] hay que tener en cuenta además la relación fluido-grano, llevándonos a modelos más complejos.

En este trabajo nos enfocamos en sistemas como estos últimos, creando una aplicación computacional que permita estudiar la respuesta de *medios granulares húmedos* y ayude a comprender el comportamiento de este tipo de material, sobre todo en estados estacionarios fuera del equilibrio.

Al estar los granos en contacto con un fluido pierden energía y después de un tiempo llegan a estar en reposo, por lo tanto es necesario aplicarles un esfuerzo externo con el objetivo de alcanzar un estado estacionario en el cual se puedan medir cantidades estadistas significativas. Con este fin vamos a realizar dos tipos de simulaciones.

En una agitaremos todo el sistema, para tener resultados de la respuesta global, aplicando una fuerza aleatoria sobre cada una de las partículas. Aunque esto es un modelo idealizado, permite obtener un estado homogéneo mas fácil de estudiar.

En otro tipo de simulaciones aplicaremos una fuerza constante a una partícula seleccionada para medir propiedades microscópicas, que podremos comparar con resultados experimentales[6] obtenidos utilizando pinzas ópticas para arrastrar a velocidad constante una partícula aislada del resto.

* silvio.rene@gmail.com
† ipagonabarraga@ub.edu

[1] Bhatnagar, P. L., Gross, E. P. & Krook, M. 1954 A model for collision processes in gases. i. small amplitude processes in charged and neutral one-component systems. *Phys. Rev.* **94** (3), 511–525.
[2] Briantov, N. V. & Pöschel, T. 2004 *Kinetic Theory of Granular Gases*. Oxford University Press.
[3] Desplat, J.-C., Pagonabarraga, I. & Blandon, P. 2001 Ludwig: A parallel lattice-boltzmann code for complex fluids. *Computer Physics Communications* **134**, 273–290.
[4] Ladd, A. J. C. 1988 Hydrodynamic interactions in a suspension of spherical particles. *The Journal of Chemical Physics* **88**, 5051–5063.
[5] Ladd, A. J. C. & Nguyen, N.-Q. 2002 Lubrication corrections for lattice-boltzmann simulation of particles suspentions. *Phys. Rev.* **66**.
[6] Meyer, A., Marshall, A., Bush, B. G. & Furst, E. M. 2006 Laser tweezer microrheology of a colloidal suspension. *Journal of Rheology* **50** (1), 77–92.
[7] Möbius, M. E., Cheng, X., Karezmar, G. S., Nagel, S. R. & Jaeger, H. M. 2004 Intruders in the dust: Air-driven granular size separation. *Physical Review Letters* **93**.
[8] van Noije, T. P. C., Ernst, M. H., Trizac, E. & Pagonabarraga, I. 1999 Randomly driven granular fluids: Large-scale structure. *Physical Review* **59**, 4326–4341.
[9] Squires, T. & Brady, J. 2004 A simple paradigm for active and nonlinear microrheology. *APS Meeting Abstracts* pp. 2–+.

Análisis numérico del *stress* inducido por bombardeo iónico

Ana Moreno Barrado[1], Mario Castro[1]
[1] *Grupo Interdisciplinar de Sistemas Complejos (GISC). Universidad Pontificia Comillas. Madrid, España.*

Uno de los primeros sistemas experimentales en los que se observó la formación de patrones a escala nanométrica es el bombardeo de superficies mediante haces iones energéticos[1]. Desde los primeros estudios teóricos de Sigmund[2] el mecanismo responsable de la formación de estos patrones se ha atribuido a la erosión del material. Así, cuando un ion impacta con la superficie de un material, deposita energía en dicho material por medio de colisiones con los átomos del *blanco*. Parte de esta energía es suficiente para romper los enlaces de los átomos de la superficie, eliminando así material. La tasa de erosión depende de la curvatura local de la superficie: los *picos* son erosionados más rápidamente que los *valles* dando lugar a una inestabilidad morfológica que es la responsable de la formación del patrón.

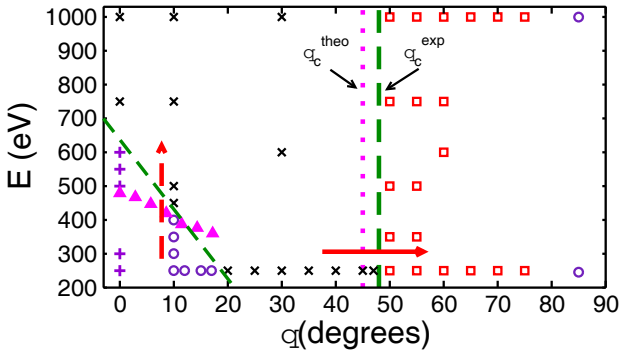

Figura 1. Diagrama morfológico teórico de la formación de patrones por bombardeo de haces de iones[4]. La transición morfológica a $\theta = 45$ se puede explicar a través de la ecuación (1).

Esta visión de la erosión se ha visto recientemente cuestionada tanto por trabajos experimentales[3] como teóricos[4].

En estos trabajos se apunta a otras causas como responsables últimas de la inestabilidad morfológica como la redistribución de material por efecto del impacto o el stress producido por la deformación causada en el material.

En particular en[4] se muestra que es la competición entre el *stress* causado por la deformación del material como respuesta al impacto del ion y el flujo viscoso inducido en el material. De hecho, aunque el material es inicialmente cristalino, los iones producen la amorfización del blanco y el eventual flujo de defectos (como vacantes e intersticiales). La relajación de estos efectos tiene como consecuencia el flujo viscoso del sólido (con una viscosidad estimada del orden de 10^8 Pa s).

De esta competición, se puede deducir un diagrama morfológico como el mostrado en la figura 1 que separa una región *plana* de una región con patrones, siendo la transición morfológica de segundo orden.

En esta contribución se propone un estudio de simulación basado en dinámica molecular para discriminar entre los dos mecanismos mencionados.

Así, se plantea la evolución del *stress* con el tiempo en función de diversos parámetros controlables experimentalmente, como la energía del ión, el flujo de partículas o el ángulo de incidencia.

En particular, se pretende realizar una conexión multiescala entre los resultados de simulación y los parámetros numéricos. Esta conexión permitiría entender la relevancia de, por ejemplo, la energía o el ángulo de incidencia sobre el blanco en la formación de la inestabilidad a través de la relación de dispersión del problema:

$$\omega_q = \frac{\tau h^2 \cos(2\theta)}{3\mu} q^2 - \frac{\sigma h^3}{3\mu} q^4, \qquad (1)$$

donde h es la anchura de la zona dañada por la radiación iónica, τ es el stress inducido por el daño, μ es la viscosidad y σ la tensión superficial.

Este tipo de simulación impone algunas limitaciones en cuanto a las escalas de tiempo que el sistema puede alcanzar, por lo que se discuten, asimismo, algunas de las posibilidades para conectar las simulaciones con las teorías continuas basadas en ecuaciones en derivadas parciales[4,5].

* ana.moreno@upcomillas.es

[1] M. Navez, C. Sella, and D. Chaperot, C. R. Acad. Sci. Paris **254**, 240 (1962).
[2] P. Sigmund, Phys. Rev. **184**, 383 (1969).
[3] C. S. Madi, H. B. George, and M. J. Aziz, J. Phys.: Condens. Matter **21**, 224010 (2009).
[4] M. Castro, R. Cuerno, enviado a Phys. Rev. Lett (2011).
[5] M. Castro, R. Cuerno, L. Vázquez, and R. Gago, Phys. Rev. Lett. **94**, 016102 (2005).

Integrating multiple signals into cell decisions by networks of protein modification cycles

Luca Cerone[†], Javier Muñoz-García[*], Zoltán Neufeld[†]

[*] *Departamento de Matemáticas and Grupo Interdisciplinar de Sistemas Complejos, Universidad Carlos III de Madrid, 28911 Leganés, Spain*

[†] *School of Mathematical Science and Complex Adaptive Systems Laboratory, University College Dublin, Dublin 4, Ireland*

Cell responses to internal and external stimuli are governed by protein interactions. The enzymatic activity and biological function of proteins is modulated by reversible post-translational modifications such as phosphorylation, acetylation, methylation, ubiquitination, sumoylation, etc[1]. Thus, post-translational protein modifications play a key role in regulating cellular processes. Here we present a general mathematical model of reversible protein modification networks and demonstrate that a single protein modified by several enzymes is capable of integrating multiple signals into robust digital cellular decisions by switching between multiple forms that can activate distinct cellular processes. We develop an analytical approach for constructing the phase diagram of such systems from the structure of the protein modification network, determining how switching between distinct responses take place. This method can be applied to a broad class of protein modification systems and provides an alternative to numerical approaches that give limited insight when the number of unknown parameters is large.

First we consider a system of two competing protein modification cycles connecting three different protein forms. We show that in the steady state most of the protein is concentrated into a single form determined by the enzyme activities representing the input signals of the system when the total protein concentration is large compared to the Michaelis-Menten saturation constants. We generalize this model to protein modification networks with tree structure and describe the mechanism of complex switching behavior of proteins arising from coupled cycles of reversible modifications controlled by multiple enzymes. These systems can be characterized by constructing their phase diagram, that is a partition of the space of enzyme activities into regions corresponding to different dominant forms. We show that the phase diagram can be obtained analytically from the wiring diagram of the modification network by recursively solving a set of balance equations for the steady state protein distributions and then applying a positivity condition to determine the regions corresponding to the different types of solutions. This method can be implemented in a computer algebra system that automatically generates the phase diagram as a set of inequalities with the parameter treated symbolically.

---

[*] javiermunozgarcia@gmail.com
`http://gisc.uc3m.es/~javier`

[1] C. T. Walsh, *Posttranslational modification of proteins: expanding nature's inventory*. Roberts and Company Publishers (2006).

Macroscopic effects of internal noise on Fisher fronts

Svetozar Nesic*, Esteban Moro, Rodolfo Cuerno
Grupo Interdisciplinar de Sistemas Complejos(GISC) and Departamento de Matemáticas, Universidad Carlos III de Madrid, Avenida de la Universidad 30, E-28911 Leganés, Spain

Continuum representation of the dynamics of spatially extended system subject to fluctuations is a very active area of research in statistical mechanics and nonlinear dynamics. An important instance is that of reaction-diffusion systems subject to internal (or microscopic) fluctuations. In the last years, particular attention has been paid to the so called Fisher-Kolmogorov-Petrovsky-Piscounov (FKPP) equation,[1]

$$\frac{\partial \rho}{\partial t} = D\Delta\rho + \rho - \rho^2 + \sqrt{\rho/N}\ \eta(x,t), \qquad (1)$$

where $\eta(x,t)$ is a Gaussian white noise and N is approximately the number of particles per unit volume.[2] This equation is also known as the Reggeon model, which provides a minimal representation of the Directed Percolation (DP) universality class.[4] Specifically, for $N = N_c$ equation (1) undergoes a transition between an active phase ($\rho \neq 0$) and an absorbing state ($\rho = 0$).[4–6] In addition, for very large $N \gg N_c$ the FKPP equation displays *pulled fronts* in which the active phase invades the absorbing state.[3] The properties of the front (velocity, fluctuations, etc.) are extremely sensitive to microscopic fluctuations. In particular, there are strong corrections to the velocity of the front for finite N when compared to the deterministic $N \to \infty$ equation.[7]

However, most of the studies of front dynamics in the FKPP equation have been done in one-dimensional setups. In this work we study what is the effect of those internal fluctuations in the dynamics of the one-dimensional front line of the two-dimensional FKPP equation. Using a non-negativity preserving algorithm to integrate equation (1),[5,6] we find that the front roughens in time and that its fluctuations can be described asymptotically by the Kardar-Parisi-Zhang universality class. Contrary to the standard perturbation theory or the standard moving boundary approximation, the effective temperature effectively felt by the front scales as $T_{\text{eff}} \sim 1/\log N$. This means that even in macroscopic systems ($N = 10^{23}$), internal fluctuations strongly influence the front dynamics.

* snesic@math.uc3m.es

[1] R. A. Fisher, Ann. Eugenics VII, 355 (1936); A. Kolmogorov, I. Petrosvky, and N. Piscounov, Moscow Univ. Bull. Math. A **1**, 1 (1937).
[2] N. G. van Kampen Stochastic Processes in Physics and Chemistry,(North-Holland, 1992) ; C. W. Gardiner, Handbook of Stochastic Methods, (Springer-Verlag, Berlin 1985).
[3] W. van Saarloos, Phys. Rep. **386**, 29 (2003); D. Panja, ibid. 393, 87 (2004).
[4] H. Hinrichsen, Adv. Phys. **46**, 815 (2000).
[5] E. Moro, Phys. Rev. E **70**, 045102(R) (2004)
[6] I. Dornic, H. Chate, and M. A. Muñoz, Phys. Rev. Lett. **94** 100601 (2005)
[7] E. Brunet and B. Derrida, Phys. Rev. E **56**, 2597 (1997); J. Stat. Phys. **103**, 269 (2001)

Digital key for chaos communication performing time delay concealment

Romain Modeste Nguimdo[1], Pere Colet[1], Laurent Larger[2], Luís Pesquera[3]

[1] *Instituto de Física Interdisciplinar y Sistemas Complejos, IFISC (CSIC-UIB),Campus Universitat de les Illes Balears, E-07122 Palma de Mallorca, SPAIN.*

[2] *UMR CNRS FEMTO-ST 6174/Optics Department, University of Franche-Comté, 16 Route de Gray, 25030 Besançon cedex, France*

[3] *Instituto de Física de Cantabria, (CSIC-Universidad de Cantabria), Santander E-39005,Spain*

Time delay is well known as playing a key role in inducing strong chaotic behaviors, which are typically exploited for chaos communications. Unfortunately, this sensitive key parameter has also been found vulnerable when using standard time series identification techniques. Another limit of hardware cryptography relies on the fact that its parameter space dimension (a kind of equivalent to the digital key size in algorithmic encryption) is relatively low compared to software cryptography. To circumvent these drawbacks, we propose here to implement a currently suggested principle in algorithmic cryptography, which consists in mixing different algebra when constructing the encryption algorithm. In the context of secure chaos-based communications, a possible implementation of this idea would consist in combining a pseudo-random bit sequence (PRBS) typically used in standard encryption, together with an analog physical chaos, in order to provide an enhanced cryptographic security through the reciprocal concealment between the boolean pseudo-random sequence and the high dimensional continuous time chaotic motion. The proposed scheme is a double opto-electronic feedback system based on high speed phase chaos[1], with constant intensity and an essentially featureless power spectrum. it allows on one hand to integrate a digital key required for decoding and on the other to conceal the delay time so that it cannot be identified from the time series using the typical methods. The emitter dynamics is given by the dimensionless variables $x_1(t)$ and $y_2(t)$

$$x_1 + \tau_1 \frac{dx_1}{dt} + \frac{1}{\theta_1} u_1 = \beta_1 \cos^2\left[\Delta(y_2 + R)_{T_1} + \phi_1\right], \quad (1)$$

$$y_2 + \tau_2 \frac{dy_2}{dt} + \frac{1}{\theta_2} u_2 = \beta_2 \cos^2\left[\Delta(x_1 + m)_{T_2} + \phi_2\right], \quad (2)$$

where $du_1/dt = x_1$, $du_2/dt = y_2$ and $\Delta(F)_{t_0} = F(t - t_0) - F(t - t_0 - \delta t_0)$. The parameters are the feedback strengths $\beta_1 = \beta_2 = 5$, the delay times $T_1 = 17$ñs and $T_2 = 15$ñs, the fast (slow) filter characteristic response times $\tau_1 = 20$ ps ($\theta_1 = 1.6$ μs) and $\tau_2 = 12.2$ ps ($\theta_2 = 1.6$ μs), the MZI imbalanced delays $\delta T_1 = 510$ ps and $\delta T_2 = 400$ ps, and the MZI static phases $\phi_1 = \pi/4$ and $\phi_2 = \pi/8$. Figures. 1 b) and c) display DMI of the chaotic carrier as function of the delay without and with PRBS, respectively. It is seen that without PRBS, clear peaks appear at time-delays T, $T + \delta T_1$, $T + \delta T_2$ and $T + \delta T_1 + \delta T_2$. However, when PRBS is employed, time-delays cannot be identified anymore. Similar results were obtained from the computation of the autocorrelation function. Figures 1 d) and e) show the effects of mismatch η in the key by measuring the root-mean-square synchronization error σ and quality factor, respectively. Considering 10 Gb/s message with amplitude of $\pi/2$ for Fig 1 e), it appears that even 4% of PRBS-mismatch is enough to considerably degrade the synchronization quality. Thus, we have shown that PRBS can be an efficient way to both provide further security and conceal the time delays in some electro-optic systems.

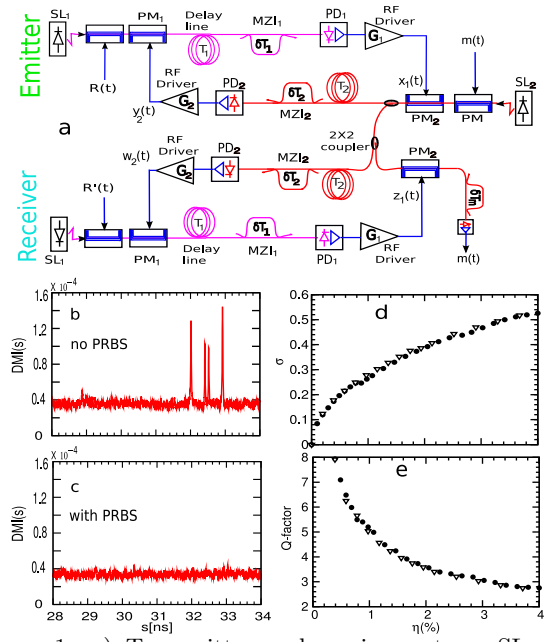

Figura 1. a) Transmitter and receiver setup: SL: semiconductor laser, PM: phase modulator, MZI: passive imbalanced Mach-Zehnder interferometer, PD: photodiode, $x_1(t)$ and $y_2(t)$ are dimensionless output voltages of the RF drivers in chains 1 and 2 respectively. $R(t)$ and $m(t)$ are the PRBS and message signals respectively. Sub-indices $i = 1, 2$ refer to the first and second processing chains, both at the emitter and the receiver. Mutual information of the chaotic carrier $x_1(t)$ zooming around the total time delays b) without PRBS and c) with PRBS at 3 Gb/s and amplitude $\pi/2$. d) Root-mean square synchronization error σ and e) Q-factor vs. percentage of receiver PRBS bits differing from the emitter PRBS considering PRBS $R(t)$ of length 1024 (•) and 512 (∇) bits

[1] R. Lavrov, M. Peil, M. Jacquot, L. Larger, V. Udaltsov, and J. Dudley, Phys. Rev. E **80**, 026207 (2009).

How do cells break their symmetry? A simple reaction-diffusion mechanism for cell polarization during asymmetric cell division

Ernesto M. Nicola[a,b], Philipp Khuc Trong[b,c], Nathan W. Goehring[c], Stephan W. Grill[b,c]
[a] *IFISC (CSIC-UIB), Institute for Cross-Disciplinary Physics and Complex Systems, Campus Universitat Illes Balears, E-07122 Palma de Mallorca, Spain.*
[b] *Max-Planck Institute for the Physics of Complex Systems, Noethnitzer Strasse 38, D-01187 Dresden, Germany.*
[c] *Max-Planck Institute of Molecular Cell Biology and Genetics, Pfotenhauerstrasse 108, D-01307 Dresden, Germany.*

Symmetry breaking processes not only occur in physical and chemical systems. In biology this effect is encountered in many different circumstances either inside single cells or in hole organisms. One example of a symmetry-breaking process occurring inside cells takes place during the phenomenon called *cell polarization*. Polarity, the asymmetry in shape present in many cells, is a common feature of many different cell types. The initial establishment of cell polarity can be considered as a symmetry-breaking process and has attracted much attention during the last years.

Cell polarization happens, *e.g.*, when cells divide asymmetrically during the development of most organisms and is an important mechanism to achieve functional specialization. This process has been intensively studied in embryos of the worm *Caenorhabditis elegans*[1,2] where, prior to the first cell division, the distribution of some characteristic proteins becomes asymmetrical (see Fig. 1). This asymmetric distribution of proteins in distinct anterior and posterior domains is responsible for the different fates that each daughter cell has after the asymmetric cell division.

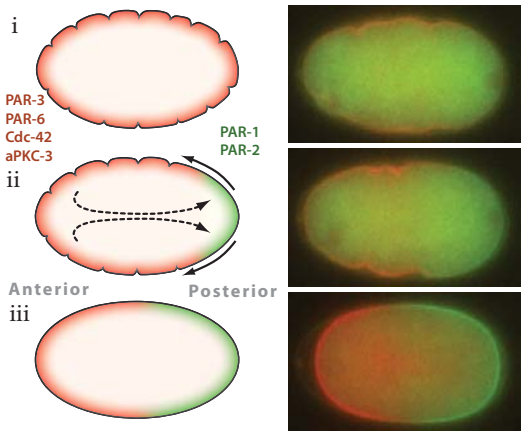

Figura 1. Example of polarization of the one-cell embryo of the *C. elegans* worm. Red indicates a high concentration of the protein PAR-6 and green PAR-2 (schematic on the left and experimental data on the right) for three subsequent stages: (i) initial (unpolarized), (ii) transitory and (iii) final (polarized) state.

Motivated by recent experimental evidence[1–3], we present and study a simple two-variable, reaction-diffusion system that describes the asymmetric distribution of the characteristic proteins in the cell membrane[4]. The model exhibits a symmetry-breaking mechanism that leads to protein segregation and accounts for many experimental observations done in the worm *C. elegans* and other organisms[4]. We show that this spontaneous symmetry breaking is induced by a mechanism similar to a Turing instability (see example in Fig. 2). However, in our model the wavelength of the fastest growing spatial pattern is always equal to the system size.

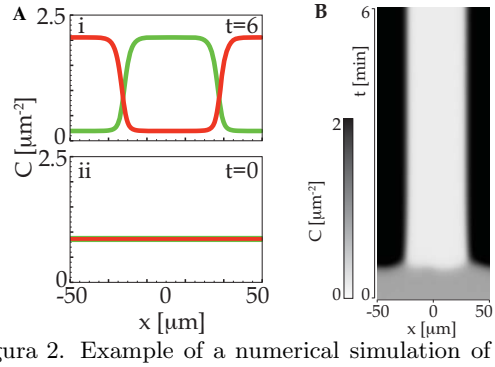

Figura 2. Example of a numerical simulation of the reaction-diffusion model illustrating the symmetry-breaking phenomenon occurring during cell polarization. A space-time plot of the concentration of PAR-6 (red) is shown in (B) and in (A) the initial and final profiles of proteins PAR-2 and PAR-6 in the cell membrane are displayed.

We also derive a minimal mathematical model (an amplitude equation) that describes polarization in a vast number of biological systems. We find that the topology of the bifurcations present in the parameter-space of our minimal model is equivalent to the parameter-spaces of a number of more realistic reaction-diffusion models proposed in the literature. The minimal model also suggests that the instability mechanism leading to polarization is generically subcritical and leads to a typical coexistence between the homogeneous- and asymmetric-states.

[1] Grill, Gonczy, Stelzer and Hyman, Nature **409**, 630 (2001).
[2] Grill, Howard, Schaffer, Stelzer and Hyman, Science **301**, 512 (2003).
[3] Goehring, Chowdhury, Hyman and Grill, Biophys. J. **99**, 2443 (2010).
[4] Goehring, Khuc-Trong, Bois, Nicola, Chowdhury, Hyman and Grill, submitted (2011).

Dynamical study of the three dimensional Saffman-Taylor problem

Matteo Nicoli*, Hervé Henry, Mathis Plapp
Laboratoire de Physique de la Matiére Condensèe
École Polytechnique, CNRS
Palaiseau - France

When a fluid of negligible viscosity displaces a more viscous one an instability develops at their interface. This problem has been originally studied by Saffman and Taylor[1] in a Hele-Shaw cell. In this set-up, the two fluids obey Darcy's law and the interfacial instability can create either a stable finger or a pattern of unstable fractal structures. Here, we consider only the case when the Saffman-Taylor finger develops.

Saffman and Taylor solved this problem in case of negligible surface tension, γ, finding that every finger of width λ is an admissible solution of the problem. Later on, McLean and Saffman[2] showed that, introducing γ as model parameter, only one finger is selected and its width is a monotonous increasing function of the rescaled surface tension $\bar{\gamma} \sim \gamma(v\mu)^{-1}$ (where μ is the viscosity of the displaced fluid and v is the finger velocity). Moreover, $\lambda = 1/2$ is the minimum of this function, such that for $\bar{\gamma} = 0$ the finger invades half of the cell.

The mathematical generalization of the Saffman-Taylor problem to three spatial dimensions is straightforward but, nevertheless, it has not been widely studied. Only recently, Levine and Tu[3] solved numerically the problem in the axisymmetric tube geometry. Employing a boundary integral method, they found several solution branches merging for positive values of the rescaled surface tension parameter $\bar{\gamma}$ (of the order of 10^{-3}). Unlike the two dimensional case, it seems that for this geometry does not exists any axisymmetric solution below this threshold.

Motivated by this result, we have developed a phase-field model of two viscous flows to investigate the dynamics of the three dimensional Saffman-Taylor problem in the regime of small surface tension. Our numerical method allows us to simulate the dynamics of the finger for fluids with arbitrary viscosity contrast and for a wide range of $\bar{\gamma}$.

We have performed full three dimensional simulations in a channel with square section and two dimensional axisymmetric simulations in the tube geometry. For these two cases we observe that the growing finger undergoes a Plateau-Rayleigh instability leading to pinch-off at the finger tail. In fact, according to the Young-Laplace equation, when a three dimensional fluid stream falls, the pressure due to surface tension increases for decreasing stream radius. This mechanism leads to the stream breaks up into droplets of same volume but smaller surface area.

Moreover, through the linear stability analysis of the tube solution in the axisymmetric geometry, we show that the solutions found in[3] are unstable for any value of the surface tension. Our phase-field model reproduces accurately this linear prediction and allows to study the influence of the finger tip on the pinch-off velocity.

---

* matteo.nicoli@polytechnique.edu

[1] P. G. Saffman and G. I. Taylor, Proc. R. Soc. London Ser. A **245**, 312 (1958).
[2] J. W. McLean and P. G. Saffman, J. Fluid Mech. **102**, 455 (1981).
[3] H. Levine and Y. Tu, Phys. Rev. A **45**, 1044 (1992).

Unified paradigm for interface dynamics

J. C. R. E. Oliveira*, P. P. Avelino†, R. Menezes‡
Centro de Física do Porto
Departamento de Engenharia Física
Universidade do Porto
Rua Dr. Roberto Frias, Porto PORTUGAL

In this work we develop a common theoretical framework for the dynamics of thin featureless interfaces. Phase field models have been applied with success to describe the dynamics of various nonrelativistic systems of featureless interfaces, including foams and grain growth. In the simplest cases with nonconserved order parameters cellular patterns bounded by an interface network tend to evolve toward configurations with less interfacial energy (or equivalently, less surface area). In these systems the velocity is proportional to the mean curvature of the interface at each point. This is the crucial ingredient behind von Neumann's law for the evolution of the area of individual domains in two-dimensional interface networks with (free) Y-type junctions: $da_n/dt \propto (n-6)$, where a_n is the area of a domain with n edges. If the interfaces have a finite width, von Neumann's law may not apply to individual domains but is reasonably obeyed on average. Also extended versions of von Neumann's law exist in three dimensions. Other laws, such as Lewis's law and Aboav's law have also been used in the characterization of classical patterns. In this work we shall focus on von Neumann's law which is more directly relevant for the evolution of an interface network. On the other hand, the dynamics of relativistic interface networks, considering various possible types of defect junctions, has been studied in detail in a cosmological context, where domain walls have been proposed in the past as an interesting dark energy candidate. However a large and accurate sets of field theory numerical simulations in combination with semi-analytical analysis have been used by the present authors to provide very strong evidence for a no-frustration conjecture, which invalidates domain walls as a viable dark energy candidate.

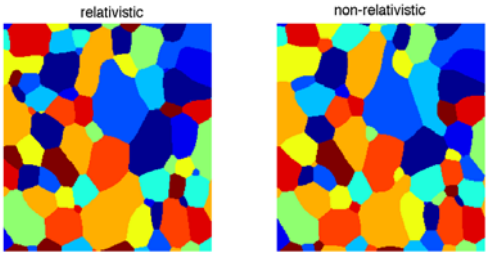

Figura 1. Two-dimensional simulation snapshots of relativistic and non-relativistic interface networks with similar characteristic lengths.

The main aim of this work is the development of a unified theoretical paradigm for interface dynamics which includes both relativistic and nonrelativistic systems in a unified framework. We set up a velocity-dependent onescale (VOS) model and use it to describe the evolution of the characteristic length and velocity of thin, featureless interface networks both in the relativistic and nonrelativistic limits. We show that the same models which describe the dynamics of cosmic relativistic interfaces also account, in a friction dominated regime, for the dynamics of cellular patterns in many material systems, such as soap froths, lipid monolayers, and other material systems. We further show that a statistical version of von Neumann's law applies in the case of scaling relativistic interface networks, implying that, although relativistic and nonrelativistic interfaces have very different dynamics, a single simulation snapshot is not able to clearly distinguish the two regimes. We highlight that crucial information is contained in the probability distribution function for the number of edges of domains bounded by the interface network and explain why laboratory tests with nonrelativistic interfaces can be used to rule out cosmological domain walls as a significant dark energy source.

* jespain@fe.up.pt
† Centro de Física do Porto, Rua do Campo Alegre 687, 4169-007 Porto, Portugal
‡ Departamento de Ciências Exatas, Universidade Federal da Paraíba, 58297-000 Rio Tinto, PB, Brazil

Cooperative tube extraction by single-headed kinesin motors

David Oriola*, Jaume Casademunt
Departament d'Estructura i Constituents de la Matèria, Universitat de Barcelona, Avinguda Diagonal 647, E-08028 Barcelona, Spain

Kinesins are a large family of processive molecular motors involved in many tasks of intracellular traffic. Most of them are dimeric motors composed by two motor "heads"which walk in a hand-over-hand fashion by alternating sequentially the motor domains attached to a microtubule. However, this model fails to describe the dynamics of KIF1A[1], a monomeric kinesin motor which moves processively by "hopping"along the microtubule track and is able to freely diffuse while still weakly bound to the filament, without detaching during many steps.

KIF1A is mostly found in neurons and it plays a fundamental role in anterograde axonal transport. Large vesicles that contain synaptic precursors are carried from the cell body over long distances along the axon in order to supply dendrites. It remains unknown why monomeric and not the most common dimeric kinesins are the ones involved specifically in this process. This is an intriguing question since dimeric kinesins largely outperform monomeric kinesins, while at the same time, axonal transport is the most demanding one in terms of force, velocity and distance. On the other hand, long processivity and large forces can naturally be achieved by assembling large numbers of motors to the same vesicle. We propose that the reason why KIF1A motors are specific to the most demanding tasks could be an unusual and remarkable adaptation to cooperative action, which could largely compensate their individual inefficiency. Incidentally, intracellular traffic disorders are associated to many neurodegenerative disorders such as Alzheimer's disease, hence a deeper understanding of collective self-organization of motors in axonal transport is potentially relevant to neuromedicine.

To study the cooperative action of small groups of motors pulling on membrane-bound cargoes, a series of biomimetic experiments has been proposed in recent years, which address the problem of the spontaneous formation and extraction of membrane tubes out of giant vesicles by molecular motors, under controlled conditions *in vitro*[2]. Most studies have been performed with conventional (dimeric) kinesins. The fluidity of the membrane and the kinetic properties of motors lead to the self-organization of motors clusters at the tube tip. The cooperative action of clusters is indeed required to explain the phenomenon and, for conventional kinesins, the problem is satisfactorily well understood at a quantitative level[3,4]. However, recent studies of Brownian ratchets that mimic the behaviour of monomeric kinesin under the conditions of the experiments of tube extraction, have revealed non-trivial dynamics leading to a dramatic enhancement of efficiency of groups of motors with respect to what one would expect from pure superposition of individual motors[5,6]. The exchange kinetics of motors between the microtubule and the membrane that controls the problem of tube extraction, however, has not been addressed.

Here we develop a quantitatively realistic and predictive model of a proposed experiment of tube extraction by collective action of KIF1A motors. We simulate the statistics of the motor cluster at the tip of a membrane tube under tension including the motor exchange kinetics, and compute both the collective force-velocity curves and the fluctuations of the tip position. These nontrivial observables behave very differently from their counterparts of conventional kinesin. The experiment proposed is expected to shed light onto the biological function of monomeric kinesin in intracellular traffic and will also allow to determine some of the unknown parameters governing the action of these motors.

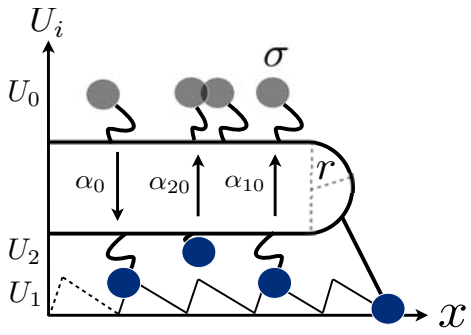

Figura 1. Tube extraction diagram showing the transition rates between the ratchet potential and the membrane tube. r is the curvature radius of the tip and σ is the motor size. Motors diffuse freely in U_2 and U_0 states.

* oriola@ecm.ub.es

[1] Y. Okada, H. Higuchi and N. Hirokawa, Nature **424**,574 (2003).
[2] C. Leduc, O. Campàs, J-F. Joanny, J. Prost, and P. Bassereau, Biochem. et Biophys. A, **1798**, 1418-1426 (2010)
[3] O. Campàs, Y. Kafri, K.B. Zeldovitch, J. Casademunt and J.-F. Joanny. Pys. Rev. Lett. **97**, 038101 (2006)
[4] O. Campàs, C. Leduc, P. Bassereau, J. Casademunt, J.-F. Joanny and J. Prost, Biophys. J. **94**, 5009-5017 (2008)
[5] J. Brugués and J. Casademunt, Pys. Rev. Lett., **102**, 118104 (2009)
[6] J. G. Orlandi, C. Blanch-Mercader, J. Brugués and J. Casademunt, Phys. Rev. E, **82**, 061903 (2010).

Unraveling spontaneous activity in neuronal cultures

Javier G. Orlandi[1*], Enric Álvarez-Lacalle[2], Sara Teller[1], Jordi Soriano[1], Jaume Casademunt[1]
[1] *Departament d'Estructura i Constituents de la Matèria, Universitat de Barcelona, Barcelona, Spain*
[2] *Departament de Física Aplicada, Universitat Politècnica de Catalunya, Barcelona, Spain*

Brain rhythms, retinal waves, epileptic seizures, Parkinson's tremors and many other neurological processes share a common feature: they are driven by the spontaneous activity of neuronal networks. And yet, the origins of this activity remain poorly understood.

In order to approach a quantitative understanding of the common mechanisms that initiate and sustain spontaneous activity in neuronal networks we focus our attention on neuronal cultures[1], which are assemblies of neurons and glial cells grown *in vitro*. The neurons in a culture start as independent units, but they grow and form connections with each other, creating a network that after a few days *in vitro* shows spontaneous activity[2]. This activity first appears in only some neurons, and is uncorrelated with its neighbors; but when the neurons have matured, the behaviour of the whole system changes and all neurons appear to fire in what seems a synchronized fashion, showing global bursts of activity. Until today, there has been no agreement on the mechanisms that originate and control this behaviour. There exists contradictory experimental evidence, some showing synchronized activity and some showing unsynchronized (and also unlocalized) activity.

We have explored both theoretically and experimentally how this spontaneous activity can appear and be maintained. In our scenario we build a model system where we first create a complex network that takes into account all the metric properties in the real system. By mimicking the way in which neurons grow and form connections, we can obtain a complex network with the appropriate correlations between its elements, which are essential to explain the dynamics of the system. Then we couple the network properties with the dynamics of the neurons through an adaptive integrate and fire model, and also taking into account that the connection itself is dynamic[3] (a depressive synapse). Coupling these ingredients with a realistic noise source (the spontaneous discharge of vesicles at the synapse) is enough to explain and understand all the observed experimental behaviour.

In this scenario, the episodes of spontaneous activity are initiated by a process that we call an activity cascade; the activity cascade is initiated by the spontaneous firing of a neuron, which transiently modifies the firing probability of its neighbors, and through a rapid succession of these correlated events, the amount of active neurons can reach a critical size that is enough to ignite the whole system. This is a localized process that is heavily influenced by network correlations (transitivity), which only appear when the network is built under its metric space. When the critical size is reached, and if all neurons are excitatory, the activity can propagate through the system as a spherical wave, as it would do in a continuous excitable medium.

The emerging picture is that the spontaneous activity of a neuronal culture must be understood as a nucleation plus propagation process rather than a synchronization phenomenon. The nontrivial topology of the underlying neuronal network, inherited from the dynamical process of neuronal growth in a metric space, makes the local nucleation of waves a highly nontrivial process of noise amplification. Regions of high clustering are typically the candidates to nucleation points, but the detailed local wiring of the network strongly affects the probability of nucleation of a given region. The directed nature of the network is essential since the statistics of feedback and feedforward loops controls the effectiveness of the nucleation process. Once the activity has built up to the critical size the propagation proceeds to ignite the whole system.

In the presence of inhibitory neurons, the propagation of activity is much more complex and far from the spherical wave picture; in this case there is a competition between excitation and inhibition that breaks the excitation front into patches of activity that propagate following complex paths.

To check these predictions we have developed an experimental setup in which neurons grow in a patterned substrate made of a topographical PDMS mould. Neurons grow and connect only along the valleys of the mould following predefined paths. In this way we are able to guide or restrict the connectivity of the network and mimic the effect of inhibition in a controlled manner. The neurons in these patterned networks also show spontaneous activity, but its propagation speed is dramatically slowed down, by about a factor of one hundred compared to standard, non–patterned cultures. This slow velocity allows the activity front to be resolved, showing that the picture of heterogeneous nucleation and propagation in a disordered medium is correct.

---

* orlandi@ecm.ub.es

[1] J. P. Eckmann , O. Feinerman, L. Gruendlinger, E. Moses, J. Soriano and T. Tlusty, Phys. Rep., **449**, 54 (2007).
[2] J. Soriano, M. Rodríguez Martínez, T. Tlusty and E. Moses, Proc. Natl. Acad. Sci. USA, **105**, 13758 (2009).
[3] E. Alvarez-Lacalle and E. Moses, J. Comput. Neurosci., **26 (3)**, 475, (2009).

Translational and rotational dynamics in a supercooled molecular liquid

Jordi Ortiz de Urbina[‡], Gemma Sesé[†], Ricardo Palomar
Departament de Física i Enginyeria Nuclear
Universitat Politècnica de Catalunya
Campus Nord UPC, 08034 Barcelona

Dynamics in supercooled liquids depends strongly on temperature, whereas both structural and themodynamic properties show a relatively weak dependence on temperature, which can often be extrapolated smoothly from the data obtained at higher temperatures[1].

We have studied the dynamics of a supercooled molecular liquid by means of molecular dynamics simulations. The molecular model has been built from the one of methanol molecules, but lacking sites for hydrogen bonding. Then, rigid diatomic molecules with an associated dipole moment have been considered[2]. Bond orientational order and translational order parameters have been evaluated. It has been found that both parameters increase upon cooling.

Time correlation functions that characterize translational dynamics of the system, as the incoherent intermediate scattering function (fig. 2), reveal the existence of three dynamic regimes at very low temperatures. The initial decay is the so-called ballistic regime. Next to it, the correlators display a *plateau* at intermediate times, in the β - relaxation regime, which is followed by a *stretched* exponential decay at long times. The picture of molecules moving in the cage made by their nearest neighbors or *cage-effect* applies to this system during the β-relaxation regime[3].

We have evaluated the mean square displacement (MSD) of the molecular centers-of-mass, and the three dinamical regions are apparent when it is plotted in a log-log scale. Diffusion coefficients (D) have been evaluated from the slope of the MSD at very long times. They follow an Arrhenius temperature dependence at high temperatures.

Molecular reorientation has also been investigated, and it can be described as a sequence of small amplitude angular steps. The reorientational relaxation times increase with temperature, and they are always smaller than the ones associated with translation. Angular velocities have been evaluated. The angular velocity autocorrelation functions display a *backscattering* area, which becomes more important upon cooling the system. The angular velocities have been used to compute the *rotational mean square displacement* (RMSD) at several temperatures. The rotational self-diffusion coefficients (D_r) have been obtained from the long-time slope of such functions. They decrease with temperature, but their temperature dependence is weaker than the one of D. Moreover, the slope of the intermediate region in RMSD functions is larger than in MSD ones.

The breakdown of the *Stokes-Einstein* and of the *Stokes-Einstein-Debye* relations at low temperatures has also been analyzed, as well as the extent of the translation-rotation coupling.

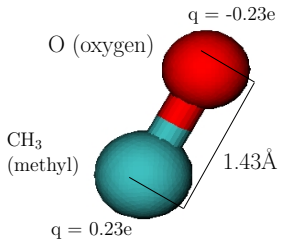

Figura 1. Molecular model

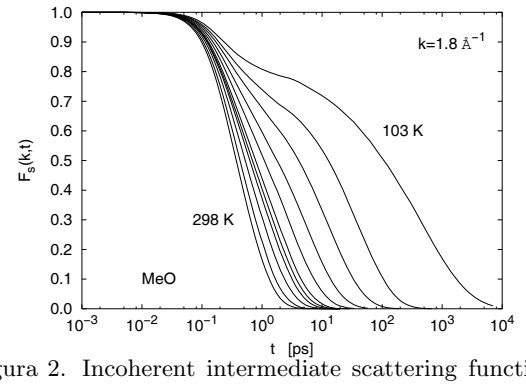

Figura 2. Incoherent intermediate scattering function for $k = k_0$, which maximizes the static structure factor, $S(\vec{k})$.

‡ jordi.ortiz@upc.edu
† gemma.sese@upc.edu

[1] C.A. Angell, K.L. Ngai, G.B. MacKenna, P.F. McMillan and S.W. Martin, J. Applied Physics **88**, 3113 (2000).
[2] R. Palomar and G. Sesé, J. Phys.Chem. B **109**, 499 (2005).
[3] R. Palomar and G. Sesé, Phys. Rev. E **75**, 011505 (2007).

Fluctuaciones de la velocidad en fluidos en flujo

José María Ortiz de Zárate*
Facultad de Física
Universidad Complutense
28040 Madrid

Todos los sistemas termodinámicos tienen fluctuaciones espontáneas (ruido térmico) cuyo origen es el carácter estoscástico de las colisiones moleculares. Cuando el sistema está en equilibrio estas fluctuaciones se pueden estudiar con la hidrodinámica fluctuante de Landau[1]. Esencialmente, a los flujos disipativos que aparecen al establecer los balances (de masa, de momento...) se le añade un componente estocástico (ruido térmico, blanco aditivo y gaussiano). La parte determinista de los flujos disipativos se expresa de la forma tradicional (leyes de Newton, Fourier, Fick...), mientras que la intensidad de la parte estocástica viene dada por el teorema de fluctuación-disipación. Este esquema asegura, para sistemas en equilibrio, que la intensidad de las fluctuaciones en las variables termodinámicas (densidad, energía específica...) coincide con lo que se obtiene de la Física Estadística.

Por consiguiente, la teoría de las fluctuaciones para sistemas en equilibrio está bien establecida y sus predicciones verificadas experimentalmente desde hace tiempo[2], en particular por la técnica de dispersión de la luz. En las últimas décadas se ha estado trabajando en la extensión de la hidrodinámica fluctuante para estados estacionarios de no-equilibrio[3]. Se ha encontrado una diferencia fundamental entre las fluctuaciones de equilibrio y las de no-equilibrio: mientras en las primeras las correlaciones estáticas son de corto alcance espacial (excepto en la vecindad de puntos críticos), fuera del equilibrio las correlaciones son -genéricamente- de largo alcance espacial. Estas predicciones se han comprobado experimentalmente[3].

El problema de no-equilibrio estudiado en más detalle ha sido el de un fluido sometido a un gradiente de temperatura[4] (problema de Rayleigh-Bénard). Recientemente[5] hemos estudiado en detalle las fluctuaciones de la velocidad en el flujo isotermo de un fluido viscoso en configuración plana de Couette (ver FIG. 1). Bajo la hipótesis de flujo incompresible, en aproximación lineal, las fluctuaciones en este problema pueden evaluarse a partir de la ecuación estocástica de Orr-Sommerfeld:

$$\partial_t(\nabla^2\delta v_z) + z\,\partial_x(\nabla^2\delta v_z) - \frac{1}{\mathrm{Re}}\nabla^4(\delta v_z) = -\left\{\nabla\times\nabla\times\left[\nabla\left(\delta\Pi\right)\right]\right\}_z, \quad (1)$$

y la ecuación estocástica de Squire[5]:

$$\partial_t(\delta\omega_z) + z\,\partial_x(\delta\omega_z) - \partial_y\delta v_z - \frac{1}{\mathrm{Re}}\nabla^2(\delta\omega_z) = \left\{\nabla\times\left[\nabla\left(\delta\Pi\right)\right]\right\}_z. \quad (2)$$

En estas expresiones $\delta v_z(\mathbf{r},\mathbf{t})$ (y $\delta\omega_z(\mathbf{r},\mathbf{t})$) son las fluctuaciones en la componente de la velocidad (y de la vorticidad) perpendicular a las paredes, z; $\delta\Pi(\mathbf{r},\mathbf{t})$ es la parte estocástica del tensor de tensiones (ruido térmico) y Re el número de Reynolds.

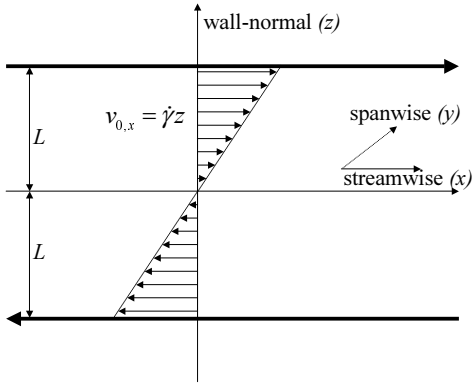

Figura 1. Fluido en flujo plano de Couette. Corresponde a un valor uniforme de la cizalla. Las paredes están ubicadas en $z = \pm L$, y se mueven con velocidades opuestas.

En nuestra comunicación presentaremos soluciones a las Eqs. (1) y (2), donde las propiedades estadísticas (correlaciones) de las fluctuaciones de la velocidad están calculadas en función de las correlaciones de $\delta\Pi(\mathbf{r},\mathbf{t})$. Se han tenido en cuenta condiciones de contorno. Se compara con resultados asintóticos, válidos para fluctuaciones de vector de onda largo, obtenidos previamente por otros autores[6]. Como conclusión se observa que el ruido térmico es amplificado por el flujo, como corresponde a un sistema fuera del equilibrio. Además, las correlaciones entre las fluctuaciones de la velocidad se hacen de largo alcance espacial.

---

* email: `jmortizz@fis.ucm.es`. Este trabajo se realizó en colaboración con el Prof. Sengers, de University of Maryland.

[1] L. D. Landau and E. M. Lifshitz, *Fluid Mechanics* (Pergamon, London, 1959), 2nd revised English version, 1987.
[2] J. P. Boon and S. Yip, *Molecular Hydrodynamics*, (Dover edition, 1991). B. J. Berne and R. Pecora, *Dynamic Light Scattering*, (Dover edition, 2000).
[3] J. M. Ortiz de Zárate and J. V. Sengers, *Hydrodynamic Fluctuations in Fluids and Fluid Mixtures* (Elsevier, Amsterdam, 2006).
[4] T. R. Kirkpatrick, E. G. D. Cohen, and J. R. Dorfman, Phys. Rev. A **26**, 995 (1982). D. Ronis and I. Procaccia, Phys. Rev. A **26**, 1812 (1982).
[5] J. M. Ortiz de Zárate and J. V. Sengers, Phys. Rev. E **77**, 026306 (2008).
[6] J. F. Lutsko and J. W. Dufty, Phys. Rev. E **66**, 041206 (2002).

Propiedades interfaciales de fluidos moleculares

Jose M. G. Palanco†, Jorge Benet‡, Luis G. MacDowell‡
†*Departamento de Física y Química Aplicadas a la Técnica Aeronáutica, Escuela de Ingeniería Aeronáutica y del Espacio, Universidad Politécnica de Madrid* ‡*Departamento de Química Física, Facultad de Ciencias Químicas, Universidad Complutense de Madrid*

El estudio de fenómenos interfaciales y de tensión superficial viene concitando un gran interés en los estudios de simulación de los últimos años. Pese a las indudables dificultades prácticas, entre ellas la aplicación de correcciones de largo alcance inhomogéneas, en la actualidad son ya importantes los avances conseguidos.

Una gran variedad de modelos moleculares han sido empleados para este tipo de estudios, desde simples esferas Lennard-Jones, a cadenas moleculares flexibles con este mismo tipo de esferas[1], y más recientemente, modelos moleculares multicentro con estructura rígida y con flexibilidad de enlaces.

El potencial intermolecular de Kihara esférico, ha sido tradicionalmente utilizado como una alternativa más sofisticada al simple potencial de Lennard-Jones para la descripción de interacciones entre fluidos -reales. Pese a su aparente simplicidad, es capaz de describir de forma razonablemente eficaz las propiedades termodinámicas volumétricas de numerosas sustancias reales simples, con geometrías no necesariamente esférica. Ello es posible mediante la cuidosa optimización de un diámetro de núcleo duro interno y del alcance efectivo de la interacción, características ambas que pueden ser esencialmente relacionadas con el comportamiento de los promedios orientacionales del potencial en modelos multicentro. Pese a estas indudables ventajas, hasta el momento no se disponía de un estudio de simulación completo de dicho sistema, ni tan siquiera de ecuaciones de estado teóricas, aplicables a este modelo de potencial.

Nosotros hemos realizado un extenso estudio de simulación por Monte Carlo de diversos sistemas Kihara, cubriendo una amplia gama de valores de interés para su aplicación a la descripción de sustancias reales. Se ha determinado así una amplio conjunto de datos de energía interna, presión, densidad y temperatura de la región de fluido único, tanto subcrítico como supercrítico, así como las coordenadas de coexistencia hasta temperaturas de 0.9 Tc. Este estudio se ha completado con el cálculo de la tensión superficial y de los perfiles de densidad en todas las temperaturas de coexistencia.

Se ha obtenido también, la curva de coexistencia y la tensión superficial de algunos modelos teóricos con dos centros de interacción, que emulan el comportamiento del etano. Este estudio de simulación es el inicio de otros similares sobre modelos multicentro, encaminados a la verificación de un nuevo modelo teórico para el cálculo de la tensión superficial, en conjunción con modelos de potencial esfericalizados a partir de promedios orientacionales, y estrechamente relacionados con el potencial de Kihara.

El nuevo modelo de tensión superficial, ha sido planteado a partir de un desarrollo funcional de la función de correlación singlete el cual, ofrece resultado teóricos prometedores para comprender mejor los mecanismos que permiten establecer puentes entre las propiedades de los fluidos homogéneos en equilibrio de fases, las cuales empiezan a ser bastante bien conocidas, y la estructura de fluidos inhomogéneos.

Paralelamente se ha utilizado el desarrollo perturbativo de Tang basado en las soluciones de la ecuación integral de Ornstein-Zernike con la aproximación MSA[2], aplicado al potencial de Kihara, obteniéndose una magnífica concordancia con los datos de simulación, tanto en la región de coexistencia no crítica como en la región del bulk. Más aún, estos resultados siguen manteniendo la analiticidad que caracteriza al desarrollo de Tang aplicado a potenciales tipo Yukawa.

---

* jose.gpalanco@upm.es

[1] L. G. MacDowell y P. Bryk, *Phys. Rev. E* **75**, 061609 (2007).

[2] Y. Tang, Z. Tong, B.C.-Y. Lu, *Fluid Phase Equilib.* **134**, 21 (1997)

Collective and individual cell memory in multistable biochemical switches

David Palau-Ortín*, Marta Ibañes
Departament d'Estructura i Constituents de la Matèria.
Facultat de Física
Universitat de Barcelona
08028 Barcelona

Developmental biology gives many examples of processes that can be understood in terms of bifurcations of nonlinear dynamical systems. One example is cell fate choice for color vision in the compound eye of the fruit fly *Drosophila melanogaster*. *Drosophila* compound eye is formed of units named ommatidia. Color vision depends on two types of ommatidia which have a different set of expressed genes in the so-called R8 photoreceptor cell. These R8 photoreceptor cells are initally in the same state. At a given time point in development, 30% of these cells change their state to another state called *Pale*, while the remaining 70% change towards a new state named *Yellow*. The *Yellow* and *Pale* state can be characterized by expression of just two genes (hereafter X and Y) which are asymetrically expressed on each state: $(x,y)_{yellow} = (ON, OFF)$ and $(x,y)_{pale} = (OFF, ON)$. The fate decisions seem to be autonomous for each ommatidia and involve a switch and a transient inducting signal[1]. The switch arises from a mutual inhibition with positive auto–regulation molecular circuit[2]. It has been shown experimentally that the switch outcome is locked when the inducting signal acts twice[1]. Herein we have investigated what drives this locking property.

Inspired in recent studies[3,4], we have performed a theoretical and numerical analysis of this molecular circuit architecture to decipher the properties of different types of switches upon transient signal repetition. We have used the model proposed by Guantes & Poyatos[3],

$$\frac{dx}{dt} = a_x \frac{1+\rho x^2}{1+x^2+\sigma y^2} - x \qquad (1)$$

$$\frac{dy}{dt} = a_y \frac{1+\rho y^2}{1+y^2+\sigma x^2} - y \qquad (2)$$

We have focused in two types of signals: (1) Those that generate a transient regime of monostability and (2) those that generate a transient regime of bistability. The first ones enable differentiation towards a single new state in a threshold-like fashion (bistable switches), while the second type drives graded differentiation towards two distinct cell fates (multistable switches) (FIG. 1) in agreement with theoretical results by Guantes & Poyatos[3].

We have analysed collective and individual cell memory when these signals act periodically.

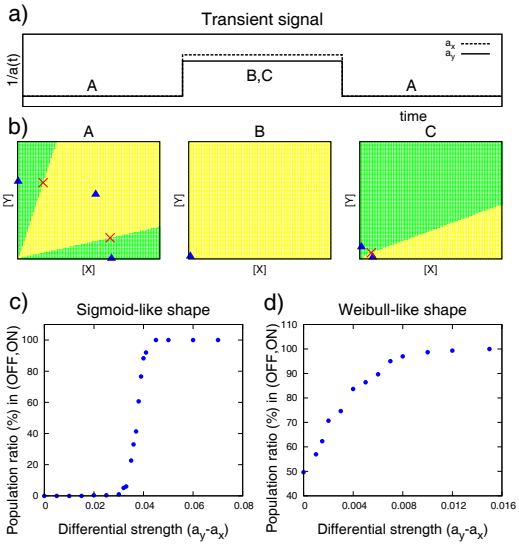

Figura 1. (a) We have studied differentiation processes driven by signals which act with different strength to X and Y genes. According to the parameter modification during the effect of the signal, this signal generates either mono (B) or bistability (C). (b) In the absence of signal (A), there are three stable states, (ON, OFF), (ON, ON) and (OFF, ON) (blue triangles). The yellow and green areas in the phase space diagram (A,B,C) denote the basin of attraction of each stable state. Unstable states are denoted by red crosses. Parameter values are: $\rho = 10$, $\sigma = 0.2$, $a_x = a_y = 1$ (A), $a_x = 0.14$, $a_y = 0.175$ (B) and $a_x = 0.2$, $a_y = 0.209$ (C). (c) A signal which genereates a transient monostable regime (B), induces a sigmoid-like shape in the response of the differentiated population rate. (d) A signal which genereates a transient bistable regime (C), induces a weibull-like shape in the response of the differentiated population rate.

Our study reveals that multistable switches, as opposed to bistable ones, have locking properties at the collective and individual cell levels and suggests color vision differentation in fruit flies may involve such multistable switches.

* palau@ecm.ub.es

[1] M. F. Wernet, E. O. Mazzoni, A. Celik, D. M. Duncan, I. Duncan, and C. Desplan, *Nature* **440**, 9, pp. 174-180 (2006)
[2] T. Mikeladze-Dvali, M. F. Wernet, D. Pistillo, E. O. Mazzoni, A. A. Teleman, Ya-Wen Chen, S. Cohen and C. Desplan, *Cell* **122**, pp. 775-787 (2005)
[3] R. Guantes and J. F. Poyatos, *PLOS Comp Bio* **4**, 11, pp. 1-13 (2008)
[4] S. Huang, Y. Guo, G. May and T. Enver, *Dev Bio* **305**, pp. 695-713 (2007)

Simulación numérica de fluidos Newtonianos y no-newtonianos en cilindros cerrados bajo forzamientos periódicos

Carles Panadès Guinart*, Francico Marques
Departament de Física Aplicada, Universitat Politècnica de Catalunya, Campus Diagonal Nord,Edifici B4, Carrer Jordi Girona 1-3, 08034 Barcelona

En la actualidad se están haciendo grandes esfuerzos para entender la turbulencia de origen elástico en fluidos no-Newtonianos. Este trabajo pretende analizar las inestabilidades elásticas en una cavidad cilíndrica llenada con un fluido no-Newtoniano y forzada periódicamente. No obstante, en primer lugar se ha considerado el mismo problema con un fluido Newtoniano[1] ya que entenderlo puede resultar muy útil para aclarar el caso no-Newtoniano y establecer analogías relevantes entre las inestabilidades causadas por la inercia y la elasticidad[2]. Los fluidos Newtonianos están governados por la usual ecuación de Navier-Stokes y los no-Newtonianos por una versión modificada de ésta, acoplada con la versión más sencilla de ecuación constitutiva para el tensor de esfuerzos (modelo de Oldroyd-B). Los dos sistemas se resuelven por medio de métodos espectrales[3]. Se han hecho progresos significativos en la comprensión del problema Newtoniano[4], mientras que se han obtenido algunos resultados preliminares prometedores para el caso no-Newtoniano. Futuros trabajos se centrarán en trabajar con diferentes modelos de ecuaciones constitutivas y encontrar evidencias de inestabilidades elásticas.

* panades@fa.upc.edu

[1] En un fluido Newtoniano, el esfuerzo y la deformación (gradiente de velocidades) son proporcionales y la viscosidad es el factor de proporcionalidad. En los fluidos no-newtonianos, la relaciones entre ambas magnitudes suelen ser mucho más complicadas.

[2] A. N. Morozov and W. van Saarlos. An introductory essay on subcritical instabilities and the transition to turbulence in visco-elastic parallel shear flows. Physics Reports 447 (2007) 112-143.

[3] I. Mercader, O. Batiste and A. Alonso. An efficient spectral code for incompressible flows in cylindrical geometries. Computers and Fluids 39 (2010) 215-224.

[4] C. Panades *et al.* Oscillatory flow enclosed in a finite cylinder. Under consideration for publication in Journal of Fluid Mechanics

Microbes answer to Santa Rosalia: reconsidering the importance of aggregation in ecological networks.

Alberto Pascual-García*, Javier Tamames, Ugo Bastolla
Centro de BiologÃa Molecular Severo Ochoa (CSIC-UAM)
Universidad Autónoma de Madrid
Cantoblanco 28049 Madrid

Homage to Santa Rosalia or *Why are so many kinds of animals?*[1] With this question has opened Hutchinson in 1959 the seminal work that aimed to reconsider the niche conception that was taking place at that time after the foundation of the competitive exclusion principle, stated by Gause in 1934 and even previously formalized by Volterra in 1926. Hutchinson's question has probably in the microbial world one of its most interesting challenges. Microorganisms represent an amount of biomass at least as big as that of plants with and an amazing diversity, and have a key role in the evolution of the biosphere.

An increasing number of available data coming from high-throughput experiments has boosted the efforts to find ecological trends, and there is an increasing evidence pointing to a qualitative similar picture between the patterns found in macro and microorganisms[2]. Some progress have been made identifying important trends as taxa-area and distance decay relationships[3], or the influence of environmental and geographic variables as depth or salinity. These progresses have been possible in part thanks to the reemergence of prokaryotic biogeography, but little attention have been made to the methodological differences that microbiological data impose over classical analysis methods of absence presence matrices. The fact that there are many cosmopolitan microorganisms, recovers the debate between deterministic and chance based explanations for the observed diversity distribution.

The classic (and vigorous) discussion between deterministic and neutral based explanations for the different interaction patterns found in community ecology, boosted the development of null models. Null model analysis finds today a new challenge: the analysis of high throughoutput microbiological data, were some additional difficulties to handle arise respect to those obtained from macroscopic observations. Another challenge in the analysis of absence presence matrices, also present in macroscopic data, is to address the meaningfulness of single pairwise associations. Whole community analysis metrics as nestedness, or the C-Score are often used to understand the community structure instead, and there are few attemps to address the meaningfulness of single pairwise associations, as the pairwise normalization of the C-Score[4], what requires a posterior statistical analysis. We propose here to construct both pairwise aggregation and segregation scores, based in a recently proposed random fill procedure[5] inspired in the well known empirical approach, that solves the problem of parameter estimation. This model avoids any bias based on the assumption that all matrices with the same row and column totals are equally likely to occur as those generated by swapping algorithms but, unlike them, it sample a canonical ensemble which is more compatible with the particularities of high throughoutput data. It also obtains a row and column total distribution maximally similar to the observed one using a maximum likelyhood procedure, generating in this way the most difficult to falsify model. Interestingly, the scores we construct from this model can be computed exactly, avoiding a posterior statistical analysis, and can be easily extended to the computation of whole community metrics.

The comparison between the observed data and the respective randomizations, leads to a strikling result: aggregation is as frequent as segregation, a result that is apparently in opposition to the macroscopic observed behavior where segregation rather than aggregation have been found[4]. This result is also consistent with a recently proposed Lotka-Volterra model[6] for plant-pollinator networks, where it is shown how mutualistic interactions allow to the system to host a higher biodiversity, as these interactions increase the structural stability of the network. This model together with the results presented here suggest that the importance of aggregation should be (re)considered to address Santa Rosalia's question: Why are so many kinds of animals *in* there?

(*) apascual@cbm.uam.es

[1] G. E. Hutchinson: *The American Naturalist* **93** (1959) 145
[2] M. C. Horner-Devine, K. M. Carney, B. J. M. Bohannan: *Proc. R. Soc. Lond. B* **271** (2003) 113
[3] M. C. Horner-Devine, M. L. andJennifer B. Hughes, B. J. M. Bohannan: *Nature* **432** (2004) 750
[4] N. J. Gotelli, W. Ulrich: *Oecologia* **162** (2010) 463
[5] J.Ñavarro-Alberto, B. Manly: *Population Ecology* **51** (2009) 505: 10.1007/s10144-008-0137-x
[6] U. Bastolla, M. A. Fortuna, A. Pascual-García, A. Ferrera, B. Luque, J. Bascompte: *Nature* **458** (2009) 1018

La estructura de redes mutualistas pesadas. Medida del clustering en redes bipartitas

Juan Manuel Pastor*, Luis J. Gilarranz±, Javier Galeano+
Depto. Ciencia y Tecnología Aplicadas
E.U.I.T. Agrícola Universidad Politécnica de Madrid
28040 Madrid

Las redes mutualistas en Ecología muestran las interacciones de beneficio mutuo entre especies. En este tipo de redes hay dos conjuntos de especies (por ejemplo, animales y plantas) y las relaciones sólo ocurren entre especies pertenecientes a conjuntos distintos. Este tipo de redes en las que existen dos tipos diferentes de nodos se denominan *bimodales* o *bipartitas*.

El estudio de estas redes mutualistas ha revelado una estructura en la matriz de interacciones. Existen especies, llamados especialistas, que interactúan con pocas especies del otro conjunto de nodos. Pero dichos especialistas siempre interactúan con las especies que llamamos generalistas, porque se relacionan con un gran número de especies. A esta propiedad se la denomina *anidamiento*. Recientes estudios sobre estas redes muestran gran robustez y una estructura que favorece la biodiversidad[1].

Aunque se han realizado numerosos trabajos sobre este tipo de redes, la práctica totalidad se han ceñido a las interacciones binarias. Sin embargo, cuando se trata de estudiar la robustez de la red o las posibles vías de extinción de especies, parece claro que es primordial conocer la "fuerza"de cada enlace. El dato cuantitativo que representa la "fuerza"del enlace en este tipo de redes es el número de visitas contabilizadas entre cada especie de animal y cada especie de planta, aunque debido al mayor esfuerzo que requiere la recolección de este tipo de datos, no existen numerosas bases de datos que proporcionan esta información.

Con este tipo de redes "cuantitativas"hemos realizado nuestro estudio sobre la influencia del peso de los enlaces en la determinación de los parámetros habituales de estas redes. En concreto, hemos trabajado con 29 bases de datos que incluyen redes polinizador-planta, planta-dispersor de semilla y hormiga-planta.

Hemos realizado una comparativa de los parámetros clásicos utilizados para caracterizar este tipo de redes[2]. Hemos calculado la distribución del "strength"con el grado, el peso medio del link en función del producto de los grados de sus nodos, el coeficiente de clustering y la distribución de grado de los próximos vecinos.

En la distribución del strength se observa que los nodos de mayor grado tienen un valor del strength mayor del que le corresponderÌa en una distribución aleatoria. También, en el peso medio del link en función del "endpoint-degree", se observa una correlación con el producto de los grados. Respecto al clustering, hemos definido un coeficiente adaptado a las redes bipartitas y de éste hemos hecho la generalización para redes bipartitas pesadas. Con este nuevo coeficiente de clustering se observa que el correspondiente valor para la red pesada es mayor que los que se obtendrían con la misma red pero cualitativa. Además este diferencia aumenta con el grado del nodo. Por último, la distribución de grado de próximo vecino, que para redes mutualistas binarias muestra una clara *desasortatividad*, al tener en cuenta el peso de los enlaces, esta tendencia parece que tiende a desaparecer, lo que indicaría que aunque las especies con las enlaces parece que tienen preferencia a relacionarse con especies con pocos enlaces, sin embargo las interacciones más fuertes suceden entre generalistas.

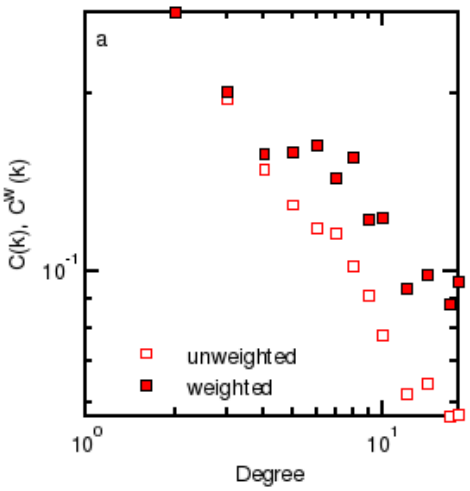

Figura 1. Coeficientes de Clustering binario (puntos sin relleno) y pesado (puntos con relleno). Valores promediados en función del grado.

* juanmanuel.pastor@upm.es
+ javier.galeano@upm.es
± Integrative Ecology Group, Estación Biológica de Doñana, CSIC, Sevilla.

[1] Bascompte J. y Jordano P. (2007), Plant-Animal Mutualistic Networks: The Architecture of Biodiversity. Annu.Rev.Ecol.Evol.Syst. 38, 567-593
[2] Barrat, A., Barthelemy, M., Pastor-Satorras, R., y Vespignani, A. (2004). The architecture of complex weighted networks. P.N.A.S. 101 (11), 3747-52

Thresholds for epidemic spreading in networks

Romualdo Pastor-Satorras*
Dept. Fisica i Enginyeria Nuclear
Universitat Politecnica de Catalunya
Campus Nord, Modul B4
08034 Barcelona

We study the threshold of epidemic models in quenched networks with degree distribution given by a power-law. For the susceptible-infected-susceptible model the activity threshold λ_c vanishes in the large size limit on any network whose maximum degree k_{max} diverges with the system size, at odds with heterogeneous mean-field (HMF) theory. The vanishing of the threshold has nothing to do with the scale-free nature of the network but stems instead from the largest hub in the system being active for any spreading rate $\lambda > 1/\sqrt{k_{max}}$ and playing the role of a self-sustained source that spreads the infection to the rest of the system. The susceptible-infected-removed model displays instead agreement with HMF theory and a finite threshold for scale-rich networks. We conjecture that on quenched scale-rich networks the threshold of generic epidemic models is vanishing or finite depending on the presence or absence of a steady state.

* romualdo.pastor@upc.edu

Vectores de Lyapunov característicos en sistemas con retraso

Diego Pazó*, Juan M. López
Instituto de Física de Cantabria (IFCA)
CSIC-Universidad de Cantabria
39005 Santander

En un sistema dinámico el espectro de exponentes de Lyapunov indica las tasas de crecimiento (y decrecimiento) exponencial en distintas direcciones de perturbaciones infinitesimales. Es bien conocido que la existencia de uno o más exponentes de Lyapunov positivos es un signo, o una definición si se prefiere, de que el atractor en el que un sistema evoluciona es caótico.

Mucho menos conocidos son, sin embargo, los vectores asociados a los exponentes de Lyapunov que indican en que direcciones se produce la amplificación de las perturbaciones. Un mejor conocimiento de estas direcciones tiene aplicación a problemas que impliquen una mejora de la predicibilidad (como es el caso de la predicción por conjuntos en meteorología), a procesos de mezclado turbulento, o, en un ámbito más matemático, a la propiedad de hiperbolicidad de un sistema dinámico.

Existe una confusión generalizada respecto a que son los vectores de Lyapunov. Muchos autores los identifican con la base ortonormal que resulta del método estándar de cálculo de los exponentes de Lyapunov. Estos vectores, llamados vactores de Lyapunov backward[1] no son intrínsecos al sistema puesto que dependen de la definición adoptada para el producto escalar (que determina su ortogonalidad). Desde hace bastantes años[2] se sabe que existe una única base de vectores de Lyapunov unívocamente definida: los vectores de Lyapunov característicos. Una perturbación alineada con uno de estos vectores se amplificará con una tasa de crecimiento dada por el exponente de Lyapunov asociado. A su vez si la evolución se hace hacia atrás en el tiempo se contraerá con el mismo exponente. Esta propiedad hace que también se hable de vectores de Lyapunov covariantes.

Recientemente se ha propuesto un algoritmo[3] eficiente para el cálculo de vectores de Lyapunov característicos en sistemas dinámicos con muchas variables. Este algoritmo nos ha permitido calcular los vectores de Lyapunov característicos en sistemas extendidos en una dimensión, observando la existencia de universalidad en su estructura espacial[4–6] de la que sólo se apartan de forma cuantitativa (no cualitativa) los sistemas Hamiltonianos[7] (FPU, Φ^4,...).

En esta comunicación nos ocupamos de las ecuaciones diferenciales con retraso, como los modelos de Mackey-Glass o de Ikeda:

$$\frac{d\,y(t)}{dt} = \mathcal{F}[y(t), y(t-\tau)] \qquad (1)$$

La dinámica gobernada por este tipo de ecuaciones es habitualmente caótica si el retraso τ es grande.

Nuestros resultados[8] hacen uso del mapeo de un sistema retrasado a un sistema extendido de tamaño igual al retraso, y son los siguientes:

1. Indicamos como hay que adaptar a los sistemas con retraso el algoritmo usado hasta ahora[3] para calcular vectores de Lyapunov característicos.

2. Encontramos numéricamente que en los sistemas con retraso los vectores de Lyapunov se organizan (cuando el retraso es grande) igual que en los sistemas disipativos con caos espacio-temporal extendidos en una dimensión espacial. La equivalencia entre ambos tipos de sistema es completa, también a nivel cuantitativo.

3. El vector de Lyapunov principal escala en espacio y tiempo como las soluciones de la ecuación de Kardar-Parisi-Zhang[9]. Nuestros resultados teóricos y numéricos esclarecen la controversia[10,11] en torno a la clase de universalidad del vector de Lyapunov.

---

* pazo@ifca.unican.es

[1] B. Legras y R. Vautard, en *Proc. Seminar on Predictability Vol. I*, ECWF Seminar, editado por T. Palmer (ECMWF, Reading, UK, 1996), pp. 135–146.
[2] J.-P. Eckmann y D. Ruelle, Rev. Mod. Phys. **57**, 617 (1985).
[3] C. L. Wolfe y R. M. Samelson, Tellus **59A**, 355 (2007).
[4] I. G. Szendro, D. Pazó, M. A. Rodríguez, y J. M. López, Phys. Rev. E **76**, 025202 (2007).
[5] D. Pazó, I. G. Szendro, J. M. López, y M. A. Rodríguez, Phys. Rev. E **78**, 016209 (2008).
[6] D. Pazó, M. A. Rodríguez, y J. M. López, Tellus **62A**, 10 (2010).
[7] M. Romero-Bastida, D. Pazó, J. M. López, y M. A. Rodríguez, Phys. Rev. E **82**, 036205 (2010).
[8] D. Pazó y J. M. López, Phys. Rev. E **82**, 056201 (2010).
[9] M. Kardar, G. Parisi, y Y.-C. Zhang, Phys. Rev. Lett. **56**, 889 (1986).
[10] A. Pikovsky y A. Politi, Nonlinearity **11**, 1049 (1998).
[11] A. D. Sánchez, J. M. López, M. A. Rodríguez, y M. A. Matías, Phys. Rev. Lett. **92**, 204101 (2004).

Additivity of Current Fluctuations in Two Dimensions and its Breakdown

Carlos Pérez-Espigares*, Pedro L. Garrido, Pablo I. Hurtado
Departamento de Electromagnetismo y Física de la Materia, and Instituto Carlos I de Física Teórica y Computacional, Universidad de Granada, Granada 18071, Spain

In this work we study the large deviations of the time-averaged current in the two-dimensional (2D) Kipnis-Marchioro-Presutti model of energy transport when subject to a boundary temperature gradient. We use the tools of hydrodynamic fluctuation theory, supplemented with an appropriate generalization of the Additivity Principle. As compared to its one-dimensionl counterpart, which amounts to assume that the optimal profiles responsible of a given current fluctuation are time-independent, the 2D Additivity conjecture requires an extra assumption, i.e. that the optimal, divergence-free current vector field associated to a given fluctuation of the time-averaged current is in fact constant across the system. Within this context we show that the current distribution exhibits in general non-Gaussian tails. The ensuing optimal density profile can be either monotone for small current fluctuations, or non-monotone with a single maximum for large enough current deviations. Furhermore, this optimal profile remains invariant under arbitrary rotations of the current vector, providing a detailed example of the recently introduced Isometric Fluctuation Relation (IFR)[1]. We have confirmed in extensive computer simulations for the 2D-KMP model the validity of the Additivity principle and the IFR for a wide current interval. However, we have also observed that for extreme fluctuations the Additivity hypothesis breaks down and the optimal density profiles become time-dependent in the form of traveling waves, giving rise to a dynamical phase transition, already observed in the 1D-KMP model[2]. In this case the IFR does not hold because it is known to break down in the regime where the Additivity Principle is violated.

* cpespigares@onsager.ugr.es

[1] P.I. Hurtado, C. Pérez-Espigares, J.J. del Pozo and P.L. Garrido, arXiv:1009.1243

[2] P.I. Hurtado and P.L. Garrido, to appear.

Modelling the F_1-ATPase

R. Perez-Carrasco*, J.M. Sancho
Departament d'Estructura i Constituents de la Materia, Facultad de Fisica, Universidad de Barcelona

The cellular environment is an out of equilibrium system in which there is a continuous transduction of matter and energy. The mechanisms driving this processes are the Molecular Motors. There are many different Molecular Motors with many different functions. For instance, kinesin, which can transport cargos along microtubule tracks; or BFM, which rotates the flagella of bacteria propelling them. What is even more interesting is that Molecular Motors are able to achieve its goal despite the high noise media in which the live.

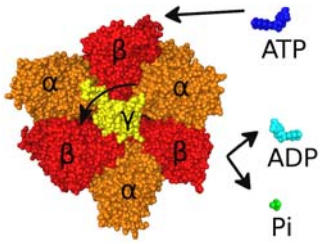

Figura 1. Working of the F_1-ATPase, the hydrolysis process in the β domain produces a rotation of the central γ shaft.

One particular molecular motor is the F_1-ATPase, part of the ATPsyntase holoenzyme. F_1-ATPase is a rotatory motor that uses the hydrolysis energy of ATP to rotate its central shaft. F_1-ATPase is reversible and can also synthesize ATP out of its hydrolysis products when the shaft is mechanically rotated in the proper direction. The rotation trajectories can be experimentally studied by attaching a load to the shaft. The aim of our work is to analyze such trajectories studying the mechanico-chemical properties of the motor and the biochemical information available.

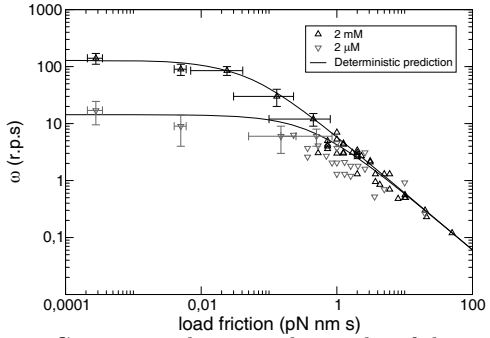

Figura 2. Comparison between the results of the model and the experimental data[3] for the dependence of the main velocity with the load friction.

The resulting model is a flashing ratchet model able to reproduce the stepping trajectories observed through Langevin dynamics. The model also returns simple analytical expressions for the average velocity of the motor that compare accurately with the dependence of the velocity on external parameters such as the ATP concentration, the friction of the load, ATP hydrolysis energy or thermal fluctuations. In addition, This model is the first model able to predict the complete substep phenomenology observed in experiments, obtaining an universal value for the susbtep angle[1].

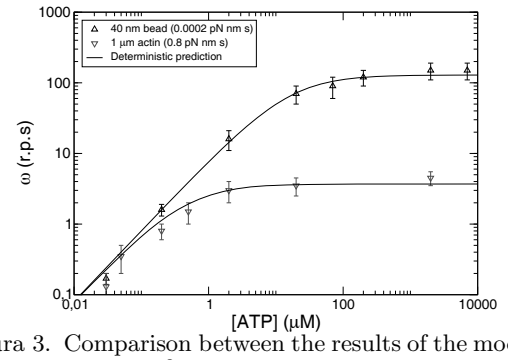

Figura 3. Comparison between the results of the model and the experimental data[3] for the dependence of the main velocity with the ATP concentration.

For the study of the molecular motors, it is often useful to describe the dynamics of the motor through a single coordinate Fokker-Planck equation. However, the translation of a dichotomous Langevin equation into a single coordinate FP equation is not straightfroward and needs of a correct interpretation of the white noise limit for the dichotomous noise driving the flashing of the motive potential. We present also a correct approach for such a problem and it is applied to the F_1 motor obtaining a good match with the experiments[2].

* rperez@ecm.ub.es

[1] R. Perez-Carrasco and J.M. Sancho, Biophys. J. **98**, 2591 (2010)
[2] R. Perez-Carrasco and J.M. Sancho, Eur. Phys. Lett. **91** 60001 (2010)
[3] Yasuda R. *et al.*, Nature **410** 898-904 (2001)

La línea de coexistencia hielo seco-CO_2 fluido: un análisis a través de simulación por el método de Monte Carlo

G. Pérez-Sánchez[1], J. M. Míguez[1], D. González-Salgado[2], M. M. Piñeiro[1]
[1] *Departamento de Física Aplicada, Facultad de Ciencias del Mar*
Campus Lagoas-Marcosende, Universidad de Vigo
36200 Vigo, España.
[2] *Departamento de Física Aplicada, Laboratorio de Termofísica de Ourense*
Campus As Lagoas, Universidad de Vigo
32004 Ourense, España

El equilibrio sólido-líquido de dióxido de carbono (CO_2) ha sido determinado a través de simulaciones por el método de Monte Carlo para el modelo MSM[1–4] y algunas actualizaciones de éste como el EPM2[5], TraPPE[6], Errington[7] y el recientemente propuesto por Zhang[8]. Se ha considerado únicamente la fase sólida de grupo espacial Pa3[9] conocida comúnmente como hielo seco. El procedimiento de cálculo es el estándar para estos casos[10] y ha consistido en los siguientes pasos. En primer lugar, se ha determinado la energía libre para la fase sólida a lo largo de una isobara de referencia (en nuestro caso 1000MPa), utilizando el "Einstein molecule method"[11] para su evaluación en un estado de referencia (100K y 1000MPa) e integración termodinámica[12] desde este estado. En segundo lugar, se han evaluado las energías libres del fluido a lo largo de la misma isobara utilizando integración termodinámica[12] desde un estado donde el CO_2 se comporta como gas ideal (800K y 1bar). Una vez que las energías libres de ambas fases se han obtenido en la misma isobara, se ha determinado un punto de coexistencia a través de la condición de igualdad de potenciales químicos. Finalmente, se ha utilizado el método Gibbs-Duhem (la integración de la ecuación de Clapeyron)[13–15] desde este punto para trazar la curva de equilibrio. Con el objeto de evaluar la consistencia de nuestros resultados, se han determinado puntos adicionales de coexistencia a 200MPa y 4MPa utilizando el cáculo de energías libres. Los resultados obtenidos han sido comparados con datos seleccionados de la bibliografía.

[1] C. S. Murthy, K. Singer, and I. R. McDonald, *Mol. Phys.*, **44** 135 (1981).
[2] D. Moller and J. Fischer, *Fluid Phase Equilib.*, **100** 35(1994).
[3] J. Vrabec, J. Stoll, and H. Hasse, *J. Phys. Chem.* B, **105** 12126 (2001).
[4] C. S. Murthy, S. F. Oshea, and I. R. McDonald, *Mol. Phys.*, **50** 531 (1983).
[5] J. G. Harris and K. H. Yung, *J. Phys. Chem.* **99** 12021 (1995).
[6] J. J. Potoff and J. I. Siepmann, AIChE J. **47** 1676 (2001).
[7] J. R. Errington, Ph.D. thesis, Cornell University, 1999.
[8] Z. Zhang and Z. Duan, *J. Chem. Phys.*, **122** 214507 (2005).
[9] H. H. Keesom and J. W. L. Kohler, *Physica*, **1** 655 (1934).
[10] C. Vega, E. Sanz, J. L. F. Abascal, E. G. Noya, *J. Phys. Condens. Matter*, **20** 153101 (2008).
[11] E. G. Noya, M. M. Conde, C. Vega, *J. Chem. Phys.*, **129** 104704 (2008).
[12] D. Frenkel, B. Smit, Understanding Molecular Simulation, Academic Press, New York 2002.
[13] D. A. Kofke, *J. Chem. Phys.*, **98** 4149 (1993).
[14] D. A. Kofke, *Mol. Phys.*, **78** 1331 (1993).
[15] D. A. Kofke, Monte Carlo Methods in Chemical Physics, edited by D. M. Ferguson, J. L. Siepmann, and D. G. Truhlar (Wiley, New York, 1998), Vol. 105 p. 404.

Chiral Selection by Interfacial Shearing of Self-Assembled Achiral Molecules

Núria Petit-Garrido, Jordi Ignés-Mullol, Josep Claret, Francesc Sagués
SOC & SAM group, IN2UB and Departament de Química Física, Universitat de Barcelona, Martí i Franquès 1, 08028 Barcelona, Spain

Chiral symmetry breaking, i.e., the absence of mirror symmetry, is a pervasive phenomenon encompassing from self-organizing galaxies to the molecular architecture of biopolymers. In materials science this is a relevant issue in self-assembling processes, as well as in asymmetric catalysis. Although spontaneous chiral resolution has been observed during aggregation of either chiral or achiral molecules, we are in general unable to realize a robust process of chiral selection. Here we report a novel phenomenon of chiral selection in self-assembled condensates of achiral amphiphiles[1]. The handedness of chiral textures, reproducing the collective rotational component of the molecular orientation inside submillimeter circular domains, is correlated with the sign of a vortical stirring in the aqueous subphase. We propose an explanation based on the distinctive kinetics of topological defect annihilation during domain coalescence at the initial coarsening stage of a phase-separating monolayer. Different from dichroism-based techniques, applied to supramolecular aggregates, we here directly observe how a macroscopic chiral force may be imprinted downscale during bottom-up molecular assembling.

Acknowledgement: This work has been supported by MICINN (Project No. FIS2006-03525) and by DURSI (Project 2005 SGR 00653). N. P. acknowledges support from MICCINN (Grant No. AP2007-01103).

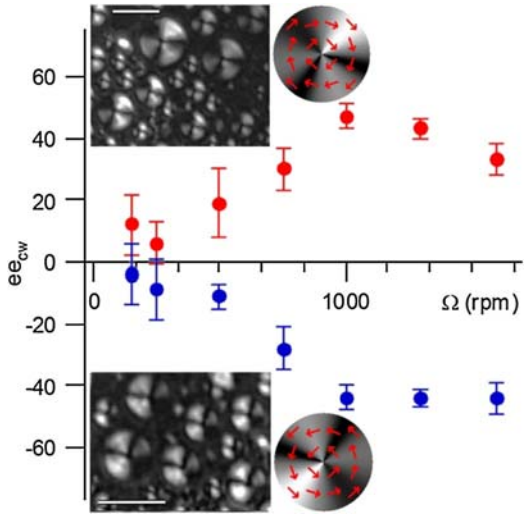

Figura 1. The enantiomeric excess, ee_{CW}, is plotted as a function of the rotating rate of the stirrer, Ω. BAM images with an ensemble of the chiral mesostructures after 5 minutes under 1000 r.p.m. stirring are shown next to each branch, along with a sketch of the resolved in-plane orientational field. Qualitatively, BAM textures appear as three black brushes, with either two upwards brushes (CCW orientation) or two downwards brushes (CW orientation). The maximum reflectivity appears in the first and third quadrants of the domains for CW and CCW orientation, respectively. White bar corresponds to 100 μm.

[1] N. Petit-Garrido, J. Ignés-Mullol, J. Claret and F. Sagués, Phys. Rev. Lett. **103**, 237802 (2009).

Blood flow in microvessels

Clara B. Picallo*† Tomás Alarcón**,‡, Aurora Hernández-Machado*¶
* *Departament de Estructura i Constituents de la Matèria. Universitat de Barcelona. 08028 Barcelona.*
** *Centre de Recerca Matemàtica. Campus de Bellaterra. Edifici C. 08193 Bellaterra.*

Vascular networks are flexible systems, able to evolve and adapt in response to the needs of the surrounding tissue. Long-term hemodynamic changes may induce permanent morphological transformations in the vessels, affecting its diameter[2] and wall thickness. However, besides this ability to deform plastically, vascular networks also are able to undergo acute regulations in the short term, for instance to fulfill a sudden high demand of oxygen in the medium.

Here we focus on the blood flow in microvessels[3] and its adaptation dynamics. Capillaries, the smallest blood vessels with diameters from 6 to 10 μm -close to the size of the red blood cells-, are responsible for the distribution of blood within tissues. Blood flow in capillaries occurs at very low Reynolds numbers and it is traditionally modeled as a stationary motion within a solid cylindrical channel, giving rise to a so-called Poiseuille velocity profile, that depends parabolically on the vessel radius and is linearly related to the pressure gradient between the ends of the capillary. However, vessel walls are far from being rigid. Here we are interested in the elastic changes in the lumen radius of capillaries due to the variations in the blood flow rate in response to the oxygen demand of the surrounding tissue. An increase in the incoming flow induces an expansion of the vessel to stand the new flow rate. Here we discuss the mechanisms that govern this expansion, the dynamics of the flow and the arising morphology of the microvessels.

† clara.picallo@gmail.com
‡ talarcon@crm.cat
¶ a.hernandezmachado@gmail.com

[1] A. R. Pries, T. W. Secomb, and P. Gaehtgens, American Journal of Physiology - Heart and Circulatory Physiology **275**, H349 (1998).
[2] T. Alarcón, H. M. Byrne, and P. K. Maini, Journal of Theoretical Biology **225**, 257 (2003).
[3] P. Bagchi, Biophysical Journal **92**, 1858 (2007).

A microcanonical multifractal approach to the characterization of heartbeat dynamics

Oriol Pont*[1], Michel Haïssaguerre[2] , Hussein Yahia[1], Nicolas Derval[2] , Méléze Hocini[2]
[1] *EPI GeoStat - INRIA Bordeaux Sud-Ouest, Campus Bdx I, F-33405 Talença*
[2] *Hopital du Haut-Lévêque, Ave. de Magellan, F-33604 Peçac*

Heartbeat dynamics is a complex system whose analysis becomes essential in order to detect arrhythmias and other life-threatening conditions. To achieve a proper analysis and characterization of it, advanced methods based on nonlinear processing are needed. In this context, the recent developments in the field of reconstructible signals and multiscale information content have led to the Microcanonical Multifractal Formalism (MMF). This framework provides a number of signal analysis techniques that are particularly suited to the study of heartbeat dynamics. In particular, the analysis of electrocardiogram signals and the electrical potential measured via catheters in different parts of the human heart allows the detection of slow changing transitions. Detecting different regimes of transition between atrial fibrillation and healthy cases could be used for early warning and treatment of cardiac arrhythmias.

Heart rhythm is the result of a complex process of synchronization between pacemaker cells and consequently displays chaotic rate fluctuations. Under normal conditions, the amplitude of these fluctuations is much smaller than the average interval between beats, which makes the healthy heartbeat (sinus rhythm) appear as periodic. However, the fluctuations around this main period is not just random noise but an structured complex dynamics. Moreover, the characterization of these fluctuations is of vital importance in determining if a heart is healthy or is showing signs of transition to an arrhythmia, despite still appearing regular.[2]

The human heart has a complex structure and a complex electrical activity. Cardiac action potential is led by polarization of pacemaker cells. These cells are not homogeneous, but mainly concentrate on nodes (sinoatrial and atrioventricular), and the Purkinje fibers that innervate the whole ventricular myocardium. The action of pacemaker cells controlling heart contractions (atrial and ventricular systole) and relaxation (diastole) in an organized manner to ensure the optimal pumping.

Early studies of fluctuations between beats found them to have a scale-invariant structure. Later developments based on multiresolution analysis allowed to describe them as multifractal,[2] though based solely on numerically-evaluated Legendre spectra, i.e., corresponding to a canonical formalism. The multifractal structure observed in cardiac rates is the result of a synchronization process in a complex hierarchical network[1] made of pacemaker cells. Therefore, a multifractal analysis of the resulting signal reflects the manifestation of the network topology generating it. As a consequence, the microcanonical approach provided by the MMF[4][5] becomes especially suitable for the analysis of this dynamic structure. In particular, a analysis based on the singularity exponents and the optimal wavelet[3] allows a direct access to the geometric characteristics of the multiscale behavior. This methodology is known to give more accurate estimation of the tails of the singularity spectrum and is generally more robust on empirical data.[5]

Having accurate estimates is of paramount importance to anticipate as much as possible when the dynamics heartbeat starts to drift from the healthy behavior. Given the the speed with which heart failure can be fatal or leave irreversible sequelae, identification of the relevant features has great potential to help to save lives and improve the health of people with heart diseases.

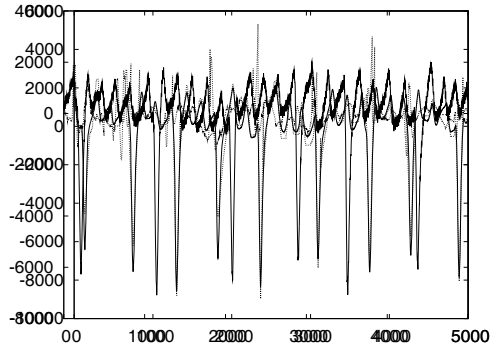

Figura 1. Measures from the V1 electrode (solid) and its reconstruction (dashed) based our model. The reconstruction shown is of very high quality, especially for the peaks, meaning that we capture and characterize most of the signal.

* oriol.pont@inria.fr

[1] P. Chainais, R. Riedi, and P. Abry. On non-scale-invariant infinitely divisible cascades. *Information Theory, IEEE Transactions on*, 51(3):1063 – 1083, march 2005.
[2] P. Ivanov, L. Amaral, A. Goldberger, S. Havlin, M. Rosenblum, Z. Struzik, and H. Stanley. Multifractality in human heartbeat dynamics. *Nature*, 399:461–465, 1999.
[3] O. Pont, A. Turiel, and C. Perez-Vicente. On optimal wavelet bases for the realization of microcanonical cascade processes. *Int. J. Wavelets Multi., IJWMIP*, 9(1):35–61, January 2011.
[4] O. Pont, A. Turiel, and C. J. Pérez-Vicente. Application of the microcanonical multifractal formalism to monofractal systems. *Physical Review E*, 74:061110–061123, 2006.
[5] A. Turiel, H. Yahia, and C. Pérez-Vicente. Microcanonical multifractal formalism: a geometrical approach to multifractal systems. Part I: Singularity analysis. *Journal of Physics A*, 41:015501, 2008.

Computación distribuída sobre redes complejas. Aplicación a la optimización de tiempos de ejecución de tareas en entornos GRID.

Francisco Prieto Castrillo*, A. Astillero†, Elena Rey Espada**
Unidad de Ciencia y Tecnología
Centro Extremeño de Tecnologías Avanzadas (CETA-CIEMAT)
10200 Trujillo (Cáceres)

Este trabajo propone un modelo teórico para el estudio de los tiempos de ejecución en un sistema de computación distribuido desde el punto de vista de las redes complejas entendiendo la infraestructura como un sistema dinámico en evolución. En particular, el modelo obtenido se aplica a la optimización del servicio WMS (*Workload Management System*) para despliegue de tareas en las tecnologías GRID. Se estudian los efectos en el rendimiento de la GRID de distintas topologías de red generadas por un modelo de crecimiento de grafos basado en el método de *Preferential Attachment*[1–3]. Como modelo de cómputo en el sistema distribuido se utiliza un esquema de tipo MMPP[4] (*Markov Modulated Poisson Process*) donde los estados finitos de la cadena de Markov representan modos de cómputo accesibles en la infraestructura dada. En este caso, cada modo hace el papel de un servidor en un modelo de colas con tasas de servicio dadas por una distribución de Poisson.

También se están recogiendo experimentalmente datos disponibles de uso de la grid para poder comparar con el modelo teórico.

---

* francisco.prieto@ciemat.es
† Departamento de Tecnología de Computadores y Comunicaciones, Universidad de Extremadura, 06800 Mérida (Badajoz)
aavivas@unex.es
`http://www1.unex.es/eweb/fisteor/antonio_astillero/`
** elena.rey@ciemat.es

[1] A. Barabasi y R. Albert, Science **286**, 509 (1999).
[2] R. Albert y A. Barabasi, Rev. Mod. Phys. **74**, 47 (2002).
[3] L. Costa, G. Travieso y C. A. Ruggiero, Euro Phys. J. B **44**, 119 (2005).
[4] Y. Wu, L. Liu, J. Mao, G. Yang and W. Zheng, *An analytical model for performance evaluation in a computational grid*, (2010).

Phase Transition of a Meniscus in a Capillary under the Influence of Gravity

C. Rascón[1], A.O. Parry[2], S. Ivell[3], A. Thorneywork[3], D. Aarts[3]
[1] *GISC, Departamento de Matemáticas. Universidad Carlos III de Madrid.*
[2] *Department of Mathematics, Imperial College London*
[3] *Department of Physical Chemistry, Oxford University*

Phase transitions of inhomogeneous fluids such as wetting and capillary-condensation that occur when a fluid is confined near a substrate or in parallel-plate geometries have received enormous attention over the last few decades. In most theoretical studies of these transitions the influence of a gravitational field is either considered secondary or, more often, completely neglected. However, it is clear that gravity plays a central role in many practical situations and, in combination with the confinement, induces further interfacial behaviour. Consider, for example, a large volume of a non-volatile liquid in a tall vertical capillary-slit or cylindrical pore which is capped at its bottom. What happens to the liquid when the capillary is slowly turned to the horizontal? Common experience tells us that the liquid will escape from the open end if the capillary is wide, as when water drains from a tipped glass, but will remain trapped if it is sufficiently narrow such as a drinking straw. It is somewhat surprising to find that this rather basic aspect of capillarity has not been investigated in depth. We show here some theoretical and experimental results of this phenomenon, and point out that this common phenomena is analogous to an interfacial unbinding phase transition involving the meniscus shape and reveals an unexpected connection between capillary-condensation and the theory of wetting transitions.

* carlos.rascon@uc3m.es

Coexistencia de cooperadores y no cooperadores en poblaciones bien mezcladas: Un escape del dilema del prisionero en la competición por recursos

Rubén J. Requejo, Juan Camacho

El origen de la cooperación es una de las ramas principales de la biología evolutiva. El análisis exhaustivo del dilema del prisionero ha permitido encontrar varios mecanismos que promueven su evolución; sin embargo, las implicaciones de la existencia de una cantidad finita de recursos no han sido estudiadas en detalle. ¿Puede la limitación de recursos por sí misma promover la cooperación? En esta charla presentaré un modelo simplificado de una población bien mezclada de cooperadores y parásitos (no cooperadores), en el que se explicita la limitación de recursos. Cuando el resultado de las interacciones no se ve afectado por dicha limitación, su estructura es la de un dilema del prisionero no iterado y bien mezclado, lo cual conlleva la extinción de la cooperación. Sin embargo, mostraré que la limitación de recursos es capaz de alterar la estructura del dilema del prisonero permitiendo coexistencia estable entre cooperadores y parásitos, lo cual sucede gracias a un proceso de auto-organización que iguala beneficios y costes de no cooperar, sin que sea necesario introducir memoria, capacidad de reconocimiento, conceptos de reputación u otras abilidades. Los resultados sugieren que la asunción de pagos constantes podría no ser válida en escenarios más amplios, en los que la limitación de recursos se considera de manera explícita, y podría ayudar a explicar el origen de la cooperación en los primeros estados evolutivos.

Towards an understanding of nucleic acids stucture in gas phase

Annalisa Arcella*, Modesto Orozco
Institute for Research in Biomedicine
Cientific Parc of Barcelona
Barcelona 08028

In the last years studies of triplex DNA have been paid much more attention because of its importance as a tool for DNA sequencing, gene control and therapeutic application. Properties of the Triplex DNA have been studied experimentally using Electrospray Soft Ionization Mass Spectrometry techniques. Where DNA undergoes a transition from solvent to vacuum changing its ionization pattern, the process is too fast to follow the structural changes with resolution. Here is where computational techniques come in handy. By performing simulations in environments that simulate conditions before and after the ionization we can better understand the nature of these triplexes and how we might be able to improve this sequences for antigene therapy. Intrinsic properties of Triplex are studied exploring its configurational space through Molecular Dynamics simulation in gas phase. Gas phase trajectrories are compared with solution ones.

Simulations have been performed for different structures, such as (GCC^+)x12mer/18mer, (GCC^+/ATT)x6mer/9mer and (ATT)x12mer/18mer, where C^+ stands for protonated cytosine. According to electrospray experiments[1] a net charge of -6/-9 is assigned to the 12mer/18mer triplexes respectively. Since there is no information about the location of these charges, two neutralization protocols were considered. First, the total charge was equally distributed along all phosphates by appropriate scaling of their charges. In the second protocol a set of 6/9 phosphates which minimize the coulombic potential is chosen, while the rest of the phosphates are neutralized by protonating phosphate groups. Unrestrained MD simulations at constant pressure and temperature in water yields stable structures, as noted in the RMSd values. Hydrogen bonds are fully preserved along the whole trajectory. After 100 ns MD simulations, the structures of the triplex in vacuum are distorted. During the dynamics in gas phase helices fold and the whole structure appears more compacted as shown by the collision cross section and radius of gyration time behaviour. In general hydrogen bonds are not preserved unlike stacking interactions which instead appear not so different from in solution one as aspected from DNA behaviour in gas[2]. Hoogsteen duplexes which compose the triplexes look like more stable than Watson-Crick one probably because of presence of positive charge of the protoneted cytosine.

* annalisa@mmb.pcb.ub.es

[1] Wan C., Guo X., Liu, Z. And S., *J. Mass spectrom.* (43,164-172, 2008).

[2] Rueda M., KalKo G.S., Luque F.J., Orozco.,*J. Mass spectrom.* .Am. Chem. Soc. 125, 8007-8014, 2003)

Efectos de tamaño iónico finito en suspensiones coloidales concentradas salt-free

Rafael Roa[1]*, Félix Carrique[1], Emilio Ruiz-Reina[2]
[1] *Física Aplicada I, Universidad de Málaga, 29071 Málaga (Spain)*
[2] *Física Aplicada II, Universidad de Málaga, 29071 Málaga (Spain)*

En este trabajo hemos estudiado la influencia del tamaño de los contraiones en la doble capa eléctrica de equilibrio y en la movilidad electroforética DC de partículas coloidales esféricas en suspensión.

La doble capa eléctrica de equilibrio en suspensiones concentradas salt-free incluyendo efectos de tamaño iónico finito ha sido estudiada recientemente por los autores[1] y constituye la base para el estudio de la movilidad electroforética. Una suspensión salt-free contiene únicamente partículas cargadas y los contraiones añadidos que contrarrestan su carga superficial. Hemos hecho uso de una aproximación de modelo de celda esférica para tener en cuenta las interacciones electro-hidrodinámicas de partícula-partícula en suspensiones concentradas. El tamaño finito de los contraiones se ha considerado incluyendo una contribución entrópica, relacionada con el volumen excluido de los iones, en la energía libre de la suspensión[2], dando lugar a una ecuación de Poisson-Boltzmann modificada. La movilidad electroforética y la doble capa eléctrica en el equilibrio han sido estudiadas previamente por Aranda-Rascón *et al.*, basándose en una corrección similar de tamaño iónico finito para el caso de suspensiones diluidas electrolíticas[3]. Para suspensiones salt-free, la ecuación de Poisson-Boltzmann modificada y las ecuaciones electrocinéticas asociadas aumentan su complejidad, lo que dificulta su resolución numérica. En este trabajo presentamos resultados numéricos para un amplio rango de fracciones de volumen y de densidades superficiales de carga de partícula, así como para distintos tamaños de contraión.

Encontramos que el efecto de tamaño iónico finito es bastante importante para cargas de partícula moderadas y altas a una fracción de volumen dada. Además, en el caso de la movilidad electroforética, estos cambios son claramente más importantes cuanto mayor es la fracción de volumen para estos valores de carga de partícula. Los efectos anteriores cobran mayor importancia cuanto mayor es el tamaño del contraión. Creemos que el presente estudio establece las bases de modelos futuros para la respuesta electrocinética AC de suspensiones concentradas salt-free que incluyan efectos de tamaño iónico finito.

---

* rafaroa@uma.es

[1] R. Roa, F. Carrique, and E. Ruiz-Reina, Phys. Chem. Chem. Phys. (2011), DOI:10.1039/C0CP02303E.
[2] I. Borukhov, D. Andelman, and H. Orland, Phys. Rev. Lett. **79**, 435 (1997).
[3] M. J. Aranda-Rascón, C. Grosse, J. J. López-García, and J. Horno, J. Colloid Interface Sci. **335**, 250 (2009).

Formulación dinámica del Efecto Casimir

Pablo Rodriguez-Lopez*, Ricardo Brito†, Rodrigo Soto‡
GISC y Departamento de Física Aplicada I (Termología), Facultad de CC. Físicas, Universidad Complutense, 28040 Madrid.

Debido a las fluctuaciones de vacío, entre dos placas metálicas descargadas aparece una fuerza atractiva[1]. Estas fuerzas de Casimir tienen una naturaleza cuántica, pero se han obtenido análogos clásicos de fuerzas de Casimir en sistemas en equilibrio sometidos a ruido térmico[2].

Estas fuerzas de Casimir son ubicuas en la Naturaleza, y han sido estudiadas en muy diferentes contextos, pero siempre en sistemas en equilibrio termodinámico[3].

En este trabajo[4] proponemos un modelo de fuerzas de Casimir general tomando como punto de partida las ecuaciones dinámicas del medio fluctuante. Junto con las propiedades estadísticas de las fluctuaciones y las condiciones de contorno de las intrusiones podemos derivar la fuerza de Casimir.

Como resultado, obtenemos una fórmula explícita de la fuerza de Casimir entre intrusiones. En particular, este formalismo contiene el efecto Casimir térmico del equilibrio como un caso particular. Además, posibilita el estudio del efecto Casimir en sistemas en los que sólo tengamos sus ecuaciones de evolución dinámicas y una fórmula de la presión del campo. Entonces, no necesitamos ni una formulación Hamiltoniana del medio, ni una formulación del equilibrio termodinámico del sistema para obtener dichas fuerzas. Por tanto, el modelo es válido tanto para sistemas en equilibrio como fuera del equilibrio.

Como aplicación, estudiamos la fuerza de Casimir entre dos placas plano paralelas infinitas con condiciones de contorno de Dirichlet o Neumann, inmersas en medios con longitud de correlación finita sometidos a distintos tipos de ruido Gaussiano. Comprobamos que cuando se cumple el Teorema Fluctuación-Disipación se recupera la fuerza de Casimir del equilibrio entre placas, mientras que cuando dicho teorema no se cumple, también obtenemos fuerzas de Casimir, pero de distinta naturaleza.

También presentamos un método numérico de cálculo de fuerzas de Casimir diréctamente inspirado en le modelo aquí propuesto.

Gracias a la generalidad del modelo presentado, podemos obtener el caso cuántico original de Casimir como un caso particular mediante el uso del formalismo de Parisi-Wu.

Además, al ser el origen de las fuerzas de Casimir las fluctuaciones del medio, estas fuerzas son de origen fluctuante. Nuestro modelo nos permite calcular la varianza de las fuerzas y demostrar que, si el ruido al que está sometido el sistema es Gaussiano, las fuerzas de Casimir son también variables Gaussianas.

---

* pablo.rodriguez@fis.ucm.es.
† brito@fis.ucm.es.
‡ rsoto@dfi.uchile.cl. Departamento de Física, FCFM, Universidad de Chile, Casilla 487-3, Santiago, Chile.

[1] H. B. G. Casimir, Proc. K. Ned. Akad. Wet. **51**, 793 (1948).
[2] M. Kardar and R. Golestanian, Rev. Mod. Phys. **71**, 1233 (1999).
[3] A. Ajdari, B. Duplantier, D. Hone, L. Peliti and J. Prost, J. Phys. II France **2**, 487-501 (1992).
[4] P. Rodriguez-Lopez, R. Brito and R. Soto, Accepted in Phys. Rev. E (2011).

Irreversibilidad y disipación en procesos estocásticos

Édgar Roldán*, Juan M.R. Parrondo†
Facultad de Ciencias Físicas y GISC
Universidad Complutense de Madrid
28016 Madrid

La entropía relativa de orden n entre dos distribuciones de probabilidad p y q de variables discretas se define como

$$D_n(p||q) = \sum_{x_1,\cdots,x_n} p(x_1,\cdots,x_n) \log \frac{p(x_1,\cdots,x_n)}{q(x_1,\cdots,x_n)}, \quad (1)$$

y es una medida de la distinguibilidad entre ambas distribuciones de probabilidad: es igual a 0 sí y sólo sí ambas distribuciones son iguales y mayor que 0 en cualquier otro caso, siendo mayor cuanto más distinguibles son[1].

Consideremos un proceso estocástico de no equilibrio en estado estacionario (NESS) del cual extraemos información discreta. Sea $(x_1, x_2, \cdots, x_n)$ una trayectoria de n pasos de una variable del sistema x. Podemos medir la entropía relativa de la distribución de probabilidad de las trayectorias del proceso $p(x_1, \cdots, x_n)$ con respecto a la distribución de probabilidad de las trayectorias invertidas temporalmente $p(x_n, \cdots, x_1)$,

$$d(x) = \lim_{n\to\infty} \frac{1}{n} D_n[p(x_1,\cdots,x_n)||p(x_n,\cdots,x_1)]. \quad (2)$$

Esta magnitud mide como de distinguible es un proceso con respecto a su inverso temporal, es decir, es una medida de la asimetría temporal o irreversibilidad del proceso que genera la variable x. Si consideramos trayectorias en el espacio de fases del sistema (Γ) o bien la variable en consideración es la entropía del sistema (s), la entropía relativa es precisamente igual a la disipación promedio del proceso[2,3]. Es decir,

$$\beta\langle w_{diss}\rangle = d(\Gamma) = d(s), \quad (3)$$

donde $\beta = 1/(k_B T)$ y $\langle w_{diss}\rangle$ es la disipación media por paso, entendida como el exceso de trabajo realizado en el proceso con respecto a la diferencia de energía libre entre el estado final y el estado inicial, $W_{diss} = W - \Delta F$. La ecuación (3) cuantifica por tanto un asunto central de la mecánica estadística, la relación entre disipación e irreversibilidad en procesos de no equilibrio.

En caso de utilizar información parcial del sistema, se obtiene una cota inferior a la disipación. Sea x una variable arbitraria del sistema, entonces en general se tiene

$$\beta\langle w_{diss}\rangle \geq d(x). \quad (4)$$

El miembro izquierdo de la ecuación anterior es una cantidad física mientras que el miembro derecho es una magnitud puramente estadística. Esto implica que incluso desconociendo de donde proviene una serie temporal podemos inferir una propiedad física del mecanismo que generó dicha serie.

El objetivo de nuestro estudio es analizar la relación entre disipación e irreversibilidad de forma cuantitativa en el NESS. Tratamos de ver si es posible estimar la disipación media de un proceso cuando solo se tiene acceso a información parcial del mismo[4].

Trabajamos con un modelo sencillo de ratchet discreta que nos permite comparar resultados analíticos de la disipación con estimaciones empíricas de la entropía relativa. Utilizando la informacion de una única trayectoria estacionaria comprobamos la igualdad (3) cuando utilizamos información total, mientras que con información parcial obtenemos una cota inferior (4).

Sin embargo, incluso con información parcial podemos inferir algunas propiedades físicas del sistema. Por ejemplo, podemos predecir el comportamiento asintótico de la disipación cuando hacemos tender un parámetro del sistema a su valor en el equilibrio. Además, somos capaces de distinguir cuantitativamente entre trayectorias en equilibrio y trayectorias fuera del equilibrio.

En algunas situaciones, un sistema disipa energía pero está aparentemente en equilibrio al no exhibir flujos o corrientes. Un ejemplo es un motor molecular en un baño térmico bajo la acción de una fuerza que anule, en promedio, su movimiento (*fuerza de parada*). Observamos que en esta situación, incluso utilizando información parcial del sistema que no exhibe corrientes, podemos predecir que el sistema está fuera del equilibrio con la entropía relativa de tres pasos. Concluimos por tanto que en un proceso genérico fuera del equilibrio, la entropía relativa, y no los flujos del sistema, es el indicador que nos dice si el proceso es o no reversible, y cuan irreversible es.

Nuestro trabajo tiene aplicaciones potenciales en biología. El grupo de Frank Julicher (MPI-PKS, Dresden) ha estudiado las células ciliares del oído, encontrando un método para diferenciar células activas y pasivas mediante un test experimental del teorema de fluctuación-disipación[5]. Nuestro estudio podría mejorar dicho método con la medida de la entropía relativa de las oscilaciones espontáneas de estas células.

* edgar.roldan@fis.ucm.es
† parrondo@fis.ucm.es

[1] T. M. Cover and J. A. Thomas, *Elements of information theory* (Wiley, Hoboken, New Jersey, 2006), 2nd ed.
[2] E. Cohen and G. Gallavotti, *J. Stat. Phys.* **96**, 1343(1999).
[3] R. Kawai, J. M. R. Parrondo, and C. V. den Broeck, *Phys. Rev. Lett.* **98**, 080602 (2007).
[4] E. Roldán and J. M. R. Parrondo, *Phys. Rev. Lett.* **105**, 150607 (2010).
[5] P. Martin, A. J. Hudspeth, and F.Julicher, Proc. Natl. Acad. Sci. U.S.A. 98, 14 380 (2001).

Escalamiento de tamaños finitos en la transición de rellenado de cuña del modelo de Ising tridimensional

J. M. Romero-Enrique[1]*, L. F. Rull[1], A. O. Parry[2]
1. Departamento de Física Atómica, Molecular y Nuclear, Area de Física Teórica, Universidad de Sevilla, Apartado de Correos 1065, 41080 Sevilla (España)
2. Department of Mathematics, Imperial College 180 Queen's Gate, London SW7 2BZ, United Kingdom

La adsorción de fluidos sobre sustratos microestructurados es un área de investigación que ha despertado gran interés en los últimos años. Un ejemplo muy estudiado es el fenómeno de rellenado en geometrías de cuña, donde se considera la interfase entre un vapor saturado en volumen y una cuña formada por la intersección entre dos sustratos homogéneos con un ángulo de abertura $\pi - 2\alpha$. Argumentos termodinámicos[1] muestran que hay una transición entre un estado de rellenado parcial (donde la cuña condensa parcialmente líquido) y una transición de rellenado total (donde la cuña está llena completamente de líquido), y que precede a la transición de mojado característica de los sustratos. Estudios de modelos mesoscópicos de fluidos con interacciones de corto alcance para valores de α pequeños[2,3] muestran que la geometría potencia las fluctuaciones interfaciales, que son dominadas por los "modos de respiración" de gran longitud de onda a lo largo de la cuña, ya que en la dirección transversal la interfase se puede considerar indeformable. Este carácter cuasi-monodimensional de las fluctuaciones ha permitido estudiar de manera analítica el comportamiento de la capa adsorbida en las cercanías de las transiciones continuas[3].

Desde un punto de vista más microscópico, esta transición de rellenado ha sido estudiada mediante simulación de Monte Carlo en el modelo de Ising, usando una geometría de doble cuña[4]. Dichos estudios muestran evidencias de la existencia de una transición de rellenado crítica, con unos exponentes críticos consistentes con los valores predichos por las teorías mesoscópicas. Sin embargo, no se consigue mostrar de manera satisfactoria el colapso de las distribuciones reescaladas de probabilidad de magnetización en una curva universal, lo que es el fundamento de la técnica de escalamiento de tamaños finitos para la localización de la transición continua de rellenado. En esta contribución reanalizamos el problema considerado por dichos autores. Desde un punto de vista teórico, y haciendo uso de las técnicas aplicadas al estudio de la transición de rellenado de una cuña infinita[3], obtenemos la distribución universal de la magnetización en la transición de rellenado del sistema infinito en la geometría finita. Comparamos dichos resultados con los obtenidos mediante simulación del modelo de Ising para diferentes tamaños, obteniéndose un acuerdo razonable entre ambos. Ello nos permite, usando técnicas de repesado de histogramas, localizar de manera precisa la transición de rellenado de cuña crítica.

* enrome@us.es

[1] P. Concus y R. Finn, Proc. Natl. Acad. Sci. USA **63**, 292 (1969); Y. Pomeau, J. Colloid Interface Sci. **113**, 5 (1985); E. H. Hauge, Phys. Rev. A **46**, 4994 (1992).

[2] A. O. Parry, C. Rascón y A. J. Wood, Phys. Rev. Lett. **85**, 345 (2000); A. O. Parry, A. J. Wood y C. Rascón, J. Phys.: Condens. Matter **13**, 4591 (2001); M. J. Greenall, A. O. Parry y J. M. Romero-Enrique, J. Phys.: Condens. Matter **16**, 2515 (2004).

[3] J. M. Romero-Enrique y A. O. Parry, Europhys. Letters **72**, 1004 (2005); J. M. Romero-Enrique y A. O. Parry, J. Phys.: Condens. Matter **17**, S3487 (2005); J. M. Romero-Enrique y A. O. Parry New J. Phys. **9**, 167 (2007).

[4] A. Milchev, M. Müller, K. Binder y D. P. Landau, Phys. Rev. Lett. **90**, 136101 (2003); A. Milchev, M. Müller, K. Binder y D. P. Landau, Phys. Rev. E **68**, 031601 (2003).

Large Scale Modeling of the Self-Assembly of Nano-Objects using a Grid Interpolation technique

Thomas Roussel*, Lourdes F. Vega
[1] *Institut de Ciéncia de Materials de Barcelona Consejo Superior de Investigaciones Cientifícas*
[2] *MATGAS Research Center (Carburos Metalicos/Air Products, CSIC, UAB).*
Campus de la UAB, 08193 Bellaterra, Spain

One of the main challenges is to precisely position the first molecular building blocks in the first layer of thin films in order to tune their hetero-epitaxial properties, or else to adjust the substrates for further steps of growth. A fine balance of weak lateral molecule-molecule interactions and stronger molecule-substrate interactions governs their thermodynamic properties, nucleation and growth mechanisms. Especially with multi-components monolayers since their physical properties are composition dependent. To simulate the self-assembly of large flat-molecules (*i.e.*more than 50 atoms/molecule), the computational effort required increases rapidly with the number of molecules, and drastically when their number of atoms is consequent. Hence, to model the adsorption of several hundreds to thousands of molecules (meaning systems of 10^5 atoms) with a statistical mechanics approach, the internal degrees of freedom of the molecules and the substrates were frozen. It allows us performing full Grand Canonical Monte-Carlo calculations by implementing the grid interpolation technique[1]. We describe the system using empirical model, which provides transferability to many organic molecules[2] and metal surfaces[3] and the approach keeps the same precision than atomistic simulations.

We will first discuss study cases: the adsorption of Metal-Phthalocyanines-Halogenated ($ZnPcCl_8$ and $CuPcF_{16}$) on dense metal-transition surfaces (respectively Ag and Au). In the following figure, we show the typical self-assembled square phases of $ZnPcCl_8$ adsorbed on Ag_{111}, with a lattice spacing about 15.3 Å. The colors are scaled within the molecule-molecule (MOL-MOL) and molecule-substrate (MOL-SURF) potential energies. The closest matching supercell of the silver along the dense directions of the surface is about 14.5 by 15 Å. We observe directly the *point-line* hetero-epitaxial structure forming blue lines along the [110] direction of the surface every two rows of molecule, in agreement with already detailed experimental and DFT calculation[4]. We analyze the energetic balance related of the cluster size and orientations within their respective orientations with the substrate.

To demonstrate the transferability of the approach we will provide some other examples on Di-indenoperylene (DIP) on Au and Cu, and the consequences of edges on the metal surface on the resulting structures. Finally, we will discuss their bi-molecular stability.

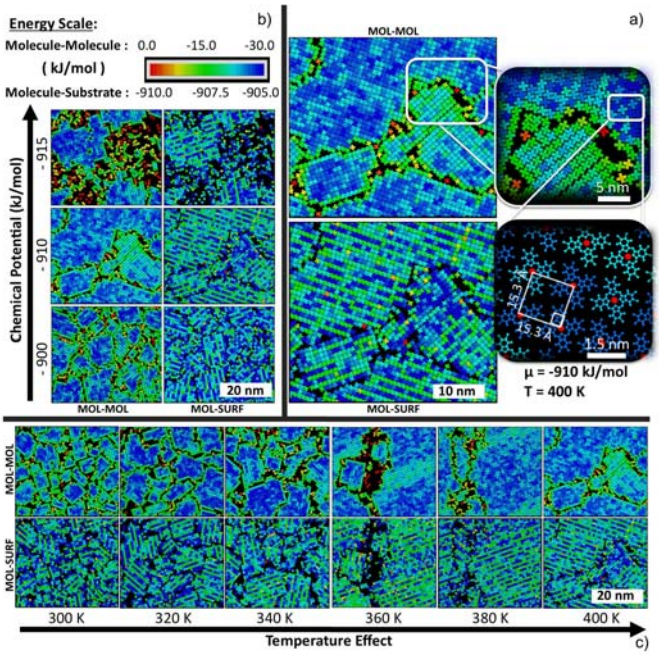

Figura 1. The different snapshots are illustrating a) the typical self-assembled square phases of $ZnPcCl_8$ adsorbed on Ag_{111}, and b) the chemical potential and c) temperature effects on the cluster size distribution and orientations.

* troussel @ icmab.es
This work is supported by the Spanish Government under NANOSELECT CSD2007-00041 and CTQ2008-05370 projects.

[1] Mannsfeld, S.C.B.; et al. *Modern Phys. Let. B*, 20, 11, 585 (2006)
[2] Jorgensen, W.L. et al. *JACS*, 118, 11225 (1996)
[3] Heinz, H.; et al. *J. Phys. Chem. C*, 112, 17281, (2008)
[4] Oison, V.; *Surf Sci.*, 601, 1040, (2007)

Propagación de Daño y orden ferromagnético en vidrios de spin tridimensionales

M. L. Rubio Puzzo*†, F. Romá‡, S. Bustingorry, P. M. Gleiser
Centro Atómico Bariloche, San Carlos de Bariloche, Río Negro, Argentina

El Modelo ±J de Edwards-Anderson (MEA)[1] exhibe una transición vítrea en tres dimensiones a una temperatura finita T_g la cual ha sido calculada numéricamente por diversos métodos, la mayoría de los cuales utilizan la idea de una longitud característica *global* que crece en la fase vítrea[2]. Sin embargo, no está esclarecido el origen del "orden" detrás de esta longitud creciente, así como la estructura subyacente de la fase vítrea a bajas temperaturas. En este marco, se ha propuesto recientemente un nuevo enfoque en el cual se identifican estructuras *locales* con características típicas de estados ordenados. Estas ideas se han extendido en la última década a través de un estudio sistemático de las heterogeneidades espacial y dinámica en los vidrios de spin[3–5]. En particular, el origen de las fuertes heterogeneidades dinámicas se ha revelado a partir del estudio de las heterogeneidades espaciales en el Estado Fundamental (EF) en el MEA[6]. En efecto, el estudio de las propiedades topológicas de las configuraciones del EF ha revelado que para una dada realización del desorden, los spines de cada configuración del EF de una muestra pueden ser separados en dos subgrupos: los spines *solidarios*, que mantienen su orientación relativa en todas las configuraciones de la muestra; y los spines *no-solidarios*, que no cumplen con esta condición[7]. La fracción de spines solidarios –en tres dimensiones– es aproximadamente el 76% de la muestra, y los mismos estan distribuídos en un gran cluster percolante y una serie de pequeñas islas cuyo tamaño se distribuye según una ley de potencias[7].

A partir de la información topológica, y luego de extensas simulaciones numéricas, es posible identificar exactamente para cada muestra el conjunto de spines solidarios y no-solidarios. Esto ha permitido estudiar la propagación de Daño[8] en el modelo, identificando y restringiendo las medidas de Daño a cada uno de los subconjuntos ya descriptos.

Los resultados obtenidos para el caso tridimensional muestran que cuando el sistema evoluciona según la regla dinámica de Metrópolis (spin-flipping)[9], el Daño crece para temperaturas mayores a T_g, la temperatura de la transición vítrea. Por otra parte, cuando se aplica dinámica de Baño Térmico (spin-orienting)[9], y para temperaturas en el rango $T_g < T < T_d$, el Daño se propaga sobre una región finita del sistema, formada por clusters finitos de carácter ferromagnético. En este caso, T_d es la temperatura crítica de la Transición de Daño en el MEA con dinámica de Baño Térmico (con $T_d \simeq T_c$, la temperatura crítica del modelo de Ising).

La existencia de estas dos temperaturas bien definidas (T_g y T_d) en el comportamiento del Daño, ha permitido caracterizar e identificar el origen de los clusters ferromagnéticos presentes en el sistema y de esta manera construir una imagen completa, e intuitiva, del origen del orden creciente en los vidrios de spin[10,11].

* lrubio@inifta.unlp.edu.ar; leticia.rubio@gmail.com
† Current Address: Instituto Carlos I de Física Teórica y Computacional, Universidad de Granada, Granada, España; Permanent Address: Instituto de Investigaciones Fisicoquímicas Teóricas y Aplicadas (INIFTA), Universidad Nacional de La Plata, CONICET, La Plata, Argentina.
‡ Permanent Address: Departamento de Física, Universidad Nacional de San Luis, San Luis, Argentina.

[1] S. F. Edwards and P. W. Anderson, *J. Phys. F* **5**, 965 (1975).
[2] H. G. Katzgraber, M. Körner and A. P. Young, *Phys. Rev. B* **73**, 224432 (2006).
[3] C. Chamon, M. P. Kennett, H. E. Castillo and L. F. Cugliandolo, *Phys. Rev. Lett.* **89**, 217201 (2002).
[4] H. E. Castillo, C. Chamon, L. F. Cugliandolo and M. P. Kennett, *Phys. Rev. Lett.* **88**, 237201 (2002).
[5] A. Montanari and F. Ricci-Tersenghi, *Phys. Rev. Lett.* **90**, 017203 (2003).
[6] F. Romá, S. Bustingorry, P. M. Gleiser, *Phys. Rev. Lett.* **96**, 167205 (2006); F. Romá, S. Bustingorry, P. M. Gleiser, D. Domínguez, *Phys. Rev. Lett.* **98**, 097203 (2007).
[7] F. Romá, A. J. Ramírez-Pastor, F. Nieto, S. Risau-Gusman and E. E. and Vogel, arXiv:1008.1249v1 (2010).
[8] M. L. Rubio Puzzo and E. V. Albano, *Commun. Comput. Phys.* **4**, 207 (2008).
[9] H. Hinrichsen, *Adv.Phys.* **49**, 815 (2000).
[10] M. L. Rubio Puzzo , F. Romá, S. Bustingorry and P. M. Gleiser, J. Stat. Mech. P09017 (2010).
[11] M. L. Rubio Puzzo , F. Romá, S. Bustingorry and P. M. Gleiser, Europhys. Lett. **91**, 37008 (2010).

Resonant cycle length polymodality and coherence in a noise-induced genetic oscillator

Pau Rué, Jordi Garcia-Ojalvo*
Departament de Física i Enginyeria Nuclear, Universitat Politècnica de Catalunya, Edifici GAIA, Rambla de Sant Nebridi s/n, Terrassa 08222, Barcelona, Spain

Gürol Süel
Green Center for Systems Biology and Department of Pharmacology, University of Texas Southwestern Medical Center, Dallas, TX 75390

Biological oscillations underlie many cellular functions, from basic processes such as cell growth and division to evolutionary environmental adaptations such as circadian rhythmicity. Some of these self-repeating processes exhibit a polymodal distribution of cycle lengths, consequence of the skipping of some periods. This is the case, for instance, of the cell cycle oscillations exhibited by Chinese hamster cells[1], fission yeast cells[2], and *Xenopus laevis* blastomeres[3]. In these organisms, cells not always divide when they are supposed to, giving rise to a distribution of cell-cycle periods that is not unimodal, but which exhibits secondary peaks at multiples of the cell-cycle period.

In this contribution we address the general question of how a limit cycle behavior with polymodal period distribution can arise in minimal oscillator models. To that end we consider a simple activator-inhibitor system operating in an excitable regime and subject to noise. We recently showed that such a model system exhibits noise-induced stabilization of an unstable focus point[4]. This system displays noise-triggered excursions away from the rest state, during which the cell passes through a region near the unstable focus. The stabilization mechanism consists in the appearance of oscillations around the unstable state, due to the stochastic fluctuations. As a consequence of these oscillations, the distribution of excursion times exhibits a marked polymodality: each oscillation around the unstable state introduces a well defined delay in the pulse duration. The pulses, however, are randomly triggered by noise and thus far from occurring regularly, a requirement for this mechanism to explain the polymodal cell-cycle duration distributions mentioned above. Nevertheless, excitable systems are known to exhibit stochastic coherence, with optimal period regularity observed for intermediate levels of noise. Here we show that stochastic coherence can be invoked, together with the noise-induced stabilization effect to provide a minimal mechanism for the generation of polymodal distributions of cycle lengths in an otherwise periodic behavior. In our setting, the level of intrinsic molecular noise is characterized by the system size, Ω, whose increase effectively scales up the numbers of molecular species (thus reducing the noise), while maintaining the concentrations constant.

Our results show that noise, besides enhancing the regularity of the pulse activations, also optimizes polymodality in the system's response. Furthermore, optimization of periodicity and polymodality are achieved when noise levels are comparable. Thus, when the coherence of the excitable pulses is maximized, so is the probability that the pulses undergo oscillations around the unstable spiral state. There is a range of noise levels for which optimization holds. Together, these results show that noisy activator-repressor genetic circuits can naturally behave as polymodal oscillators.

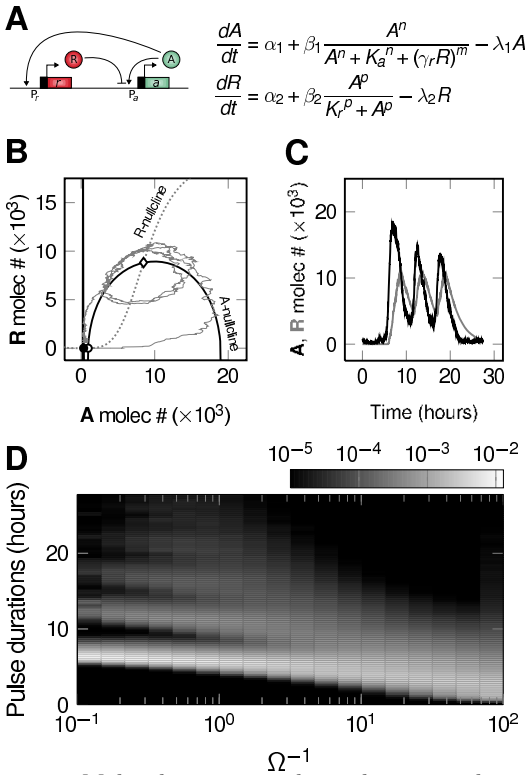

Figura 1. Molecular noise induces bursts with multiple pulses in the genetic activator-repressor model (**A**) by stabilizing an unstable spiral point (**B**, **C**). Optimal levels of molecular noise optimize the polymodality of the cycle lengths (**D**).

* jordi.g.ojalvo@upc.edu

[1] R. R. Klevecz, Proc Natl Acad Sci USA **73**,4012 (1976).
[2] A. Sveiczer, B.Ñovak,and J. M.Mitchison, J Cell Sci **109**,2947 (1996).
[3] Y. Masui and P. Wang, Biol Cell **90**, 537 (1998).
[4] M. Turcotte, J. Garcia-Ojalvo, and G. M. Süel, Proc Natl Acad Sci USA **105**,15732 (2008).

Dynamical simulations of virus wrapping and budding

Teresa Ruiz-Herrero *, Michael F. Hagan **, Enrique Velasco*
* *Departamento Física Teórica de la Materia Condensada, Universidad Autónoma de Madrid, Madrid, Spain*
** *Department of Physics, Brandeis University, Waltham, MA, 02454, USA*

Enveloped viruses bud through the cell membrane as the final step in their replication process. For many enveloped viruses, a nucleo-protein capsid first assembles in the cytoplasm, attaches to the membrane, and then buds. We explore this process through modeling the wrapping of a spherical particle by a model bilayer membrane, using coarse-grained molecular dynamics simulations and a theoretical elastic model. Specifically, we study the kinetics and morphologies of wrapping as a function of the relevant system parameters, including the particle radius, the strength of the membrane-particle interaction, and the membrane bending rigidity. The theoretical model predicts a phase diagram as a function of the system parameters, which is compared to results of the dynamics simulations. Furthermore, the simulations elucidate the dynamical mechanisms by which budding occurs and the structures of intermediate configurations.

* teresa.ruiz@uam.es

[1] S.Tzlil, M. Deserno, W. M. Gelbart and A. Ben-Shaul Biophysical Journal, Volume 86, Issue 4, 2037-2048, 1 April 2004

[2] Rui Zhang and Toan T. Nguyen. Phys. Rev. E 78, 051903 (2008)

Confined aqueous electrolytes within cylindrical nanocavities

J. Sala[†*], P. Videla[‡], D. Laria[‡], J. Martí[†], E. Guàrdia[†]
[†] *Departament de Física i Enginyeria Nuclear, Universitat Politécnica de Catalunya, Campus Nord, B4-B5 08034 Barcelona, Spain*
[‡] *Departamento de Química Inorgánica, Analítica y Química-Física e INQUIMAE. Facultad de Ciencias Exactas y Naturales. Universidad de Buenos Aires, Ciudad Universitaria, Pabellón II, 1428, Buenos Aires, Argentina*

With recent advances in nanotechnology, physicochemical processes at the nanoscale will become increasingly important. Many processes, such as nanoparticle synthesis and reverse osmosis, involve aqueous electrolytes confined in nanostructures. In this communication we present the results of a series of molecular dynamics (MD) simulation studies on sodium chloride aqueous solutions confined within cylindrical silica pores. Confinement was examined in fully periodic systems comprising a single pore immersed in a sodium chloride aqueous solution at 1 molar concentration. The silica pore was generated following closely the procedure described in previous papers.[1] Two different pores, differing in their interface structures, were analyzed. (i) The first ones, hereafter referred to as hydrophobic cavities, were modeled by assuming that liquid-solid site-site interactions were exclusively of the Lennard-Jones type. (ii) Effects from chemical functionalization in the pore walls were examined in hydrophilic cavities, in which dangling oxygen atoms lying at the pore interface were hydroxylated. Silanol groups were generated by attaching mobile hydrogen atoms, with a geometrical arrangement similar to the one described in Ref. 2. In each case, three different values of the pore radius, i. e. R=10, 15 and 17.5 Å, were considered. A snapshot of a typical MD configuration corresponding to a hydrophobic cavity is depicted in Fig. 1.

MD simulations were performed with the NAMD package.[3] Each system was simulated for a time period of approximately 30 ns. A thorough analysis of the structure, single particle and collective dynamic properties was carried out. Special attention was devoted to separately analyze the properties of bulk and interfacial ions. Finally, our present results were compared with previous studies of unconfined electrolyte solutions.[4,5]

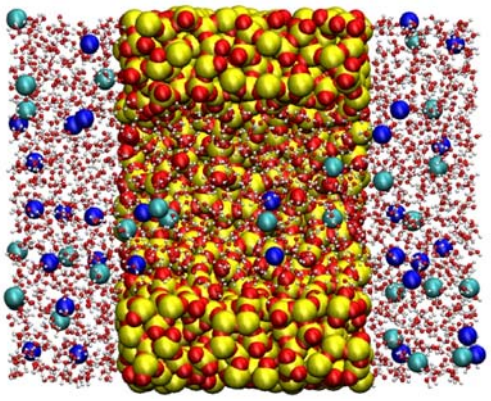

Figura 1. Snapshot of a typical MD configuration corresponding to a hydrophobic cavity. Si atoms are in yellow and O atoms are in red. Na^+ and Cl^- ions are in blue.

* jonas.sala@upc.edu

[1] J. Rodriguez, M. D. Elola, and D. Laria, J. Phys. Chem. B **114**, 7900 (2010) and references therein.
[2] N. Giovambattista, P. J. Rossky, and P. G. Debenedetti, Phys. Rev. E **73**, 041604 (2006).
[3] `http://www.ks.uiuc.edu/Research/namd/`
[4] E. Guàrdia, D. Laria and J. Martí, J. Phys. Chem. B **110**, 6332 (2006)
[5] J. Sala, E. Guàrdia, and J. Martí, J. Chem. Phys. **132**, 214505 (2010).

Numerical Study of Natural Convection Inside a Horizontal Cylinder

O. Sánchez Casals*, I. Mercader, O. Batiste
Departamento de Física Aplicada
Universidad Politècnica de Catalunya
08034 Barcelona

The numerical study of convective flows of enclosed fluids has attracted much research activity in the past due to its relevance in many engineering applications such as crystal growth of semiconductors. During this process, natural convection may generate defects like striations. For a low Prandtl number fluid contained in a differentially heated horizontal cylindrical cavity, convection always exists, but above a critical temperature difference between the endwalls of the cavity, the flow changes from a stationary to an oscillatory behavior. This passage from one state to another could affect the quality of grown crystal due to the complex dynamics of flow. Several authors have investigated numerically the thermogravitational flows for cylindrical enclosures[1–3].

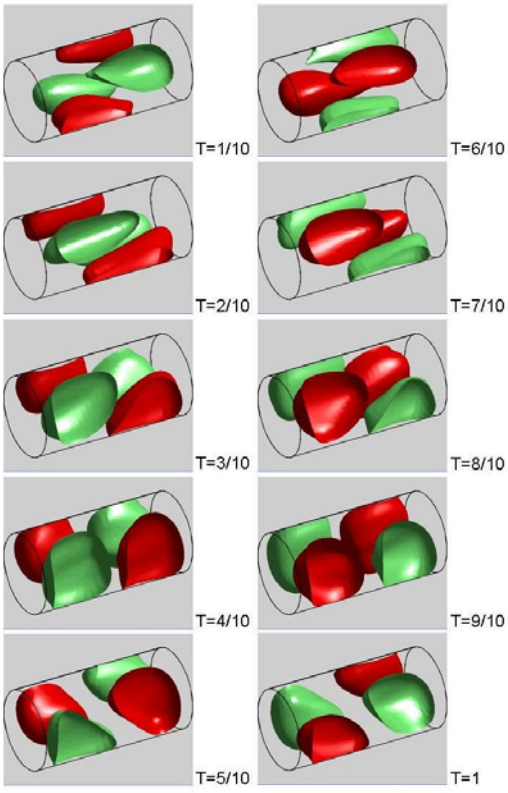

Figura 1. One period time sequence of bubble-like perturbations of temperature field.

In this work, a numerical study for analyzing the main features of the basic flow and the instability of natural convection in a cylindrical enclosure is performed by using a combination of a second order time-splitting method and a pseudo-spectral approach[4]. The efficient code used for solving the Navier Stokes equations in a vertical cylinder[4] has been adapted for studying the three-dimensional convective flow in a horizontal cylinder. In the vertical mid-plane *XZ (Y = 0)*, we expect to find some agreement with 2D simulations of Mercader et al[5].

We have also chosen an aspect ratio $\Gamma = 2$ ($\Gamma = length/diameter$) as in Mercader et al.[5] with Prandtl number $\sigma = 0.00715$, such that the system maintains a basic single-roll flow configuration. In this basic configuration, the vector plot reveals that the fluid flows from the hot to the cold wall in the upper part of the cylinder, and flows back from the cold to the hot wall in the lower part. It is responsible for heat convection, leading to vertical temperature gradients within the central region.

The dependence of the threshold value of Rayleigh number and critical frequency with the aspect ratio is also studied. The nature of the instability is the same in the range of aspect ratios from 1.5 to 2.5: a supercritical Hopf bifurcation that breaks two reflection symmetries of the basic flow and maintains their product. The instability is characterized by a periodic movement of bubble-like perturbations traveling along the contour of the basic roll (see FIG. 1).

* odlyss@gmail.com

[1] V. Kurian, M. Varma, A. Kannan, Numerical studies on laminar natural convection inside inclined cylinders of unity aspect ratio,*Int. J. of Heat and Mass Transfer* 52, pp. 822-838 (2009).
[2] L. Davoust, R. Moreau, M.D. Cowley, P.A. Tanguy, F. Bertrand, Numerical and analytical modelling of the MHD buoyancy-driven flow in a Bridgman crystal growth configuration,*Journal of Crystal Growth* 180, pp. 422-432 (1997).
[3] S. Vaux, H. Ben Hadid, D. Henry, Study of the hydrodynamic instabilities in a differentially heated horizontal circular cylinder corresponding to a Bridgman growth configuration, *Journal of Crystal Growth* 290, pp. 674–682 (2006).
[4] I. Mercader, O. Batiste, A. Alonso. An efficient spectral code for incompressible flows in cylindrical geometries, *Computers and Fluids* 39 pp. 215-224 (2010).
[5] I. Mercader, O. Batiste, L. Ramirez-Piscina, X. Ruiz, S. Rüdiger, J. Casademunt, Bifurcations and chaos in single-roll natural convection with low Prandtl number, *Physics of Fluids* 17, 104108 (2005).

Frequency detuning and communication between brain areas

Belén Sancristóbal, Raul Vicente†, Gordon Pipa†, Jordi Garcia-Ojalvo
Departament de Física i Enginyeria Nuclear
Universitat Politècnica de Catalunya Rambla de Sant Nebridi s/n 08222 Terrassa, Spain

Coupled oscillators are well known to shift their natural frequencies and eventually reach a frequency locking regime. Usually these oscillators are supposed to be harmonic and the coupling diffusive. This is a rare situation in nature, since biological oscillators, for instance, have a broad frequency spectrum and their phase dynamics are highly non-stationary due to the variety of incoming inputs. In many cases, diffusive coupling (if at all present) is not the most relevant type of connection, as most biological systems rely on a chemical transmission of information that is closer to pulse coupling rather than to diffusive coupling.

We have studied the relevant case of coupled brain oscillations, in particular those recorded in *the local field potential (LFP)* that reflects the average synaptic activity of a neuronal network. To that end, we have modeled a cortical population composed of randomly connected Hodgkin-Huxley neurons, including both excitatory and inhibitory elements. The parameters characterizing the dynamics of the ionic channels in the neuronal membrane, as well as the time constants of the neurons and the synapses (both GABA and AMPA), are tuned according to experimental observations.

Each neuron receives a Poisson train of excitatory action potentials of slowly varying rate, resulting in a firing activity of the individual neurons that is low and irregular (Fig. 1, top). In spite of the seemingly irregular dynamics of single neurons, a faster collective rhythm emerges (bottom panel of Fig. 1), apparent in the LFP, resulting from the recurrence within the population that gives place to alternation of periods of excitation and inhibition.

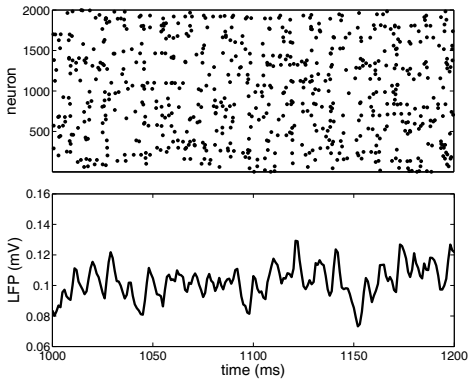

Figura 1. Rasterplot (top panel) and LFP (bottom panel) of a simulated cortical network of 2000 neurons receiving a non-homogeneous Poisson train of action potentials at an average rate of 2.4 kHz.

We have characterized the changes in the frequency peak in the gamma range (30 Hz–80 Hz) of the LFPs of two cortical populations in terms of the coupling strength and directionality.

Using these neuronal oscillations, we have tested the hypothesis of *communication through coherence*[1], according to which oscillations emerging as a collective behavior of a group of neurons provide a mechanism for the control of communication between distinct brain areas. We have found, in a simple scheme of brain connectivity, the conditions for which two neuronal populations oscillate coherently (see Fig. 2), so that their phase difference at precise frequencies remains constant for some interval of time and is unchanged from trial to trial.

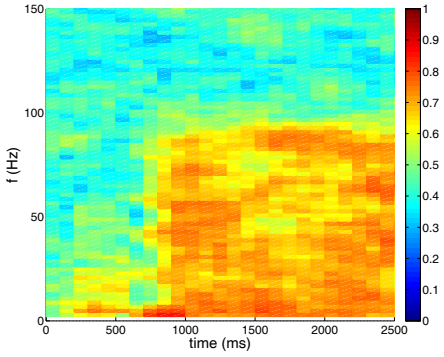

Figura 2. Coherence index (colored scale) between two neuronal populations. A value of 1 indicates that the phase difference between two oscillatory signal is unchanged across trials. In this case the two signals are the LFPs of two neuronal populations bidirectionally coupled at $t = 1000$ ms.

If the two neuronal groups maintain their phase coherence, the transmission delay of action potentials from one group to the other can be expected to play a crucial role in order to choose at which LFP-phase of the postsynaptic group the presynaptic action potentials arrive. Depending on that phase, the receiving neurons will be excited above threshold or not, as has been experimentally proven by Singer and colleagues[2]. Our modeling results indicate that this firing selectivity might underlie the mechanism of communication through coherence.

---

† Department of Neurophysiology, Max Planck-Institut, Deutschordenstraβe 46, 60528 Frankfurt am Main, Germany

[1] P. Fries, Trends Cogn Sci **9**, 474, (2005).
[2] M. Volgushev, M. Chistiakova, and W. Singer, Neuroscience **83**, 15 (1998).

Translational and rotational velocity correlations and cumulants in a granular gas

Andrés Santos*, Gilberto M. Kremer†
Departamento de Física, Universidad de Extremadura, E-06071 Badajoz, Spain

We consider a dilute granular gas of hard spheres (of diameter σ, mass m, and moment of inertia I) colliding inelastically with coefficients of normal and tangential restitution α and β, respectively. The basic quantities characterizing the distribution function $f(\mathbf{r},\mathbf{v},\boldsymbol{\omega};t)$ of linear ($\mathbf{v}$) and angular ($\boldsymbol{\omega}$) velocities are the second-degree moments defining the translational ($T^{\rm tr}$) and rotational ($T^{\rm rot}$) temperatures. The deviation of f from the Maxwellian distribution parameterized by $T^{\rm tr}$ and $T^{\rm rot}$ can be represented by the cumulants a_{20}, a_{11}, a_{02}, and b associated with fourth-degree velocity moments. They are defined as[1–3]

$$\langle(\mathbf{v}-\mathbf{u})^4\rangle = \frac{15}{4}\left(\frac{2T^{\rm tr}}{m}\right)^2(1+a_{20}), \tag{1}$$

$$\langle\omega^4\rangle = \frac{15}{4}\left(\frac{2T^{\rm rot}}{I}\right)^2(1+a_{02}), \tag{2}$$

$$\langle(\mathbf{v}-\mathbf{u})^2\omega^2\rangle = \frac{9}{4}\frac{2T^{\rm tr}}{m}\frac{2T^{\rm rot}}{I}(1+a_{11}), \tag{3}$$

$$\langle[(\mathbf{v}-\mathbf{u})\cdot\boldsymbol{\omega}]^2\rangle - \frac{1}{3}\langle(\mathbf{v}-\mathbf{u})^2\omega^2\rangle = \frac{5}{4}\frac{2T^{\rm tr}}{m}\frac{2T^{\rm rot}}{I}b. \tag{4}$$

The parameters a_{20} and a_{02} measure the kurtosis of the translational and rotational distribution functions, respectively. The translational-rotational correlations are measured by a_{11} and b.

The main objective of this work is the evaluation of the collisional rates of change of these second- and fourth-degree moments by means of a Sonine approximation

$$\phi(\mathbf{c},\mathbf{w}) \approx \phi_M(\mathbf{c},\mathbf{w})\Big\{1 + a_{20}S^{(2)}_{\frac{1}{2}}(c^2) + a_{02}S^{(2)}_{\frac{1}{2}}(w^2) + a_{11}S^{(1)}_{\frac{1}{2}}(c^2)S^{(1)}_{\frac{1}{2}}(w^2) + b\left[(\mathbf{c}\cdot\mathbf{w})^2 - \frac{1}{3}c^2w^2\right]\Big\}, \tag{5}$$

where $S^{(n)}_p(x)$ are Sonine polynomials of degree n and

$$\mathbf{c} \equiv \frac{\mathbf{v}-\mathbf{u}}{\sqrt{2T^{\rm tr}/m}}, \quad \mathbf{w} \equiv \frac{\boldsymbol{\omega}}{\sqrt{2T^{\rm rot}/I}}, \tag{6}$$

$$\phi(\mathbf{c},\mathbf{w}) \equiv \frac{1}{n}\left(\frac{4T^{\rm tr}T^{\rm rot}}{mI}\right)^{3/2} f(\mathbf{v},\boldsymbol{\omega}), \tag{7}$$

$$\phi_M(\mathbf{c},\mathbf{w}) = \pi^{-3}e^{-c^2-w^2}. \tag{8}$$

The results are subsequently applied to the computation of the temperature ratio $T^{\rm rot}/T^{\rm tr}$ and the cumulants of two paradigmatic states: the homogeneous cooling state and the homogeneous steady state driven by a white-noise stochastic thermostat. It is found in both cases that the Maxwellian approximation for the temperature ratio does not deviate much from the Sonine prediction. On the other hand, non-Maxwellian properties measured by the cumulants cannot be ignored, especially in the homogeneous cooling state for medium and small roughness. In that state, moreover, the cumulant directly related to the translational velocity differs in the quasi-smooth limit $\beta \to -1$ from that of pure smooth spheres ($\beta = -1$), as illustrated in Fig. 1. This singular behavior is directly related to the unsteady character of the homogeneous cooling state and thus it is absent in the stochastic thermostat case.[3]

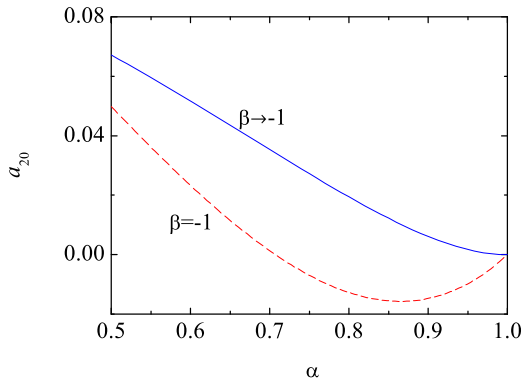

Figura 1. Plot of the HCS cumulant a_{20} (assuming $b = 0$) versus the coefficient of normal restitution α for $\beta = -1$ (dashed line) and in the limit $\beta \to -1$ (solid line).

* andres@unex.es
† Departamento de Física, Universidade Federal do Paraná, Curitiba, Brazil; kremer@fisica.ufpr.br

[1] N. V. Brilliantov, T. Pöschel, W. T. Kranz, and A. Zippelius, Phys. Rev. Lett. **98**, 128001 (2007).
[2] W. T. Kranz, N. V. Brilliantov, T. Pöschel, and A. Zippelius, Eur. Phys. J. Spec. Top. **179**, 91 (2009).
[3] A. Santos, G. M. Kremer, and M. dos Santos, Phys. Fluids (in press).

Teoría y simulación de Histéresis Angular en gotas sésiles

M. J. Santos*, J. A. White†
Departamento Física Aplicada. Facultad de Ciencias
Universidad de Salamanca
37008 Salamanca

La ecuación de Young[1] describe el ángulo de contacto de equilibrio θ_{Young} para una gota sobre un substrato. De acuerdo con esta ecuación, θ_{Young} tiene un valor único que sólo depende de las energías libres interfaciales entre las fases sólida, líquida y vapor. En la práctica, sin embargo, debido a la naturaleza heterogénea del substrato sólido se observan una serie de ángulos de contacto estables, este fenómeno es conocido como *histéresis del ángulo de contacto*, o *histéresis angular*.

Experimentalmente es posible obtener un ciclo de histéresis aumentando (con una jeringuilla o una pipeta) el volumen de una gota de líquido depositada sobre un substrato y posteriormente retirando el líquido, disminuyendo así su volumen. Se observa que el ángulo de contacto no es el mismo durante estos dos procesos. Denominando θ_a al *ángulo de contacto de avance* (primera fase) y θ_r al *ángulo de contacto de retroceso* (segunda fase), se verifica: $\theta_r \leq \theta_{Young} \leq \theta_a$.

En este trabajo se trata de reproducir los resultados experimentales obtenidos por C.N.N. Lam *et al.*[2] en un ciclo de histéresis de una gota de agua depositada en una superficie sólida consistente en una oblea de silicio recubierta de ácido poliláctico. Para ello se siguen dos métodos, por un lado la resolución de la ecuación de *Young-Laplace* y por otro una simulación con el programa *Surface Evolver*[3]. En ambos casos, se introduce en término de fricción que permite describir adecuadamente la histéresis angular.

a) Se resuelve la *ecuación de Young-Laplace en coordenadas cilíndricas*. Se evoluciona la gota variando el volumen en pequeños incrementos, aumentándolo desde V_i a V_f y luego disminuyéndolo, a velocidad constante en ambos casos. En la Fig. 1 se representan los resultados obtenidos para el radio de contacto, ρ, y el ángulo de contacto, θ, en función del tiempo. También se representa la variación del volumen V frente al tiempo.

b) *Surface Evolver*[3] es un programa informático destinado al modelado de la forma de superficies sometidas a diferentes fuerzas o ligaduras. Dadas sus características *Surface Evolver* es una herramienta ideal para el análisis de gotas sésiles a partir de sus interfaces. Éstas son descritas por medio de una triangulación (Fig. 2) que puede modificarse (refinándose) y reajustarse durante el proceso de minimización de la energía del sistema. Posteriormente se comparan los resultados con los obtenidos experimentalmente por Lam *et al.*[2] y resolviendo la ecuación de Young-Laplace (Fig. 1).

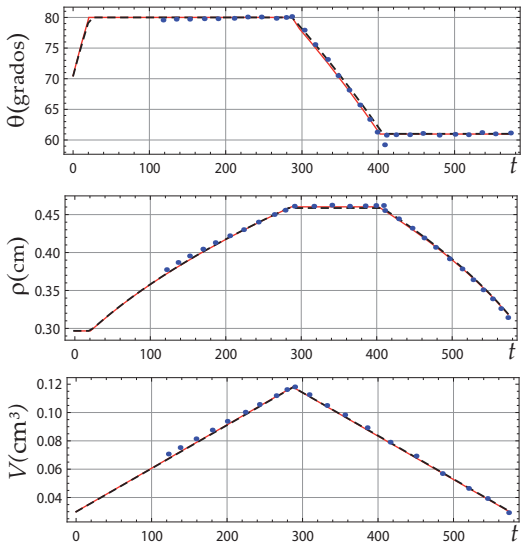

Figura 1. Ciclo de histéresis de una gota de agua. Comparación de los resultados experimentales de Lam *et al.*[2] (puntos azules) con los obtenidos a partir de la *ecuación de Young-Laplace* (línea continua roja) y de simulación con *Surface Evolver* (línea discontinua negra).

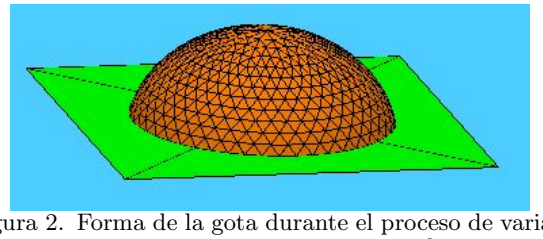

Figura 2. Forma de la gota durante el proceso de variación de volumen con el programa *Surface Evolver*[3].

* smjesus@usal.es
† white@usal.es

[1] T. Young, Philos. Trans. R. Soc. London, 95 (1805) 65.
[2] C.N.C. Lam et al. *Advances in Colloid and Interference Science* 96 (2002) 169-191
[3] Brakke, K.A., *Exp. Math.* 1(2), 141 (1992).

Crystallization Mechanism of Hard Sphere Glasses

Eduardo Sanz, Chantal Valeriani, Emanuela Zaccarelli, Wilson Poon, Peter Pusey, Mike Cates
SUPA School of Physics and Astronomy, University of Edinburgh, Mayfield Road, Edinburgh EH9 3JZ, United Kingdom.

In supercooled liquids, vitrification generally suppresses crystallization. Yet some glasses can still crystallize despite the arrest of diffusive motion. This ill-understood process may limit the stability of glasses, but its microscopic mechanism is not yet known. Here we present extensive computer simulations addressing the crystallization of monodisperse hard-sphere glasses at constant volume (as in a colloid experiment). Multiple crystalline patches appear without particles having to diffuse more than one diameter. As these patches grow, the mobility in neighbouring areas is enhanced, creating dynamic heterogeneity with positive feedback. The future crystallization pattern cannot be predicted from the coordinates alone: crystallization proceeds by a sequence of stochastic micro-nucleation events, correlated in space by emergent dynamic heterogeneity.

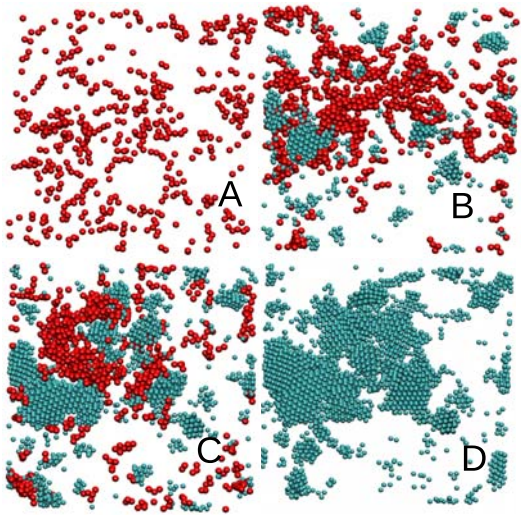

Figura 1. Slab in the xy plane showing the 5% most mobile particles (in red) and the crystalline particles (in light blue)at time $t = 0$ (A), $t = 320$ (B), $t = 640$ (C) and $t = 1280$ (D). Mobile particles are ranked by the distance they move between the time of the frame at which they are shown and the subsequent frame (accordingly, frame D does not show mobile particles). Mobile particles are spatially correlated with crystalline ones and have a higher tendency to become crystalline than "average" amorphous particles.

* esanz@ph.ed.ac.uk

[1] E.Sanz,C.Valeriani,E.Zaccarelli,W.C.K.Poon,P.N.Pusey and M.E.Cates *Phys.Rev.Lett.* in press (2011).

Network-based scoring system for genome-scale metabolic reconstructions

M. Ángeles Serrano, Francesc Sagués
Departament de Química Física, Universitat de Barcelona, Martí i Franquès 1, 08028 Barcelona, Spain

Network reconstructions at the cell level are a major development in Systems Biology. However, we are far from fully exploiting its potentialities. Often, the incremental complexity of the pursued systems overrides experimental capabilities, or increasingly sophisticated protocols are underutilized to merely refine confidence levels of already established interactions. For metabolic networks, the currently employed confidence scoring system rates reactions discretely according to nested categories of experimental evidence or model-based likelihood. Here, we propose a complementary network-based scoring system that exploits the statistical regularities of a metabolic network as a bipartite graph. As an illustration, we apply it to the metabolism of *Escherichia coli*. The model is adjusted to the observations to derive connection probabilities between individual metabolite-reaction pairs and, after validation, to assess the reliability of each reaction in probabilistic terms. This network-based scoring system uncovers very specific reactions that could be functionally or evolutionary important, identifies prominent experimental targets, and enables further confirmation of modeling results. We foresee a wide range of potential applications at different sub-cellular or supra-cellular levels of biological interactions given the natural bipartivity of many biological networks.

Drift of a spiral wave in a heterogeneous heart tissue

Ana Simic, Jean Bragard
Departamento de Fisica y Matematica Aplicada
Facultad de Ciencias
31008 Pamplona

It is widely accepted, based on numerous numerical, experimental and theoretical studies, that spiral wave reentry underlies different types of cardiac arrhythmia. Moreover, such patterns are present in great variety of excitable systems. Dynamics of such a wave is characterized by motion of it's tip, which depending on the system's parameters and model in use, can produce diverse patterns ranging from rigid rotation to meander patterns with inward or outward petals differing in shape and length. It has been shown that presence of different heterogeneities or particular conditions can significantly affect the motion of a spiral wave causing it to drift in particular direction. Drift of a spiral wave has also been reported experimentally in cardiac tissue[1]. As heterogeneities are very important in the genesis and stability of cardiac arrhythmias, we have numerically explored the drift of an induced spiral in a piece of a two dimensional heterogeneous tissue. Gradient is applied in a form of smooth gradient of system's parameters. Some basic mechanisms for spiral wave drift using simple two variable models and Luo-Rudy 1 model for excitable tissue have been elucidated[2,3]. However, as the time scale of spiral drift is similar to the one of calcium dynamics, it makes it interesting to study drift in physiologically detailed model.

[1] Davidenko, A. V. Pertsov, R. Salomonsz, W. Baxter, J. Jalife, *Nature* **355**, 349(1992)
[2] V. Krinsky, E. Hamm, V. Voignier,*Physical Review Letters*, **76**, 3854(1996)
[3] K. H. W. J. Ten Tusscher, A. V. Panfilov, *Am J Physiol Heart Circ Physiol* **284**, H542 (2003)

Magneto-rheological properties of stiff magnetic filaments near an adsorbing surface

Pedro A. Sánchez[1], Joan J. Cerdá[1], Tomás Sintes[1]*, V. Ballenegger[2], Christian Holm[2]
[1] *Instituto de Física Interdisciplinar y Sistemas Complejos, IFISC (CSIC-UIB), Universitat de les Illes Balears, 07122 Palma de Mallorca, Spain*
[2] *Institute for Computational Physics. Universität Stuttgart. 70569 Stuttgart, Germany*

Despite magnetic filaments have been used by nature since long time ago in magnetostatic bacterias[1], Humankind has just begun to caress its potential for novel applications[2]. The continuous improvements on the synthesis of artificial magnetic filaments, reducing the size of the magnetic particles and improving the grafting between particles, has set the onset in the creation of particles which resemble magnetic polymers but in the scale of tenths of nanometers. In difference to the magnetic polymers[3], the magnetic filaments can exhibit non-zero magnetization at room temperature. The study of the physical properties of such systems via numerical simulations can help to elucidate the potential of the magnetic filaments for practical applications.

In the present work[4] the adsorption of stiff magnetic filaments close to an attractive surface is studied thoroughly via extensive Langevin dynamics simulations (LD). Magnetic filaments are represented by a coarse-grained bead-spring model where each bead bears a point dipole located at its center and the excluded volume interaction is introduced via a soft-core repulsive potential. We find strong evidence for the existence of two transitions as the temperature is lowered. First, the system undergoes a continuum phase transition from the desorbed to the adsorbed state. This transition is followed by a second structural transition that takes place when the filaments are already adsorbed. The adsorption transition is found to be very similar to the one observed for stiff non-magnetic polymer chains[5] where the chain bending interaction plays a similar role as the magnetic component of the present case. However, the tendency of the magnetic chains to stretch is reversed by a further reduction in temperature and the chains tend to form closed adsorbed loops leading to a second structural transition. A representation of the phase diagram for the adsorption of magnetic filaments is determined here for the first time. We also present a novel way to determine the temperature at which the chain is adsorbed that is based on the analysis of the change in the number of trains, tails and loops developed by the polymer chain during the adsorption process.

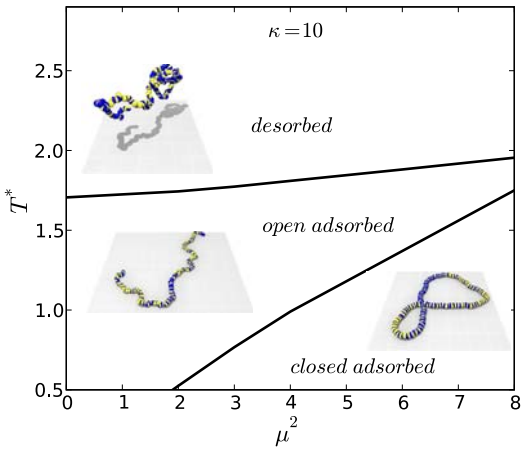

Figura 1. Representation of the phase diagram of a single stiff magnetic filament near an adsorbing surface for moderate values of the magnetization ($\mu^2 < 10$)

* tomas@ifisc.uib-csic.es

[1] A. Komeili *et al.*, *Science* **311**, 242 (2006)
[2] S. J. Blundell *et al.*, *J. Phys. Condens. Matter* **16**, R771 (2004)
[3] M. Kamachi, *J. Macromol. Sci.* **C42**, S41 (2002)
[4] Sánchez, *et al.*, *Soft Matter* DOI 10.1039/c0sm00772b (2011)
[5] T. Sintes, *et al.*, *Macromolecules* **34**, 1352 (2001)

Investigating the folding kinetics in DNA hairpins using molecular constructs with short and long handles

N. Forns, S. de Lorenzo, M. Manosas, K. Hayashi, J. M. Huguet, and F. Ritort*
Small Biosystems Lab
Facultad de Física
Universidad de Barcelona
08028 Barcelona

Laser optical tweezers is a single molecule technique that allow us to exert and to measure the mechanical forces on individual biological systems. By measuring tiny forces and distances (in the pN and nanometer ranges, respectively), this technique allows us to investigate the folding kinetics and the free energies of formation of single molecules such as DNA, RNA or proteins. In optical tweezers experiments the molecular setup consists of the molecule of interest flanked by two handles, generally double stranded DNA (dsDNA), one handle located at each side of the molecule and this construct is tethered between two polystyrene beads. Previous works (1,2) have revealed the influence of the length of the handles on the folding/unfolding kinetics. Longer handles (less stiff) tend to give faster kinetics that short handles. Here we show the results of our experiments on the folding kinetics in DNA hairpins using dsDNA handles of 700bp, and a new extremely short design dsDNA handles of 29 bp (3). Moreover we present a novel method based on the analysis of high-bandwidth noise force fluctuations at different forces that provides a way to measure the stiffness of the optical trap and the stiffness of the molecular system tethered between the beads.

* fritort@gmail.com

[1] Wen J.-D, et al. Force unfolding kinetics of RNA using optical tweezers. I. Effects of experimental variables on measured results. *Biophys.J.92:2996-3009 (2007)*

[2] Manosas M., et al. Force unfolding kinetics of RNA using optical tweezers. II. Modeling experiments. Biophys.J.92:3010-3021 (2007). *Biophys.J.92:3010-3021 (2007)*

[3] Forns.N., et al. Improving signal-to-noise resolution in single molecule experiments using molecular constructs with short handles. *Biophys.J.100:1765-1774 (2011)*

Experiments on Patterned Neuronal Cultures

Sara Teller*[1], Javier G. Orlandi[1], Enric Álvarez-Lacalle[2], Jaume Casademunt[1], Elisha Moses[3], Jordi Soriano[1]
[1] *Departament d'Estructura i Constituents de la Matèria, Universitat de Barcelona, Barcelona, Spain*
[2] *Departament de Física Aplicada, Universitat Politècnica de Catalunya, Barcelona, Spain*
[3] *Department of Physics of Complex Systems, Weizmann Institute of Science, Rehovot, Israel.*

Neuronal networks, from the smallest culture to the entire brain, are characterized by a rich repertoire of spontaneous rhythmic dynamics, in the form of electric activity that propagates throughout the system. Spontaneous activity in the brain plays a fundamental role in the development of synaptic connections and is crucial for proper synchronization between brain areas. The principles that govern the emergence, propagation, and stability of spontaneous activity fronts are proving elusive to the neuroscience community. In particular, the interplay between the connectivity of a neuronal network and its dynamics is still a fundamental paradigm.

Neuronal cultures are excellent model systems to study fundamental questions of neuronal networks, from connectivity and structure to learning, plasticity, and propagation of information[1,2]. Here we present experiments designed to shed light on the role of neuronal connectivity on spontaneous neuronal dynamics. We use the concept of *patterned neuronal cultures*, where neurons and connections are guided or constrained along predefined circuits.

We consider one–dimensional (1D) and two–dimensional (2D) patterns. 1D patterns are prepared by chemically printing a circuit on a glass substrate[1,3]. The circuit is typically 70 μm wide and $3-5$ cm long. Activity starts spontaneously at any point of the circuit and propagates with a stable velocity towards its ends. By increasing or reducing the connectivity of the network using different chemical agents one can extract important information on the mechanisms that sustain a stable propagating front[3].

2D patterns are prepared by using a topographical mold made of PDMS and manufactured using soft–lithography. Neurons are then placed over the mold in such a way that they grow and connect only along the valleys of the pattern. Patterned cultures show a repertoire of activity that is much richer and complex than standard, non–patterned cultures. For instance, we observe that the front advances in the form of patches of activity that propagate following complex paths, and with a velocity that is about 100 times slower than standard cultures. We also observe that activity preferentially starts in specific areas known as 'Burst Initiation Zones'. Altogether, patterned cultures offer an excellent and versatile tool to understand the emergence and maintenance of spontaneous activity in neuronal networks. They also provide the experimental platform for our theoretical modelling of spontaneous activity based on dynamical systems and complex networks.

---

* teller.sara@gmail.com

[1] J. P. Eckmann , O. Feinerman, L. Gruendlinger, E. Moses, J. Soriano and T. Tlusty, Phys. Rep., **449**, 54 (2007).
[2] J. Soriano, M. Rodríguez Martínez, T. Tlusty and E. Moses, Proc. Natl. Acad. Sci. USA, **105**, 13758 (2009).
[3] S. Jacobi, J. Soriano and E. Moses, J Neurophysiol **104**, 2932 (2010).

Inter-spike correlations induced by dichotomous noise modulation in an excitable laser

Jordi Tiana-Alsina[1*], Tilo Schwalger[2] , M. Carme Torrent[1], Benjamin Lindner[2], Jordi Garcia-Ojalvo[1]
[1] *Departament de Física i Eng. Nuclear, Universitat Politècnica de Catalunya, Edif. GAIA, 08222 Terrassa, Barcelona, Spain*
[2] *Max-Planck-Institut für Physik komplexer Systeme, Nöthnitzer Strasse 38, 01187 Dresden, Germany.*

The behavior of certain natural and technological systems often takes the form of sequences of discrete events (point processes), whose statistical properties can be controlled both by the internal dynamics of the system and by the environmental conditions to which the system is subjected. Correlations in the time intervals between subsequent events (named inter-spike intervals, ISIs, in what follows) arise in certain circumstances and can be functionally relevant. This is the case, for instance, of sensory neurons, in which ISI correlations are known to increase information transfer[1] by reducing low-frequency noise[2]. A natural question is then, what is the simplest mechanism leading to ISI correlations?

In this contribution we show experimentally that environmental conditions alone can lead to correlations, by examining the response of an excitable laser to a random dichotomous modulation of its pump current. Our experimental system consists in a diode laser subject to optical feedback through an external mirror. Due to the action of the delayed feedback, the laser exhibits (provided the feedback strength is moderate and the pump current is close to threshold) a spiking dynamics in the form of uncorrelated trains of brief power dropouts that can be interpreted as excitable pulses[3] as shown in Fig. 1(a). The spiking rate (k_i) depends on the laser pump current. In Fig. 1(b), we plot the autocorrelation function of the ISI intervals. Note that, for this particular case, ISIs at non-zero lags are completely uncorrelated, and thus we can interpret this dynamical regime as a renewal point process.

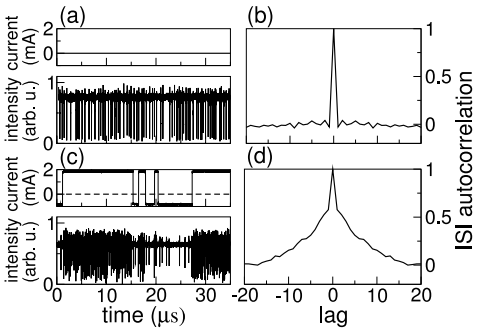

Figura 1. Dichotomous noise modulation induces ISI correlations. Laser output [bottom traces in (a,c)] in response to a given pump current [top traces in (a,c)]. The corresponding autocorrelation functions of the ISI sequence are shown in plots (b,d).

Next, we analyze the effect of environmental variations on the ISI statistics of the laser emission. Dichotomous noise leads to a varying firing rate (Fig. 1(c)) that results in a pattern of ISI correlations (Fig. 1(d)) that matches the one obtained analytically from a discrete, M-state kinetic model[4,5]. This agreement supports our interpretation of the experimentally observed correlations as arising solely from the environmental driving, and not from the (somewhat complicated) dynamics of the laser.

Figure 2 plots the first-order correlation coefficient ρ_1 versus the ratio of the firing rates, k_2/k_1, corresponding to the two pump current levels of the dichotomous modulation. The experimental results exhibit, in qualitative agreement with the theoretical analysis, a local maximum of the first-order correlation as the variable firing-rate ratio decreases. The three data sets combine measurements of two different lasers, different reference levels of the pump current, and different feedback characteristics. The fact that the system behaves in the same qualitative way for these very varied conditions highlights the reproducibility of the results.

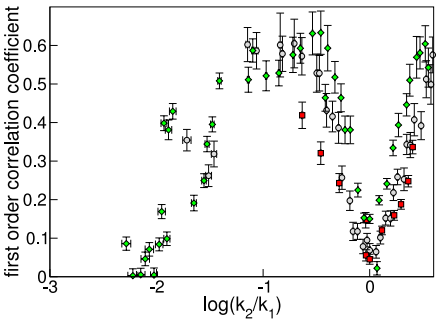

Figura 2. First-order correlation coefficient ρ_1 as function of $\log(k_2/k_1)$, for three different values of k_1: 6.5 MHz (grey circles), 10 MHz (red squares), and 15 MHz (green squares). The switching rate for the dichotomous modulation is in all cases $\lambda = 100$ kHz.

These results shed light on the minimal requirements to generate correlations in spike time series, showing in particular, that no specific mechanisms intrinsic to the spiking system are necessary.

* jordi.tiana@upc.edu

[1] M. J. Chacron, A. Longtin, and L. Maler, *J. Neurosci.*, **21**, 5328 (2001).
[2] M. J. Chacron, B. Lindner, and A. Longtin, *Fluct. Noise Lett.* **4**, 195 (2004).
[3] J. Mulet and C. R. Mirasso, *Phys. Rev. E* **59**, 5400 (1999).
[4] B. Lindner and T. Schwalger, *Phys. Rev. Lett.* **98**, 210603 (2007).
[5] B. Lindner and T. Schwalger, *Eur. Phys. J. Special Topics* **187**, 211 (2010).

Transversal dynamics of paramagnetic colloids in a longitudinal magnetic ratchet

Pietro Tierno*
Departament de Química Física, Universitat de Barcelona, Martí i Franquès 1, 08028 Barcelona, Spain

In this talk I will describe the transversal motion of paramagnetic particles above the magnetic stripe pattern of a uniaxial garnet film, exhibiting a longitudinal ratchet effect in the presence of an oscillating magnetic field[1]. First I will focus on the behaviour of one colloid. Without the field, the thermal diffusion coefficient obtained by video microscopy is $D_0 \sim 10^{-4}\mu m^2/s$. With the field, the transversal diffusion exhibits a giant enhancement by almost four decades and a pronounced maximum as a function of the driving frequency. It is possible to explain the experimental findings with a theoretical interpretation in terms of random disorder effects within the magnetic film[2].

On the second part of this talk I will focus on the collective dynamics of an ensemble of paramagnetic particles organized as a one-dimensional chain and driven above the magnetic film. The centre of mass of the chain shows a diffusive behavior with mean square displacement $\sim t$, while its end-to-end distance shows anomalous kinetics with a sub-diffusive growth $\sqrt{t}$. It is possible to extract the potential of mean force between the particles within the chain by invoking the Pope-Ching equation[3]. Thus the experimental data are interpreted by using the Rouse model, originally developed for polymers, and all relevant parameters are extracted experimentally[4].

---

* ptierno@ub.edu

[1] P. Tierno, S. V. Reddy, T. H. Johansen, and T. M. Fischer Phys. Rev. E **75**, 041404 (2007); P. Tierno, S. V. Reddy, M. G. Roper, T. H. Johansen, and T. M. Fischer, J. Phys. Chem. B , **112**, 3833 (2008).

[2] P. Tierno, P. Reimann, T. H. Johansen, and Francesc Sagués Phys. Rev. Lett. **105**, 230602 (2010).

[3] S. B. Pope and E. S. C. Ching, Phys. Fluids A 5, 1529 (1993); E. S. C. Ching, Phys. Rev. E 53, 5899 (1996).

[4] P. Tierno, Francesc Sagués, T. H. Johansen, and I. M. Sokolov in preparation.

On the Gaussian approximation for master equations

R. Toral, L. F. Lafuerza
IFISC, Instituto de Física Interdisciplinar y Sistemas Complejos, CSIC-Universitat de les Illes Balears, Campus UIB, 07122 Palma de Mallorca

Master equations are a convenient tool to treat stochastic Markov processes[1,2]. In some cases, they offer an alternative approach to the Chapman-Kolmogorov equation and have been used extensively in discrete-jumps, or birth-death, processes, such as chemical reactions (including those happening inside a cell), population dynamics or other ecology problems[3], opinion formation and cultural transmission in the field of sociophysics[4], etc. In all these cases, it is important to consider that the population number (whether molecules, individuals, agents, etc.) might not be very large (maybe ranging in the tens or hundreds) and the fluctuations, whose relative magnitude typically scales as the square root of the inverse of this number, can not be considered as negligible. It is therefore, of the greatest importance to derive evolution equations for the average behavior and the fluctuations. The important work by van Kampen[1] offers a systematic way of deriving these equations from an expansion of the master equation in a parameter Ω, typically the system volume. The Ω-expansion is mostly used in its lowest order form, in which one can prove that the error in the average value, the second moment and the fluctuations (the variance), scale at most as Ω^0, Ω^1 and $\Omega^{1/2}$, respectively. The van Kampen Ω-expansion, furthermore, shows that, at this lowest order, the fluctuations follow a Gaussian distribution. We take this result of van Kampen's theory and, considering from the very beginning that fluctuations are Gaussian, we derive a closed system of equations for the average value and the second moment[5]. This Gaussian closure of the hierarchy of moments turns out to be more accurate than the Ω-expansion as the above-mentioned errors scale at most as $\Omega^{-1/2}$, $\Omega^{1/2}$ and $\Omega^{1/2}$, respectively. Furthermore, the Gaussian closure scheme is very simple to carry on in practice and can be easily generalized to systems described by more than one variable. Therefore, the Gaussian approximation is more accurate, which turns out to be important, specially for small values of Ω. This scaling of the errors is valid for all times provided that the macroscopic law has a fixed point as a single attractor[1]. In both schemes the validity of the approximations might be limited for large times when there is more than one absorbing state, or a single one different from the attractor of the macroscopic law, since in those cases the distribution eventually approaches a sum of delta-functions. We have checked these results by comparing the performance of the two methods in three examples: (i) a binary chemical reaction $A + B \underset{\omega}{\overset{\kappa}{\rightleftarrows}} C$, (ii) an autocatalytic reaction $A \overset{k}{\longrightarrow} X$, $2X \overset{k'}{\longrightarrow} B$ and (iii) a recently introduced model[6] in which the process of opinion formation in a society considers two main parties, A and B, plus an intermediate group of undecided agents I; the supporters of A and B do not interact among them, but only through their interaction with the group I, convincing one of its members with a given probability. In all cases studied, the Gaussian closure has given a better approximation to the average and the second moment, although the Ω-expansion, due to a cancellation of errors, yields a somehow smaller numerical error in the variance. In general, and compared to other field-theoretical methods available in the litrature[7,8], the Gaussian closure scheme is very simple to carry on in practice and this simplicity and the improvement of the predictive power is more apparent in many-variable systems. We believe that this method can be usefully applied to the study of other problems of recent interest in the literature involving stochastic processes in systems with a small number of particles.

[1] N. G. van Kampen, *Stochastic Processes in Physics and Chemistry*, (North-Holland, Amsterdam, 2004).
[2] C. W Gardiner, *Handbook of Stochastic Methods for Physics, Chemistry and the Natural Sciences* (Springer-Verlag, 1990).
[3] D. T. Gillespie, *Exact stochastic simulation of coupled chemical reactions* J. Phys. Chem. **81**,2340 (1977).
[4] Castellano, C., Fortunato, S., Loreto, *Statistical physics of social dynamics* V. Rev. Mod. Phys. **81**, 591 (2009).
[5] L.F. Lafuerza, R. Toral, J. Stat. Phys. **140**, 917-933 (2010).
[6] M. S. de la Lama, I.G. Szendro, J.R. Iglesias, H.S. Wio, *Van Kampen's expansion approach in an opinion formation model*, Eur. Phys. J. B **51**, 435 (2006).
[7] M.Doi, *Second quantization representation for classical many-particle system*, J. Phys. **A 9**, 1469 (1976).
[8] L. Peliti, *Path integral approach to birth-death processes on a lattice*, J. Physique **46**,1469 (1985).

Delivering nutrients to a tissue: blood flow and capillary growth

Rui D. M. Travasso*, Tobias Schwartz, Eugenia Corvera Poiré†, Mario Castro‡, Juan Carlos Rodríguez-Manzaneque§, Orlando Oliveira, Joana Oliveira††, A. Hernández-Machado§§
Centro de Física Computacional
Universidade de Coimbra
Rua Larga, 3004-516 Coimbra, Portugal

Understanding angiogenesis (the growth of new vessels starting from existing vasculature) is a challenging problem with important consequences for the treatment of cancer and other pathological situations. We present different aspects of an integrated approach to the description of capillary growth and blood flow in heath and disease.

We introduce a multi-scale phase-field model for the description of angiogenesis that combines the benefits of continuum physics description and the capability of tracking individual cells. The model allows us to discuss the role of the endothelial cells' chemotactic response and proliferation rate as key factors that tailor the neovascular network. Importantly, we also test the predictions of this theoretical model against relevant experimental approaches in mice that displayed distinctive vascular patterns. The model reproduces the in vivo patterns of newly formed vascular networks, providing quantitative and qualitative results for branch density and vessel diameter on the order of the ones measured experimentally in mouse retinas.

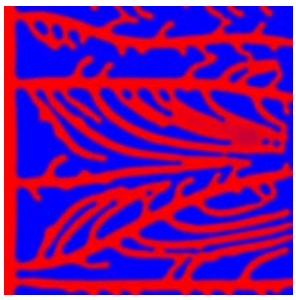

For a correct understanding of capillary dynamics it is also necessary to analyze tissue irrigation resulting from the blood flow in the newly formed network. In particular we analyze the alterations in irrigation of a tissue where there is local vessel disruption (due to low levels of VEGF and high concentrations of Ang-2), an event that occurs in the early stages of diabetic retinopathy. We identify the foci of neo-vascularization and show that there is a vascular network dependent critical disrupted area above which non-local hypoxia exists in the tissue, leading to an hyper-vascularized phenotype.

Our results highlight the ability of physical models to suggest relevant hypotheses with respect to the role of different parameters in these process, hence underlining the necessary collaboration between modeling, in vivo imaging and molecular biology techniques to improve current diagnostic and therapeutic tools.

* rui@teor.fis.uc.pt
† Departamento de Física y Química Teórica, Facultad de Química, Universidad Nacional Autónoma de México. México DF 04510, Mexico
‡ GISC and Grupo de Dinámica No-lineal (DNL), Escuela Téc. Sup. de Ingeniería (ICAI), Universidad Pontificia Comillas, E28015, Madrid, Spain
§ GENYO (Pfizer-University of Granada-Andalusian Government Centre for Genomics and Oncological Research), 18007, Granada, Spain
†† CFP and Departmento de Enginharia Física, R. Dr. Roberto Frias, 4200-465 Porto, Portugal
§§ Departament ECM, Facultat de Física, Universitat de Barcelona. Diagonal 647, E-08028 Barcelona, Spain

The role of asymmetric interactions on the effect of habitat destruction in mutualistic networks

Guillermo Abramson[†], Claudia Trejo Soto[*‡], Leonardo Oña[§]

[†] *Centro Atómico Bariloche, R8400AGP Bariloche, Argentina*

[‡] *Departament de d'Estructura i Constituents de la Màteria, Universitat de Barcelona, Avinguda Diagonal 647, E-08028 Barcelona, Spain*

[§] *Department of evolutionary genetics, Max Planck Institute for Evolutionary Anthropology, Deutscher Platz 6, 04103 Leipzig, Germany*

Plant-pollinator mutualistic networks are asymmetric in their interactions: specialist plants are pollinated by generalist animals, while generalist plants are pollinated by a broad involving specialists and generalists. It has been suggested that this asymmetric —or disassortative— assemblage could play an important role in determining the equal susceptibility of specialist and generalist plants under habitat destruction. At the core of the argument lies the observation that specialist plants, otherwise candidates to extinction, could cope with the disruption thanks to their interaction with generalist pollinators. We present a theoretical framework that supports this thesis. We analyze a dynamical model of a system of mutualistic plants and pollinators, subject to the destruction of their habitat. We analyze and compare two families of interaction topologies, ranging from highly assortative to highly disassortative ones, as well as real pollination networks. We found that several features observed in natural systems are predicted by the mathematical model. First, there is a tendency to increase the asymmetry of the network as a result of the extinctions. Second, an entropy measure of the differential susceptibility to extinction of specialist and generalist species show that they tend to balance when the network is disassortative. Finally, the disappearance of links in the network, as a result of extinctions, shows that specialist plants preserve more connections than the corresponding plants in an assortative system, enabling them to resist the disruption.

[*] claudiat@ecm.ub.es

Análisis de la variabilidad multiescala en series temporales de precios de materias primas

Antonio Turiel*, Conrad Pérez-Vicente**
* *Institut de Ciències del Mar, CSIC, Passeig Marítim de la Barceloneta, 37-49, 08003 Barcelona.*
** *Facultat de Física, Universitat de Barcelona, Martí i Franqués, 1, 08028 Barcelona.*

El análisis multifractal es una herramienta muy potente para el estudio y descripción de series temporales complejas con propiedades multiescala. Por medio de la correcta estimación de los exponentes de singularidad en cada punto (que son medidas de la regularidad o irregularidad locales) se puede descomponer la señal bajo análisis en dos componentes: una señal reducida, que es funcionalmente muy simple (el dominio de su derivada contiene sólo tres valores, -1,0 y 1) pero que incorpora toda la variabilidad de pequeña escala (dinámica rápida) asociada a la estructura multifractal de la señal original; y un campo de fuentes, de variación suave (dinámica lenta) y cuya estructura es continua excepto en determinados puntos de transición, que delimitan los dominios de validez de la descripción. En los últimos años, la introducción de este tipo de descomposición para el análisis de series econométricas ha permitido empezar a analizar las propiedades estocásticas que están directamente asociadas a las características geométricas de las series, simplemente analizando las matrices de transición que operan sobre el campo de tres valores de la derivada de la serie reducida.

Sin embargo, la separación de las series en componente reducida y componente de fuentes no es excesivamente estable debido a que en esencia implica una segunda derivada, con lo que el ruido obscurece casi completamente la señal al aplicarse a datos reales. Se han propuesto diversas aproximaciones metodológicas para obtener una estimación robusta de esta descomposición, del enfoque más restrictivo al más general; en este trabajo discutiremos las diferentes metodologías y sus virtudes y defectos, hasta centrarnos en el método más estable de determinación de fuentes, el de la regresión multiescala bilateral.

Demostraremos la potencia de esta aproximación metodológica aplicándola a series temporales de precios de materias primas, que han sido muy volátiles durante los últimos años. El objetivo de nuestro estudio es clasificar algunas signaturas características de estos mercados mediante el análisis multifractal de las series de sus precios. Hemos analizado dos tipos de serie, la serie de precios spot del barril de petróleo Brent y la serie de cotizaciones diarias de la onza de oro, y hemos intercomparado sus resultados para tratar de cuantificar la importancia relativa de algunos factores que los analistas suelen arguir para justificar la volatilidad de los precios.

Colloids in a bacterial bath: simulations and experiments

Chantal Valeriani, Martin Li, John Novosel, Jochen Arlt, Davide Marenduzzo
SUPA School of Physics and Astronomy, University of Edinburgh, Mayfield Road, Edinburgh EH9 3JZ, United Kingdom.

We present a joint experimental and computational study of the effect of bacterial motion on micron-scale colloids contained in a two-dimensional suspension of Bacillus Subtilis. With respect to previous work using E. coli, here we introduce a novel experimental set-up that allows us to realise a two-dimensional bacterial suspension insensitive to either evaporation or fluid flow.

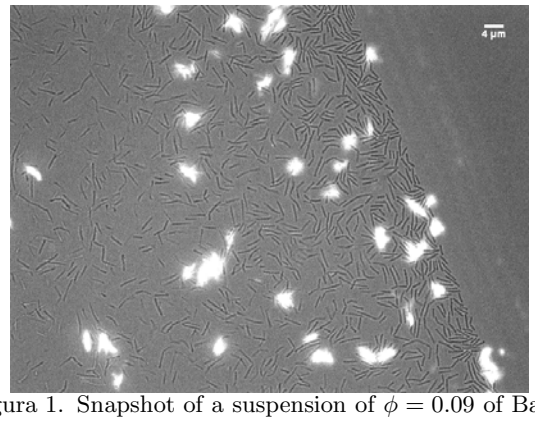

Figura 1. Snapshot of a suspension of $\phi = 0.09$ of Bacillus Subtilis cells sandwiched between two oxygen-plasma-treated cover-slips, where 5% of cells are fluorescently stained. Bacterial cell bodies appear black in the figure.

By analysing the mean square displacements of both bacteria and colloids, we confirm the existence of a crossover from super-diffusive behaviour at short time scales to normal diffusion at longer times. We also study the same two-dimensional system by means of numerical simulations, using a suspension of self-propelled dumbbells or the Vicsek model, which has been previously used to study the dynamics of active particles. Our numerical results obtained with both models are in broad agreement with the experimental trends, but only the dumbbell simulations can match the experimental data quantitatively. The level of agreement we find suggest that steric interactions due to collisions are important players in determining collective motion of the bacterial bath, and should complement hydrodynamic interactions in experiments.

---

* cvaleria@ph.ed.ac.uk

[1] C.Valeriani,M.Li,J.Novosel,J.Arlt and D.Marenduzzo, *Soft Matter* in press (2011).

Divide and Conquer

Teresa Vaz Martins*, Raúl Toral
IFISC, Instituto de Física Interdisciplinar y Sistemas Complejos, CSIC-UIB
Campus UIB
E- 07122 Palma de Mallorca

We consider systems composed of many units forced by signals that too weak to be detected by a single uncoupled unit. We show that when the units interact via a combination of attractive and repulsive links, the sensitivity of the system to weak signals increases for a given proportion of repulsive links, leading to a significant collective coherent response.

We establish the mechanism of response enhancement through competitive interactions in different types of systems, whose common characteristic is the possession of some form of threshold. Thus, we consider prototypical bistable[1],[2], oscillatory[3] or excitable[3] systems, as well as models of opinion formation[4]. Although different systems exploit different routes to achieve an optimization of the response, we observe in all cases a coincidence between the proportion of repulsive links that optimizes the response, and the one that leads to some particular form of disorder.

Thus, we can place the research in a broader context of the effects of disorder on the response properties of nonlinear systems subjected to weak forcing. Competitive interactions are taken as a source of disorder, as an alternative to previous studies where response was amplified by disorder induced by noise[5] or diversity[6].

This work opens up wider perspectives about the role of repulsive links in information processing in various systems where the presence of competitive interactions is known to exist, but its function hasn't been yet established.

---

* teresa@ifisc.uib-csic.es

[1] T. Vaz Martins, V. N. Livina, A. P. Majtey, R. Toral, Physical Review E **81**, 041103 (2010).
[2] T. Vaz Martins, R. Toral, M. A. Santos, European Physical Journal B **67**, 329-336 (2009).
[3] T. Vaz Martins, R. Toral, Synchronisation Induced by Repulsive Interactions in a System of van der Pol Oscillators, Submitted, (2011)
[4] T. Vaz Martins, M. Pineda, R. Toral, EPL **91**, 48003 (2010).
[5] L. Gammaitoni, P. Hänggi, P.Jung, F. Marchesoni, Rev. Mod. Phys. **70**, 223, (1998).
[6] C. Tessone, C.R. Mirasso, R. Toral, J.D. Gunton, Phys. Rev. Lett. **97**, 194101, (2006).

Effect of polydispersity and soft interactions on the nematic vs. smectic phase stability in platelet suspensions

Y. Martínez-Ratón[1], E. Velasco[2]
[1] *GISC, Departamento de Matemáticas, Escuela Politécnica Superior, Universidad Carlos III de Madrid, E-28911 Leganés (Madrid)*
[2] *Departamento de Física Teórica de la Materia Condensada, Universidad Autónoma de Madrid, E-28049 Madrid*

The issue of polydispersity is crucial to understand phase behaviour in experiments on colloidal suspensions of particles with rod- or plate-like shape, since colloidal particles can never be made truly identical and phase equilibria is very much affected by polydispersity. Non-spherical colloidal particles are known to form liquid-crystalline phases, such as nematic, smectic and columnar, but the nematic phase is difficult to obtain experimentally in charge-stabilised platelike particles before the formation of smectic, columnar or gel phases. The observation of equilibrium nematic phases in platelets requires fine-tuning of the ionic strength of the solvent. Therefore, the concomitant effects of polydispersity and soft interactions seem to be an important issue as regards the stabilisation of the nematic phase.

In this communication we discuss theoretically, using density-functional theory, the phase stability of nematic and smectic ordering in a suspension of platelets of the same thickness but with a high polydispersity in diameter, and study the influence of polydispersity on this stability[1]. The platelets are assumed to interact like hard objects, but additional soft attractive and repulsive interactions, meant to represent the effect of depletion interactions due to the addition of non-absorbing polymer, or of screened Coulomb interactions between charged platelets in an aqueous solvent, respectively, are also considered. The aspect (diameter to thickness) ratio is taken to be very high, in order to model solutions of mineral platelets recently explored experimentally[2]. In this régime a high degree of orientational ordering occurs; therefore the model platelets can be taken as completely parallel and are amenable to analysis via a fundamental-measure theory. Our focus is on the nematic vs. smectic phase interplay, since a high degree of polydispersity in diameter suppresses the formation of the columnar phase due to incommensuration with a single lattice parameter of the triangular lattice formed by the columns.

When interactions are purely hard, the theory predicts a continuous nematic-to-smectic transition, regardless of the degree of diameter polydispersity. However, polydispersity enhances the stability of the smectic phase against the nematic phase. Predictions for the case where an additional soft interaction is added are obtained using mean-field perturbation theory. In the case of the one-component fluid, the transition remains continuous for repulsive forces, and the smectic phase becomes more stable as the range of the interaction is decreased. The opposite behaviour with respect to the range is observed for attractive forces, and in fact the transition becomes of first order below a tricritical point. Also, for attractive interactions, nematic demixing appears, with an associated critical point. When platelet polydispersity is introduced the tricritical temperature shifts to very high values.

Finally, we discuss the implications of our theoretical approach for recent experiments being performed on colloidal platelets made of α-Zirconium phosphate in an aqueous solution, for which the nature of interactions between the platelets is not clear and the interpretation of their phase behaviour is uncertain.

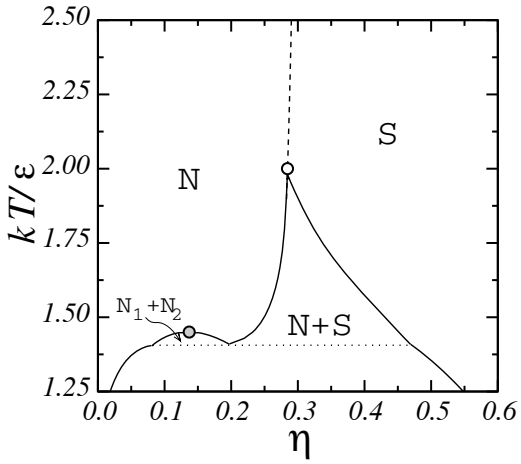

Figura 1. Temperature-scaled density phase diagram of the polydisperse attractive platelet model for medium-range interactions.

[1] Y. Martínez-Ratón and E. Velasco, submitted to J. Chem. Phys.
[2] D. Sun, H.-J. Sue, Z. Cheng, Y. Martínez-Ratón and E. Velasco, Phys. Rev. E **80**, 041704 (2009).

Malware como depredador en ecosistemas ip

Rafael Vida[1], Elka Korutcheva[2]
[1] *Grupo Interdisciplinar de Sistemas Complejos (GISC). Departamento de Fisica Fundamental, Universidad Nacional de Educacion a Distancia, Madrid, España,*
[2] *Departamento de Fisica Fundamental, Universidad Nacional de Educacion a Distancia, Madrid, España*

La transferencia de datos de malware (abreviatura de Malicious Software) supone en ocasiones cerca del 60% del volumen mundial de datos en Internet, y en el caso de correo electrónico en España cerca del 97%. Para asegurar la continuidad de éste tipo de servicios de comunicaciones es necesario *limpiar* la red de datos no deseados.

Hasta ahora los esfuerzos se concentran en la verificación de malware en los extremos, o en la comprobación de la existencia de vulnerabilidades (debilidades en la protección del software) conocidas en los sistemas que acceden a las redes de comunicaciones.

Esta aproximación *a posteriori* ha demostrado ser, además de ineficaz, costosa desde un punto de vista computacional.

El funcionamiento del malware es tal que la eliminación de una botnet, por ejemplo, tarda semanas en ser reemplazada por otra nueva redistribución de software distinto, pero que se distribuye usando las mismas vulnerabilidades. Los sistemas de detección de intrusos y antivirus están diseñados, en general, de forma que detectan patrones o firmas en el software que se distribuye, pero no consideran la red lógica que establecen las vulnerabilidades.

Como las vulnerabilidades persisten, los nuevos virus y ataques compiten por ella como *recursos*, y la velocidad de propagación de la nueva infección es mayor que la capacidad de reacción del software de protección. Véase la figura III, en la que se representan datos reales de la caída de la botnet McColo y la evolución del malware en los dos meses siguientes.

Este tipo de comportamiento permite modelizar el conjunto de sistemas como un *ecosistema*, en el que el software atacante compite por los recursos, es decir, las vulnerabilidades existentes en los elementos de la red.

Este trabajo pretende analizar y entender la dinámica poblacional del *ecosistema virtual* y la relación entre dicha dinámica y la estructura lógica subyacente. Para ello se estudiará el proceso de difusión del malware hasta su situación de equilibrio que se alcanza (según [1]). Adicionalmente nos interesa conocer el efecto de la topología de la red compleja sobre el tiempo en alcanzar el nuevo equilibrio.

Se abordará la topología lógica desde varios niveles de abstracción, definida por el malware en diferentes niveles de capas de red de comunicaciones (IP, TCP, aplicación).

De esta manera, se analizará el efecto de la introducción de un nuevo elemento depredador en la red, que imitando el comportamiento del malware, permitirá identificar las posiciones lógicas en las redes IP que permitan romper el equilbrio alcanzado, de tal manera que se mitigue o elimine el efecto del virus, a base de competir con los *depredadores* por los recursos existentes.

El mismo análisis permitirá, adicionalmente, localizar las zonas lógicas en las que los sistemas de análisis de tráfico en busca de anomalías y recogida de información de seguridad relevante son más eficientes.

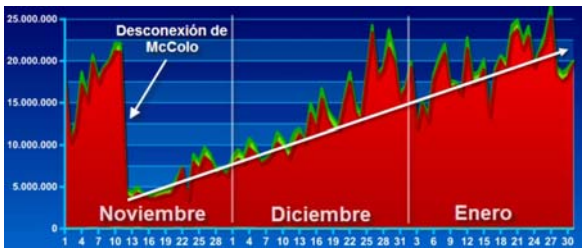

Figura 1. Recuperación del malware tras la eliminación de la botnet Mccolo. Fuente: Telefònica Grandes Clientes, España.

* rvida@upcomillas.es

[1] Z. Chen and C. Ji, *Spatial-temporal modeling of malware propagation in networks*, IEEE Transactions on Neural Networks (2005).
[2] Y. Song, G.P. Jiang, Y. Gu, *Modeling malware propagation in complex networks based on cellular automata*, Circuits and Systems, 2008. APCCAS 2008. IEEE Asia Pacific Conference on, (2009).
[3] P.P. Reddy and P.R. Reddy, *Modeling the Spread of Malware in Computer Networks* (2009).
[4] K.I. Goh, W. Cho, J. Choi, L.M. Lee, and I.M. and Kim, *Correlated couplings and robustness of coupled networks*, Bulletin of the American Physical Society (2011).

Crystal polymorphism of a water monolayer under hydrophobic nanoconfinement

Oriol Vilanova*, Giancarlo Franzese*
Departament de Física Fonamental, Universitat de Barcelona, Barcelona, Spain

Bulk water presents a large number of crystalline and amorphous ices. Hydrophobic nanoconfinement is known to affect the tendency of water to form ice and to reduce the melting temperature. However, a systematic study of the ice phases in nanoconfinement is hampered by the computational cost of simulations at very low temperatures. Here we develop a coarse-grained model for a water monolayer in hydrophobic nanoconfinement and study the formation of ice by Mote Carlo simulations. We find two ice phases: low-density-crystal ice at low pressure and high-density hexatic ice at high pressure, an intermediate phase between liquid and high-density-crystal ice[1].

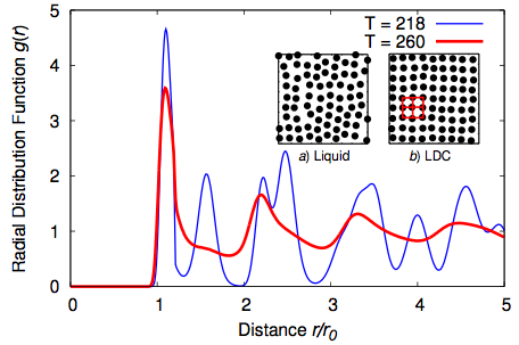

(a) Low pressure at $P = 0.06$ GPa

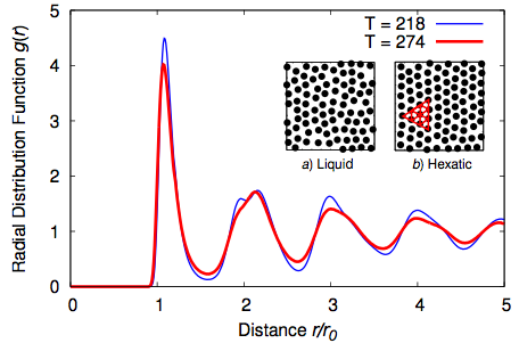

(b) High pressure at $P = 0.24$ GPa

Figura 1. Radial Distribution Functions for different state points. (a) At $P = 0.06$ GPa and $T = 246$ K (in the liquid phase) and $T = 218$ K (in the LDC phase). Here and in the next panel, insets show a portion of typical configurations at the state points represented in the main panels. The $g(r)$ for the LDC has many peaks correspoding to the long-range trans- lational order of the square crystal, while the $g(r)$ for the liquid near the coexistence shows precursors of the LDC structure. (b) At $P = 0.24$ GPa and $T = 274$ K (in the liquid phase) and $T = 218$ K (in the hexatic phase). The liquid $g(r)$ has a shoulder in the second peak that splits into a small peak in the hexatic phase. The hexatic phase has liquid-like short-range translational order due to the pres- ence of many disclinations, but crystal-like long-range ori- entational order, emphasized by links in the inset describ- ing the hexatic phase.

* oriol.vilanova@gmail.com, gfranzese@ub.edu

[1] O. Vilanova and G. Franzese, Structural and dynamical properties of nanoconfined supercooled water, pre-print arXiv:1102.2864 (2011).

Diffusion in macromolecular crowded media: Monte Carlo simulation of obstructed diffusion vs. FRAP experiments

Eudald Vilaseca*, Isabel Pastor†, Adriana Isvoran††, Sergio Madurga†††, Josep-Lluís Garcés‡, Francesc Mas‡‡
Departament de Química Física i Institut de Química Teòrica i Computacional (IQTCUB)
Facultat de Química, Universitat de Barcelona
Martí i Franquès, 1. 08028 Barcelona

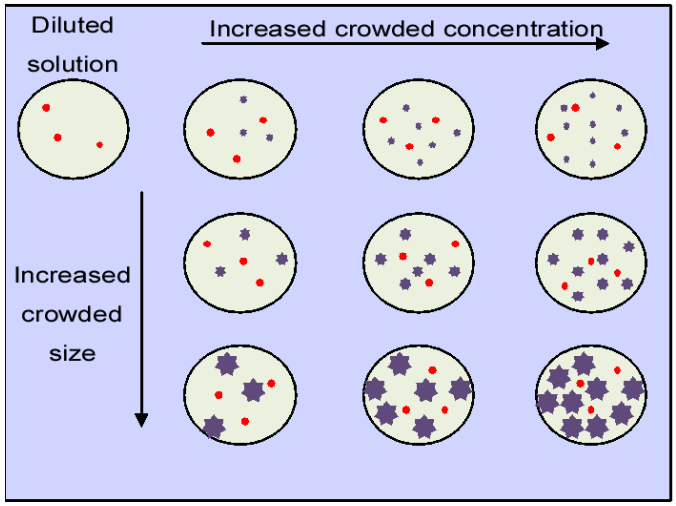

Figura 1. Different system conditions for simulations and experiments. Red points represent tracer particles and star markers represent obstacles at different concentrations and sizes.

The diffusion of tracer particles in 3D macromolecular crowded media has been studied using two methodologies, simulation and experimental, with the aim of comparing their results.
First, the diffusion of a tracer in an obstructed 3D lattice with mobile and big size obstacles has been analyzed through a Monte Carlo (MC) simulation procedure[1]. Secondly, fluorescence recovery after photobleaching (FRAP) experiments have been carried out to study the diffusion of a model protein (alpha-chymotrypsin) in in vitro crowded solution where two type of Dextran molecules are used as crowder agents[2]. To facilitate the comparison, the relative size between the tracer and the crowder is the same in both studies.
The results indicate a qualitative agreement between the diffusional behaviors observed in the two studies. The dependence of the anomalous diffusion exponent and the limiting diffusion coefficient on the obstacle size and excluded volume shows, in both cases, a similar tendency. The introduction of a reduced mobility parameter in the simulation model accounting for the short-range tracer-obstacle interactions allows obtaining a quantitative agreement between the limiting diffusion coefficient values yielded by both procedures[3].

The simulation-experiment quantitative agreement for the anomalous diffusion exponent requires further improvements. As far as we know, this is the first reported work where both techniques are used in parallel to study the diffusion in macromolecular crowded media.

* eudald.vilaseca@ub.edu
† i.pastor@ub.edu
†† Department of Chemistry, University of the West Timisoara, Timisoara, Romania. aisvoran@cbg.uvt.ro
††† s.madurga@ub.edu
‡ Departament de Química. Universitat de Lleida. Lleida. jlgarces@quimica.udl.es
‡‡ fmas@ub.edu
[1] E. Vilaseca, A. Isvoran, S. Madurga, J.L. Garcés, I. Pastor, F. Mas Phys. Chem. Chem. Phys. DOI: 10.1039/C0CP01218A
[2] I. Pastor, E. Vilaseca, S. Madurga, J.L. Garcés, M. Cascante, F. Mas J. Phys. Chem. B **114**, 4028 (2010).
[3] E. Vilaseca, I. Pastor, A. Isvoran, S. Madurga, J.L. Garcés, F. Mas Theor. Chem. Acc. DOI: 10.1007/s00214-010-0840-5

Critical, interfacial and surface properties of ionic liquids by a molecular-based equation of state

O. Vilaseca[1]*, F. Llovell[1], L.F. Vega[1]
[1] *Institut de Ciència de Materials de Barcelona / MATGAS2000 AIE*
Campus de la UAB
08193 Bellaterra, Barcelona

Precise measurements of ionic liquids (IL) physical properties near the critical point are an unexplored field. Experimental data at these extreme conditions is very difficult to achieve due to the low vapor pressures and the thermal degradation of ionic liquids far before the critical region is reached. However, in order to design thermally stable ILs, information about the critical region is a requirement for industrial purposes. Hence, the need of a reliable prediction of the critical properties of ionic liquids has pushed the development of theoretical methods based on molecular-based approaches with physical meaning. In this contribution, within the framework of the soft-SAFT EoS[1] coupled with the Density Gradient Theory (DGT)[2], the surface tension as well as the critical temperature, pressure and density have been estimated, for three different ionic liquid families, and compared with those reported in the literature from expe

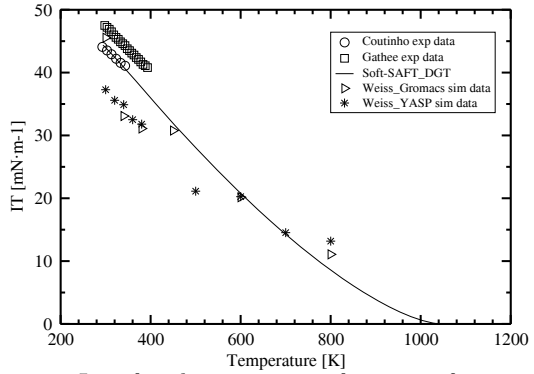

Figura 1. Interfacial tension as a function of temperature for [C4-mim][PF6]

In addition, for the [Cn-mim][Tf2N] ILs family a correlation for the influence parameter as a function of the molecular weight was obtained, empowering the predictive capabilities of the equation for interfacial tensions of compounds of the family for which experimental data is scarce or unavailable[3]. Finally, surface thermodynamic properties were also derived from the dependence of the surface tension values, and compared with those obtained with Guggenheim's and Eötvos empirical equations[3–5]. The results presented here show the robustness of using an accurate and versatile equation of state for the evaluation of bulk, interfacial[7] and surface properties[8] with a very modest computational effort.

This work is partially financed by the Spanish Government under project CTQ2008-05370 and NANOSELECT and CEN2008-01027, a Consolider and a CENIT project belonging to the Programa Ingenio 2010). Additional support from the Catalan Government is also acknowledged (SGR-2005-00288 and 2009SGR-666). F. Llovell acknowledges a JAE-Doctor fellowship from the Spanish Government.

* ovilaseca@gmail.com

[1] F.J. Blas, L.F Vega, Mol. Phys., 92, 135 (1997).
[2] J.D. van der Waals, Z. Phys. Chem. 13, 657 (1894).
[3] P. J. Carvalho, M. G. Freire, I. M. Marrucho, A. J. Queimada, and J. A. P. Coutinho, J. Chem. Eng. Data 53, 1346 (2008).
[4] L.P.N. Rebelo, J.N. Canongia Lopes, J.M.S.S. Esperanca, E. Filipe, J. Phys. Chem. B 109, 6040 (2005).
[5] M. G. Freire , P. J. Carvalho , A. M. Fernandes , I. M. Marrucho, A. J. Queimada , J. A.P. Coutinho , J. of Colloid and Interface Science 314, 621 (2007).
[6] V. C. Weiss, B. Heggen and F. Müller-Plathe J. Phys. Chem. C 114, 3599 (2010).
[7] O.Vilaseca and L.F. Vega, Fluid Phase Equilib. 2010. doi:10.1016/j.fluid.2010.09.018
[8] O.Vilaseca and L.F. Vega, Submitted for publication

Chaos and unpredictability in evolutionary dynamics in discrete time

Daniele Vilone*,1, Alberto Robledo[1,2], Angel Sánchez[1,3]

1 - Grupo Interdisciplinar de Sistemas Complejos (GISC), Departamento de Matemáticas, Universidad Carlos III de Madrid, 28911 Leganés (Madrid)

2 - Universidad Nacional Autónoma de México, México D.F., México

3 - Instituto de Biocomputación y Física de Sistemas Complejos (BIFI), Universidad de Zaragoza, 50018 Zaragoza

Cooperative behaviours are commonly observed in nature. However, explaining their origin is not a trivial task, and game theory provides a useful framework to shed light on such phenomenon. The starting point is a so called 2×2 game, in which two individuals, or players, can adopt one of two possible strategies (usually cooperation, C, and defection, D), and earn a payoff Π according to the strategy chosen by both. Subsequently, a great deal of individuals playing 2×2 among themselves are taken into consideration. The first step is to study such population in the mean-field approximation ("well-mixed" case). In this case the dynamics is often ruled by the replicator equation[1]

$$\dot{x} = x \cdot (\Pi_C - \bar{\Pi}) \ , \qquad (1)$$

where $x = x(t)$ is the density of cooperators at time t and Π_C the average payoff of a cooperator (possibly function of t, too), while $\bar{\Pi}$ is the average payoff of the entire population. Of course, the defector density y is easily given by the relation $x + y = 1$. According to the details of the game, that is, to the values of the payoff parameters, the dynamical behaviour of the system will be different.

Let us consider for example a well-mixed population of individuals playing the Prisoner's Dilemma Game (PDG) among themselves. In a PDG played by only two players the rational choice for both is the defection, even though the highest joint payoff would be obtained with mutual cooperation (technically speaking, the Nash equilibrium of the PDG is not a Pareto optimum). Now, equation (1) predicts that a population of PDG players evolves towards an all-defectors final state. Analogously, if the game by which indivuduals interact is the Harmony Game (HG, whose equilibrium in the 2×2 case is mutual cooperation), the population will end up in the all-cooperators configuration, and so on with all the possible 2×2 games. In general, the dynamics given by the replicator equation is deterministic and perfectly predictable. Nevertheless, it must be noticed that in nature there are species which reproduce in discrete-time path: every new generation replaces the previous one, that is, all the old individuals die before their offspring reproduce on its turn[2]. In this case, it is better to take into consideration a discretized version of the differential equation (1), where the variable t is an integer instead of a real number.

In the present work, we focus on the map derived by the direct discretization of the replicator equation, which then assumes the form

$$x_{N+1} = x_N \cdot (\Pi_C - \bar{\Pi}) + x_N \qquad N \in \mathbf{N} \ . \qquad (2)$$

This map returns the same well determined results of its continuous version only for a restricted set of the values of the parameters, which coincides with the set usually studied by researchers until now[3]. In fact, for different values of the parameters we have found distinct and somehow exotic results: in particular, the system does not end up in the frozen configuration provided by the replicator equation, but in periodic orbits around such solution. Moreover, for other values of the parameters, the system becomes chaotic, so that its behaviour is totally unpredictable.

In this work we present evidence supporting those phenomena (see for instance FIG. 1), characterize the regions on which they are observed and the implications for the corresponding games, and analyse the implications for the very debated issue of the evolution (and possibly the emergence and stability) of the cooperation in real systems.

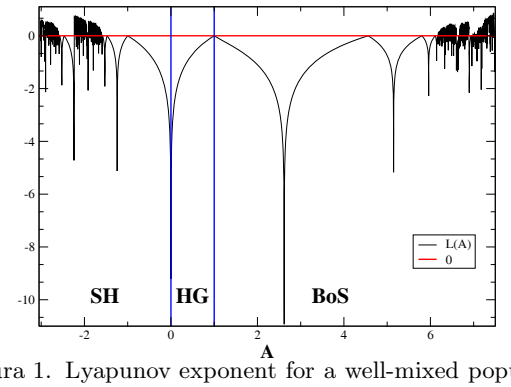

Figura 1. Lyapunov exponent for a well-mixed population following the discrete dynamics of eq. (2). According to the value of the parameter A, the individuals interact by Battle of Sex (BoS), HG or Stug Hunt (SH) games. Independently of the details of such games, it can be seen how the dynamics turns chaotic (positive Lyapunov exponent) for $A \lesssim -1.6$ and $A \gtrsim 6$, (it never happens in the continuous case).

* daniele.vilone@gmail.com

[1] Hofbauer J. and Sigmund K., "Evolutionary Games and Population Dynamics", Cambridge (1998).

[2] It is the case of several species of insects and most bacteria.

[3] C. P. Roca, J. A. Cuesta and A. Sánchez, *Phys. of Life Rev.*, **6**, 208 (2009).

La ecuación de Kuramoto-Sivashinsky estocástica pertenece a la clase de universalidad Kardar-Parisi-Zhang en dos dimensiones

Matteo Nicoli,[1] Edoardo Vivo y Rodolfo Cuerno
Departamento de Matemáticas y Grupo Interdisciplinar de Sistemas Complejos (GISC), Universidad Carlos III de Madrid, Avenida de la Universidad 30, 28911 Leganés (Madrid)

La ecuación de Kuramoto-Sivashinsky estocástica (nKS) aparece en numerosos contextos físicos, como la erosión de superficies y el crecimiento limitado por difusión. Su versión determinista (dKS) surge también en la descripción de multitud de sistemas espacialmente extensos, hasta el punto de considerarse un paradigma en el estudio del caos espaciotemporal.[2]

Una de las características mas interesantes de la ecuación dKS es que, al menos en $d = 1$, presenta rugosidad cinética en la clase de universalidad de la ecuación de Kardar-Parisi-Zhang (KPZ), como ocurre para la ecuación nKS.[3,4] Sin embargo, en $d = 2$ su comportamiento a grandes escalas no se comprende del todo, existiendo resultados analíticos contradictorios respecto al comportamineto asintótico de la ecuación dKS frente al de la ecuación de KPZ.[5,6] En el caso de la ecuación nKS, las simulaciones numéricas sugieren un comportamiento no-KPZ,[8] lo que contradice expectativas teóricas basadas en la estructura detallada del grupo de renormalización.[4]

En este trabajo,[9] retomamos el estudio numérico de la ecuación nKS en $d = 2$. Utilizando un esquema pseudoespectral, es posible realizar simulaciones de sistemas con tamaños lo suficientemente grandes como para poder confirmar un comportamiento de escala tipo KPZ en el estado asintótico. Para ello, aprovechamos que, en coordenadas adecuadas, la ecuación nKS depende únicamente del acoplo KPZ, g,[7] al poderse escribir como

$$\frac{\partial h}{\partial t} = -\nabla^2 h - \nabla^4 h + \frac{\sqrt{g}}{2}(\nabla h)^2 + \xi(\mathbf{r}, \mathbf{t}),$$

donde ξ es un ruido de amplitud fija. Así, podemos estudiar el espacio de fases completo de la ecuación nKS en términos de g y del tamaño del sistema, L.

Nuestros principales resultados se resumen en la figura 1. Mediante el colapso de datos de la densidad espectral de potencia con los exponentes de KPZ en $d = 2$,[7] identificamos tres regímenes para la ecuación nKS: i) Preasintótico en el que el colapso no es bueno para ninguno de los valores L estudiados (punto A). ii) Régimen con buen colapso sólo para pequeños números de onda (punto B). iii) Régimen en el que el estado asintótico KPZ se alcanza incluso a tiempos cortos (punto C). Este tipo de análisis permite concluir que las simulaciones anteriores de la ecuación nKS[8] no alcanzaban a observar el estado asintótico KPZ por corresponder a valores de g y L en el régimen de acoplo KPZ débil.

En el contexto de la controversia sobre la clase de universalidad de la ecuación determinista de KS en $d = 2$, si se pudiera probar su equivalencia con la ecuación nKS como en $d = 1$,[10] nuestros resultados implicarían que el escalado asintótico de la ecuación dKS también estaría en la clase de universalidad de la de KPZ en $d = 2$. En ausencia de una conexión explícita entre las dos ecuaciones en $d = 2$, dicha controversia sigue constituyendo un importante problema abierto en Ciencia No Lineal.

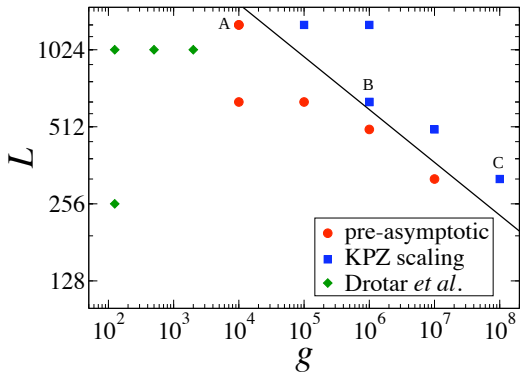

Figura 1. Diagrama de fase cualitativo para la ecuación nKS en $d = 2$. Los puntos rojos corresponden a escalado preasintótico (tipo i). Los cuadrados azules corresponden a un acoplo KPZ fuerte (tipos ii y iii). Los diamantes son los resultados de [8]. La línea continua se ha calculado por mínimos cuadrados, y separa las regiones de acoplo débil y fuerte.

[1] Laboratoire de Physique de la Matière Condensée, École Polytechnique - CNRS, 91128 Palaiseau, Francia.

[2] M. Cross y H. Greenside, *Pattern Formation and Dynamics in Nonequilibrium Systems* (Cambridge University Press, Cambridge, 2009).
[3] R. Cuerno, H. A. Makse, S. Tomassone, S. T. Harrington y H. E. Stanley, Phys. Rev. Lett. **75**, 4464 (1995).
[4] R. Cuerno y K. B. Lauritsen, Phys. Rev. E **52**, 4853 (1995); K. Ueno, H. Sakaguchi y M. Okamura, *ibid.* **71**, 046138 (2005).
[5] C. Jayaprakash, F. Hayot y R. Pandit, Phys. Rev. Lett. **71**, 12 (1993).
[6] I. Procaccia, M. H. Jensen, V. S. L'vov, K. Sneppen y R. Zeitak, Phys. Rev. A **46**, 3220 (1992).
[7] A.-L. Barabási y H. E. Stanley, *Fractal Concepts in Surface Growth* (Cambridge University Press, Cambridge, 1995).
[8] J. T. Drotar, Y.-P. Zhao, T.-M. Lu y G.-C. Wang, Phys. Rev. E **59**, 177 (1999).
[9] M. Nicoli, E. Vivo y R. Cuerno, Phys. Rev. E (Rapid Comm.) **82**, 045202(R) (2010).
[10] C. C. Chow y T. Hwa, Physica D **84**, 494 (1995).

Variational formulation for the KPZ equation: consistency, Galilean-invariance, and other issues in real-space discretization

H.S. Wio[1,*], J.A. Revelli[1], C. Escudero[2], R.R. Deza[3], M. S. de La Lama[4]
(1) Instituto de Física de Cantabria (UC and CSIC), Spain,
(2) Dep. Matemáticas, Fac. Cs., Univ. Aut. de Madrid, Spain,
(3) Physics Dept. and IFIMAR (UNMdP and CONICET), Argentina,
(4) Max-Planck-Institute, Göttingen, Germany.
(*) E-mail: wio@ifca.unican.es, URL: http://www.ifca.unican.es/users/wio/

We present a variational formulation for the Kardar-Parisi-Zhang (KPZ) equation that leads to a thermodynamic-like potential for the KPZ as well as for other related kinetic equations [1]. We prove some global shift invariance properties previously conjectured by other authors, and also show a few results about the form of the stationary probability distribution function for arbitrary dimensions. In addition, strong constraints are drawn for the choice of real-space discretization schemes, using the known fact that the KPZ equation results from a diffusion equation (with multiplicative noise) through a Hopf–Cole transformation. Whereas the nearest-neighbor discretization passes the consistency tests, known examples in the literature do not. We propose a consistent and highly accurate scheme, and emphasize the importance of the Lyapunov functional as a natural starting point for real-space discretization. Also, in the light of these findings, the mainstream opinion on the relevance of Galilean invariance and the fluctuation–dissipation theorem (peculiar of 1D) is challenged [2,3,4].

References

[1] Wio H.S., Int. J. Bif. Chaos **18**, 2813 (2009)

[2] H.S.Wio, J.A.Revelli, R.R.Deza, C.Escudero and M.S. de La Lama, Europhys.Lett. **89**, 40008 (2010)

[3] H.S.Wio, J.A.Revelli, R.R.Deza, C.Escudero and M.S. de La Lama, Phys. Rev. E **81**, 066706 (2010)

[4] H.S.Wio, J.A.Revelli, R.R.Deza, C.Escudero and M.S. de La Lama, Phil. Trans. Royal Soc. A **369**, 396 (2011).

Crowd Synchrony and Quorum Sensing Transition in Star-coupled Non-identical Semiconductor Lasers with Time Delay

Jordi Zamora-Munt, C. Masoller, Jordi Garcia-Ojalvo
*Departament de Física i Eng. Nuclear, Universitat Politècnica de Catalunya, Edif. GAIA, Rambla de Sant Nebridi s/n, 08222 Terrassa, Barcelona, Spain**

Rajarshi Roy
Institute for Research in Electronics and Applied Physics, Department of Physics, and Institute for Physical Science and Technology, University of Maryland, College Park, MD 20742, USA

Crowd synchrony and quorum sensing arise when a large number of dynamical elements communicate with each other via a common information pool. Previous evidence in different fields, including chemistry[1], biology[2,3] and civil engineering[4], has shown that this type of coupling leads to synchronization, when coupling is instantaneous and the number of coupled elements is large enough. Here we consider a situation in which the transmission of information between the system components and the coupling pool is not instantaneous.

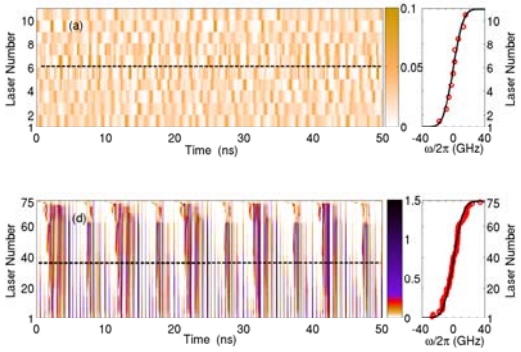

Figura 1. The color coding shows the intensity for each star laser as a function of time. In the vertical axis the lasers are sorted by their solitary frequency with number 1 corresponding to the most negative detuning. The black dashed line shows the laser for which $\omega = 0$. (a) for 10 lasers, (d) for 75 lasers. The right column shows the frequency of the lasers (dots), in relation with the normailized cumulative Gaussian distribution (solid line). The star-lasers are pumped above the lasing threshold and the Hub laser is pumped below threshold.

We show numerically that a system of non-identical semiconductor lasers (star-lasers) coupled to a common hub laser with time delay can be synchronized with zero lag[5,6] (Fig. 1).

The transition to the synchronization occurs above a certain critical number M_c of coupled lasers, provided the pump current of the hub laser is smaller than the solitary pump current threshold μ_{th}. The type of synchronization transition can be controlled via the pump current, μ of the star lasers (Fig. 2): a gradual (first-order-like) transition is observed for star lasers with $\mu > \mu_{th}$, and an abrupt (second-order-like) transition arises for $\mu < \mu_{th}$. A similar behavior has been exhibited by a chemical quorum sensing system[1].

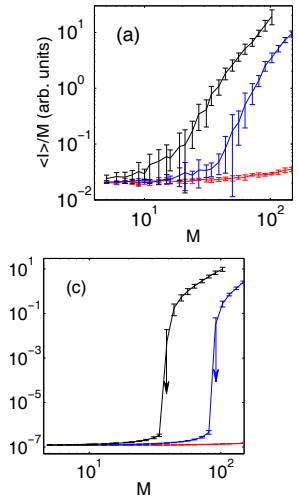

Figura 2. Ratio between the averaged coherent intensity $\langle I \rangle$ and the number of star lasers M, as a function of M itself and for different coupling strengths: From top to bottom $\kappa = 30$ ns^{-1}, $\kappa = 20$ ns^{-1} and $\kappa = 10$ ns^{-1}. (a) $\mu = 1.02$, $\mu_H = 0.4$. (c) $\mu = 0.7$, $\mu_H = 0.4$. Each point is averaged over 10 to 40 different initial conditions and detuning frequencies. The arrows mark errorbars out of the axis limits.

The critical number of lasers increases linearly with the width of frequency distribution, and depends on the coupling strength via a power-law with negative exponent, in agreement with the crowd synchronization transition reported in the Millenium bridge[4]. On the other hand, the coupling delay reduces the critical number of lasers while it has no influence on it for large enough time delays, even though the delay is evident through the lag time with which the hub laser is synchronized with the star lasers (which are synchronized isochronously to one another).

* jordi.zamora.munt@upc.edu

[1] A. F. Taylor, M. R. Tinsley, F. Wang, Z.Huang and K. Showalter, Science **323**, 614 (2009).
[2] J. Aldridge and E. K. Pye, Nature **259**, 670 (1976).
[3] S. De Monte *et al.*, Proc. Natl. Acad. Sci. U.S.A. **104**, 18377 (2007).
[4] S. H. Strogatz, D. M. Abrams, A. McRobie, B. Eckhardt and E. Ott, Nature **438**, 43 (2005).
[5] I. Fischer, R. Vicente, J. M. Buldú, M. Peil, C. R. Mirasso, M.C. Torrent and J. Garcia-Ojalvo, PRL **97**, 123902 (2006).
[6] J. Zamora-Munt, C. Masoller, J. Garcia-Ojalvoa and R. Roy, PRL **105**, 264101 (2010).

Tapping vertical en una capa granular

José Damas*, Iker Zuriguel y Diego Maza
Departamento de Física y Matemática Aplicada
Universidad de Navarra
Irunlarrea S/N 31008 Pamplona, Navarra

En éste trabajo presentamos nuevos resultados experimentales acerca de una capa granular perturbada verticalmente mediante un *tapping*, en concreto, acerca de la fracción de compactación en función de la amplitud de la perturbación (Γ). Experimentos previos[1] han demostrado la existencia de estados estacionarios de compactación que evolucionan de forma monótona cuando se incrementa Γ. Estos resultados están de acuerdo con la propuesta teórica de S. Edwards[2]. Sin embargo estudios númericos recientes[3] predicen que si la aceleración aplicada al sistema es lo suficientemente alta, la fracción de compactación (Φ) se incrementa. Así, sería posible encontrar dos estados con el mismo Φ para valores diferentes de aceleración. Consecuentemente se hace necesario explorar experimentalmente valores de aceleración de mayor amplitud[4].

El arreglo experimental utilizado consiste en una celda cuasi-bidimensional de plexiglass con 25 mm de ancho y 1.1 mm de espesor, en la cual se colocaron 900 esferas de cerámica de aluminio de 1 ± 0.05 mm de diámetro. Para realizar la perturbación se utilizó un oscilador con el que se genera un tap de una frecuencia característica de 30 Hz.

Para medir la fracción de compactación, se tomaron 500 fotos de alta resolución después de haber alcanzado un estado estacionario de compactación. Se ha encontrado experimentalmente que la compactación granular no decae monótonamente como se creía. Esto ha dado lugar a nuevas propuestas que consideran un mayor numero de variables de estado para realizar una descripción adecuada de los estados granulares de equilibrio[5].

Se incluyen aquí, resultados preliminares sobre la diámica del sistema durante el tapping midiendo el desplazamiento de su centro de masas. También se modificó el número de partículas contenidas en la celda, para estudiar la dependencia de la fracción de compactación con este parámetro (Figura 1).

III

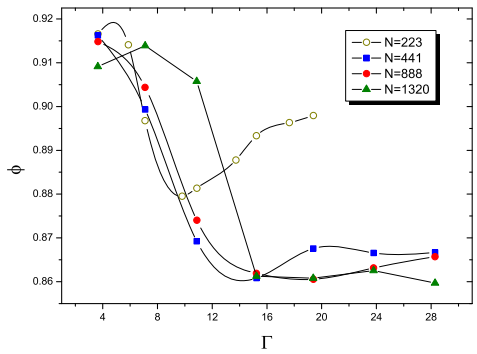

Figura 1. Curva de Compactación.

Es posible que esta dependencia sea la responsable de que no se haya observado este comportamiento previamente en situaciones experimentales.

* jdelacruz@alumni.unav.es

[1] E. R. Nowak, J. B. Knight, E. Ben-Naim, H. M. Jaeger and S. R. Nagel, *Phys. Rev. E* (57, 1971, 1998).
[2] S. F. Edwards and R. B. S. Oakeshott, *Physica A* (157, 1080, 1989).
[3] L. A. Pugnaloni, M. Mizrahi, C. M. Carlevaro and F. Vericat, *Phys. Rev. E* (78, 051305, 2008).
[4] P. A. Gago, N. E. Bueno and L. A. Pugnaloni, *Gran. Matt.* (11, 365, 2009).
[5] L. A. Pugnaloni, Iván Sanchez, P. A. Gago, José Damas, Iker Zurigel and Diego Maza, *Phys. Rev. E* (82, 050301, 2010).

Thermodynamics of RNA hybridization inferred from out of equilibrium unzipping experiments

C. V. Bizarro, J. M. Huguet and F. Ritort*

Small Biosystems Lab†, Departament de Física Fonamental
Facultat de Física, Universitat de Barcelona
Diagonal 647
08028 Barcelona

We have recently developed a methodology to infer the free energy of hybridization of DNA with a single molecule technique[1]. It consists in unzipping a molecule of DNA of a few thousands of base pairs with optical tweezers. These pulling experiments provide a force vs. distance curve that is analyzed to obtain the free energy of formation of the Nearest-Neighbor motifs. However, this technique is only valid for quasistatic pulling experiments. We have extended our technique to out of equilibrium experiments, in which the force vs. distance curves are not quasistatic anymore. So we are able to analyze the data obtained from pulling experiments on RNA, which exhibits much more hysteresis than DNA. The main advantage of this technique is that it circumvents the problems of bulk experiments such as aggregation of molecules or autocatalysis of biomolecules at certain salt concentrations or pH. The results pave the way to establish the single-molecule unzipping experiments as a reliable technique to extract the free energy of formation of biomolecular motifs.

* fritort@gmail.com
† `http://www.ffn.ub.es/ritort/`

[1] Huguet *et al.*, Proc. Natl. Acad. Sci. U.S.A **107**, 15431 (2010).

How proteins fold?: Unfolding/folding of the single protein barnase induced by mechanical forces

B. Rey Serra, A. Alemany, S. Frutos, C. Larroy, C. Ceconni and F. Ritort
Departament de Física Fonamental
Facultat de Física
Universidat de Barcelona
08028 Barcelona

The functionality of proteins is determined by their tertiary structure. Typically, misfolded conformations lead to harmful states where the protein cannot function properly. Under these circumstances, the understanding of how a protein folds becomes one of the most challenging problems in molecular biology. In this project, we present single molecule studies of Barnase protein. Stretching experiments using dual-beamed optical tweezers have been performed in order to obtain relevant kinetic properties such us the unfolding forces, the elastic properties of the aminoacid chain and the free energy of formation of the protein.

Force spectroscopy of individual molecular motors

L. Bongini, M. Manosa, C. V. Bizarro, F. Ritort
Departament de Fisica Fonamental
Facultat de Fisica
Universitat de Barcelona
08028 Barcelona

The activity of an ATP dependent molecular motor, the GP41 helicase, is studied by means of optical tweezers. Helicases are polymeric proteins that convert chemical energy into useful mechanical work. By hydrolyzing ATP they can displace on single stranded DNA or unzip large portions of double stranded DNA. Although several bulk assays exist which allow to characterize both their ATP consumption and their DNA unzipping activity, a detailed understanding of their mechanical functioning is still lacking. Single molecule manipulation allows to investigate the dependence on mechanical load of the average unzipping rate as well as fluctuations in unzipping activity.

Entropy production and coarse graining in Markov processes

Simone Pigolotti*, Andrea Puglisi, Lamberto Rondoni, Angelo Vulpiani
Dept. de Fisica i Eng. Nuclear, Universitat Politecnica de Catalunya
Edif. GAIA, Rambla Sant Nebridi s/n, 08222 Terrassa, Barcelona, Spain

I will present a general method to coarse grain master equations by eliminating fast decaying states[1]. The method is based on the following recipe: states having a typical lifetime shorter than a prescribed threshold are identified, and it is imposed that the time spent in these states is zero. This prescription removes these states from the description of the system and renormalizes the other transition rates, as illustrated in Fig. 1.

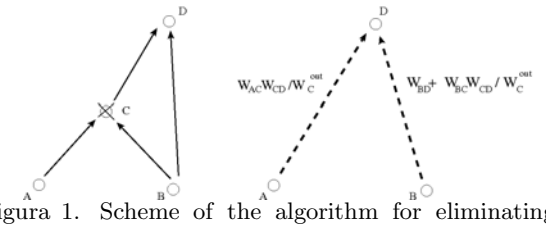

Figura 1. Scheme of the algorithm for eliminating fast states

This procedure has a number of interesting properties. It is commutative: the resulting system is independent of the order in which states are eliminated. Further, analytical results can be derived in simple cases (like one dimensional systems), so that the coarse grained system may be written in a simple closed form.

We apply the coarse graining algorithm to study the following problem: what happens to the distribution of entropy production in a non-equilibrium system after coarse graining?

More precisely, we study several non-equilibrium systems and compute in each of them the distribution of the Lebowitz-Spohn functional:

$$\Omega_t = \frac{1}{t} \ln \frac{W_{\omega_0 \to \omega_1} W_{\omega_1 \to \omega_2} ... W_{\omega_{m-1} \to \omega_m}}{W_{\omega_1 \to \omega_0} W_{\omega_2 \to \omega_1} ... W_{\omega_m \to \omega_{m-1}}}. \qquad (1)$$

and its Cramer function, $-\log[P(\Omega_t)]/t$, as a function of the coarse graining level, i.e. of the fraction of eliminated states.

In all cases, the result is that the distribution of entropy production is very robust even to extreme coarse graining, eliminating a large fraction of states from the dynamics, as shown in Fig. 2. However, when the coarse graining level passes some threshold, the entropy production suddenly drops.

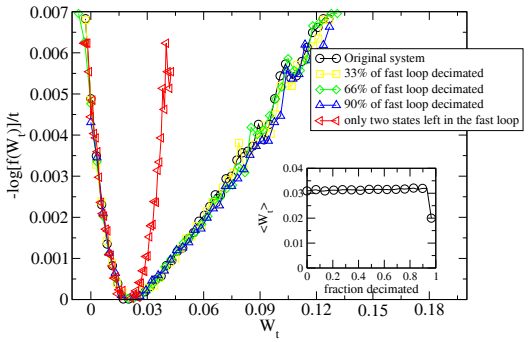

Figura 2. Cramer function and entropy production after progressive decimation

We interpret this result in terms of Schnakenberg's network theory: the entropy production can be decomposed into contributions coming from loops in the transition networks. Decimation shortens these loops, without affecting much the entropy production. This happens until current-carrying loops are destroyed, causing the entropy production to drop down.

Finally, we apply this theory to a biophysics example, a model of the Kinesin motor protein cycle.

* simone.pigolotti@upc.edu

[1] S. Pigolotti and A. Vulpiani, J. Chem. Phys. 128(154114), 2008.
[2] A. Puglisi, S. Pigolotti, L. Rondoni and A. Vulpiani, J. Stat. Mech. P05015 (2010).

Parte IV

Índice de Autores

Índice de Autores

Parte V

Asistentes al Congreso

Lista de Participantes

1. Abad Jarillo, Enrique
   - Universidad de Extremadura
   - E-mail: eabad@unex.es
2. Acevedo Escalante, Manuel Francisco
   - Universidad de Navarra
   - E-mail: macevedo@alumni.unav.es
3. Alarcón Oseguera, Francisco
   - Universitat de Barcelona
   - E-mail: falarcon@ffn.ub.es
4. Alcaraz i Sendra, Olga
   - Universitat Politècnica de Catalunya
   - E-mail: olga.alcaraz@upc.edu
5. Alonso Muñoz, Sergio
   - Physikalisch-Technische Bundesanstalt
   - E-mail: sergio.alonso@ptb.de
6. Alonso Pereda, Juan J.
   - Universidad de Málaga
   - E-mail: jjalonso@uma.es
7. Alvarez Baños, Raquel
   - Universidad Zaragoza
   - E-mail: raquel.alvarez.ba@gmail.com
8. Alvarez Lacalle, Enrique
   - Universitat Politècnica de Catalunya
   - E-mail: enrical@fa.upc.edu
9. Aragoneses, Andrés
   - Universitat Politècnica de Catalunya
   - E-mail: andres.aragoneses@upc.edu
10. Arcella, Annalisa
    - Institute for Research in Biomedicine
    - E-mail: annalisa.arcella@gmail.com
11. Arenas, Alex
    - Universitat Rovira i Virgili
    - E-mail: alexandre.arenas@urv.cat
12. Ares, Saúl
    - Max Planck Institute
    - E-mail: saul@pks.mpg.de
13. Astillero Vivas, Antonio
    - Universidad de Extremadura
    - E-mail: aavivas@unex.es
14. Auguet Sangrá, Carlota E.
    - Universitat Politècnica de Catalunya
    - E-mail: carlota@fa.upc.edu
15. Aznar Palenzuela, María
    - Universitat de Barcelona
    - E-mail: maznar@ffn.ub.es
16. Baronchelli, Andrea
    - Universitat Politècnica de Catalunya
    - E-mail: andrea.baronchelli@upc.edu
17. Bedeaux, Dick
    - Norwegian University of Science and Technology
    - E-mail: dick.bedeaux@chem.ntnu.no
18. Bergues Cabrales, Jesús Manuel
    - Universidad San Jorge
    - E-mail: jmbergues@usj.es
19. Bianco, Valentino
    - Universitat de Barcelona
    - E-mail: vbianco@ub.edu
20. Bitlloch Puigvert, Pau
    - Universitat de Barcelona
    - E-mail: pau.bitlloch@gmail.com
21. Bitrián Varea, Vicente
    - Universitat Politècnica de Catalunya
    - E-mail: vicente.bitrian@upc.esu
22. Bitrián, Vicente
    - Universitat de Barcelona
    - E-mail: cblanchme@hotmail.com
23. Boix Deudero, Miguel
    - Universitat Rovira i virgili
    - E-mail: miguel.boix@urv.cat
24. Bonatto, Cristian
    - Universitat Politècnica de Catalunya
    - E-mail: bonatto.cristian@gmail.com

25. Bonet Avalos, Josep
    - Universitat Rovira i Virgili
    - E-mail: josep.bonet@urv.cat
26. Bongini, Lorenzo
    - Universitat de Barcelona
    - E-mail: bongini@fi.infn.it
27. Boronat, Jordi
    - Universitat Politècnica de Catalunya
    - E-mail: jordi.boronat@upc.edu
28. Borondo Rodriguez, Florentino
    - Universidad Autonoma de Madrid
    - E-mail: f.borondo@uam.es
29. Bravo Yuste, Santos
    - Universidad de Extremadura
    - E-mail: santos@unex.es
30. Brey Abalo, José Javier
    - Universidad de Sevilla
    - E-mail: brey@us.es
31. Brito, Ricardo
    - Universidad Complutense
    - E-mail: brito@fis.ucm.es
32. Buceta Fernandez, Javier
    - Parc Cientific de Barcelona
    - E-mail: javier.buceta@pcb.ub.es
33. Builes Toro, Santiago
    - ICMAB (CSIC)
    - E-mail: sbuiles@icmab.es
34. Burguete, Javier
    - Universidad de Navarra
    - E-mail: javier@fisica.unav.es
35. C. Manrubia, Susanna
    - Instituto Nacional de Técnica Aeroespacial
    - E-mail: scmanrubia@cab.inta-csic.es
36. Cabrillo García, Carlos
    - IEM (CSIC)
    - E-mail: ccabrilo@foton0.iem.csic.es
37. Cacilda Rodrigues Espain Oliveira, Joana
    - Universidade do Porto
    - E-mail: joanaespain@gmail.com
38. Calero Borrallo, Carles
    - ICMAB - CSIC
    - E-mail: ccalero@icmab.es
39. Calvo Minguillón, Ausias-March
    - Universitat Politècnica de Catalunya
    - E-mail: ausias.march@upc.edu
40. Camacho, Juan
    - Universitat Autònoma de Barcelona
    - E-mail: juan.camacho@uab.es
41. Camuñas-Soler, Joan
    - Universitat de Barcelona
    - E-mail: joancs@gmail.com
42. Cao García, Francisco Javier
    - Universidad Complutense de Madrid
    - E-mail: francao@fis.ucm.es
43. Capitan Gomez, Jose Angel
    - Universitat Rovira i Virgili
    - E-mail: jcapitan@gmail.com
44. Carballido Landeira, jorge
    - Universidad de Santiago de Compostela
    - E-mail: jorge.carballido@gmail.com
45. Carretero Campos, Concepción
    - Universidad de Málaga
    - E-mail: ccarretero@uma.es
46. Carrique Fernández, Félix
    - Universidad de Málaga
    - E-mail: carrique@uma.es
47. Casademunt Viader, Jaume
    - Universitat de Barcelona
    - E-mail: jaume.casademunt@ub.edu
48. Casanellas Vilageliu, Laura
    - Universtiat de Barcelona
    - E-mail: lauracasanellasvilageliu@gmail.com
49. Castro Mon, Jorge
    - Universidad de Santiago de Compostela
    - E-mail: jorge.castro.mon@gmail.com
50. Castro Ponce, Mario
    - Universidad Pontificia Comillas de Madrid
    - E-mail: marioc@upcomillas.es

51. Cerdà Pino, Juan Jose
    - Universitat de les Illes Balears
    - E-mail: joan@ifisc.uib-csic.es
52. Cerdeiriña, Claudio
    - Universidad de Vigo
    - E-mail: calvarez@uvigo.es
53. Cerruti, Benedetta
    - Institute for Cancer Research and Treatment
    - E-mail: benedetta.cerruti@gmail.com
54. Chacón Fuertes, Enrique
    - ICMM - CSIC
    - E-mail: echacon@icmm.csic.es
55. Clotet i Fons, Xavier
    - Universitat de Barcelona
    - E-mail: xclotet@ecm.ub.es
56. Colet, Pere
    - Universitat de les Illes Balears - CSIC
    - E-mail: pere@ifisc.uib-csic.es
57. Cornelles Soriano, Miguel
    - Universitat de les Illes Balears - CSIC
    - E-mail: miguel@ifisc.uib-csic.es
58. Corral Cano, Alvaro
    - Centre de Recerca Matemàtica
    - E-mail: alvaro.corral@uab.es
59. Corvera Poiré, Eugenia
    - Universidad Nacional Autónoma de México
    - E-mail: eugenia.corvera@gmail.com
60. Costa Ferreira, Silvio
    - Universitat Politècnica de Catalunya
    - E-mail: silviojr@ufv.br
61. Cuenda Cuenda, Sara
    - Universidad Autónoma de Madrid
    - E-mail: sara.cuenda@uam.es
62. Cuerno Rejado, Rodolfo
    - Universidad Carlos III de Madrid
    - E-mail: cuerno@math.uc3m.es
63. Cuesta Ruiz, José A
    - Universidad Carlos III de Madrid
    - E-mail: cuesta@math.uc3m.es
64. de Franciscis, Sebastiano
    - Universidad de Granada
    - E-mail: sebast@onsager.ugr.es
65. de la Torre, Jaime Arturo
    - Universidad Nacional de Educación a Distancia
    - E-mail: jatorre@bec.uned.es
66. de las Heras, Daniel
    - Universidad de Lisboa
    - E-mail: daniel.delasheras@uam.es
67. de Sancristóbal, Belén
    - Universitat Politècnica de Catalunya
    - E-mail: belen.sancristobal@gmail.com
68. Deluca Silberberg, Anna
    - Centre de Recerca Matemàtica
    - E-mail: adeluca@crm.cat
69. Diaz Guilera, Albert
    - Universidad de Barcelona
    - E-mail: albert.diaz@ub.edu
70. Dies Miracle, Marta
    - Universitat Politècnica de Catalunya
    - E-mail: marta.dies@upc.edu
71. Dinis Vizcaino, Luis
    - Universidad Complutense de Madrid
    - E-mail: ldinis@fis.ucm.es
72. Domedel-Puig, Núria
    - Universitat Politècnica de Catalunya
    - E-mail: nuria.domedel@upc.edu
73. Domínguez Alvarez, Alvaro
    - Universidad de Sevilla
    - E-mail: dominguez@us.es
74. Domínguez García, Virginia
    - Universidad de Granada
    - E-mail: domgarvir@gmail.com
75. Duque Campayo, Daniel
    - Universidad Politécnica de Madrid
    - E-mail: daniel.duque@upm.es
76. Echebarria Dominguez, Blas
    - Universitat Politècnica de Catalunya
    - E-mail: blas@fa.upc.edu

77. Erola, Pau
    - Universitat Rovira i Virgili
    - E-mail: pau.erola@urv.cat
78. Escala, Darío Martín
    - Universidad de Santiago de Compostela
    - E-mail: dmescala@gmail.com
79. Español, Pep
    - Universidad Nacional de Educación a Distancia
    - E-mail: pep@fisfun.uned.es
80. Espinar, Lorena
    - Universitat Politècnica de Catalunya
    - E-mail: lorena_espinar@hotmail.com
81. Esplugas Martí, Cristian
    - Universitat de Barcelona
    - E-mail: cristian.esplugas@gmail.com
82. Estrada Díez, Javier
    - Universidad Autónoma de Madrid
    - E-mail: javier.estrada@uam.es
83. Falo Forniés, Fernando
    - Universidad de Zaragoza
    - E-mail: fff@unizar.es
84. Faraudo Gener, Jordi
    - ICMAB - CSIC
    - E-mail: jfaraudo@icmab.es
85. Fernandez-Nieves, Alberto
    - Georgia Institute of Technology
    - E-mail: alberto.fernandez@physics.gatech.edu
86. Fernández del Río, Ana
    - Universidad Nacional de Educación a Distancia
    - E-mail: anafrio@gmail.com
87. Fernández Gracia, Juan
    - IFISC (UIB - CSIC)
    - E-mail: juanf@ifisc.uib-csic.es
88. Fernandez Lafuerza, Luis
    - IFISC (UIB-CSIC)
    - E-mail: luis@ifisc.uib-csic.es
89. Fernandez Sanchez, Eva Maria
    - Consejo Superior de Investigaciones Cientificas
    - E-mail: efernand@icmm.csic.es
90. Ferrer Savall, Jordi
    - Universitat Politècnica de Catalunya
    - E-mail: jordi.ferrer-savall@upc.edu
91. Figueras La Peruta, Luis Alfonso
    - ICMAB - CSIC
    - E-mail: lfigueras@icmab.es
92. Floria Peralta, Luis Mario
    - Universidad de Zaragoza
    - E-mail: mario.floria@gmail.com
93. Formosa Jordan, Pau
    - Universitat de Barcelona
    - E-mail: pformosa@ecm.ub.es
94. Franzese, Giancarlo
    - Universitat de Barcelona
    - E-mail: gfranzese@ub.edu
95. Frigola Tubert, David
    - Universitat de Barcelona
    - E-mail: frigola.david@gmail.com
96. Galeano, Javier
    - Universidad Politécnica de Madrid
    - E-mail: javier.galeano@upm.es
97. Gamboa, Antonio
    - Universidad Politécnica de Madrid
    - E-mail: angamboa@yahoo.com
98. Garcia-Ojalvo, Jordi
    - Universitat Politècnica de Catalunya
    - E-mail: jordi.g.ojalvo@upc.edu
99. García Almarza, Noé
    - CSIC
    - E-mail: noe@iqfr.csic.es
100. García de Soria Lucena, María Isabel
    - Universidad de Sevilla
    - E-mail: gsoria@us.es
101. García Palanco, Jose María
    - Universidad Politénica de Madrid
    - E-mail: jose.gpalanco@upm.es
102. Garcia Ratés, Miquel
    - Universitat Rovira i Virgili
    - E-mail: miquelalexandre.garcia@urv.cat

103. Garcimartín Montero, Angel
    - Universidad de Navarra
    - E-mail: angel@fisica.unav.es
104. Garrido Galera, Pedro L.
    - Universidad de Granada
    - E-mail: garrido@ugr.es
105. Goethe, Martin Johannes
    - Universitat de Barcelona
    - E-mail: martingoethe@gmx.de
106. gomes caldeira, silvia maria
    - Universitat de Barcelona
    - E-mail: silvia.caldeira@gmail.com
107. Gómez Álvarez, Paula
    - Universidad de Vigo
    - E-mail: ga_paula@uvigo.es
108. Gómez Estévez, Juan Luis
    - Universitat de Barcelona
    - E-mail: jlgomez@ffn.ub.es
109. Gómez Jiménez, Sergio
    - Universitat Rovira i Virgili
    - E-mail: sergio.gomez@urv.cat
110. Gomila Villalonga, Damià
    - Consejo Superior de Investigaciones Científicas
    - E-mail: damia@ifisc.uib-csic.es
111. González de Prado Salas, Pablo
    - Universidad Autónoma de Madrid
    - E-mail: pablogps86@gmail.com
112. González Maestre, Miguel Ángel
    - Universidad de Extremadura
    - E-mail: maestre@unex.es
113. Granell, Clara
    - Universitat Rovira i Virgili
    - E-mail: clara.granell@urv.cat
114. Grujic, Jelena
    - Universidad Carlos III de Madrid
    - E-mail: jgrujic@math.uc3m.es
115. Guardia, Elvira
    - Universitat Politècnica de Catalunya
    - E-mail: elvira.guardia@upc.edu
116. Guimerà, Roger
    - Universitat Rovira i Virgili
    - E-mail: roger.guimera@urv.cat
117. Guinea, Francisco
    - ICMM - CSIC
    - E-mail: paco.guinea@icmm.csic.es
118. Guiu, Jacobo
    - Universidad de Santiago de Compostela
    - E-mail: xakogs@hotmail.com
119. Hernandez-Machado, Aurora
    - Universitat de Barcelona
    - E-mail: a.hernandezmachado@gmail.com
120. Hernández Álvarez, Juan Antonio
    - Universidad Politécnica de Madrid
    - E-mail: jantonio.hernandez@iberbanda.es
121. Hernandez Garcia, Emilio
    - IFISC (CSIC-UIB)
    - E-mail: emilio@ifisc.uib-csic.es
122. Hernández Navarro, Sergi
    - Universitat de Barcelona
    - E-mail: sergihn@hotmail.com
123. Hidalgo Aguilera, Jorge
    - Universidad de Granada
    - E-mail: jhidalgo@onsager.ugr.es
124. Huguet Casades, Josep Maria
    - Universidad de Barcelona
    - E-mail: jhuguetub.edu
125. Huhn, Florian
    - Universidad de Santiago de Compostela
    - E-mail: florian.huhn@usc.es
126. Ibañes, Marta
    - Universitat de Barcelona
    - E-mail: marta.ibanes@gmail.com
127. Ignés Mullol, Jordi
    - Universitat de Barcelona
    - E-mail: jignes@ub.edu
128. Jacobo, Adrian
    - Max Planck Institute
    - E-mail: jacobo@pks.mpg.de

129. Janda Galán, Alvaro
    - Universidad de Navarra
    - E-mail: ajandaga@alumni.unav.es
130. Jiménez Blas, Felipe
    - Universidad de Huelva
    - E-mail: felipe@uhu.es
131. Johnson, Samuel
    - Universidad de Granada
    - E-mail: samuel@onsager.ugr.es
132. Khalil Rodríguez, Nagi
    - Universidad de Sevilla
    - E-mail: nagi@us.es
133. Kolton, Alejandro B.
    - Universitat de Barcelona
    - E-mail: alejandro.kolton@gmail.com
134. Korutcheva, Elka
    - UNED
    - E-mail: elka@fisfun.uned.es
135. Lacasa, Lucas
    - Universidad Politécnica de Madrid
    - E-mail: lucas_lacasa@yahoo.es
136. Laneri, Karina Fabiana
    - Institut Català de Ciències del Clima
    - E-mail: karinalaneri@gmail.com
137. Lasanta Becerra, Antonio
    - Universidad de Sevilla
    - E-mail: alasanta@us.es
138. Lecina Casas, Daniel
    - Universitat de Barcelona
    - E-mail: danilecina@gmail.com
139. Ledesma Aguilar, Rodrigo
    - University of Oxford
    - E-mail: ra.ledesma@gmail.com
140. Llopis Fusté, Isaac
    - Universitat Politècnica de Catalunya
    - E-mail: isaac.llopis@upc.edu
141. Llovell, Felix
    - CSIC
    - E-mail: fllovell@icmab.es
142. Lomba García, Enrique
    - CSIC
    - E-mail: E.Lomba@iqfr.csic.es
143. López Caballero, Miguel
    - Universidad de Navarra
    - E-mail: mlcdos@gmail.com
144. Lopez, Juan Manuel
    - Universidad de Cantabria
    - E-mail: lopez@ifca.unican.es
145. de Lorenzo, Sara
    - Universitat de Barcelona
    - E-mail: slorenzoros@gmail.com
146. Losada González, Juan Carlos
    - Universidad Politécnica de Madrid
    - E-mail: juancarlos.losada@upm.es
147. Lozano Grijalba, Celia
    - Universidad de Navarra
    - E-mail: clozano@alumni.unav.es
148. Lugo Vélez, Carlos Antonio
    - Universitat Politècnica de Catalunya
    - E-mail: carlos.lugo@fa.upc.edu
149. Luque Santolaria, Antoni
    - Universitat de Barcelona
    - E-mail: tonisantolaria@gmail.com
150. Luque Serrano, Bartolo
    - Universidad Politécnica de Madrid
    - E-mail: bartolome.luque@upm.es
151. Lyra Gollo, Leonardo
    - Universitat de les Illes Balears - CSIC
    - E-mail: leonardo@ifisc.uib-csic.es
152. Lythe, Grant
    - Univesity of Leeds
    - E-mail: grant@maths.leeds.ac.uk
153. Mackie, Allan
    - Universitat Rovira i Virgili
    - E-mail: allan.mackie@urv.cat
154. Madurga Díez, Sergio
    - Universitat de Barcelona
    - E-mail: s.madurga@ub.edu

155. Mandrà, Salvatore
    - Universitat de Barcelona
    - E-mail: smandra@ffn.ub.es
156. Mareschal, Michel
    - ZCAM - Universidad de Zaragoza
    - E-mail: mmaresch@ulb.ac.be
157. Martí Rabassa, Jordi
    - Universitat Politècnica de Catalunya
    - E-mail: jordi.marti@upc.edu
158. Martinez Bennassar, Hector
    - Universidad Autonoma de Madrid
    - E-mail: hector.martinez@uam.es
159. Martínez García, Ricardo
    - Universitat de les Illes Balears - CSIC
    - E-mail: ricardo@ifisc.uib-csic.es
160. Martínez Llinàs, Jade
    - Universitat de les Illes Balears - CSIC
    - E-mail: jade@ifisc.uib-csic.es
161. Martínez Piñeiro, Manuel
    - Universidade de Vigo
    - E-mail: mmpineiro@uvigo.es
162. Martinez Raton, Yuri
    - Universidad Carlos III de Madrid
    - E-mail: yuri@math.uc3m.es
163. Martínez Vaquero, Luis Alberto
    - Universidad Carlos III de Madrid
    - E-mail: luisalberto.martinez@uc3m.es
164. Masoller, Cristina
    - Universitat Politècnica de Catalunya
    - E-mail: cristina.masoller@gmail.com
165. Matas Navarro, Ricard
    - Universitat de Barcelona
    - E-mail: rmtn83@gmail.com
166. Matías, Manuel A.
    - Universitat de les Illes Balears - CSIC
    - E-mail: manuel@ifisc.uib-csic.es
167. Maynar Blanco, Pablo
    - Universidad de Sevilla
    - E-mail: maynar@us.es
168. Mederos, Luis
    - ICMM - CSIC
    - E-mail: lmederos@icmm.csic.es
169. Meléndez Schofield, Marc
    - Universidad Nacional de Educación a Distancia
    - E-mail: mmelendez@fisfun.uned.es
170. Miguel López, M. Carmen
    - Universitat de Barcelona
    - E-mail: carmen.miguel@ub.edu
171. Míguez Díaz, José Manuel
    - Universidade de Vigo
    - E-mail: miguezjm@uvigo.es
172. Miritello, Giovanna
    - Universidad Carlos III de Madrid
    - E-mail: gmiritel@math.uc3m.es
173. Monforte García, Jorge
    - Universidad de Zaragoza
    - E-mail: jmonforte@bifi.es
174. Montbrió Fairen, Ernest
    - Universitat Pompeu Fabra
    - E-mail: ernest.montbrio@upf.edu
175. Morales Suaréz, Silvio René
    - Universitat de Barcelona
    - E-mail: silvio.rene@gmail.com
176. Moreno Barrado, Ana
    - Universidad Pontificia de Comillas
    - E-mail: anamorenob@gmail.com
177. Moretti, Paolo
    - Universitat Politècnica de Catalunya
    - E-mail: paolo.moretti@upc.edu
178. Moro, Esteban
    - Universidad Carlos III de Madrid
    - E-mail: esteban.moroegido@gmail.com
179. Mullin, Tom
    - University of Manchester
    - E-mail: tom@reynolds.ph.man.ac.uk
180. Muñoz García, Javier
    - Universidad Carlos III de Madrid
    - E-mail: javiermunozgarcia@gmail.com

181. Muñoz, Miguel A.
    - Universidad de Granada
    - E-mail: mamunoz@onsager.ugr.es
182. Muñuzuri, Alberto P.
    - Universidad de Santiago de Compostela
    - E-mail: uscfmapm@cesga.es
183. Muratov, Alexander
    - Universitat Rovira i Virgili
    - E-mail: alexander.muratov@urv.cat
184. Nesic, Svetozar
    - Universidad Carlos III de Madrid
    - E-mail: snesic@math.uc3m.es
185. Nguimdo, Romain Modeste
    - IFISC
    - E-mail: modeste@ifisc.uib.es
186. Nicola, Ernesto M.
    - Universitat de les Illes Balears - CSIC
    - E-mail: ernesto.nicola@gmail.com
187. Nicoli, Matteo
    - Ecole Polytechnique
    - E-mail: matteo.nicoli@polytechnique.edu
188. Oriola Santandreu, David
    - Universitat de Barcelona
    - E-mail: davidoriola@gmail.com
189. Orlandi, Javier G.
    - Universitat de Barcelona
    - E-mail: dherkova@gmail.com
190. Ortin Rull, Jordi
    - Universitat de Barcelona
    - E-mail: ortin@ecm.ub.es
191. Ortiz de Urbina i Viadé, Jordi
    - Universitat Politècnica de Catalunya
    - E-mail: jordi.ortiz@upc.edu
192. Ortiz de Zárate, José M.
    - Universidad Complutense de Madrid
    - E-mail: jmortizz@fis.ucm.es
193. Pagonabarraga Mora, Ignacio
    - Universitat de Barcelona
    - E-mail: ipagonabarraga@ub.edu
194. Palassini, Matteo
    - Universitat de Barcelona
    - E-mail: palassini@ub.edu
195. Palau Ortín, David
    - Universitat de Barcelona
    - E-mail: david.palau.ortin@gmail.com
196. Panadès Guinart, Carles
    - Universitat Politècnica de Catalunya
    - E-mail: panades@fa.upc.edu
197. Pardo, Luis Carlos
    - Universitat Politècnica de Catalunya
    - E-mail: luis.carlos.pardoupc.edu
198. Pascual García, Alberto
    - Centro de Biología Molecular Severo Ochoa (CSIC-UAM)
    - E-mail: apascual@cbm.uam.es
199. Pastor Ruiz, Juan Manuel
    - Universidad Politécnia de Madrid
    - E-mail: juanmanuel.pastor@upm.es
200. Pastor Satorras, Romualdo
    - Universitat Politècnica de Catalunya
    - E-mail: romualdo.pastor@upc.edu
201. Patti, Alessandro
    - IQAC - CSIC
    - E-mail: alpnqb@iqac.csic.es
202. Pazó, Diego
    - CSIC-Universidad de Cantabria
    - E-mail: pazo@ifca.unican.es
203. Peñaranda Ayllón, Angelina
    - Universitat Politècnica de Catalunya
    - E-mail: angelina@fa.upc.edu
204. Perez-Espigares, Carlos
    - Universidad de Granada
    - E-mail: cpespigares@onsager.ugr.es
205. Pérez Carrasco, Ruben
    - Universitat de Barcelona
    - E-mail: 2piruben@gmail.com
206. Pérez Sánchez, Germán
    - Universidad de Vigo
    - E-mail: gperez@uvigo.es

207. Picallo Gonzalez, Clara B.
    - Universitat de Barcelona
    - E-mail: clara.picallo@gmail.com

208. Pigolotti, Simone
    - Universitat Politècnica de Catalunya
    - E-mail: simone.pigolotti@gmail.com

209. Pons Rivero, Antonio Javier
    - Universitat Politècnica de Catalunya
    - E-mail: a.pons@upc.edu

210. Pont, Oriol
    - INRIA
    - E-mail: oriol.pont@inria.fr

211. Pradas, Marc
    - Imperial College London
    - E-mail: m.pradas-gene@imperial.ac.uk

212. Prados Montaño, Antonio
    - Universidad de Sevilla
    - E-mail: prados@us.es

213. Prieto Castrillo, Francisco
    - CETA-CIEMAT
    - E-mail: francisco.prieto@ciemat.es

214. Prignano, Luce
    - Universitat de Barcelona
    - E-mail: luceprignano@ffn.ub.es

215. Ramasco, José Javier
    - IFISC (CSIC-UIB)
    - E-mail:

216. Ramírez de la Piscina Millán, Laureano
    - Universitat Politècnica de Catalunya
    - E-mail: laure@fa.upc.edu

217. Rascón Díaz, Carlos
    - Universidad Carlos III de Madrid
    - E-mail: carlos.rascon@uc3m.es

218. Requejo, Rubén
    - Universitat Autònoma de Barcelona
    - E-mail: rubenfisico@gmail.com

219. Rey Serra, Blanca
    - Universitat de Barcelona
    - E-mail: breyserra@gmail.com

220. Rios i Rubiras, Oriol
    - Universitat de Barcelona
    - E-mail: oriolrios@gmail.com

221. Roa Chamorro, Rafael
    - Universidad de Málaga
    - E-mail: rafaroa@uma.es

222. Rodríguez Cantalapiedra, Inmaculada
    - Universitat Politècnica de Catalunya
    - E-mail: inma@fa.upc.edu

223. Rodríguez Díaz, Miguel Angel
    - CSIC-Universidad de Cantabria
    - E-mail: rodrigma@ifca.unican.es

224. Rodriguez Lazaro, Guillermo
    - Universitat de Barcelona
    - E-mail: grolazaro@gmail.com

225. Rodríguez López, Pablo
    - Universidad Complutense de Madrid
    - E-mail: parodrilo@gmail.com

226. Rodríguez Parrondo, Juan Manuel
    - Universidad Complutense de Madrid
    - E-mail: parrondo@fis.ucm.es

227. Roldán Estébanez, Edgar
    - Universidad Complutense de Madrid
    - E-mail: callmeyaw@gmail.com

228. Romero Enrique, José Manuel
    - Universidad de Sevilla
    - E-mail: enrome@us.es

229. Roussel, Thomas
    - ICMAB - CSIC
    - E-mail: troussel@icmab.es

230. Rovira, Carme
    - Parc Científic de Barcelona
    - E-mail: crovira@pcb.ub.es

231. Rubí Capaceti, Miguel
    - Universitat de Barcelona
    - mglrb2@gmail.com

232. Rubio Puzzo, Maria Leticia
    - Universidad Nacional de La Plata, Argentina
    - E-mail: leticia.rubio@gmail.com

233. Rué Queralt, Pau

- Universitat Politècnica de Catalunya
- E-mail: pau.rue@upc.edu

234. Ruiz Herrero, Teresa

- Universidad Autónoma de Madrid
- E-mail: teresa.ruiz@uam.es

235. Ruiz Montero, Maria Jose

- Universidad de Sevilla
- E-mail: majose@us.es

236. Sala Viñas, Jonàs

- Universitat Politècnica de Catalunya
- E-mail: jonas.sala@upc.edu

237. San Miguel, Maxi

- IFISC (CSIC-UIB)
- E-mail: maxi@ifisc.uib-csic.es

238. Sanchez Casals, Odalys

- Universitat Politècnica de Catalunya
- E-mail: odlyss@gmail.com

239. Sánchez Sánchez, Anxo

- Universidad Carlos III de Madrid
- E-mail: anxo@math.uc3m.es

240. Sancho, José M.

- Universitat de Barcelona
- E-mail: josemsancho@gmail.com

241. Santalla Arribas, Silvia Noemí

- Universidad Carlos III de Madrid
- E-mail: silvia.santalla@uc3m.es

242. Santos Reyes, Andrés

- Universidad de Extremadura
- E-mail: andres@unex.es

243. Santos Sanchez, Maria Jesus

- Universidad de Salamanca
- E-mail: smjesus@usal.es

244. Sartori-Velasco, Pablo

- Max Planck Institute
- E-mail: pablo.sartori@gmail.com

245. Scagliarini, Andrea

- Universitat de Barcelona
- E-mail: ascagliarini@gmail.com

246. Serral, Maria

- Universitat Rovira i Virgili
- E-mail: maria.serral@urv.cat

247. Serrano Moral, M. Ángeles

- Universitat de Barcelona
- E-mail: marian.serrano@ub.edu

248. Sesé Castel, Gemma

- Universitat Politècnica de Catalunya
- E-mail: gemma.sese@upc.edu

249. Simic, Ana

- Universidad de Navarra
- E-mail: asimic@alumni.unav.es

250. Sintes Olives, Tomas

- Universitat de les Illes Balears - CSIC
- E-mail: tomas@ifisc.uib-csic.es

251. Tarazona Lafarga, Pedro

- Universidad Autonoma de Madrid
- E-mail: pedro.tarazona@uam.es

252. Teller Amado, Sara

- Universitat de Barcelona
- E-mail: teller.sara@gmail.com

253. Tiana Alsina, Jordi

- Universitat Politècnica de Catalunya
- E-mail: jordi.tiana@upc.edu

254. Tierno, Pietro

- Universitat de Barcelona
- E-mail: ptierno@ub.edu

255. Tondelier, Paul

- Universitat de Barcelona
- E-mail: paul.tondelier@ens.fr

256. Toral, Raúl

- Universitat Illes Balears
- E-mail: raul@ifisc.uib-csic.es

257. Torrent Serra, M. Carme

- Universitat Politècnica de Catalunya
- E-mail: carme.torrent@upc.edu

258. Trejo Soto, Claudia

- Universitat de Barcelona
- E-mail: trejo.claudia@gmail.com

259. Trepat, Xavier

- Universitat de Barcelona
- E-mail: xtrepat@ub.edu

260. Trullas Simo, Joaquim

- Universitat Politècnica de Catalaunya
- E-mail: quim.trullas@upc.edu

261. Turiel Martínez, Antonio

- Institut de Ciències del Mar, CSIC
- E-mail: turiel@icm.csic.es

262. Valeriani, Chantal

- Universidad Complutense
- E-mail: cvaleria@ph.ed.ac.uk

263. Vaz Martins, Teresa

- IFISC (UIB-CSIC)
- E-mail: teresa@ifisc.uib-csic.es

264. Vega de las Heras, Carlos

- Universidad Complutense de Madrid
- E-mail: cvega@quim.ucm.es

265. Vega Reyes, Francisco

- Universidad de Extremadura
- E-mail: fvega@unex.es

266. Velasco Caravaca, Enrique

- Universidad Autónoma de Madrid
- E-mail: enrique.velasco@uam.es

267. Vida Delgado, Rafael

- Facultad de Ciencias, Físicas, UNED
- E-mail: rvida1@alumno.uned.es

268. Vilanova Gabarrón, Oriol

- Universitat de Barcelona
- E-mail: oriol.vilanova@gmail.com

269. Vilaseca, Eudald

- Universitat de Barcelona
- E-mail: eudald.vilaseca@ub.edu

270. Vilaseca i Vidal, Oriol

- ICMAB - CSIC
- E-mail: ovilaseca@gmail.com

271. Vilone, Daniele

- Universidad Carlos III de Madrid
- E-mail: daniele.vilone@gmail.com

272. Vivo, Edoardo

- Universidad Carlos III de Madrid
- E-mail: doc.cap@gmail.com

273. White Sánchez, Juan Antonio

- Universidad de Salamanca
- E-mail: white@usal.es

274. Wio Beitelmajer, Horacio S.

- Universidad de Cantabria
- E-mail: wio@ifca.unican.es

275. Zamora Munt, Jordi

- Universitat Politècnica de Catalunya
- E-mail: jordi.zamora.munt@upc.edu

276. Zuriguel, Iker

- Universidad de Navarra
- E-mail: iker@fisica.unav.es

Organismos patrocinadores

Programa FisEs 2011

Hora	Jueves, 2 de junio	Viernes, 3 de junio	Sábado, 4 de Junio
8:15-9:00	**Inscripción**		
9:00-9:30	**Inauguración**	F. Guinea (I-4)	D. Bedeaux (I-1)
9:30-10:00	T. Mullin (I-5)		
10:00-10:30		S. N. Santalla (O-20)	J. Burguete (O-3)
		A. J. Pons (O-19)	F. Vega Reyes (O-22)
10:30-11:00	R. Ledesma-Aguilar (O-14)	J. Grujić (O-9)	M.I. García de Soria (O-7)
	A. P. Muñuzuri (O-17)	J. A. Hernández (O-11)	A. Janda (O-12)
11:00-11:30	**Café**		
11:30-12:00	A. Fernández-Nieves (I-3)	J. J. Ramasco (I-7)	L. C. Pardo (I-6)
12:00-12:30	A. Patti (O-18)	P. Moretti (O-16)	A. Corral (O-6)
	P. L. Garrido (O-8)	R. Guimerà (O-10)	C. Bonatto (O-2)
12:30-12:45	P. Colet (O-5)	S. Johnson (O-13)	**Clausura**
12:45-13:00		M. Mareschal (I-11)	
13:00-15:00	**Comida**		
15:00-16:30	**Paneles (sesión 1)** **P 1-90**	**Paneles (sesión 2)** **P 91-**	
16:30-17:00	**Café**		
17:00-18:00	C. Rovira (I-8)	J. M. Sancho (I-9)	
18:00-18:30	P. Español (I-2)	X. Trepat (I-10)	
18:30-19:00	M. Castro (O-4)	S. Ares (O-1)	
	P. Sartori (O-21)	A. Luque (O-15)	